International Committee for Future Accelerators

Sponsored by the Particles and Fields Commission of IUPAP

Beam Dynamics Newsletter

No. 43

Issue Editor:
C.R. Prior

Editor in Chief:
W. Chou

August 2007

Contents

4

8

1   Foreword

1.1   From the Chair

Weiren Chou, Fermilab
mail to: chou@fnal.gov

The ICFA Beam Dynamics Panel met on June 25, 2007 in Albuquerque, New Mexico, U.S.A. during the PAC07 conference. Sixteen people including panel members or their delegates and several invitees attended. The meeting agenda and minutes can be found in Section 5.

The meeting received reports from the Panel Chair and four working group leaders about the activities in the past two years and plans for the next two years. At the meeting the Panel unanimously approved a letter to Stan Schriber, Organizing Committee Chair of PAC07, endorsing the creation of the International Particle Accelerator Conference (IPAC), a 3-year cycle of PAC, EPAC and APAC. For the latest development on this subject, refer to the letter to the Editor from the PAC Coordination Committee (PACCC) in Section 2.

The meeting discussed the important issue of turnover of panel membership and working group leadership and unanimously approved a mechanism to enforce the length of terms on the panel. This mechanism is described in the meeting minutes in Section 5.

The meeting also discussed Open Access (OA) Publishing, a campaign currently going on in the world high-energy physics community. The panel supports this initiative and urges the ICFA to play a leading role in this campaign.

A number of new workshop proposals were discussed. The meeting also decided the issue editors of this newsletter for the next two years.

Organization of *The Second International Accelerator School for Linear Colliders*, which will take place at the Ettore Majorana Center, Erice (Sicily), Italy from October 1 – 10, 2007, is proceeding smoothly. The school received 243 applications from around the world and accepted 69 students. The selection was based on merit only and did not consider financial need. The students come from 18 countries in the three regions: Asia and Oceania, Europe and Africa, and North and South America. A list of the students as well as the lecturers and a complete curriculum can be found on the school web site: http://www.linearcollider.org/school/2007/.

The editor of this issue is Dr. Chris Prior, a panel member and a senior scientist from the Rutherford Appleton Laboratory, England. Dr. Prior has assembled 14 excellent articles on FFAGs. This is a record number for the theme section of this newsletter. I'd like to congratulate him for this remarkable success. I'd also like to express my sincere gratitude to him for producing a well-organized fine Newsletter on schedule.

1.2   From the Editor

Christopher R Prior

http://www.astec.ac.uk/intbeams

STFC Rutherford Appleton Laboratory, Harwell Science and Innovation Campus,
Chilton, Oxfordshire OX11 0QX, U.K.

Mail to: c.r.prior@rl.ac.uk

The theme of this edition of the ICFA Beam Dynamics Newsletter is Fixed-Field Alternating Gradient (FFAG) accelerators. FFAGs have enjoyed something of a revival in recent years, spurred by the demands for rapid acceleration of unstable particles and parallel developments in the necessary associated technologies. New concepts in FFAG beam dynamics have been discovered, opening up a host of possibilities for study, with practical applications as diverse as cancer therapy and ADS.

The centre-piece of this Newsletter must be the article on EMMA, written by Scott Berg. EMMA will be the world's first non-scaling FFAG and the first FFAG ever to be built in Europe. A small electron model of a much larger muon accelerator, EMMA will enable tests of many of the new theories, including non-linear beam dynamics and resonance crossing. Construction is about to start at the Daresbury Laboratory, U.K., and experiments are due to begin in September 2009.

Since the literature on FFAGs is rather diffuse, members of the community have taken the opportunity in this edition to write a series of articles which I hope will provide a coherent overview of the subject. We start with an introduction that touches on the history of FFAGs and describes the main features of the different types currently under study. Other articles cover the adventurous R&D programme in Japan; the basic theory of the different types of FFAG accelerator; special simulation codes that have had to be developed to understand FFAG beam dynamics; designs for muon and proton FFAGs, including special acceleration techniques like harmonic number jumps; and finally the development of non-scaling FFAGs for medical purposes. Much of this work is very recent and some is being published here for the first time.

I am extremely grateful to all the friends and colleagues who have responded so positively to my proposal to focus this Newsletter on FFAGs. The stimulus to write up their work will perhaps lead to a full exposition of the subject in book or booklet form at a later date.

FFAGs aside, there are two articles in the regular section on the International Linear Collider, and summaries of two recent workshops: the ICFA-sponsored workshop on Energy Recovery Linacs in the UK, and the 18th Meeting of the International Collaboration on Advanced Neutron Sources, in China, which had a substantial element devoted to high power proton accelerators. Finally, there are summaries of four recent Ph.D. theses. This is an important but sometimes neglected section of the Newsletter. We are keen to know about novel ideas and this is a good opportunity for young people to advertise themselves and make their progress known.

2 Letters to the Editor

2.1 A Three-year Cycle of International Particle Accelerator Conferences

Dear Sir,

We write to draw your readers' attention to recent decisions made by the organising committees of the main American, Asian and European accelerator conferences regarding the structure and timing of future events.

The conferences concerned are the U.S., European and Asian Particle Accelerator Conferences, PAC, EPAC and APAC respectively.

Up to now, PAC and EPAC have held alternating conferences biennially, whereas APAC has operated three-yearly, always coinciding with one or other of the main European and US events. Recognising the growth of APAC, the rapid development of accelerator projects in the Far East and the detrimental effect of the timing, the committees of all three conferences recently voted unanimously to merge into a three-year cycle, thereby creating a series that can be developed into an annual International Particle Accelerator Conference (IPAC). Details are shown in the table, which highlights the clash between PAC and APAC this calendar year.

Year	Asia	Europe	Americas
2007	APAC, Indore, India		PAC, Albuquerque
2008		EPAC, Genoa, Italy	
2009			PAC, Vancouver
2010	IPAC, Kyoto, Japan		
2011		IPAC, Valencia, Spain	
2012			IPAC, mid-USA
2013	IPAC, probably Shanghai, China		
2014		IPAC	
2015			IPAC

Conferences have already been agreed and venues chosen for the near future, so it has been decided that the first IPAC will be the Asian event, in Kyoto in May 2010. The cycle will continue in Europe in 2011, the USA in 2012, Asia in 2013 etc, as shown. The organizational structure is still being worked out, but seems likely to be much as at present, though with a more international flavour.

In reaching this decision, the committees were mindful of the need to reduce the number of major conferences in an already busy schedule. Discussions had been going on for a number for years, but were given a timely push towards agreement by a call from ICFA and its Chairman, Albrecht Wagner, in mid 2006. With the added support of laboratory directors worldwide, we feel confident that the decision to move to a three-year cycle is right.

The way is still open for smaller regional conferences between major events – and the US seems likely to follow this route with a regional accelerator conference in New York in 2011 – but this will be for individual groups to decide.

Yours faithfully,

Stan Schriber, Chris Prior, Shin-ichi Kurokawa
on behalf of the Particle Accelerator Conferences Coordination Committee (PACCC)

3   International Linear Collider (ILC)

3.1   The ILC Engineering Design Phase – Towards the Production of an Engineering Design Report

Marc Ross, Fermilab
mail to: mcrec@fnal.gov

3.1.1   International Linear Collider Engineering Design Phase – Introduction

In August 2007, the International Linear Collider Global Design Effort (ILC GDE) published the ILC Reference Design Report (RDR) [1], which contains a description of the design of the linear collider and a "value" cost estimate. The RDR was developed over a two-year period starting in August 2005 with the creation of the GDE at the Second ILC workshop, held at Snowmass, Colorado, USA. The design described in the RDR and its associated estimate allow the GDE to plan and prioritize the next phase of the ILC, the creation of an Engineering Design and the production, by mid 2010, of an Engineering Design Report (EDR).

The EDR will contain, in addition to a more mature design and an updated value estimate, a plan for executing the ILC Project. The purpose of the EDR is to facilitate formal international negotiations at government level on siting, funding, organization and execution of the ILC project with a timescale consistent with the start of construction in 2012. The creation of the ILC Engineering Design will include:

- Basic R&D to demonstrate that all components can be engineered.
- R&D into alternative solutions to mitigate remaining risk.
- An overall design to allow machine construction to start within 3 years following its completion.
- Selection between high tech options to allow industrialization efforts.
- A comprehensive value-engineering exercise.
- A complete value cost estimate for the machine, including a funding profile consistent with the project schedule.
- A project execution plan including a realistic schedule.

- Designs for facilities shared between different "area systems", and for site-specific infrastructure. The designs must include the level of detail needed for regions to estimate the cost to host.
- All necessary information must be provided to regions to evaluate project technical and financial risks in support of a bid to host.

With the completion of the EDR, the ILC GDE leadership will be able to seek approval of the ILC Project from governmental agencies.

3.1.2 ILC Reference Design Report – Guidance for the ED Phase

The RDR "value estimate" methodology is based on experience with large multilateral international scientific projects such as the International Tokamak Experimental Reactor (ITER) and experiments at the LHC. The value of a component is defined as the lowest reasonable estimate of the procurement cost of that component. It is effectively the barest cost estimate that would be used by any of the funding agencies. Individual nation's funding agencies can then add to the base value any other items usually included in their own estimating system. Value is a particularly convenient concept for dealing with "in-kind" contributions, where project participants provide equipment rather than directly providing funds.

The RDR value estimate and the ongoing ILC R & D effort allow a quantitative assessment of the leverage that Engineering Design Phase efforts will have on the ILC Project. A good example is the R&D aimed at justifying the superconducting RF (SCRF) linac cavity design gradient choice of 31.5 MV/m. This R&D task, which involves a coordinated effort in all regions participating in the ILC work, consists of repeated processing and testing of SCRF cavities in order to demonstrate the expected yield and to prove the effectiveness of the chosen "baseline" cavity preparation procedure. In this example, a 10% reduction in the design gradient would raise the estimated cost of the ILC by about 7%. Each ongoing R&D effort can be ranked in this way resulting in a cost and risk mitigation priority assessment.

3.1.3 Towards the Production of an EDR

The GDE is now in the process of restructuring itself and making plans for the engineering design phase, leading to the completion of the ILC Engineering Design Report (EDR) in 2010. The scope of the EDR necessitates a robust management and an appropriate organization with resources sufficient to accomplish its aims. The Engineering Design phase organization must have clear lines of authority and responsibility and must effectively connect tasks with human and financial resources (often from multiple resources across the regions). This must be accomplished while maintaining a strong international collaboration in the absence, at least initially, of centralized funding.

As the RDR neared completion, a Task Force was launched to collect input from the GDE and from contributors to the RDR and to apply Project Management principles in order to propose an appropriate, functional, Work Breakdown Structure (WBS) to be used during the ED phase. The Task Force report is due in August 2007.

The Engineering Design phase organizational alignment highlights the cost drivers identified in the RDR. Production of high-technology SCRF components and Conventional Facilities and Siting (CFS) together account for 70% of the RDR value

estimate. Accordingly, each has its own branch in the top level EDR Work Breakdown Structure. The third branch is allocated to Accelerator Systems.

A fundamental management principle of the Engineering Design phase will be the containment of the RDR Value estimate. Areas of potential cost-reduction via good engineering practices have been clearly identified in the RDR. While the RDR conceptual design is sound and complete, the overall engineering design remains immature, and the ED phase will bring the application of accelerator systems engineering, industrial development investment and value engineering processes. Value Engineering is an iterative process whereby the ratio of [cost/"worth"], where "worth" is the lowest possible cost, is minimized. Similar terms are "trade studies" and "cost benefit analysis."

One of the greatest challenges of the ILC is to maintain effective communication paths between co-workers separated by great distances. A great strength of the ILC GDE collaboration is the diverse technical expertise and wide ranging laboratory infrastructure that can be applied to any given problem. This strength is often the result of years of hard work and preparation. In the ED phase, as during the period leading up to the RDR, the community will continue to rely on remote teleconferencing tools, such as the "WebEx" product. In addition, due to the need to iterate through the value engineering process and maintain a strong project management, we will also rely on multi-day, internal, topical face-to-face meetings which have a strong technical focus. These will be summarized three times per year at the Global Design Effort International Collaboration Meetings.

3.1.4 Reference

1. A link to the Reference Design Report can be found on the web: http://www.linearcollider.org/cms/?pid=1000025

3.2 Simulations of Fast-Ion Instability in the ILC Electron Damping Ring

Eun-San Kim
Mail to: eskim1@knu.ac.kr
Department of Physics, Kyungpook National University, Daegu, Korea

3.2.1 Abstract

We investigate the fast-ion instability in the ILC electron damping ring with high beam intensity and low-emittance. It is shown that the ion instability can cause beam oscillations that grow exponentially and give a significant limitation in the damping ring. We have performed a weak-strong simulation to show characteristic phenomena of the instability in the damping ring. In particular, we investigated the effects of the various different bunch filling patterns, vacuum pressures and a feedback system on the fast-ion instability. It is shown that the fast-ion instability can be cured by a bunch-bunch feedback about every 50 turns.

3.2.2   Introduction

When electron beams circulate in the ring, ions are generated by the ionization of residual gas in the ring. The ions may be trapped by the electron beams and oscillate in a certain frequency ω_i in the electric potential of the electron beam. A coherent motion between the beam and the ions may cause the beam instability [1] and then the frequency of the ion oscillation is given by

$$\omega^2_{i,x(y)} = \frac{2\lambda_e r_p c^2}{A} \frac{1}{\sigma_{x(y)}(\sigma_x + \sigma_y)} \quad , \tag{1}$$

where λ_e, r_p, A, c and $\sigma_{x(y)}$ are the averaged line charge density of the beam, the proton classical radius, the atomic number of the ion, velocity of the light and the horizontal (vertical) beam size, respectively.

The fast-ion instability can cause an exponential growth of the vertical amplitude in the beam. Then the oscillation frequency of the ions is related to beam sizes as shown in Eq. (1). The beam size at a longitudinal location is varied depending on the beta and dispersion functions in the ring. Thus, the frequency is changed from position to position and the frequency spread may act as the Landau damping in the coherent ion oscillation.

In the ILC damping ring, a bunch includes a population of about $1 \sim 2 \times 10^{10}$ to optimize or relax the beam-beam effect at the interaction point. Thus, to keep a high luminosity for a low bunch population, the bunch spacing becomes narrower. Because the fast-ion instability strongly depends on the bunch filling patterns in the ring, we investigate in detail the ion instabilities in the various filling patterns in the ILC damping ring that has a very low-emittance of 5×10^{-10} m. We also show the growth time and characteristics of the fast-ion instability in the ILC damping by using a simulation method. Table 1 shows the basic parameters of the OCS6 damping ring [2].

Table 1: Basic parameters in OCS6 damping ring.

Variable	*Value*	*Variable*	*Value*
Circumference	6695 m	Beam energy	5 GeV
Betatron tune	52.39 / 49.30	Momentum compaction	0.00042
Transverse damping time	25.6 ms	Energy spread	0.00128
RF frequency	650 MHz	Normalized emittance	5 micron

Table 2: Bunch filling patterns in the OCS6 damping ring

Variable	*Case A*	*Case B*	*Case C*	*Case D*	*Case E*
Number of bunches	5782	5658	4346	3646	2767
Bunch population	0.97×10^{10}	0.99×10^{10}	1.29×10^{10}	1.54×10^{10}	2.20×10^{10}
Number of bunch in a train	49	46	53	25	22
Bunch spacing in a train	2	2	2	3	4

3.2.3   A Simulation Model

We consider CO^+ ion as the instability source, because the major components of the residual gas are CO and H_2, and the ionization cross-section of CO is five times higher than that of H_2. We assume that the partial pressure of CO gas is $P = 3 \times 10^{-8}$ Pa. The number of ions that are generated by an electron beam with the population of N_e is given by $n_i[m^{-1}] = 0.046\ N_e P$ [Pa]. For our parameters, n_i is 27 m^{-1} for $N_e = 2 \times 10^{10}$ and $P = 3 \times 10^{-8}$ Pa.

In our simulation method, the ions are represented by macro-particles and each bunch is represented by a rigid Gaussian macro-particle. The beam sizes of the bunches are fixed and only their dipole motions are investigated. The dipole moment of each bunch is computed every turn [3]. Ions are generated at positions located by all magnetic components and drift spaces. New macro-particles for the generated ions are produced at the transverse position (x, x´, y, y´) of the beam where the ionization occurs. The beam motion and the ion motion are tracked at the positions of all magnets and drift spaces. Ionization in a long drift space is examined every 2 m. All electron beams are initially set to zero displacement.

Incoherent behavior of the ions is obtained by our simulations, but features of the beam, such as emittance growth, cannot be computed. We compute the time evolution of the growths of the dipole amplitudes of the beam, where the vertical amplitude is half of the Courant-Snyder invariant $J_y = (\gamma_y y^2 + 2\alpha_y yy´ + \beta_y y´^2)/2$, where γ_y, α_y and β_y are the Twiss parameters. The ILC damping ring has a circumference of 6.6 km and the number of trains is 61 to 123, depending on the filling patterns, in the ring. For the fast simulations, one bunch train and 1/6 section of the whole lattice are considered by our simulations. Beam-ion interaction is expressed by the Basetti-Erskine formula for the beam with a Gaussian distribution in the transverse direction [4]. Various bunch trains and ring lattices are covered by our simulation. Bunch-by-bunch feedback is also involved in the simulation. The feedback system has a damping time of 50 turns and fluctuation of 0.02 σ_y. The gain is rather conservative with the present technology.

3.2.4   Simulation Results for the Various Filling Patterns

Table 2 shows the various bunch filling patterns for the ILC damping ring. Simulations are performed to show the aspects on the fast-ion instability for the five filling patterns. The simulation provides the positions of all bunches, turn-by-turn. The horizontal and vertical maximum amplitudes in the all bunches, $J_{x,y}$, are obtained turn-by-turn in the simulation. Figure 1 shows the evolution of the vertical maximum values J_y for the five filling patterns in Table 2 in a vacuum pressure of 0.23 nTorr without (top) and with (bottom) the bunch-by-bunch feedback per 50 turns, respectively. It is shown that the maximum amplitudes are saturated for all the filling patterns when the feedback is off. It is shown that the Case C (green line) gives the fastest exponential growth time, as shown in analytical estimation. It is also shown that vertical maximum amplitudes can be well suppressed by the feedback per 50 turns for all the filling patterns.

Figure 2 shows the effects of the vacuum pressures on the fast-ion instability. Top and bottom in Figure 2 show evolutions of the maximum values of J_y and exponential growth times for the different vacuum pressures when the feedback is off in Case A, respectively. Figure 3 (top) shows evolution of the maximum values of J_y in all bunches for the different turns of feedback in Case A. It is shown that feedback per 50 turns

provides a sufficient damping. Figure 3 (bottom) shows evolution of the maximum values of J_y in all bunches for the different bunch intensities in case A with the feedback per 50 turns. It is shown that vertical amplitude in bunch intensity larger than 2×10^{10} is not well suppressed by the feedback.

3.2.5   Summary

We have investigated the simulation studies on the fast-ion instability in the ILC electron damping ring. By using a weak-strong simulation method, we showed aspects of fast-ion instabilities for various bunch filling patterns in the ring. The simulation results also showed bunch-by-bunch feedback of about 50 turns is required to cure the fast-ion instability in the damping ring.

3.2.6   References

1. T.O. Raubenheimer and F. Zimmermann, Phys. Rev. E 52 p. 5487 (1995).
2. Reference Design Report for ILC, ILC 2007-01 (2007).
3. K. Ohmi, Phys. Rev. E 55, p. 7550 (1997).
4. M. Bassetti and G. Erskine, CERN Report No. ISR TH/80-06 (1980).
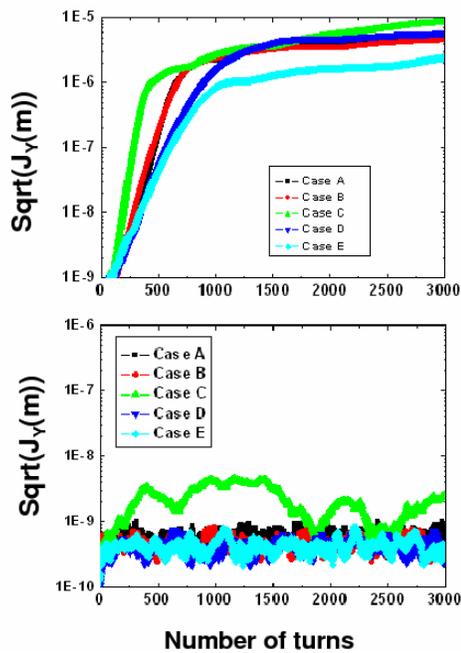
Figure 1: Vertical amplitudes without feedback (top) and with feedback (bottom) per 50 turns.
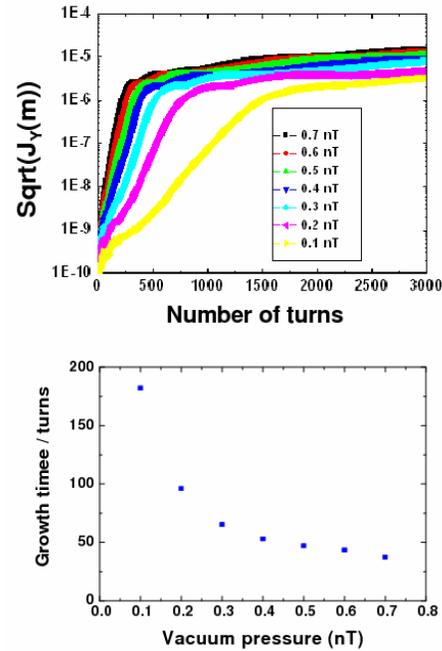
Figure 2: Vertical amplitudes and growth times v. different vacuum pressures for case A.
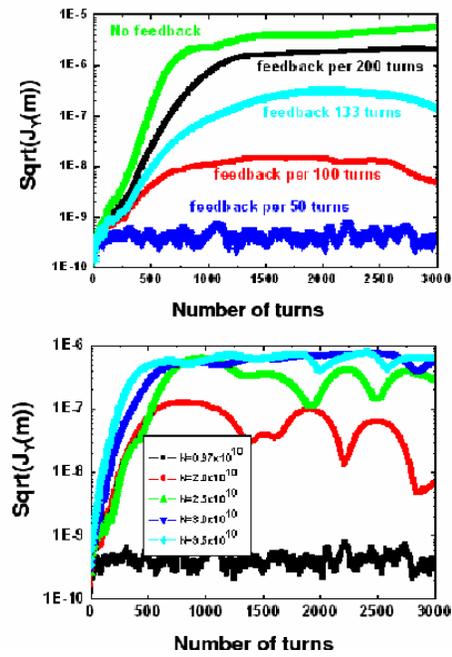
Figure 3: Vertical amplitudes with different number of feedback (top) and different currents (bottom).

4   Theme Section: FFAG Accelerators

4.1   An Introduction to FFAG Accelerators and Storage Rings

M.K. Craddock

Mail to: craddock@triumf.ca

Department of Physics and Astronomy, University of British Columbia, and
TRIUMF, 4004 Wesbrook Mall, Vancouver, B.C. V6T 2A3, Canada

Fixed Field Alternating Gradient accelerators (FFAGs) offer higher pulse repetition rates and acceptances than synchrotrons – and therefore much higher beam intensities. With a fixed magnetic field the rep rate is set by purely rf considerations, and can be several kHz, while the radially extended spiral orbit and high momentum compaction lead to large radial and momentum acceptances – at the cost of somewhat wider vacuum chambers, magnets and rf cavities. With fixed magnetic fields, modulated rf, and pulsed beams, FFAGs operate just like synchrocyclotrons, but are capable of reaching tens of GeV. The innovations were to break the magnet into radial or spiral sectors to provide edge and strong focusing, and (usually) to remove the central region – the same steps that convert a classic Lawrence cyclotron into a separated-sector isochronous ring cyclotron. The FFAG is the most general type of fixed-field accelerator (cyclotron).

Table 1: Fixed magnetic field accelerators – the cyclotron family.

Magnetic field - azimuthal variation	Fixed frequency (CW beam)	Frequency-modulated (Pulsed beam)
Uniform	Lawrence cyclotron	Synchrocyclotron
Periodic	Isochronous cyclotron	FFAG

Following the discovery of alternating gradient (AG) focusing in 1952, FFAGs were proposed independently by Ohkawa [1] in Japan, Kolomensky *et al.* [2] in the USSR and Symon and Kerst [3] in the US. The most intensive studies were carried out by Symon, Kerst *et al.* at MURA (the Mid-western Universities Research Association) in Wisconsin in the 1950s and 60s, and culminated in the construction and successful testing of electron models of radial-sector and spiral-sector designs [4] (Figure 1). But proposals for proton FFAGs were not funded at that time, nor were those for 1.5 GeV spallation neutron sources by the Argonne [5] and Jülich [6] laboratories in the 1980s.
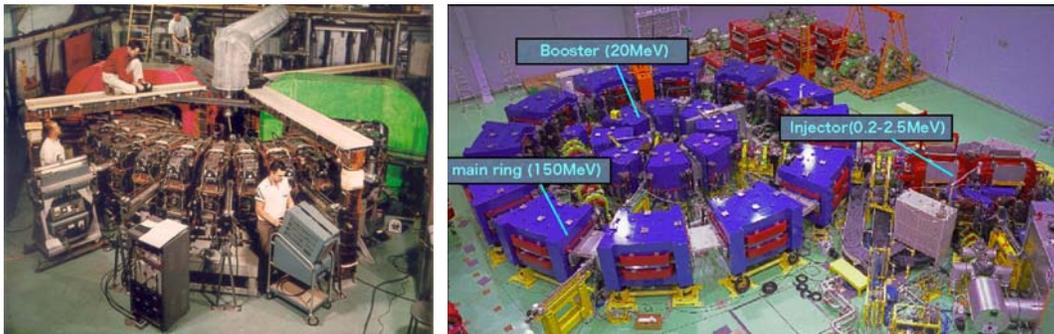
Figure 1: Scaling FFAGs. (Left): 50-MeV electron model at MURA in 1961. (Right): The three proton rings for ADSR studies at Kyoto University Research Reactor Institute in 2006.

In recent years, with improvements in magnet and rf design technology, FFAGs have become the focus of renewed attention. Four proton machines have now been built, and two more, plus three for electrons, and a muon/alpha cooling ring, are under construction. In addition, more than 20 designs are under study for the acceleration of protons, heavy ions, electrons and muons, with applications as diverse as treating cancer, irradiating materials, driving subcritical reactors, boosting high-energy proton intensity, and producing neutrinos. Moreover, it has become apparent that FFAG designs need not be restricted to the 'scaling' approach explored in the 1950s. Dropping this restriction has revealed a range of interesting new design possibilities, which have been explored in a series of FFAG Workshops since 1999 [e.g.7-11].

4.1.1 Scaling FFAGs

Resonance crossing was a big worry in the early days of AG focusing, because of the low energy-gain/turn. The *scaling* principle was therefore adopted, whereby the orbit shape, optics and tunes are kept the same at all energies. To first order the latter are given by:

$$v_r^2 \approx 1 + k \tag{1}$$

$$v_z^2 \approx -k + F(1 + 2\tan^2 \varsigma) \tag{2}$$

where the average field index $k(r) \equiv r\,(dB_{av}/dr)/B_{av}$, the azimuthally averaged field at radius r, $B_{av} \equiv \langle B(\theta) \rangle$, the magnetic flutter $F \equiv \langle (B(\theta)/B_{av} - 1)^2 \rangle$, and the spiral angle is ζ. Clearly, <u>constant v_r requires constant k</u>, implying a magnetic field profile $B_{av} = B_0(r/r_0)^k$ and a momentum profile $p = p_0(r/r_0)^{k+1}$. Consequently, constant <u>v_z requires constant $F(1 + 2\tan^2\zeta)$</u> - a quantity that must also be given a high value, since usually $k \gg 1$ to minimize the radial aperture. MURA's recipe was to keep the <u>flutter $F(r)$ = constant</u>, by using constant profile $B(\theta)/B_{av}$ and:
   - for spiral sectors: <u>constant ζ</u>, so the sector axis is a logarithmic spiral $R = R_0 e^{\theta \cot \zeta}$;
   - for radial sectors: boosting F by specifying <u>$B_D = -B_F$</u>.
Of course, reverse fields raise the average radius. The 'circumference factor' R/ρ = 4.5 if there are no straights [3], but is smaller with them (1.8 for the KEK 150 MeV ring).

4.1.1.1 FFAGs operating or under construction

Recent years have seen the construction and successful operation of the first-ever FFAGs for protons (with energies of 1 MeV [12] and 150 MeV [13]) by Mori's group at KEK, and the initiation of several more (Table 2). All follow scaling principles and all but one (with spiral sectors) employ radial-sector triplet magnets.

The KEK machines introduced important innovations in both magnet and rf design. The DFD triplets are built and powered as single units, without a steel return yoke, forcing the return flux through the Ds and automatically providing reverse field. The open structure also facilitates injection and extraction. The rf innovation (avoiding the cumbersome rotary capacitors on synchrocyclotrons) was to use Finemet metallic alloy tuners, which offer (a) rf modulation (with a 1.5-4.6 MHz sweep) at 250 Hz or more, and so high rep rates; (b) high permeability, and so short cavities with high effective fields; (c) low Q ($\approx$1), allowing broadband operation without any need for active tuning.

A 150/200 MeV FFAG of similar design is being installed at the Kyoto University reactor, together with injector and booster FFAGs [14] (Figure 1 (right)). This will

eventually provide 100-μA beams to test Accelerator-Driven Sub-critical Reactor (ADSR) operation. The Kyoto group is also building a proton FFAG ionization cooling ring ERIT (Emittance–Energy Recovery Internal Target) [15] as a neutron source for boron neutron-capture therapy. This uses FDF rather than DFD triplets.

Table 2: Scaling FFAGs operating or under construction.

	Ion	E (MeV)	Cells	Spiral angle	Radius (m)	First Beam	Comments
KEK-PoP	p	1	8	0°	0.8-1.1	2000	
KEK	p	150	12	0°	4.5-5.2	2003	100 Hz, 90% extraction
KURRI -ADSR	p	2.5	8	40°	0.6-1.0	2006	Initial spec^n: 120 Hz, 1 μA Later: 1kHz, 100μA, 200 MeV
	p	20	8	0°	1.4-1.7	2006	
	p	150	12	0°	4.5-5.1	(2007)	
NEDO-ERIT	p	11	8	0°	2.35	(2007)	70 mA ionization cooling ring
PRISM study	α	0.8	6	0°	3.3	(2008)	Phase space rotator
Radiatron	e	5	12	0°	0.3-0.7	(2008)	24 kW, 10 kHz, betatron acc^n.

FFAGs are of interest for muons too. PRISM (Phase-Rotated Intense Slow Muon source), based on a 10-cell DFD radial-sector FFAG of 6.5 m radius, is under construction at RCNP Osaka for eventual installation at J-PARC (Kuno *et al*. [16]). It will collect muon bunches at 68 MeV/c and rotate them in phase space, reducing the momentum spread from ±30% to ±3%. With a repetition rate of 100-1000 Hz the intensity will be high enough to allow ultra-sensitive studies of rare muon decays. The first six magnets will initially form an α–particle test ring to demonstrate the principle.

Finally, RadiaBeam Technologies is building "Radiatron", a compact 5-MeV high-power electron FFAG for medical and industrial applications [17]. Like ERIT, this uses FDF triplets, but employs a betatron core to accelerate by induction rather than by rf.

4.1.1.2   Scaling FFAG studies

In addition, more than a dozen different scaling FFAG designs have been published (Table 3), mostly in Japan, but also in France (RACCAM [21]) and the USA (μ cooling ring [23]). These range from a fist-sized 1-MeV prototype for electron irradiation [18], to medium-sized sources for proton and ion therapy (for which the high pulse repetition rates are clinically advantageous), to the 200-m diameter 20-GeV muon ring proposed for a neutrino factory. Both spiral- and radial-sector designs are employed, the latter all using DFD triplet cells. The proposals include some "hybrid FFAG/synchrotron" designs by MElCo (Mitsubishi Electric Co.) [18], where a limited field rise is permitted.

The KEK/Kyoto group's most ambitious plan is to build a neutrino factory [24] at J-PARC based on a chain of four FFAGs accelerating muons from 0.3 to 20 GeV. The largest would have a radius of 200 m (with a total orbit spread of 50 cm) and consist of 120 cells, each containing a superconducting DFD triplet. Most cells would also contain rf cavities to provide an overall energy gain of around 1 GeV per turn, restricting the losses through muon decay to 50% overall. The use of low-frequency rf (24 MHz) keeps the buckets wide enough to contain the phase drift occurring as the orbit expands. A major advantage of FFAGs over linacs - either single or recirculating - is that their large acceptances in *r* and *p* obviate the need for muon cooling or phase rotation. There are also significant cost savings on the accelerators themselves.

Table 3: Scaling FFAGs – design studies.

Accelerator	Ion	Energy (MeV/u)	Cells	Spiral angle	Radius (m)	Rep rate (Hz)	Comments
MElCo Laptop [18]	e	1	5	35°	0.023-0.028	1,000	Hybrid, Magnet built
eFFAG [19]	e	10	8	47°	0.26-1.0	5,000	20-100 mA
Ibaraki Med. Acc.[20]	p	230	8	50°	2.2-4.1	20	0.1 μA
LPSC RACCAM [21]	p	180	10	50°	3.2-3.9	>20	Proton therapy
MElCo p Therapy[18]	p	230	3	0°	0-0.7	2,000	SC, quasi-isochronous
MElCo	C^{6+}	400	16	64°	7.0-7.5	0.5	Hybrid
C Therapy[18]	C^{4+}	7	8	0°	1.35-1.8	0.5	FFAG/synchrotrons
NIRS Chiba [22]	C^{6+}	400	12	0°	10.1-10.8	200	Compact
Ion Therapy	"	100	12	0°	5.9-6.7	"	radial-sector
Accelerators	C^{4+}	7	10	0°	2.1-2.9	"	designs
PRISM [16]	μ	20	10	0°	6.5		Phase-space rotator
Mu Cooling Ring[23]	μ	160	12	0°	0.95±0.08		Gas-filled
J-PARC	μ	20,000	120	0°	200		Δr = 0.5 m
Neutrino	"	10,000	64	0°	90		≈10 turns
Factory	"	3,000	32	0°	30		SC magnets
Accelerators[24]	"	1,000	16	0°	10		Broadband rf

4.1.2 Linear non-scaling FFAGs (LNS-FFAGs)

In a study of FFAG arcs for recirculating muon linacs in 1997, Mills and Johnstone [25] noted that the rapid acceleration (<20 turns) essential for muons allows betatron resonances no time to damage beam quality, and so scaling can be abandoned, the tunes allowed to vary, and a wider variety of lattices explored. Moreover, using constant-gradient *"linear"* magnets greatly increases dynamic aperture and simplifies construction, while employing the strongest possible gradients minimizes the real aperture. Johnstone *et al*. [26] applied this ***non-scaling*** approach to a complete FFAG ring, showing that it would be advantageous to use superconducting magnets with positively bending Ds and negatively bending Fs; *i.e.* both B_D and $|B_F|$ decrease outwards (Figure 2). The radial orbit spread would be reduced (allowing the use of smaller vacuum chambers and magnets), and the orbit circumference $C(p)$ shortened and made to pass through a minimum instead of rising monotonically as $p^{1/(k+1)}$ (Figure 3 (left)). The variation in orbit period is thereby reduced, allowing the use of high-Q fixed-frequency rf.
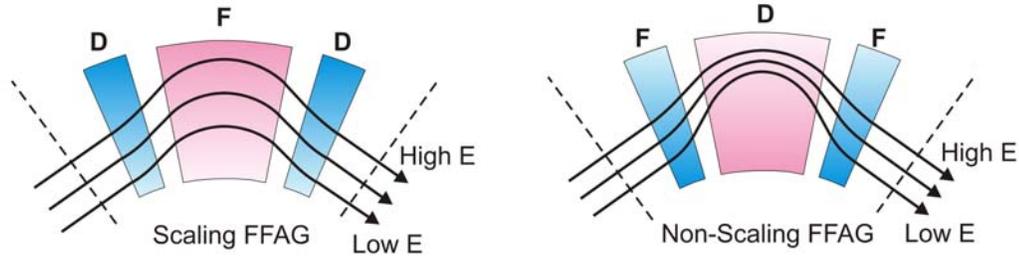
Figure 2: Scaling and non-scaling FFAG magnetic fields and orbit patterns. Positive-bending fields are shown in pink, negative in blue, with the colour density indicating the field strength. Note that FDF scaling and DFD non-scaling lattices are also possible.

$C(p)$'s parabolic variation and its parametric dependence can be derived using a simple model [27], treating the F and D magnets as thin lenses of equal strength q (gradient × length). For symmetric F0D0 or triplet cells, and assuming $q_F = q_D \equiv q$:

$$C(p) = C(p_m) + \frac{12\pi^2}{e^2 q^2 N L_{FD}} (p - p_m)^2 \qquad (3)$$

where N is the number of cells, and L_{FD} is the (shorter) F-D spacing. The minimum is at $p_m = (4p_c + eqL_{FD})/6$ where the p_c closed orbit is such that $B_F = 0$. The orbit radii $r(p)$ show similar dependence, with distinct p_{min}.

Lattices along these lines were developed [7-9] by Johnstone at Fermilab, by Berg, Courant, Trbojevic and Palmer at Brookhaven, by Keil at CERN and Sessler at LBNL, and by Koscielniak at TRIUMF. Results from a cost-optimization study of muon acceleration from 2.5-20 GeV by Berg et al. [9] favoured a chain of three rings using doublet cells with SC magnets and high-field 200 MHz SC cavities. Their top energies would be 5, 10 and 20 GeV, with circumferences of 246, 322 and 426 m, and 64, 77 and 91 cells respectively. The smallest would be similar in price to a linac, but those above 10 GeV less costly.
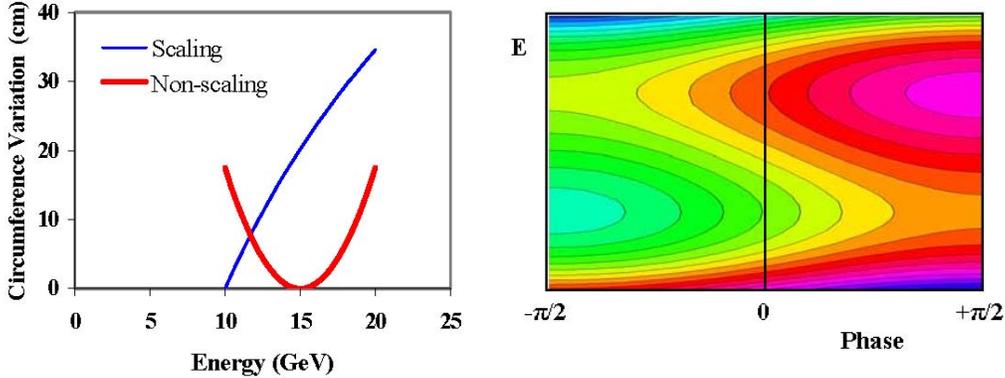
Figure 3: Linear non-scaling FFAGs. (Left): Circumference variation with energy. (Right): Acceleration path (yellow) in longitudinal phase space.

With the orbit length varying by only 20 cm, first falling and then rising, Berg [28] and Koscielniak [29] have shown that, provided a critical rf voltage is exceeded, an acceleration path can be created (Fig. 3 (right)) that stays close to the voltage peak (crossing it three times), snaking between neighbouring buckets (rather than circulating inside them) just as in an imperfectly isochronous cyclotron [30]. By using high-field superconducting 200-MHz cavities it should be possible to accelerate from 10 to 20 GeV in 17 turns, with a decay loss of 8% (25% in the three rings).

In order to demonstrate the novel features of such a design - particularly "serpentine" or "gutter" acceleration outside buckets, and the crossing of many integer and half-integer resonances (*cf.* Figure 4 (left)) - the construction of a 10-20 MeV electron model (EMMA, with $C = 16.6$ m and 42 doublet cells) [31] is under way at Daresbury, where the 8-35 MeV Energy Recovery Linac Prototype (ERLP) will act as injector.

In an effort to reduce the number of FFAG stages for muons from three to two, Trbojevic [32] has proposed an oval "racetrack" lattice, with two small-radius 90° arcs, where the magnets are close-packed, and two large-radius ones, with straights to accom-

modate the rf and other equipment. The betatron and dispersion functions are matched
at the central energy. The momentum range per stage is increased from ±33% to ±40%,
allowing two stages to span the range 3.67-20 GeV – assuming that the accelerating
gradient can be raised from 10 to 17 MeV/m. On similar principles, he and colleagues
[33] propose an electron FFAG ring composed of six small- and six large-radius arcs for
e-RHIC, to fit within the existing tunnel.

4.1.2.1   LNS-FFAGs for protons and ions

Using non-scaling FFAGs to accelerate protons or ions that are not fully relativistic
introduces two complications: first, the orbit time may vary over a wide enough range
that fixed-frequency operation is not possible; and second, cost considerations may
favour a lower energy gain per turn and longer acceleration time, so that resonance
crossing is more of a concern.

Keil, Trbojevic and Sessler [34] have proposed a system of three concentric LNS-
FFAGs for cancer therapy. Each is composed of 48 doublet cells, the largest ring having
C = 52 m. The smaller pair would accelerate protons to 250 MeV and the larger pair C^{6+}
ions to 400 MeV/u. FM operation is envisaged, with pulse rates up to ~500 Hz. As in
the muon machines, the tune per cell drops from ~0.4 to ~0.15 during acceleration, but
quite modest rf voltages (≤220 kV at ~20 MHz) are sufficient to retain good beam
quality while crossing more than a dozen integer and half-integer imperfection reson-
ances (the design avoids all intrinsic resonances below 3rd order). They also propose a
lightweight LNS-FFAG gantry [35], composed of 28 superconducting triplets, capable
of accepting the whole extracted momentum range at fixed field.

Also for cancer therapy, Johnstone and Koscielniak [36] propose a single-stage
LNS-FFAG (with 14 F0D0 cells and C = 40 m) accelerating carbon ions from
18 MeV/u to 400 MeV/u (and protons too). Their design introduces a powerful new
feature: the magnets are wedge-shaped, with opening angles chosen so that the edge
focusing compensates the other sources, minimizing the variation in tunes (Figure 4
(right)). The dynamic aperture at injection is 10-20π μm.
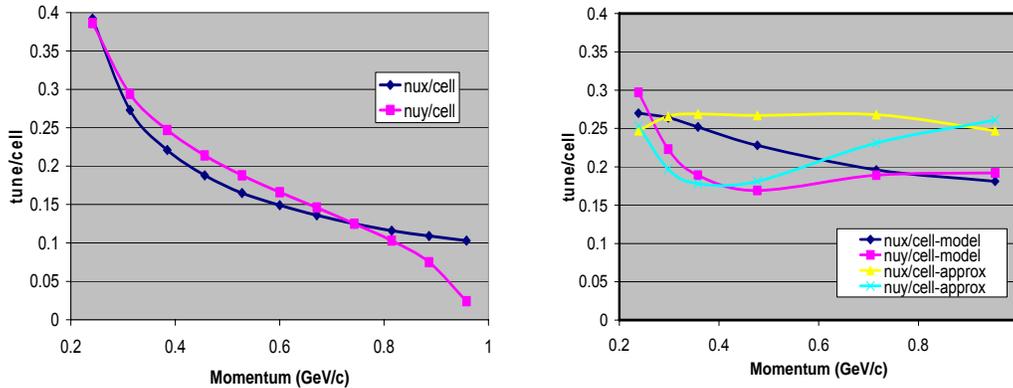
Figure 4: Dependence of cell tunes on momentum in LNS-FFAGs: (left) conventional design
for rapid, or muon, acceleration; (right) tune-stabilized for medical therapy [36]. In the legend,
approx refers to an analytic solution, model to one obtained using MAD.

A further study of an LNS-FFAG for hadron therapy (PAMELA), associated with
the EMMA project mentioned above, has been funded in the UK [37]. Its aims are to
find an optimal scheme for a 450-MeV/u carbon machine, together with designs for the

magnets and rf system and a preliminary cost estimate, then to scale it down to 70-MeV and 230-MeV proton machines as possible prototypes.

LNS-FFAGs have also been considered by Ruggiero *et al*. [38] for higher energy proton and heavy-ion drivers. For a 10-MW proton source they propose a 50-250 MeV ring followed by a 250-1000 MeV one, both with $C = 204$ m and 80 FDF cells. The frequency swing during acceleration could be accommodated by using either broadband (Finemet) cavities at a few MHz (1-kHz pulse rate), or the harmonic number jump (HNJ) technique [39] with 804-MHz cavities (either 10 kHz or cw). To ensure regular integer jumps per turn in the HNJ case, the accelerating field must change with energy (i.e. vary across the aperture). This would be achieved by grouping cavities operating in different TM modes together. An FFAG upgrade to the AGS Booster is also being considered, and one octant of a 0.2-0.8 MeV electron model (MINHA, $C = 18$ m, $N = 48$) for that is scheduled for construction 2007-8.

The heavy-ion driver for radioactive-ion production is to deliver 4.2 particle-μA of ^{238}U ions at 400 MeV/u. It would also use two rings with $C = 204$ m and 80 FDF cells (though with different field strengths), the first stage accelerating from 15-80 MeV/u. The same acceleration options and pulse rates are suggested as for protons.

4.1.3   Non-Linear Non-Scaling FFAGs

Rees [40] has designed several NS-FFAGs using non-linear field profiles and slightly more complicated dFDFd cells (termed pumplets from the Welsh word for five, pump - pronounced pimp), where the d/Ds are parallel-edged and the Fs wedge-shaped. The extra parameters provide greater control over the beta-functions and dispersion, enabling the vertical tune to be kept almost constant and, for highly relativistic particles, the orbits made exactly isochronous. Moreover, pumplet insertions can be incorporated, well-matched to the arcs - a notoriously difficult feat in an FFAG. Their long drifts allow the use of more efficient multi-cell rf cavities, shortening the circumference. For a 4-MW proton driver, he has proposed a 50-Hz 10-GeV FFAG ($C = 624$ m with 2 super-periods of 34 cells each) injected by a 3-GeV RCS. A more recent 10-MW proposal employs two 0.8-3.2 GeV FFAGs in parallel ($C \approx 439$ m with 36 identical cells).

To accelerate muons, Rees uses just two FFAGs, the first from 3.2-8 GeV, the second from 8-20 GeV ($C = 920$ m with 4 superperiods of 30 cells each), both rings being isochronous - a muon cyclotron! Although isochronous cyclotron designs in this energy range have been reported before [41], they have relied on spiral-edge focusing to counteract the high k values. What is remarkable here is that spiral is not needed. Méot *et al*. [40] have carried out tracking studies using realistic magnetic fields.

The exploration of non-scaling lattices is in its early days, but the initial efforts have already yielded some remarkable results. Who knows, maybe there are yet more varieties of FFAG waiting to be discovered?

4.1.4   Acknowledgements

4.1.5   References

1. T. Ohkawa, Bull. Phys. Soc. Jpn. (1953).
2. A.A. Kolomensky, V.A. Petukhov, M.S. Rabinovich, Lebedev Ph. I. Rpt. (1953).
3. K.R. Symon, Phys. Rev. **98**, 1152 (1955); D.W. Kerst *et al.*, *ibid*. 1153; K.R. Symon *et al.*, Phys. Rev. **103**, 1837 (1956).
4. K.R. Symon, PAC'03, 452 (2003); F.T. Cole, Cyclotrons'01, Suppl. (2001).
5. T.K. Khoe, R.L. Kustom, PAC'83, IEEE Trans. **NS-30**, 2086 (1983).
6. P.F. Meads, G. Wüstefeld, PAC'85, IEEE Trans. **NS-32**, 2697 (1985)
7. FFAG 2003 Workshop, BNL, http://www.cap.bnl.gov/mumu/conf/ffag-031013/
8. FFAG 2004 Workshop, TRIUMF, http://www.triumf.ca/ffag2004/programme.html
9. Proc. FFAG04 Workshop, KEK (2004); http://hadron.kek.jp/FFAG/FFAG04_HP/
10. FFAG05 Workshop, KEK, (2004); http://hadron.kek.jp/FFAG/FFAG05_HP/
11. FFAG 2007 Workshop, LPSC Grenoble, http://lpsc.in2p3.fr/congres/FFAG07
12. M. Aiba, Y. Mori *et al.*, EPAC'00, 299 (2000).
13. S. Machida *et al.*, PAC'03, 3452 (2003); M. Aiba *et al.*, EPAC'06, 1672 (2006).
14. M. Tanigaki, M. Inoue, Y. Mori *et al.*, EPAC'06, 2367 (2006).
15. K. Okabe, M. Muto, Y. Mori, EPAC'06, 1675 (2006).
16. A. Sato, Y.Kuno *et al.*, EPAC'06, 2508 (2006).
17. S. Boucher, R. Agustsson *et al.*, PAC'07, THPMS018 (2007).
18. H. Tanaka, in [9]; H. Tanaka, T. Nakanishi, Cyc'04, 238 (2004).
19. Y. Yuasa, *WG3 Summary*, in [9].
20. T. Yokoi, *WG3 Summary*, in [9].
21. J. Pasternak, J. Fourrier *et al.*, PAC'07, THPAN008 (2007).
22. T. Misu, Y. Iwata *et al.*, Phys. Rev. ST AB **7**, 094701 (2004).
23. A. Garren, H. Kirk, S. Kahn, in [8]; H. Kirk *et al.*, PAC'03, 2008 (2003).
24. Y. Mori, EPAC'02, 278 (2002); S. Machida, NIMPR, **A503**, 41 (2003).
25. F. Mills, Proc. 4th Int. Conf. Physics Potential and Development of μ^+ μ^- Colliders, San Francisco, 1997, 693-696; C. Johnstone, *ibid.*, 696-698 (1998).
26. C. Johnstone, W. Wan, A. Garren, PAC'99, 3068.
27. M.K. Craddock, in [7]; S. Koscielniak, M.K. Craddock, EPAC'04, 1138 (2004).
28. J.S. Berg, Proc. Snowmass 2001, T503 (2001); J.S. Berg, PAC'05, 1532 (2005).
29. S. Koscielniak, C. Johnstone, Proc. Snowmass 2001, T508 (2001); S. Koscielniak, C. Johnstone, N.I.M. **A523**, 25 (2004).
30. M.K. Craddock, C.J. Kost, J.R. Richardson, IEEE Trans. **NS-26**, 2065 (1979).
31. R. Edgecock, PAC'07, THOABOB01 (2007).
32. D. Trbojevic, PAC'07, THPMS093 (2007).
33. D. Trbojevic, R.C. Gupta *et al.*, PAC'07, THPMS094 (2007).
34. E. Keil, A.M. Sessler, D. Trbojevic, Phys. Rev. ST AB, **10**, 054701 (2007).
35. D. Trbojevic, B. Parker, E. Keil, A.M. Sessler, *ibid.* **10**, 053503 (2007).
36. C. Johnstone, S.R. Koscielniak, PAC'07, THPMN103 (2007).
37. K. Peach, J. Cobb *et al.*, PAC'07, THPMN076 (2007).
38. A.G. Ruggiero in [11]; A.G. Ruggiero *et al.*, PAC'07, THPAS104 (2007).
39. A.G. Ruggiero, Phys. Rev. ST AB, **9**, 100101 (2006).
40. G.H. Rees in [9-11]; F. Lemuet, F. Méot, G. Rees, PAC'05, 2693 (2005).
41. J. I. M. Botman *et al.*, PAC'83, IEEE Trans. **NS-30**, 2007 (1983).

4.2   Scaling FFAG Accelerators

Yoshiharu Mori
Mail to: mori@KL.rri.kyoto-u.ac.jp
Kyoto University, Research Reactor Institute, Osaka, Japan

Masamitsu Aiba
Mail to: Masamitsu.Aiba@cern.ch
CERN, Geneva, Switzerland

4.2.1   Introduction

Until recently, the FFAG (Fixed Field Alternating Gradient) accelerator meant an accelerator with a static magnetic field and zero chromaticity beam optics. Thus, the magnetic field had to be nonlinear. However, a linear lattice configuration can be adopted and the constraint of zero chromaticity may be broken, if very rapid acceleration is possible and betatron resonances can be crossed quickly. Thus, nowadays, an FFAG accelerator which satisfies the zero chromaticity beam optics is called "Scaling" and the other "Non-scaling". The scaling FFAG is based on a nonlinear magnetic field to meet the requirement for zero chromaticity beam optics. Thus, in the transverse direction, the beam behaviour is more or less nonlinear. On the other hand, since the momentum compaction factor of the scaling type of FFAG does not depend on the beam momentum, the longitudinal beam motion becomes quite linear at high energy. In the non-scaling FFAG, a linear magnetic field in transverse beam optics is exploited. Betatron resonance crossing is, therefore, inevitable. Moreover, the longitudinal beam dynamics is strongly nonlinear.

The scaling type of FFAG accelerator has unique features compared with other types of accelerator. The features of the scaling type of FFAG accelerator can be summarized by the following distinctive characteristics:

- Strong focusing: The FFAG accelerator has strong focusing characteristics in the beam optics in all directions: Alternating gradient (AG) focusing in the transverse direction and phase focusing with rf acceleration in the longitudinal direction.
- Moving orbit: The magnetic field in the FFAG accelerator is static; therefore, the beam orbits move during acceleration. This is like a cyclotron but not as pronounced because the magnetic field gradient is fairly large.
- Zero chromaticity: Because of the strong focusing behaviour as described above, a betatron resonance is a harmful problem in the beam optics. To avoid resonance crossing which leads to beam loss, the betatron tunes should remain constant during acceleration.

Various advantages exist in FFAG accelerators compared with other accelerators such as cyclotron and synchrotron. Since the magnetic field is static, there is no need to synchronize the RF pattern with the magnetic field. This results in a high repetition rate for the beam acceleration with a modest number of particles in the ring. Thus, high average beam current becomes available because space charge and collective effects are below threshold. Very large acceptances for horizontal and longitudinal directions are

also possible for the FFAG. A typical value of the horizontal acceptance is 10,000 π mm.mrad and the momentum acceptance becomes some tens of percent.

High beam current allows a new type of proton or electron driver. Fast acceleration and large acceptance may open the door for acceleration of short-lived particles such as muons, unstable nuclei, etc. A neutrino factory based on a muon accelerator and storage ring has been seriously discussed recently, and the FFAG accelerator is conceived as a most promising way for muon acceleration up to several tens of GeV.

The idea of the FFAG accelerator was originally conceived by Ohkawa in 1953 [1]. The first electron model of an FFAG was developed by Kerst, Cole and Symon in the MURA accelerator project in the late 1950s and several electron models were constructed in the early 1960s [2]. However, since then no proton and practical FFAG accelerator has been built until recently, mainly because of technical difficulties.

One of the technical problems was its complicated magnetic field configuration. The magnetic field is totally nonlinear to meet the optical constraints such as zero chromaticity adequately. The magnet design must, therefore, be accomplished with 3D magnetic field calculation. This problem has been overcome by 3D field simulation codes such as TOSCA-OPERA with recent fast computers.
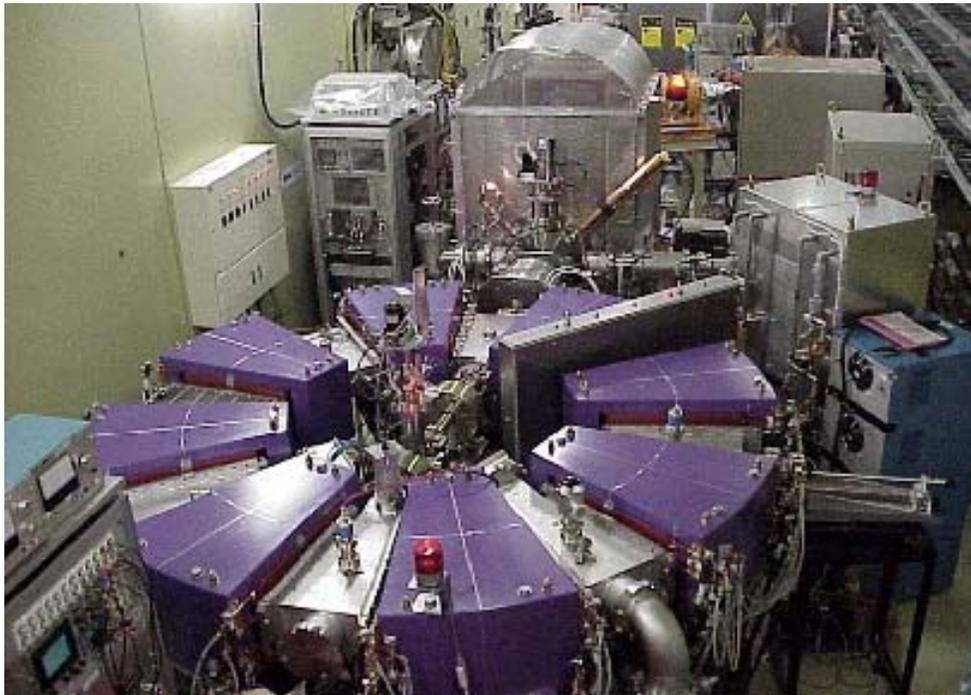
Figure 1: POP-FFAG accelerator.

The other difficulty was rf acceleration. In the electron models at the MURA project, the beam acceleration was mostly with induction and/or a fixed frequency system. In order to accelerate heavy particles such as protons, a variable frequency rf system is essential. Moreover, since room for the rf acceleration system in the ring of an FFAG accelerator is normally limited because of its compactness and high super-periodicity, a rather high rf field gradient is necessary. These requirements are difficult for an ordinary tuned rf cavity like a ferrite-loaded cavity, which is commonly used in a proton synchrotron. For a proton FFAG accelerator, a broad band and high gradient rf

cavity is required. A new type of rf cavity developed at KEK in Japan [3] made it possible to overcome this problem. This type of rf cavity uses a high permeability magnetic alloy (MA) such as FINEMET. The rf characteristics and performance of MA have proved suitable for use in rf cavities in a FFAG proton accelerator.

4.2.2 Development of Proton POP-FFAG Accelerator

In 1999, the world's first proton FFAG accelerator was demonstrated at KEK [4, 5]. Named POP-FFAG, it is shown in Figure 1. The POP-FFAG accelerates protons from 50 keV to 500 keV within 1 msec. Following this success, it has been recognized that FFAG accelerators have advantages in rapid acceleration with large momentum acceptance, which are needed both for muon accelerators and for high power proton drivers. Since then, intensive studies and discussions have been undertaken and various novel ideas have emerged. Research and development of FFAG accelerators for many applications are also in progress at many institutes.

In scaling FFAG accelerators like POP-FFAG, each beam orbit for different beam momenta has similarity in shape (curvature), and zero chromaticity in the beam optics is realized. Thus, the betatron tunes for both horizontal and vertical directions are constant during beam acceleration avoiding any problems from resonance crossing. In cylindrical coordinates, it can be shown analytically that the configuration of the magnetic field at the median plane can be expressed by the following equation [6]:

$$B(r,\theta) = B_0 \left(\frac{r}{r_0} \right)^k f\left(\theta - \varsigma \ln \frac{r}{r_0} \right) \tag{1}$$

where $\varsigma = \tan\xi$, and ξ is a spiral angle of the magnet in the azimuth plane. Accordingly, two schemes for beam focusing are invoked by this magnetic field configuration: one is radial sector focusing and the other spiral sector focusing. Radial sector focusing uses a combination of positive and negative bending magnets to create strong beam focusing with a FODO lattice configuration. In spiral sector focusing, edge focusing is used efficiently. For the POP-FFAG, a radial focusing DFD lattice was adopted. In order to design the beam optics for the POP-FFAG, we applied a linearised model [7] as the first step, which was verified by particle tracking for the hard edge magnet configuration.

One of the difficulties of designing the optics in the real FFAG machine is how to treat the effect of the fringing field of each magnet. In the FFAG accelerator, either for radial sector or spiral sector designs, the beam focusing includes the edge focusing in its structure. Therefore, careful consideration and designing for the effects of the fringing fields become very important and in practice 3D field calculations and beam tracking simulations are essential, although they are the most time consuming part of the design. Various 3D field simulation codes are available; we have been using TOSCA-OPERA.

The results of the 3D field calculation with TOSCA-OPERA for the POP-FFAG are shown in Figure 2 with blue open squares. The difference from the no-fringe hard edge model is obvious. The measured betatron tunes in the POP-FFAG are shown in the figure with red open circles. The agreement between the measurement and the design based on 3D field simulation is very impressive.

The scaling type of FFAG accelerator has a large acceptance both in transverse and longitudinal directions. In the transverse direction, especially in the horizontal direction,
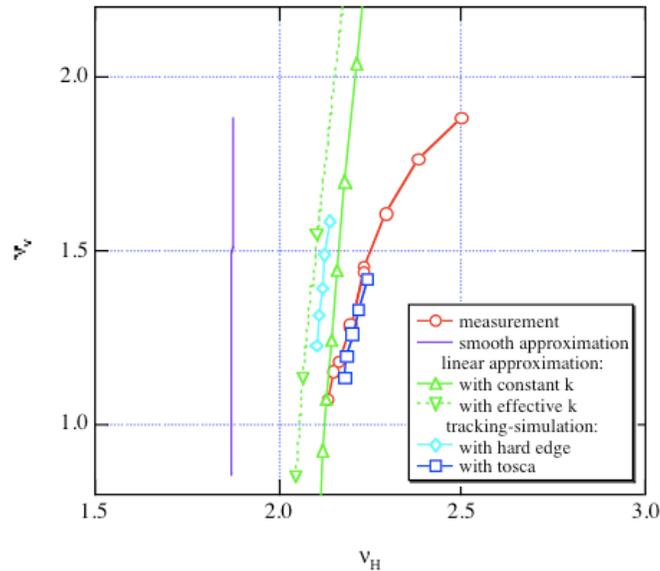
Figure 2: Tune diagram of the POP-FFAG for different operating conditions. The red open circles and the blue squares show the measured values and the beam tracking results with the TOSCA-OPERA field simulation, respectively.

the physical aperture must be large because the beam orbit should move as a function of the beam momentum. Nonlinear magnetic field components are inevitable in the scaling type of FFAG accelerator having zero chromaticity and the dynamic aperture is reduced by the nonlinear fields. If the phase advance of the betatron oscillation for each cell in both the horizontal and vertical directions is chosen to be less than 90 degrees, the effects on the dynamic aperture caused by sextupole and octupole fields can be eliminated. In Figure 3, the horizontal dynamic aperture estimated by beam tracking for the POP-FFAG is shown. As can be seen from this figure, the dynamic aperture was more than 5,000 π mm.mrad.
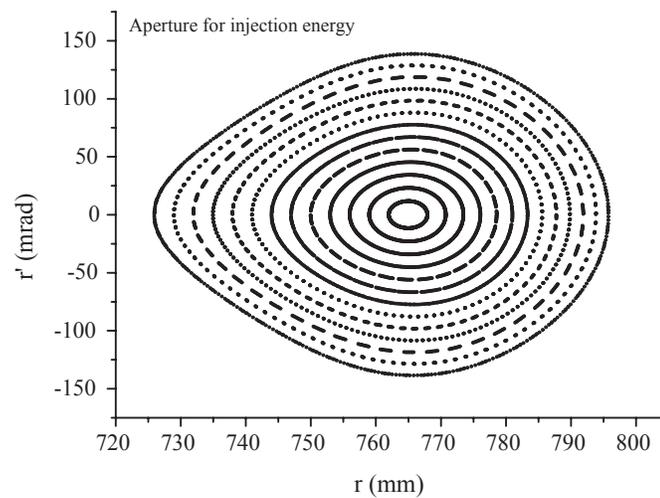
Figure 3: Dynamic aperture in the horizontal direction for the POP-FFAG.

In order to realize a scaling type of proton FFAG accelerator, various technical difficulties have to be overcome. Especially for heavy particles such as protons, a broad band and high gradient rf acceleration system working at relatively low rf frequency is necessary. The requirements of the rf cavity for heavy particle acceleration are summarized as follows:

- Broad band: A frequency sweep of a factor of two or more is needed.
- High gradient: A high field gradient makes fast acceleration possible.
- Large aperture: A large aperture, especially horizontally, can accommodate orbit excursions.
- Large longitudinal acceptance: A frequency of a few MHz provides a large longitudinal acceptance.

This type of rf system is very difficult to realize with an ordinary rf acceleration system using ferrite. A new type of rf cavity using high permeability magnetic alloys (MA cavity) has been developed to solve these problems. Characteristics of magnetic alloy are summarized as follows:

- Large permeability: ~2000 at 5 MHz
- High Curie temperature: ~570 deg.
- Thin tape: ~18 micron
- Small Q value: ~0.6. The Q value can be increased by making core cut if necessary.

The high permeability magnetic alloys, in general, have a large saturation field and the permeability is very large even at high field, compared with ferrite. Therefore, a high μQ value is realized although the Q value itself is relatively small. The μQf stays constant even at large rf field.

To achieve zero chromaticity, the magnets used in FFAG accelerators should be gradient magnets to satisfy the magnetic field configuration as described above. Several ways to realize such a type of magnet have been proposed.

- Tapered gap: The magnet pole shape has a large gap inside and small gap outside.
- Flat gap with surface coils: The gradient magnetic field can be generated by trim coils on the flat gap of the magnet.
- Cos(theta)-like magnet.

In triplet focusing structures, such as DFD in a radial sector FFAG accelerator, the return yoke of the centre magnet can be eliminated because the field directions for F and D magnets are opposite to each other. This type of magnet is called a "Return Yoke-Free Magnet", and has been used for the 150-MeV FFAG accelerator developed at KEK, described below. The magnet of the FFAG accelerator is DC, so a superconducting magnet seems to be interesting. To make a proper field gradient, a multilayer coil with single winding technique can be applied. The multilayer coil type of superconducting magnet was also developed at KEK [8].

Beam dynamics of resonance crossing have been studied on the POP-FFAG accelerator [9]. Crossing $3Q_x = 7$ has been examined (the super-periodicity is eight), and the islands in phase space move outward in this case. Then some particles are trapped by the islands and carried away to large amplitude. Figure 4 shows measured

trapping efficiencies, that is, the ratio of trapped particles to the total number of particles.
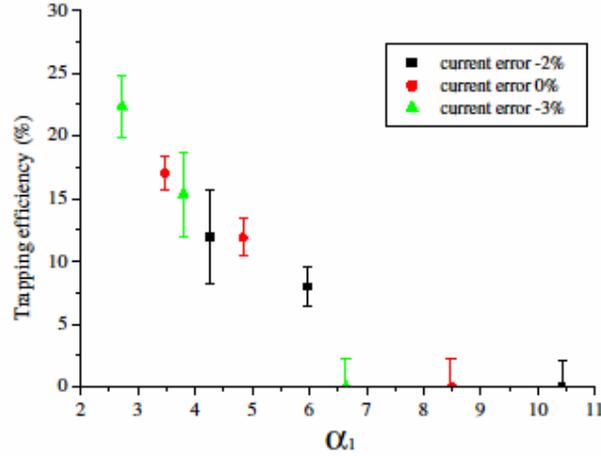
Figure 4: Trapping efficiency measured at POP-FFAG (crossing $3Q_x=7$). The horizontal axis α_1 is proportional to $(\varepsilon/\Delta e)^{2/3}$, where ε is the crossing speed and Δe is the resonance width. Details are shown in [9].

We confirmed experimentally that (non-structural) third order resonances could be crossed without beam loss. It is clear that the crossing speed alone is not enough to describe resonance crossing. Not only should the crossing speed be fast enough but the resonance width should be sufficiently narrow to avoid a deterioration of beam emittance due to resonance crossing.

4.2.3   Development of a 150 MeV proton FFAG Accelerator

A 150 MeV proton FFAG accelerator, which is expected to be a prototype FFAG accelerator for various applications such as proton therapy and an accelerator-driven reactor, has been developed at KEK [10-15]. The machine was designed in 2000, assembled and finally commissioned in March 2003. Figure 5 shows a picture of the 150 MeV FFAG, and the design parameters are summarized in Table 1.

Table 1: Design parameters of the 150 MeV FFAG.

Parameter	Value	Unit
Lattice	DFD triplet	-
Beam energy	12-150 (10-125)	MeV
Number of sectors	12	-
k-value	7.6	-
Average radius	4.47-5.20	m
Betatron tunes (H/V)	3.69-3.80 / 1.14-1.30	-
Max. magnetic field on orbit (F/D)	1.63 / 0.78	T
RF frequency	1.5 – 4.0	MHz

From the machine development point of view, beam extraction and rapid cycling operation were important subjects to explore in order to judge the potential of an FFAG for various applications. The experimental results for these topics are described in the following sections.

An FFAG has an ability to generate a high repetition pulse beam as long as the rf voltage allows since its guiding fields are constant in time. That increases the average current in general. Particularly for medical applications, a pulsed beam of time structure with several hundred Hz is desirable for cancer therapy treatment using a spot scanning technique.

The rf cavity to achieve high repetition, say 100 Hz, was however still a big challenge; high field gradient and rapid frequency variability and large horizontal aperture to accommodate beam orbits have to be fulfilled. A possible solution is the so-called MA (Magnetic Alloy) cavity, which works in the MHz band and has a low Q-value. After many tests and improvement, we finally established an rf system which can provide ~6 kV (~35 kV/m) rf continuously [16].
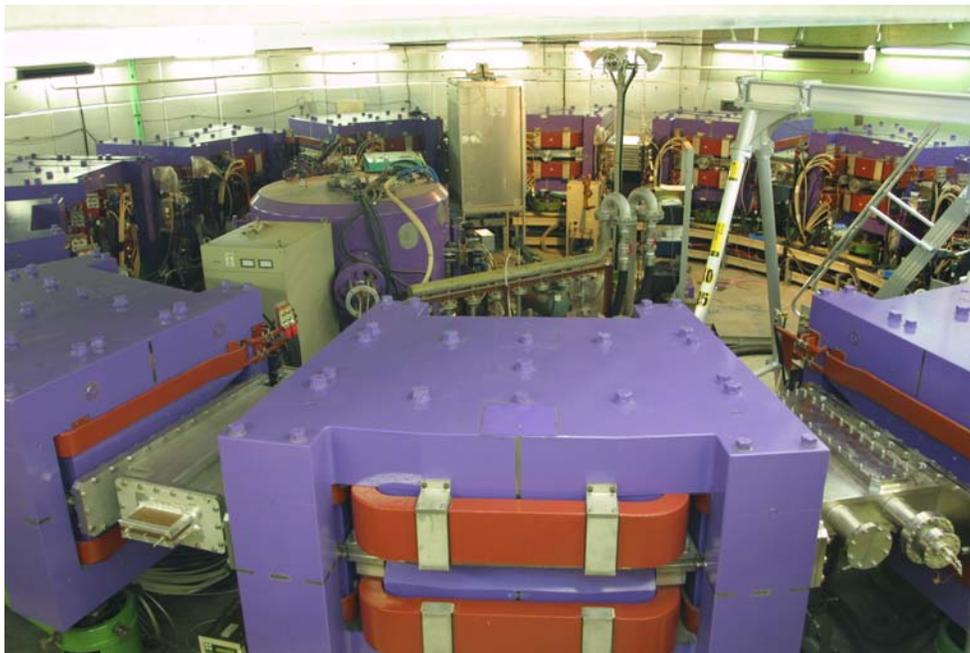
Figure 5: 150 MeV FFAG.

Beam extraction has been performed for the first time at the 150 MeV FFAG. The extraction scheme is the fast extraction commonly used in synchrotrons. A kicker magnet and a septum magnet should work at 100 Hz as well. We use an air-cored magnet as a kicker. The required kicker strength is about 500~600 Gauss with length of 0.6 m. The maximum voltage and current of the kicker power supply are 70 kV and 2000 A, respectively. The switching part is a MOSFET (Metal Oxide Semiconductor Field-effect Transistor) array. The extraction septum magnet is a pulsed magnet with a fringing field suppression plate whose thickness is less than 3 mm. The field of the septum magnet is about 4-5 kGauss with a length of 0.5 m. High extraction efficiency with these devices was expected.

   The experimental results at beam extraction with 100 Hz operation are shown in Figure 6. We compared beam currents in the ring and at the extraction line. The extraction efficiency was measured as more than 90%.

   One of the critical beam dynamics issues was resonance crossing. It was identified at an early stage of the beam commissioning. While the principle of a scaling FFAG gives a zero chromaticity condition, betatron tunes would not be exactly constant over the momentum from injection to extraction due to fringe fields and field saturation effects. The design horizontal tune was above the resonance of $3Q_x=11$ but it turned out to be slightly below the resonance in practice. Consequently, the horizontal tune has to cross the third order resonance during acceleration.
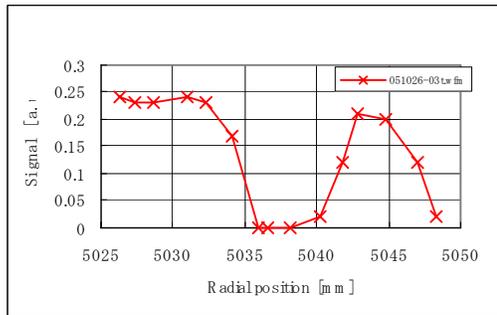
(a) measured beam separation
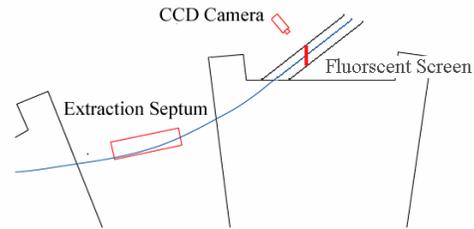
(b) setup of screen monitor and camera
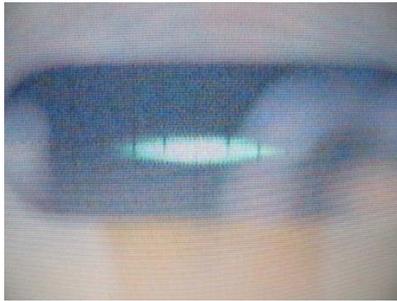
(c) beam on screen monitor
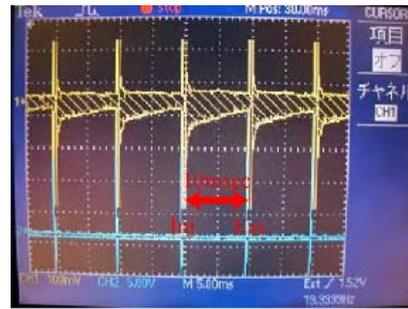
(d) beam signal of 100 Hz

Figure 6: Results of the beam extraction experiment (for 100 MeV extraction).

   In particular, when the available rf voltage was very low at the beginning of commissioning, a problem with beam loss due to resonance crossing was highlighted. One of the sources to excite the resonance is a breakdown of the 12-fold symmetry due to closed orbit distortion (COD) excited by the rf cavity since the fringe field in straight sections is absorbed by the rf cores. We put two dipole magnets on both sides of the cavity to correct the COD and the resonance. The beam loss due to the resonance crossing was respondent to the current of the correction dipoles.   There was still some beam loss even when the possible COD correction was applied because the COD and the resonance would not be perfectly corrected. The beam loss has been, however, overcome by increasing the rf voltage, thereby increasing the resonance crossing speed.

   Because of the intrinsic higher order components of scaling FFAG fields, the beam dynamics of resonance crossing would be dominated by nonlinear motion, especially

for the nonlinear resonances. The islands in phase space, which form stable fixed points in addition to the origin, disturb the transverse distribution during resonance crossing. They move inward or outward in phase space depending on the signs of tune changes and nonlinear detuning.

In the crossing of $3Q_x=11$ in the 150 MeV FFAG, the islands in phase space are initially located at a very large amplitude. They come close and penetrate the beam as the resonance is crossed, and finally disappear after crossing. When the crossing is fast compared to the particle motion in phase space, the islands disappear without deteriorating the beam emittance. When the crossing speed is relatively slow, the particles can reach large amplitude and be lost at the injection septum since the tune crosses resonance at a beam energy slightly above that at injection.

4.2.4 Emittance/energy Recovery Internal Target Ring (ERIT-ring) for Intense Secondary Particle Production with an FFAG Accelerator

Applications of FFAG accelerators for medical use have been proposed in two different fields: hadron beam therapy and boron neutron capture therapy (BNCT). In hadron beam therapy, a rapid cycling accelerator is one of the most interesting ideas that could allow spot scanning treatment. Operation at 100 Hz, demonstrated with the scaling type of proton FFAG accelerator at KEK as described above, would be a good start in this direction.
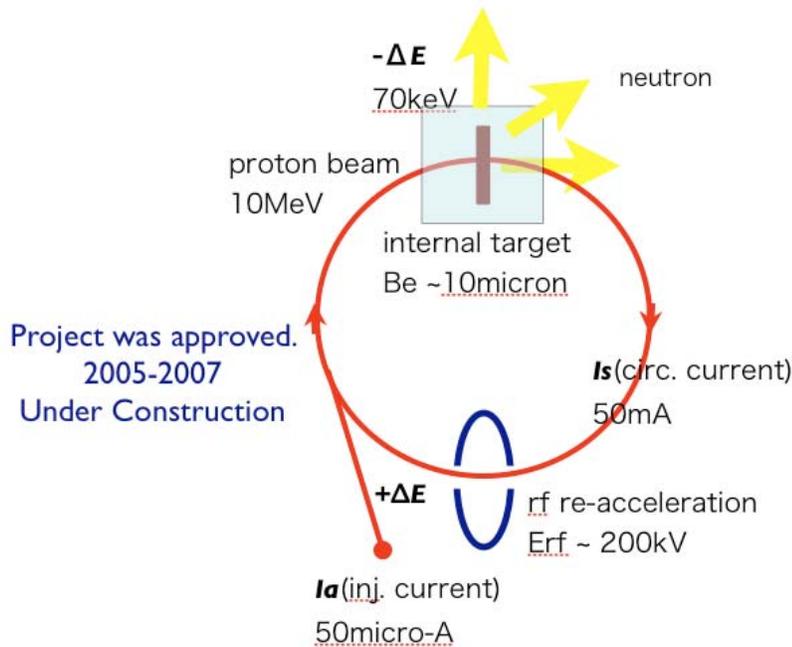
Figure 7: Schematic diagram of ERIT.

For BNCT medical applications, an accelerator-based intense thermal or epithermal neutron source has been strongly requested recently. A scaling type of FFAG accelerator with an ERIT (energy/emittance recovery internal target) concept has been proposed for this purpose and is now under construction [17, 18].   Figure 7 shows a

schematic diagram of ERIT. This scheme may also be used to produce intense beams of other secondary particles such as unstable nuclei, muons etc.

The circulating current of the beam inside a strong focusing ring accelerator, such as an FFAG, is fairly large because the bunch orbits the ring many times with large revolution frequency. For example, in the case of neutron production, when 10^{11} protons at 10 MeV orbit a ring of circumference 10 m, the circulating beam current reaches 70 mA. 10^{11} protons per bunch is a relatively modest number for such strong focusing proton accelerators of this energy. If a neutron production internal target such as a beryllium thin foil is inserted into the ring and the beam hits the target efficiently, the neutron yield should become comparable with that from a nuclear reactor.

In this scheme, however, the incident proton beam will be lost from the ring very quickly because the beam energy of the incident protons is lost to ionization of the target atoms turn by turn, and also because the beam emittances, in transverse and longitudinal directions, are blown up by multiple scatterings with the target electrons. These deleterious effects can, however, be cured by ionization cooling [19, 20, 21]. The transverse emittance reaches equilibrium because of the ionization cooling which is invoked in this energy recovery internal target scheme. For a 10 MeV proton beam with a 5 mm beryllium target, the transverse emittance reaches about 300 π mm.mrad after 3,000 turns, as shown in Figure 8.
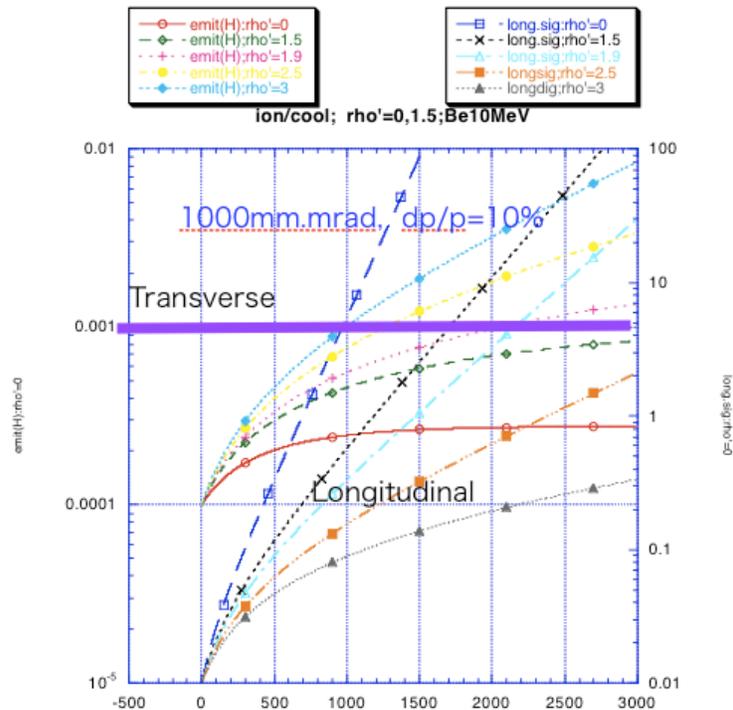
Figure 8: Transverse and longitudinal emittance growth in ERIT.

On the other hand, since there is no cooling effect expected in the longitudinal direction, a large energy spread is inevitable. For example, after 1,000 turns using the same beryllium target, the energy spread of the 10 MeV proton beam would be about 10%.In order to circulate such a large transverse and longitudinal emittance beam in the ring, the FFAG seems to be one of the most suitable accelerators. The FFAG has very large acceptance, especially in momentum space, compared with other types of ring

accelerators, because zero chromaticity in the beam focusing is fulfilled. Moreover, the FFAG ring has the functions both of acceleration and storage, which can be ideal for the internal target type of secondary particle source, and it may be applied for generating not only neutrons but other particles such as pions and unstable nuclei, although the ionization cooling efficiency may be small.

Based on the ERIT scheme, a neutron source for BNCT has been under development in Japan as a NEDO (New Energy Development Organization) project since 2005 and will be completed in 2007.

4.2.5   References

1. T. Ohkawa, Proc. annual meeting of JPS, 1953.
2. K.R. Symon et al., Phys. Rev 103 (1956), 1837.
3. Y. Mori, M. Fujieda, K. Koba, H. Nakayama, C. Ohmori, Y. Sato, Y. Tanabe, A. Takagi, M. Toda, T. Uesugi, M. Yamamoto, T. Yan, M. Yoshii, Proc. of the European Particle Accelerator Conference (EPAC'98), 1998, Stockholm, p.299.
4. Y. Mori, Proc. of EPAC'98, pp.289-292 (1998).
5. Y. Sato et al. Proc of EPAC00, pp.581-583 (2000).
6. A.A. Kolomensky and A.N. Lebedev, "Theory of Cyclic Accelerators", North-Holland, 1966, p.340.
7. S. Machida, Y. Mori, R. Ueno, Proc. of European Accelerator Conf. EPAC2000, 2000, page 557.
8. T. Obana, T. Ogitsu, T. Nakamoto, K. Sasaki, A. Yamamoto, M. Yoshimoto, Y. Mori, Nucl. Phys. B, 149(2005), pp 283-285.
9. M. Aiba, S. Machida, Y. Mori, S. Ohnuma. Phys. Rev. STAB, 9, 084001 (2006).
10. M. Aiba et al., Proc. of PAC01, pp.3254-3256 (2001).
11. J. Nakano et al., Proc. of EPAC02, pp.1028-1030 (2002).
12. T. Yokoi et al., Proc. of EPAC02, pp.1076-1078 (2002).
13. Y. Yonemura et al., Proc. of PAC03, pp.3452-3454 (2003).
14. Y. Yonemura et al., Proc. of EPAC04, pp.2640-2642 (2004).
15. M. Aiba Y. Mori, H. Nakayama, K. Okabe, Y. Sakamoto, A. Takagi, R. Taki, Y. Yonemura, Proc. of EPAC06, pp.1672-1674 (2006).
16. Y. Yonemura et al., Nucl. Instrum. Meth. Vol. 576, Issues 2-3, pp.294-300 (2007).
17. Y. Mori, presentation at the International Workshop of the FFAG Accelerators (FFAG03), Tsukuba, 2003.
18. Y. Mori, Nucl. Instr. Meth., PRS, A563 (2006) 591-595.
19. A.N. Skrinskii & V.V. Parkhomchuk, Sov. J. Part. Nucl., 12, 223 (1981).
20. D. Neuffer, Particle Accelerators 14, 75 (1983).
21. D. Neuffer, Nucl. Instr. and Meth. A532, p.26 (2004.).

4.3 Novel Longitudinal Dynamics of Non-scaling FFAGs

Shane R. Koscielniak
Mail to: shane@triumf.ca
TRIUMF, 4004 Wesbrook Mall, Vancouver, BC, V6T2A3 Canada

4.3.1 Introduction

The linear-field, Non-Scaling Fixed-Field Alternating-Gradient (NS-FFAG) accelerator emerged [1, 2, 3, 4, 5, 6, 10] in the context of fast muon acceleration for a Neutrino Factory and/or Muon Collider [8]. The novel lattice composed of combined function magnets with alternating gradients has the ability to compress a large range of momenta into a small radial aperture and boasts a large 6-dimensional acceptance. This lattice has also the feature that the path-length variation versus momentum is double valued, resulting in a unique longitudinal dynamics [3, 7, 9, 11]. Detailed analytical derivations of lattice properties and longitudinal dynamics are presented in [12, 13, 14] and [15, 16], respectively.

Nevertheless, the FFAG 'outsider' may wonder "why should this be of interest to me?" The answer is two-fold: not only does the longitudinal motion display a new and interesting non-linear thresholding behaviour, but that same motion sheds new light on the "on-crest" acceleration adopted long ago for AVF cyclotrons.

Maintaining *synchronism* between the charged particles and the rf cavity oscillating electric fields is of paramount importance if deceleration is to be avoided. Generally, two means of arranging synchronism are used. (I) There is (almost) no net arrival-time variation and acceleration proceeds on-crest, as in the isochronous cyclotron where spiral path length is adjusted to compensate varying orbit speed. (II) Speed or path-length variation of the beam is compensated by rf sweeping, as in the synchrotron and scaling FFAG respectively. For rapid acceleration of relativistic particles, completed in tens of turns or less, the NS-FFAG offers a third option: cross-crest acceleration. On the few-turn time scale, the radio frequency cannot be other than fixed. Ideally such a machine would be isochronous, but this is not possible over the ±50% Δp/p momentum range intended. The linear dependence of path-length on momentum is set to zero, leaving the quadratic term to dominate the longitudinal dynamics of this *almost isochronous* FFAG. This leads to an asynchronous acceleration in which the beam centroid crosses back and forth and back the crest of the sinusoidal waveform during the transit from injection to extraction energy.

The motion is best understood in terms of the longitudinal phase space. We begin our exposition by way of comparison with a conventional rf-bucket. Consider not acceleration of a centred beam in a moving bucket, but rather an off-centre bunch moving from bottom to top of a stationary rf bucket - whose dynamics is that of a pendulum oscillator, Fig. 1. This archetypal nonlinear system has stable oscillations (libration) within the bucket and phase slipping (rotation) outside; the phase slip reverses direction

Figure 1 pendulum

above and below the bucket. Notice in particular that no new phenomena occur as the cavity voltage is increased, the bucket height merely scales as √V.

In the NS-FFAG, quadratic dependence of path length on momentum implies that there are twice as many fixed points. Initially there are three bands of phase-slip in
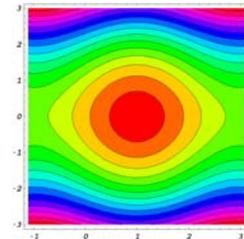
alternating directions separated by upper and lower buckets. (This behaviour is reminiscent of "transition energy" in a synchrotron.) As the voltage is raised, there appears a new phenomena: above a critical, threshold value, the rotation manifolds become linked in a serpentine path that extends from below the lower bucket to above the upper bucket - and this new serpentine channel may be used for acceleration!
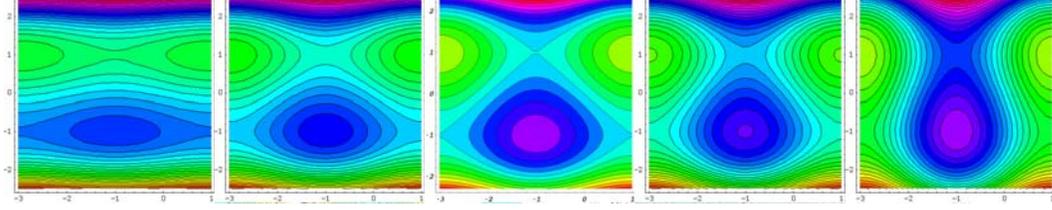
Figure 2: NS-FFAG longitudinal phase space variation as accelerating voltage is increased.

This observation leads to a general principle for acceleration over multiple fixed points: the rf voltage must exceed the critical value to link the unstable fixed points in a zig-zag ladder. The direction of phase slip reverses at each fixed point, and so the criterion is simply that the voltage be large enough that another fixed point be encountered before a π phase slip has accumulated. This same principle is at work in any imperfectly isochronous cyclotron, though the number of fixed points is probably larger.

4.3.2 Mathematical Description

We now give a quantitative description [7, 9, 11, 15, 16] of the serpentine acceleration in a NS-FFAG. Let the time of flight range per cell be ΔT over the energy range ΔE, and the peak energy increment per cell be δE. Let index n denote iteration number, E_n be the particle energy and t_n, T_n be the absolute and relative arrival times, respectively. Let τ_0 be the cell traversal time at the reference energy E_r. Then $t_n = T_n + n\tau_0$. The longitudinal motion is modelled by the difference equations:

$$E_{n+1} = E_n + \delta E \cos(\omega T_n) \quad \text{and} \quad T_{n+1} = T_n + 4\left(\frac{E_{n+1} - \overline{E}}{\Delta E}\right)^2 \Delta T - \delta T_2 \tag{1}$$

Here $\overline{E} = (\hat{E} + \breve{E})/2$, $\Delta E = (\hat{E} - \breve{E})$ and $\Delta T = \delta T_1 + \delta T_2$. The time slip δT_2 represents the fact that the radio-frequency is synchronous with the orbital period at E_r, which is not necessarily equal to the mean energy $\overline{E}$.

We introduce dimensionless variables: $x = \omega T$, $y = (E - \overline{E})/\Delta E$ and dimensionless parameters: $s \equiv n\omega\Delta T$, $a \equiv (\delta E/\Delta E)/(\omega\Delta T)$, $b \equiv (\delta T_2/\Delta T)$; and approximate the motion by differential equations:

$$x' = \frac{dx}{ds} = (2y)^2 - b \quad \text{and} \quad y' = \frac{dy}{ds} = a \cos x \tag{2}$$

The ratio b may take any value between 0 and 1. The injection and extraction energies $\breve{E}, \hat{E}$, correspond to $y = \pm 1/2$, respectively. The reference energy is the solution of $T_{n+1} = T_n$, namely $E_r = \overline{E} \pm (\Delta E/2)\sqrt{b}$. The particle motion is synchronous with the rf at these two energies and the direction of phase slip reverses above/below them. Equations (2) above may be derived from the Hamiltonian

$$H(x,y) = \frac{4}{3}y^3 - yb - a\sin x$$

Let c be some particular value of the Hamiltonian. The *central trajectory* passing through $(x,y) = (0,0)$ for $c = 0$ has special significance. It gives both the range and minimizes the dwell time; it is the reference path for acceleration.

4.3.2.1   *Choice of operating point*

The doublet (a,b) is the key parameter of the system. The condition to link the unstable fixed points by a line segment with linear acceleration is $a=(1/3)b^{(3/2)}$; this is the critical value a_c for opening of the serpentine channel. About this value, there is a discrete change in the topology of the phase space and a dramatic change in the particle transmission from low to high energy. In general, the choice of operating point will depend not only on acceleration range ($\breve{y}$ to $\hat{y}$) and acceptance, but also up on a compromise between acceleration efficiency and the dispersion of dwell time - which leads to nonlinear emittance distortion. Roughly speaking, the acceleration range and efficiency increase with b, but so does the dispersion of arrival times.

The half-period τ, the dwell time from injection to extraction, is of significance - particularly for muon decay losses.

$$\tau = \int ds = \int_{\breve{x}}^{\bar{x}} dx/x' = \int_{\breve{y}}^{\bar{y}} dy/y' . \tag{3}$$

The average value of $\cos x$ along the path indicates the efficiency of acceleration and is also of interest: $<\cos x> a\,\tau = (\hat{y} - \breve{y})$.

4.3.2.2   *Explicit trajectories and properties*

Let the cube roots of -1 be: $r_1 = -1$, $r_2 = e^{i\pi/3}$ and $r_3 = e^{-i\pi/3}$. A trajectory is a contour of constant Hamiltonian $H(x,y)=c$, with solutions $y(x)$ given by:

$$y_i = -\frac{1}{2}\left[r_i w + \frac{b}{r_i w} \right], \quad i = 1,2,3$$

and

$$w = 3^{\frac{1}{3}}\left[c + a\sin x + \sqrt{(c + a\sin x)^2 - \frac{1}{9}b^3} \right]^{\frac{1}{3}} .$$

Here y_1 is the upper, y_2 is the middle, and y_3 is the lower segment. How many of these solutions are needed depends on the values of (a,b,c) and the ranges of x. For a *centre range* of x, momentum y is triple-valued and all y_i are needed; and for *end ranges* either y_1 or y_3 is suitable. The ranges are divided by the turning points of the motion y_2, namely

$$\breve{x} = -\arcsin\left[(a_c + c)/a\right] \quad \text{and} \quad \hat{x} = \arcsin\left[(a_c - c)/a\right].$$

4.3.3   No slip reversal, case $b = 0$

Setting $b=0$ is a means to reducing the time dispersion; in this case there is no reversal of the x' slip direction. The range of the channel is given by that of the central trajectory. The width of the channel depends on paths terminating on the fixed points

for which $c = \pm a$. The acceleration range extends between $y = \pm(3a/4)^{(1/3)}$. At $x = \pm\pi/2$, the momentum width of the channel is $\delta y = (3a/2)^{(1/3)}$ – but the useful width is less.

4.3.3.1   Half period, efficiency and dispersion

The period and expectation values will vary with the range over which they are evaluated. Let us first form the values on the fixed range $x = \pm\pi/2$, which implies a varying momentum range $y = \pm(3a/4)^{(1/3)}$. For the central trajectory the total dwell time is

$$\tau_u(a,0) = \sqrt{\pi}\,\Gamma\!\left(\frac{1}{6}\right)\bigg/\!\left[(6a)^{2/3}\,\Gamma\!\left(\frac{2}{3}\right)\right].$$

On the same trajectory, the acceleration efficiency is $<\cos x> = 2(3a/4)^{(1/3)}/[a\tau] \approx 0.823503$. In order to find the time dispersion, we must compute the half period of motions for particles with differing values c of the Hamiltonian. The lowest order terms in a Taylor series about the central trajectory $c = 0$ are

$$\frac{\tau_u(a,c)}{\tau_u(a,0)} = \left[1 + \frac{2}{9}\left(\frac{c}{a}\right)^2 + \frac{32}{243}\left(\frac{c}{a}\right)^4 + \dots\right].$$

We have not yet considered whether these paths cross the nominal acceleration range $y = \pm 1/2$. This first occurs for the relatively large value $a = 1/6$, and the x-range extends between $\pm\pi/2$. For yet larger values of a, the range of x for which $|y| \leq 1/2$ is smaller and we must reduce the corresponding ranges of integration to $x = \pm\arcsin[1/(6a)]$. We refer to the dwell time between these points as the *restricted period* τ_r :

$$\tau_r(a,0) = \frac{1}{a}\,F_{21}\!\left[\frac{1}{6},\frac{1}{2},\frac{7}{6},\frac{1}{(6a)^2}\right].$$

Here F_{21} is the hypergeometric function. We may also obtain the average value of cosine over the interval $(\hat{y} - \breve{y}) = 1$, i.e. $<\cos x>_r = 1/[a\tau_r] = 1/F_{21}[\dots]$. This quickly approaches unity for $a > 1/4$.

The dwell time for paths with $c \neq 0$ can be computed. The expressions are lengthy; we present one special case.

$$\tau_r\!\left(\frac{1}{6},c\right) = \tau_r\!\left(\frac{1}{6},0\right)\left[1 + 8c^2 + \frac{512}{3}c^4 + \dots\right]$$

where

$$\tau_r\!\left(\frac{1}{6},0\right) = \sqrt{\pi}\,\Gamma\!\left(\frac{1}{6}\right)\bigg/\Gamma\!\left(\frac{2}{3}\right) \approx 7.28595.$$

4.3.4   Two slip reversals, case $b \neq 0$

The working is facilitated by writing the solutions in the form $y(x(z))$ where the relations between x, z are given in the Table 1. Here $\breve{z} = -\text{arccosh}[(a-c)/a_c]$, $\hat{z} = +\text{arccosh}[(a+c)/a_c]$. Over the end ranges $z = [\breve{z}, 0]$ and $z = [0, \hat{z}]$, the two solutions become $y_1 = -y_3 = +\sqrt{b}\cosh(z/3)$. Over the centre range $z = \pm\pi/2$, the three solutions become $y_1 = +\sqrt{b}\cos[(z-\pi/2)/3]$, $y_2 = -\sqrt{b}\sin[z/3]$, $y_3 = -\sqrt{b}\cos[(z+\pi/2)/3]$. The connection between z and time-like s is the dwell time, introduced in equation (3) and elaborated in equation (4) below.

Table 1: Relations between x and z

x range	transformation	z range
$\hat{x} \to +\pi/2$	$(c + a\sin x) = +a_c \cosh z$	$0 \to \hat{z}$
$\breve{x} \to \hat{x}$	$(c + a\sin x) = a_c \sin z$	$\mp \pi/2$
$-\pi/2 \to \breve{x}$	$(c + a\sin x) = -a_c \cosh z$	$\breve{z} \to 0$

4.3.4.1   Range and width of channel

The range of the serpentine channel, found by substituting $x = \pm\pi/2$ in the central trajectory, extends between $\pm y = \sqrt{b}\cosh[(1/3)\operatorname{arccosh}(a/a_c)]$. At the critical value a_c the range spans $y(a_c) = \pm\sqrt{b}$. The paths emanating from the unstable fixed points define the momentum width of the channel at $x = \pm\pi/2$. The lower and upper bounds are respectively $y = \sqrt{b}$ and $y = \sqrt{b}\cosh[(1/3)\operatorname{arccosh}(2a/a_c - 1)]$. Channel width rises as b falls, but collapses when $a = a_c$.

4.3.4.2   Half period, efficiency and dispersion

In general, expressions for dwell time, acceleration efficiency and time dispersion cannot be obtained in closed form. However, there are useful special cases. The simplest case is that the integration ranges are $y = \pm\sqrt{b}$, or $x = \pm\arcsin(a_c/a)$. The dwell time is

$$\tau = 2\frac{\sqrt{b}}{3a} \int_{-\pi/2}^{+\pi/2} dz \frac{\cos(z/3)}{\cos x(z)} . \tag{4}$$

When $c=0$ the integral is obtained (almost) exactly:

$$\tau(a,0) = 4\sqrt{b}/(a\pi)\boldsymbol{K}[(a_c/a)^2] \tag{5}$$

The series expansion for $\boldsymbol{K}$, the complete elliptic integral of the first kind, converges quickly for $b^{(3/2)} < a$. On the central trajectory, the acceleration efficiency is

$$<\cos x> = 2\sqrt{b}/[a\tau] = (\pi/2)/\boldsymbol{K}[\ldots], \tag{6}$$

which tends very quickly to unity because x' is smallest around the crest and largest near the zero crossing.

To find the dispersion we must find the dwell time for paths with $c \neq 0$, namely

$$\tau(a,c) \approx \tau(a,0) + \frac{2\sqrt{b}c^2}{a(a^2 - a_c^2)^2}\left(2a^2\boldsymbol{E}[\ldots] + (a_c^2 - a^2)\boldsymbol{K}[\ldots]\right) + \ldots \tag{7}$$

Here $\boldsymbol{E}$, the complete elliptic integral of the second kind, has argument $(a_c/a)^2$. A significant feature of the expansion is the resonant denominator terms $(a^2 - a_c^2)$. These occur because, for given a value, the larger is b so the motion is closer to a fixed point; and so we should expect the dispersion in arrival times to increase with b.

4.3.4.3   Choice of operating point

Corresponding to the extraction/injection momenta $y = \pm 1/2$ is the position range $x = \pm\arcsin[(1-3b)/(6a)]$; and to $y = \pm\sqrt{b}$ is $x = \pm\arcsin(a_c/a)$. These ranges become

identical when $b=1/4$. In this case, the dwell time, efficiency and dispersion over the restricted range are given by equations (5), (6) and (7) for all a. The unique values which simultaneously satisfy the channel opening condition $a = (1/3)b^{(3/2)}$ and $(x,y) = \pm(\pi/2,1/2)$ are $(a,b) = (1/24,1/4)$. This forms a starting point from which to set suitable acceleration parameters. In practice we need a channel of finite width, which implies $a > 1/24$; and the desire to optimise acceptance and dispersion suggests a lowering of b. In the proposed muon FFAGs, the acceleration rate is limited to $a \leq 1/12$ for technical reasons. The central trajectory spans exactly $(x,y) = \pm(\pi/2,1/2)$ for $(a,b) = (1/12,1/6)$ and it is anticipated that the optimum operating point is in the vicinity of these values.

For the electron model, EMMA (see section 4.7), rf voltage is less of a limitation. To give robustness and tolerance of errors, $a = 1/6$ is considered the minimum; and this allows also to investigate the $b = 0$ case. To give a full exploration capability, additional "head room" is foreseen and sufficient rf voltage to achieve $a = 1/4$ is the baseline.
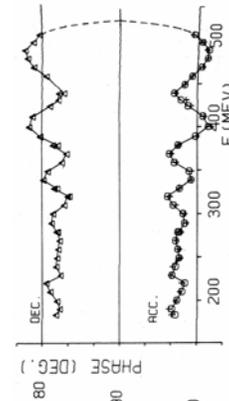
Figure 3: experiment

4.3.5 AVF Cyclotron

Developing a magnetic field shape in cyclotrons which simultaneously provides perfectly isochronous orbits and resonance-free transverse focusing over a large momentum range is not possible. In practice, the relative freedom to adjust the magnet lattice and field profile by shims and correction coils produces a residual time of flight variation that is characterized, presumably, by a high order polynomial. Hence there are expected to be alternating radial bands of phase slip around fixed points of perfect synchronism. Nevertheless, lack of isochronism can be overcome by "brute force". If the energy increment per turn is large enough, then it will be possible to achieve the final energy before an accumulated phase slip of $\pi/2$ leads to deceleration. Hence the energy range and transmission of a cyclotron will show a variation with cavity voltage that may even exhibit thresholding.
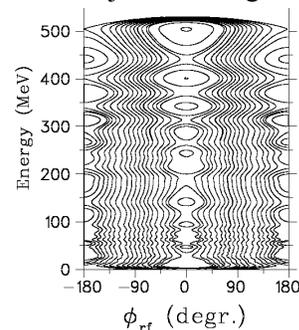
Figure 4: calculation

Experimental measurements, Fig. 3, of the phase histories versus energy (or radius) of accelerating and decelerating beams in the TRIUMF cyclotron [17] are suggestive of the existence of a serpentine channel. Baartman and Rao [18] proposed that the phase wiggles owe their existence to a ladder of fixed points. (If the machine were perfectly isochronous, the paths would be vertical with no wiggles.) Calculations verified this proposition and indicate there to be at least eight fixed points in the ladder. Fig. 4 was generated with the computer program COMA, from a magnet field model of the TRIUMF cyclotron. The D-voltage is 91 kV, and the wave crest is at 90°. Although Fig.4 is a calculation, the coarser features have been experimentally verified [17].

Thus, the serpentine cross-crest acceleration principle devised to predict the properties of the linear-field NS-FFAG is seen to be entirely at home in the world of imperfectly isochronous cyclotrons. Indeed, one may argue that the novel longitudinal dynamics seen in the NS-FFAG, with its remarkable thresholding phenomena versus accelerating voltage and leading to the serpentine channel, is just a simple and

illustrative example of the more general and more complicated dynamics in an AVF cyclotron.

4.3.6   References

1. C. Johnstone: Proc. 4th Int. Conf. Physics Potential & Development of $\mu^+\mu^-$ Colliders, San Francisco, Ca., Dec. 1997, 696-698.
2. C. Johnstone et al: Proc. 1999 Particle Accel. Conf. N.Y. City, N.Y., p. 3068.
3. C. Johnstone et al: Proc. Snowmass 2001, SLAC-R-599, eConfC010630, T508.
4. J.S. Berg et al: Proc. 2003 Particle Accel. Conf., Portland Or., May 2003, p.3413.
5. D. Trbojevic et al: *ibid*, p.1816.
6. J.S. Berg et al: *ibid*, p.2216.
7. S. Koscielniak & C. Johnstone: *ibid*, p.1831.
8. The Neutrino Factory and Muon Collider Collaboration: http://www.cap.bnl.gov/mumu/
9. S. Koscielniak & C. Johnstone: NIM-A 523. pp. 25-49, May 2004.
10. J.S. Berg: Proc. Cyclotrons 2004, 18-22 October 2004, Tokyo, Japan, 19C2.
11. S. Koscielniak: *ibid*, 19C3.
12. S. Koscielniak: TRIUMF internal report TRI-DN-05-13.
13. S. Koscielniak: TRIUMF internal report TRI-DN-03-14.
14. S. Koscielniak: TRIUMF internal report TRI-DN-06-4.
15. S. Koscielniak: TRIUMF internal report TRI-DN-03-13.
16. S. Koscielniak: TRIUMF internal report TRI-DN-05-12.
17. M. Craddock et al: IEEE Trans. Nuc. Sci. Vol. NS-24, No.3, June 1977, p.1615.
18. R. Baartman and Y-N. Rao: private commun., TRIUMF, Vancouver B.C., 2004.

4.4   6-D Beam Dynamics Simulations in FFAGs using the Ray-Tracing Code Zgoubi

François Méot
Mail to: francois.meot@lpsc.in2p3.fr
CEA DAPNIA and IN2P3 LPSC
Grenoble, France

4.4.1   Introduction

Fixed Field Alternating Gradient (FFAG) accelerators are nowadays looked upon as realistic possibilities for many types of application. Examples are the acceleration of muon beams in a Neutrino Factory, medical machines, proton drivers, and applications requiring fast acceleration. This represents a sort of rebirth [1]. Considering the difficulty of modelling FFAG optics using regular matrix or algebraic methods, stepwise ray-tracing has, from the outset, been considered a convenient, accurate way of simulating 6-D beam dynamics in these machines [2]. For this reason, the ray-tracing code Zgoubi [3] has recently been subject to much development, and is now used in several FFAG design studies [4]. Zgoubi contains models of *all* types of FFAG magnets, and can accurately simulate beam dynamics in *all* types of FFAG. This article

reports on the present status of these 6-D transport simulation methods, the associated tools and results.

4.4.2   The Zgoubi ray-tracing method

The Zgoubi integration method is based on stepwise resolution of the Lorentz equation using a technique based on Taylor series. The position and velocity of a particle at location $M_2(s+\Delta s)$ after a step Δs are computed from Taylor expansion at location $M_1(s)$. The coefficients in these Taylor expansions involve the derivatives of the velocity, which are drawn from the Lorentz equation and require knowledge (or modelling) of the magnetic field and its derivatives. Details of the method can be found in [3].

4.4.3   FFAG optical elements

Dedicated Zgoubi procedures, "FFAG", "FFAG-SPI" and "DIPOLES", have recently been developed, which allow modelling of scaling types of magnets or magnet assemblies, either radial or spiral, as well as more general dipole magnets with arbitrary radial non-linear content and shapes. These procedures include simulation of magnetic fields of the form $B_z(r,\theta) = B_{z0} F(r, \theta) R(r)$ (where r and θ are respectively the radial and axial (angle) coordinates), and take into account field fall-off at magnet ends, including possible field overlap and other r-dependent fringe extents for modelling variable gap size effects. These are all important ingredients in FFAG design.

The radial dependence of the field can take the form ("FFAG" and "FFAG-SPI" procedures) $R(r) = (r/R_0)^k$ for the simulation of normal conducting magnets, or the form ("DIPOLES") $R(r) = b_0 + b_1 (r-R_0)/R_0 + b_2 (r-R_0)^2/R^2 + ...$ in order to treat, for instance, superconducting FFAG dipoles [5]. Non-scaling FFAGs can also be simulated by using the existing "MULTIPOLE" procedure [3], and isochronous FFAGs can be treated by means of "MULTIPOLE" and/or "DIPOLES". The axial dependence of the field, $F(r, \theta)$, which includes the geometry of the effective field boundaries (EFB), with such shapes as radial or spiral, is modeled using an Enge type of field fall-off. Figures 1 and 2 below illustrate the "FFAG" and "FFAG-SPI" procedures.

4.4.3.1   Additional features

i.   The possibility of using ***fitting means*** is of key interest in developing FFAG magnet modelling. Fitting means are indispensable tools for preliminary adjustments (magnet and lattice geometry, tunes, etc.) prior to tracking, and useful for further assessment and optimization of higher order behaviour, dynamic aperture, transmission, etc. Various types of constraint, including closed orbits, tunes, chromaticities and aperiodicities, have been added to Zgoubi to fulfill the needs of FFAGs and studies of periodic structures.

ii. *Acceleration* in FFAGs is simulated using the "CAVITE" procedure [3]. The question of time of flight (TOF), either in terms of a reference particle or absolute, is handled in a manner compatible with FFAG needs and does not need special development.

iii. ***2-D and 3- field maps*** may also be used [3, 6], and yield very good symplecticity as well as fairly fast computing.
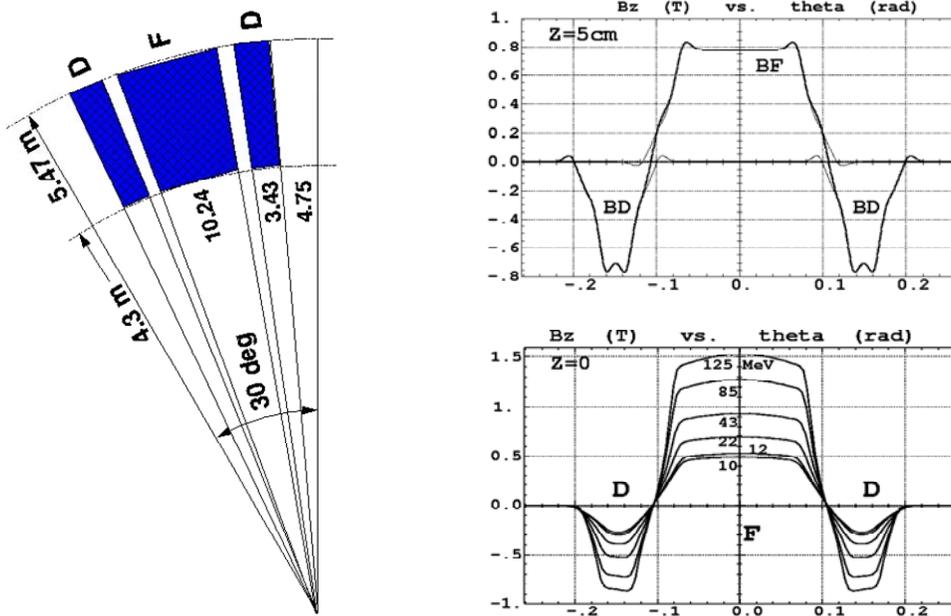
Figure 1: Left: geometry of the KEK 150 MeV radial scaling DFD FFAG triplet. Right, top: magnetic field across the triplet on an arc of a circle, at non-zero z, using the "FFAG" procedure, as obtained by superposition (thick line) of the independent contributions (thin lines).Right, bottom: field on closed orbits in the 12-cell ring, from 10 to 125 MeV.
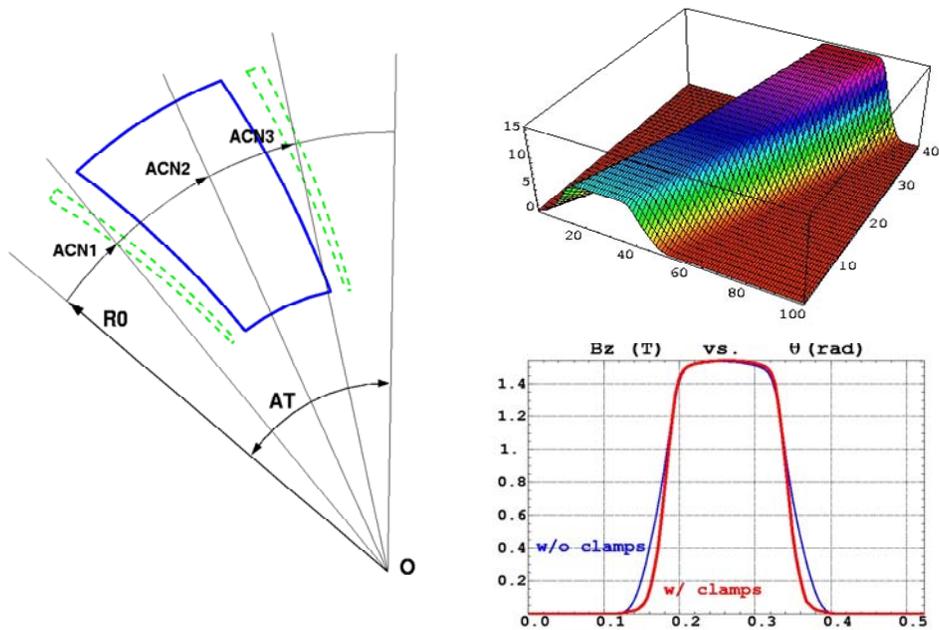
Figure 2: Left: geometry of a spiral sector dipole and typical ingredients (angles, radius, etc.) to define the optical element and positioning of its EFBs, including possible field clamps (dotted lines). Right, top: 3-D representation of the field as delivered by the "FFAG-SPI" procedure; bottom: field fall-off, together with the effect of the clamp modelling.

More details concerning these numerical methods and tools can be found in [7, 8].

4.4.4 FFAG lattice simulations

In the following we give recent examples, for various FFAG lattices, of the use of the procedures addressed above.

4.4.4.1 Radial FFAG

Figure 3 shows the vertical motion, and its damping, for a particle accelerated from 12 to 125 MeV in the modelling of the KEK 12-period ring based on the DFD triplet described above. The orbit radius increases from 4.5 to 5.2 m. The numerical integration method features high accuracy, allowing an integration step size as large as 0.5 cm despite the strong field non-linearities. Figure 4 shows sample horizontal and vertical phase space plots, the quality of the latter showing the accuracy of the integration.
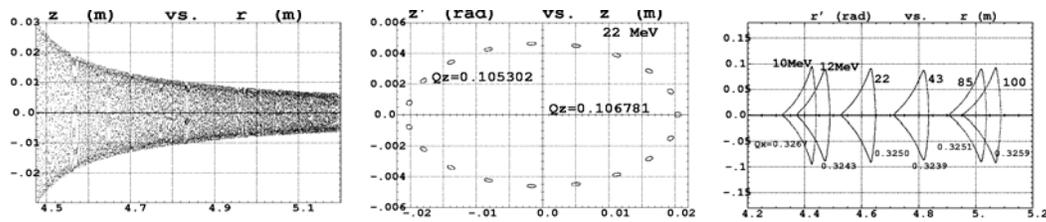
Figure 3: Left: vertical motion under acceleration from 12 to 120 MeV over 20000 turns in the 12-cell ring. Middle: vertical phase space near the stability limit at 22 MeV. Right: horizontal stability limits at various energies, 1000 turns.

4.4.4.2 Spiral FFAG

For a spiral lattice (Fig. 4), based on the FFAG sector of Fig. 2, we use the "FFAG-SPI" procedure. This lattice is designed for the acceleration of protons from 17 to 180 MeV. A scan of (k,q) space, where q is the spiral angle, in the smooth approximation yields the stability region shown in Figure 4 - middle (circles) with the corresponding tune domain shown to the right. A similar (k,q) scan, using the ray-tracing method and field modelling described above, has been superimposed (triangles). This is typical of investigations made possible by the flexibility of geometrical
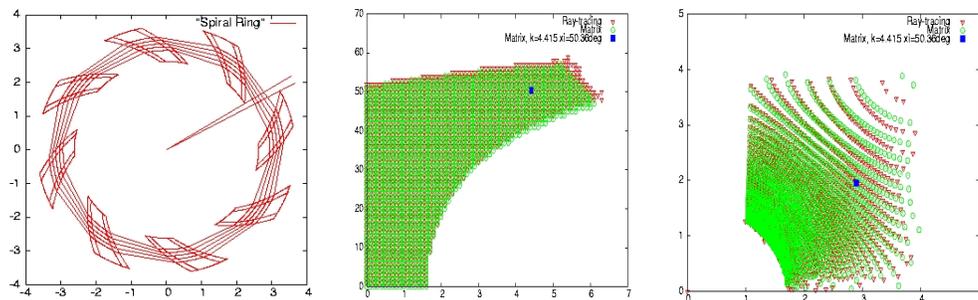
Figure 4: Left: spiral lattice ring, diameter ~7 m, maximum field 1.5 T on high energy orbit, packing factor 0.38. Middle: a scan of the stability domain in the k (field index, horizontal axis) and q (spiral angle, vertical axis) variables. Left: the corresponding stability region in the tune diagram.

modelling of FFAG optical elements in Zgoubi. The agreement between both methods is good for lower k and q values and degrades with increasing k and increasing q. This behaviour that can be attributed to (i) the loss of validity of the constant orbit radius assumption in the smooth approximation, i.e. closed orbits in the dipole sensibly depart from an arc of a circle, and to (ii) the increasing perturbative effect of fringe fields, as they are traversed over an increasingly long distance for larger q values. It can be concluded that the consistency of the two types of results is good, on the one hand confirming the efficiency of the smooth approximation for a first approach of the magnet and lattice parameters, and on the other hand showing that high precision of ray-tracing is necessary for further insight into ring design and beam dynamics.

We can also consider scanning the (k,q) space for dynamic aperture (DA). This is illustrated in Figure 5. Recent comparisons with DA tracking using 3-D field map computations (using TOSCA) have yielded surprisingly similar DA behaviour, thus confirming the usefulness of the geometrical modelling approach as a preliminary design stage.
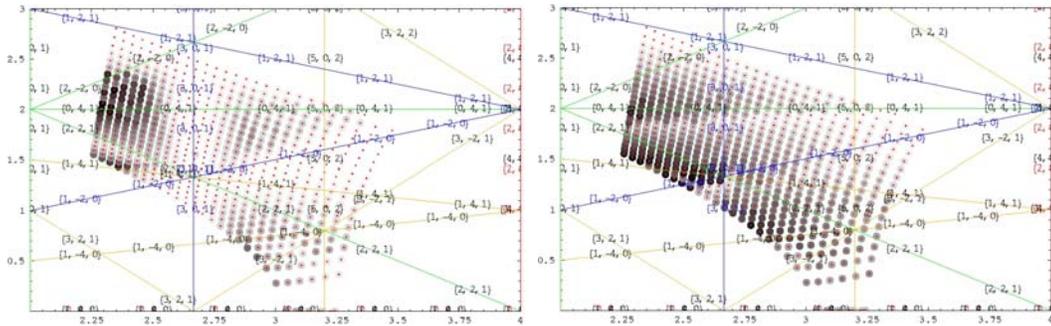
Figure 5: A scan of the horizontal (left) and vertical (right) dynamic apertures in the spiral ring, as represented in the tune diagram. The size of the dark circles indicates the DA value.

4.4.4.3   *Linear FFAG lattice, gutter acceleration*

Based on the existing "MULTIPOLE" procedure, 6-D tracking in linear FFAGs was successfully undertaken in early designs [9]. The more recent Neutrino Factory 5-10 GeV muon FFAG with ISS parameters [10] is used for the present illustration. The muon ring has a circumference of 285 m and comprises 64 quadrupole doublet (FD) cells as represented in Figure 6, which also shows closed orbits at various muon energies.
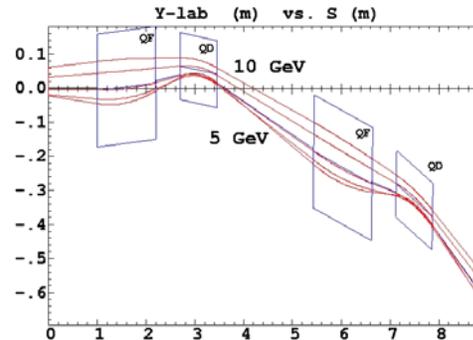
Figure 6: Muon FFAG cell and closed orbits
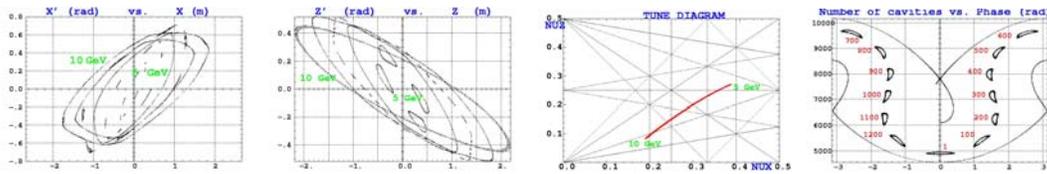
Figure 7: From left to right: horizontal stability limits around closed orbits at various energies; vertical stability limits at various energies; muon beam path in the tune diagram, from 5 to 10 GeV; muon beam motion in the longitudinal phase space.

The motion stability limits from tracking are shown in Figure 7. They are well defined – a sign of good symplecticity – and it can be checked that they correspond to particle tunes neighbouring harmful systematic resonance lines. Transmission in the 5-10 GeV and 10-20 GeV rings, with a 3 cm/0.05 eV.s emittance injected beam, has been obtained in this manner [11, 12]. Sample results showing excursion in the tune diagram and motion in longitudinal phase space are illustrated in Figure 7.

These tools are also used for extensive 6-D beam tracking simulations [13] to support the design of the EMMA electron model of a muon FFAG accelerator (J. S. Berg article, this review).

4.4.4.4 Isochronous FFAG lattice

An isochronous (non-linear) FFAG allows on-crest (cyclotron-like) acceleration of ultrarelativistic particles, and has been proposed for muons in a Neutrino Factory [14]. The lattice is based on a "pumplet" cell (Figure 8), comprised of three different, strongly non-linear magnets, including multipoles up to dodecapole and featuring positive chromaticity and $\gamma = \gamma_t$ at all energies.
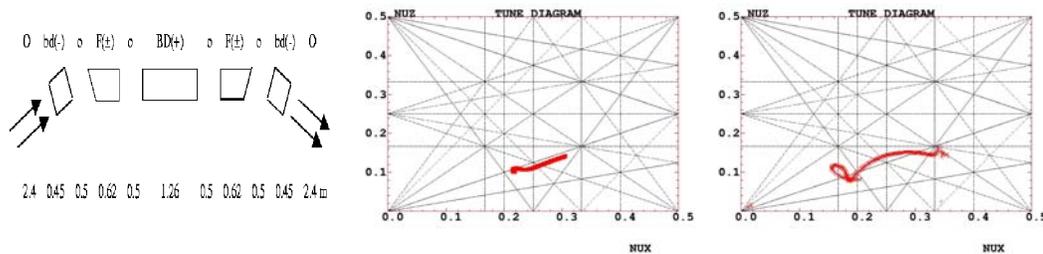
Figure 8: Left: isochronous pumplet cell. Centre: beam path in the tune diagram for the electron model. Right: beam path in the tune diagram for the 123-periodicity muon ring.

Beam optics in this lattice are simulated by means of the "MULTIPOLE" procedure applied to the central and two end rectangular magnets, and by means of the "DIPOLES" procedure for the second and fourth sector magnets. An electron model of such an isochronous FFAG has been tracked in the same way [15]. The ring comprises 45 cells, acceleration is from 11 to 20 MeV and is performed in 15 turns at a rate of 40 kV/cell using 3 GHz rf.

Computation of transverse acceptance at injection is possible in Zgoubi by tracking a beam injected with large initial 4-D emittance. The outgoing transmitted beam yields

the ring admittance. Such beam dynamics parameters as the beam path in the tune diagram, from injection to top energy, can be drawn too, as shown in Figure 8.

A muon ring of this isochronous type is currently being designed, using Zgoubi for fine tune adjustment and dynamic aperture tracking. It accelerates muons from 8 to 20 GeV in 16 turns, using 200 MHz, 18 MV/cavity rf. A preliminary version of the ring comprises 123, 10.2 m long cells. 6-D tracking results show strong beam loss in the 17 GeV region, and this is correlated to the beam straddling a resonance node in the tune diagram (Figure 8 - right). A new insertion type of lattice is under study, featuring very low chromaticity and limited resonance line traversal, aimed at improving the dynamic acceptance and beam transmission.

4.4.5   References

1. M. Craddock, "The Rebirth of the FFAG", CERN Courier 44-6 (2004), http://cerncourier.com/main/article/44/6/17.
2. F.T.Cole, "O CAMELOT! A Memoir of the MURA Years" (Section 7.1), Proc. Cycl. Conf, April 11, 1994; FFAG particle accelerators, Phys.Rev. Vol.103-6, 1837-1859, 1956.
3. F. Méot and S. Valero, Zgoubi Users' Guide, FERMILAB-TM-2010 (1997). See also, NIM A 427 (1999) 353-356.
4. F. Méot and F. Lemuet, "A modern answer in matter of precision tracking: stepwise ray-tracing", Procs. CARE/HHH workshop, CERN (Nov. 2004).
5. M. Yoshimoto et al., "SC magnets for FFAGs", Proc. NuFact03 Workshop, Columbia Univ., NY (2003).
6. M. Aiba and F. Méot, "Determination of KEK 150 MeV FFAG parameters from ray-tracing in TOSCA eld maps", CERN-NUFACT-Note-140 (2004); http://slap.web.cern.ch/slap/NuFact/NuFact/NFNotes.html.
7. F. Lemuet and F. Méot, "Developments in the ray-tracing code Zgoubi for 6-D multiturn tracking in FFAG rings", NIM A (2005) ;
8. J. Fourrier, F. Martinache, F. Méot, J. Pasternak, "Spiral FFAG lattice design tools: application to 6-D tracking in a proton-therapy class lattice", Report IN2P3/LPSC-07-40, submitted to NIM (2007).
9. F. Lemuet, "Collection and Muon Acceleration in the Neutrino Factory Project", PhD thesis, CEA Saclay & CERN, 2007.
10. F. Méot, "Tracking in an 8-16 GeV non-scaling muon FFAG", FFAG03 workshop, KEK (2003), http://hadron.kek.jp/FFAG/FFAG03 HP/menu.html.
11. ISS-NuFact Acceleration Working Group Web-page, at http://www.hep.ph.ic.ac.uk/iss/.
12. F. Lemuet and F. Méot, "6-D transmission in US-Study 2a FFAGs", ISS/NuFact Workshop, BNL (Dec. 2005).
13. F. Méot, "6-D transmission in EMMA FFAG electron model", DAPNIA-06-04, CEA Saclay (Jan. 2006).
14. G.H. Rees, "An Isochronous Ring for Muon Acceleration", FFAG04 workshop, KEK (2004), http://hadron.kek.jp/FFAG/FFAG04 HP/menu.html. See also this edition of the ICFA Beam Dynamics Newsletter.
15. F. Méot, "Beam transmission in isochronous FFAG lattices", FFAG Workshop 2005, Fermilab (Apr. 2005). http://bt.pa.msu.edu/ffag/main.html.

4.5   Emittance Dilution in Resonance Crossing of FFAG Accelerators

S.Y. Lee

Mail to: shylee@indiana.edu

Department of Physics, Indiana University, Bloomington, IN47405

4.5.1 Introduction

Emittance evolution in synchrotrons is one of many important topics in accelerator physics. There are many possible mechanisms for emittance growth. Some of these mechanisms are half integer stopbands, integer stopbands, and nonlinear resonance. There are many theoretical studies without much experimental verification. It is possible that the mechanisms of emittance growth in different accelerators are different. In 2002, S. Cousineau *et al* tried to measure the emittance evolution vs the beam intensity at the PSR and IUCF Cooler Injector Synchrotron (CIS) [1]. Unfortunately, one can not measure the evolution of the beam emittance at PSR, and the resolution of the beam profile (wire chamber) at CIS is too coarse to provide good resolution.

Since 1996, the Fermilab Booster has been equipped with an ionization profile monitor (IPM), that can measure the beam profile in each revolution (averaged over 50 bunches per revolution). In 2005, X. Huang carried out systematic emittance measurement vs the beam intensity [2]. The beam emittance can be deduced once the machine properties are measured [3]. The evolution of the normalized emittance showed that the vertical emittance growth rate depends highly on the beam intensity, while the horizontal beam normalized emittance growth rate remains nearly zero for all beam intensities from 4E11 to 7E12. Based on the accelerator lattice measured by the ICA method [3], we carried out detailed emittance evolution modelling based on a space charge potential model. In this model, the space charge kick is given by a potential-like thin lens kick at each half cell. In each half cell, we also include random dipole kicks, random quadrupole kicks, random skew quadrupole kicks, and sextupole kicks to simulate the injection closed-orbit error, the half-integer stopband, the linear coupling, and the systematic or random sextupoles. The betatron motion excitation by the energy gain in each rf cavity is introduced to simulate the rapid cycling accelerator at 15 Hz. In order to model the beam emittance evolution, we do not use the non-self-consistent potential space charge model! This means that the beam distribution may be changed by emittance growth mechanism, while the space charge force remains to be Gaussian in nature. Detailed data analysis revealed that the essential emittance dilution mechanism at the Fermilab Booster arose from the difference and sum resonances induced by the random skew quadrupole errors [4].

In recent years, the Fixed-Field-Alternating-Gradient (FFAG) accelerator concept has been seriously considered to be a possible candidate as a high power beam source. In particular, the non-scaling (NS)-FFAG was considered to be the main candidate for the proton driver for a Neutrino Factory. The problem of NS-FFAG is that the betatron tunes will pass through many resonances. One argues that the tune ramping rate is high, and thus the effect is benign. In February 2006, I started to ask the question: How fast is fast enough? What determines the ramping rate required for such an accelerator? This is the main problem to be addressed in this review and in Ref. [5, 6].

4.5.2 Systematic Space Charge Resonances

4.5.2.1   Problem

The space charge potential is a nonlinear function of x^2+z^2. The first order of the space charge force induces the incoherent space charge (Laslett) tune shift! However, the higher order space charge force can produce systematic 4th order resonances. One of these resonances is called the Montague resonance, located at $2\nu_x-2\nu_z=0$. More importantly, the resonances at $4\nu_x=mP$ and $4\nu_z=nP$ where m, n are integers, P is the superperiodicity of the accelerator can be very important too! The physics is that the space charge kicks are modulated by the beam size variation. This may occur even when the accelerator is perfectly built. In fact, this phenomenon has been observed at the KEKPS [7]. These resonances resemble the nonlinear betatron resonances [8].

4.5.2.2   Simulations

Once the problem is determined, it is easy to carry out this task. The program that I used to analyze the emittance evolution can easily be modified to study the FFAG problem!

4.5.2.3   Results

The first problem is study the emittance growth due to resonance crossing through the 4th order systematic space charge resonances. Define the emittance growth factor (EGF) as the ratio of the final emittance to the initial emittance. We can evaluate the dependence of the EGF vs the tune ramp rate ($\Delta\nu/\Delta n$), the reduced resonance strength ($g_{40\ell}$, $g_{04\ell}$), the linear space charge tune shift parameter, etc. It turns out the EGF vs the tune ramp rate obeys a scaling law. Employing the scaling law, we define a critical tune ramp rate for a tolerable emittance growth factor. The critical tune ramp rate vs the reduced resonance strength is shown in the Figure below.

In fact, the 6th order systematic space charge resonances can also cause substantial emittance growth. The momentum aperture of NS-FFAG accelerator is limited. A realistic NS-FFAG design should take this effect into consideration.

4.5.3 Linear random resonances

Besides the systematic space charge resonances, the betatron tunes of the NS-FFAG must pass through many random resonances. For linear resonances induced by the random quadrupole and skew quadrupole errors, we find EGF $\sim \exp[\lambda|g|^2/(\Delta\nu/\Delta n)]$, where λ is a constant, g is the half-integer or sum resonance stopband width [9].

4.5.4 Discussion

So far, the studies on the EGF of resonance crossing are only preliminary. There is much work needed to be carried out. Some of future studies include experimental measurements of the scaling laws of linear resonance crossing, experimental measurements of crossing the systematic space charge resonance, scaling law of nonlinear resonance crossing, etc.
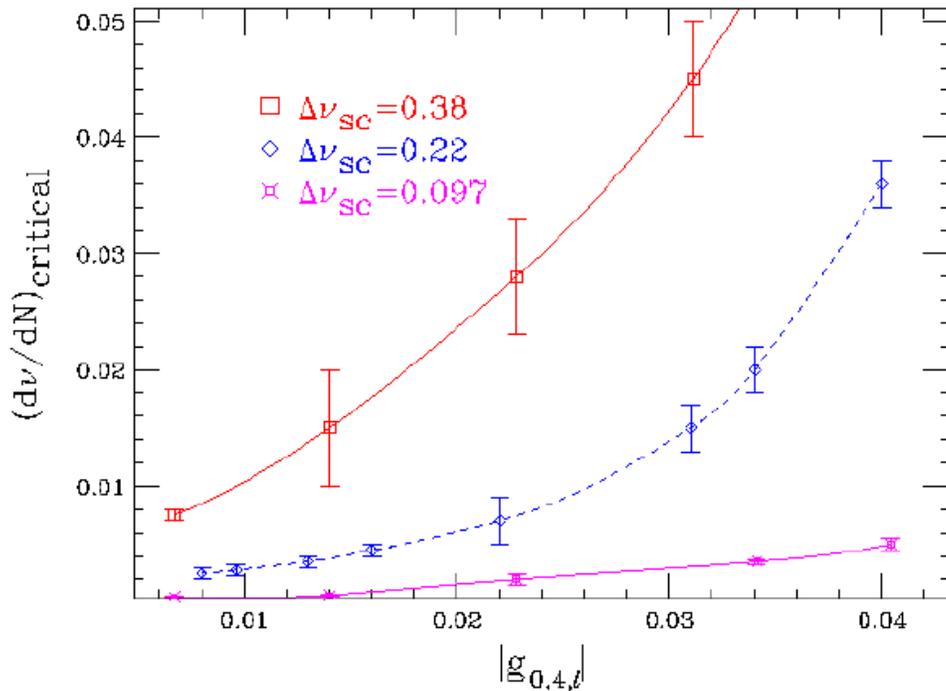
Figure 1: The critical tune ramp rate vs the reduced 4th order systematic space charge
resonance strength, which depends solely on the accelerator lattice function

4.5.5 References

1. S. Cousineau, "Understanding space charge and controlling beam loss in high intensity synchrotrons", Ph.D. thesis, Indiana University (2003).
2. X. Huang and S.Y. Lee, "Emittance Measurements and Modeling of the Fermi-. lab Booster", FERMILAB-2326-AD-AD (2005).
3. Xiaobiao Huang, S.Y. Lee, Eric Prebys, and Ray Tomlin, "Application of independent component analysis to Fermilab Booster**",** Phys. Rev. ST Accel. Beams 8, 064001 (2005).
4. Xiaobiao Huang, S. Y. Lee, K. Y. Ng, and Y. Su, "Emittance Measurements and Modeling of the Fermilab Booster", Phys. Rev. ST Accel. Beams **9**, 014202 (2006).
5. S.Y. Lee, "Fundamental Limit of Nonscaling Fixed-Field Alternating-Gradient Accelerators" Phys. Rev. Lett. **97**, 1048001 (2006).
6. S.Y. Lee, G. Franchetti, I. Hofmann, F. Wang, and L. Yang, "Emittance growth mechanisms for space-charge dominated beams in FFAG and proton driver rings" New Journal of Physics **8,** 291 (2006).
7. S. Igarashi, T. Miura, E. Nakamura, Y. Shimosaki, M. Shirakata, K. Takayama, T. Toyama, "Space Charge Effects during the Injection Period of the KEK PS Main Ring" Proc. of the PAC03, 2610 (2003).
8. D.D. Caussyn *et al.*, "Experimental studies of Nonlinear Beam Dynamics," Phys. Rev. **A46**, 7942 (1992).
9. S.Y. Lee, *Accelerator Physics*, 2nd edition (World Scientific, Singapore, 2004).

4.6 Modelling of a Nonscaling FFAG and Findings with the New Code

Shinji Machida

Mail to: s.machida@rl.ac.uk

ASTeC Intense Beams Group, STFC Rutherford Appleton Laboratory, Didcot, Oxfordshire, OX11 0QX, U.K.

4.6.1 Introduction

The basic idea that motivated me to write a new tracking code for an FFAG is a complete separation of the lattice geometry from the particle orbits. In a code such as MAD [1], the position of the lattice elements determines a particle orbit, namely, magnets such as quadrupole and sextupole magnets define the reference orbit at the center of the magnets. It is, in fact, reasonable to assume that the lattice geometry and the central orbit are coupled together because ideally the beam orbit in a synchrotron is fixed during acceleration. In a FFAG, on the other hand, particle momentum and magnet strength are completely independent. The field strength is fixed and the orbit shifts in the aperture of magnets like a cyclotron. For example, in a nonscaling FFAG [2, 3] which uses only dipole and quadrupole magnets just like an ordinary storage ring, a beam does not go through the center of the quadrupole magnet at all or does go through but at some instantaneous momentum which does not have any specific meaning. A code that can handle the lattice geometry and a particle orbit separately is definitely needed [4].

To be more specific, the new code is not for designing a nonscaling FFAG lattice. The lattice geometry should be determined, at least roughly, by another code such as MAD. This sounds contradictory to what I just said. It is not, however, because MAD and other codes for synchrotron lattice design are still useful if we only look at the optics of a fixed momentum. In these codes, there is an option to define a particle orbit at the off-center of a magnet as long as the magnitude of the displacement is constant in time. The new code tracks particles based on the predetermined location and strength of magnetic elements and rf cavities and updates three components of particle momentum.

Regarding a name of the code, I will use a temporary name "s-code", assigned by Francois Meot at a workshop about a year ago.

4.6.2 Modelling of Nonscaling FFAGs

All the elements are represented as a collection of thin lenses, which include end field regions. For example, 70 mm QD, which is for an electron model of a nonscaling FFAG (EMMA, hereafter) [5, 6], is expanded into an object with 100 mm length with
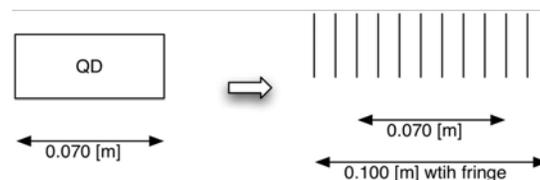
Figure 1: A magnet is represented as a collection of thin lenses including end fields.

end fields attached. Then, the whole object is split into slices making thin lens kicks as shown in Fig. 1.

At each slice, the two transverse components of momentum change as

$$p_{y,new} = p_{y,old} + \frac{k_q}{1+\delta}\left(b_x \frac{p_{z,old}}{p_{x,old}} - b_z\right)\Delta x \tag{1}$$

$$p_{z,new} = p_{z,old} + \frac{k_q}{1+\delta}\left(b_y - b_x \frac{p_{y,old}}{p_{x,old}}\right)\Delta x \tag{2}$$

b_x, b_y, b_z are the normalized strength of magnetic field. x is longitudinal, y is horizontal, and z is the vertical direction. Unless a magnet is very short with respect to the aperture, b_z is unity and b_x and b_y are zero at the middle of a magnet body. Longitudinal momenta are updated to keep the total momentum constant:

$$p_{x,new} = \sqrt{p_{old}^2 - p_{y,new}^2 - p_{z,new}^2} \tag{3}$$

Between slices, a particle travels in a straight line.

As end fields, we assume the Enge type field fall-off with proper coefficients. For a quadrupole magnet of which a nonscaling FFAG consists, we take the scalar potential in cylindrical coordinates as

$$P_2(r,\theta,z) = \frac{r^2 \sin 2\theta}{2}\left[G_{2,0}(z) + G_{2,2}(z)r^2 + \cdots\right] \tag{4}$$

where

$$G_{2,2k}(z) = (-1)^k \frac{2}{4^k k!(2+k)!} \frac{d^{2k}G_{2,0}(z)}{dz^{2k}} \tag{5}$$

and

$$G_{2,0}(z) = \frac{G_0}{1+\exp\left(\sum_{i=0}^{5} C_i z^i\right)} \tag{6}$$

$$z = \frac{s}{g} \tag{7}$$

s is the distance from the hard edge, g is the scaling parameter of the order of the gap, and C_i is the Enge coefficients. We took the potential up to $G_{2,1}$.

A closed orbit is found by tracking a particle iteratively until the initial coordinates and the final coordinates match to a reasonable accuracy. Once the closed orbit is found,

small transverse oscillations are introduced to measure betatron tunes and lattice functions. This process is repeated for different momenta to make sure orbits exist and betatron oscillations are stable in the range of acceleration. As an example, orbits in EMMA are shown in Fig. 2.

As for acceleration, a particle receives a longitudinal momentum kick at an rf cavity whereas its transverse momenta remain the same. Adiabatic damping is included in this way:

$$p_{x,new} = \sqrt{\left(E_{old} + Vsin\theta\right)^2 - m_0c^2 - p_{y,old} - p_{z,old}} \tag{8}$$

Since all the elements are thin lenses, a trajectory is a collection of consecutive straight lines. Time of flight of a particle is recorded at each element simply as an accumulation of the straight line distance divided by velocity.
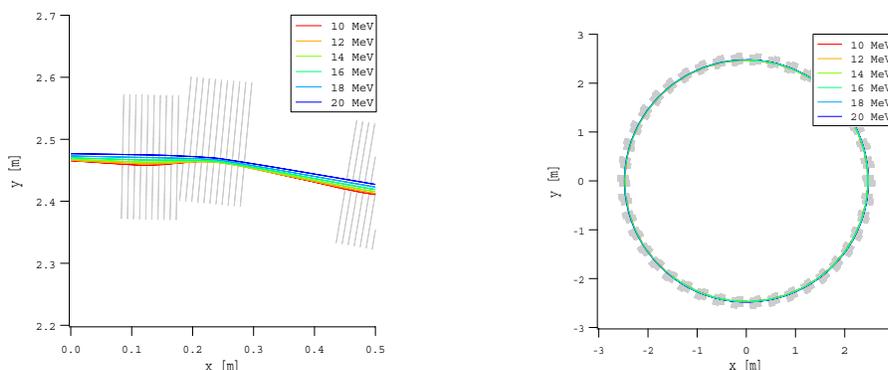
Figure 2: Closed orbits in EMMA for several fixed energies.

If necessary, time of flight and transverse tunes are adjusted by changing quadrupole and dipole strengths. In fact, in both EMMA and muon ring lattices, we use a horizontally displaced quadrupole to produce a dipole field. Therefore, machine parameters are optimized by two knobs: quadrupole strength and displacement of focusing and defocusing quadrupoles.

4.6.3　Findings

4.6.3.1　Tune excursion

Because a nonscaling FFAG is supposed to be operated with natural chromaticity, the total tune of a ring crosses several integers and half-integers. Although the tune per cell is carefully chosen between 0 and 0.5 so that there are no structure integer and half-integer resonances, a concern still remains whether integer and half-integer crossings, that may be excited by strength and alignment errors, are harmful.

A tracking study has been carried out with s-code including alignment errors of dipole magnets and gradient errors of quadrupole magnets. Figure 3 is one result. It shows the orbit distortion when the rms alignment error is 0.1 mm (rms) in both horizontal and vertical directions. Although it is just one example, it implies that there is no clear relation between integer crossing and growth of orbit distortion. Integer

"resonance" is hardly identified. In order to study the effects in more detail, we have tracked a particle in 501 different lattices with different random errors. The rms orbit distortion as a function of time is shown in Figure 4. This shows that the rms distortion is gradually increased almost as a function of the square root of time. This clearly shows that the distortion is a result of random dipole kicks by alignment errors.
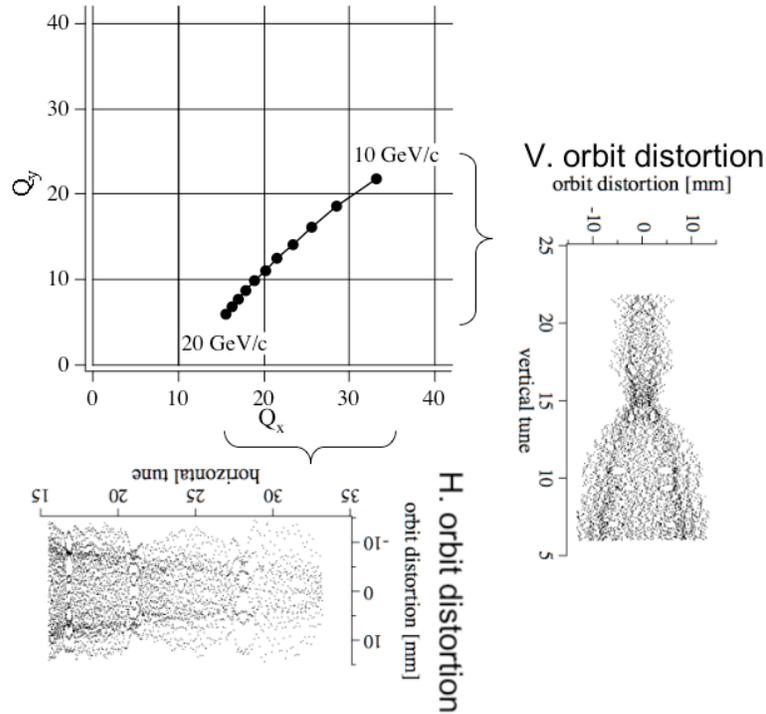
Figure 3: Tune excursion of 10 to 20 GeV/c muon ring and orbit distortion when alignment errors of 0.1 mm (rms) are included.

A similar exercise has been undertaken with gradient errors. Tracking several particles on the edge of the emittance ellipse shows the distortion of lattice functions when random gradient errors are included. The distortion, however, occurs continuously
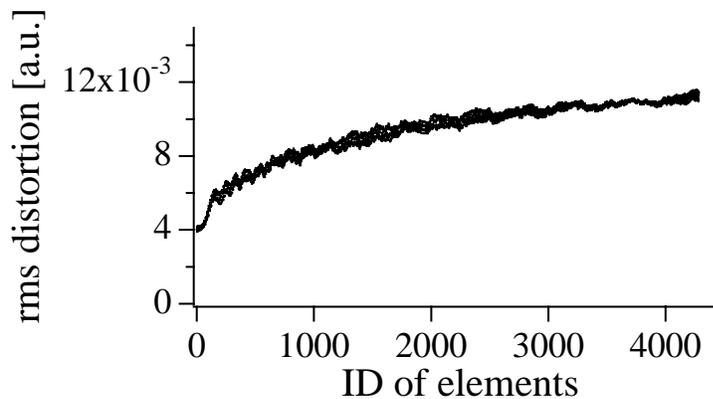
Figure 4: RMS orbit distortion out of 501 tracking results.

during acceleration, independently of total tunes. Excitation due to half-integer "resonance" is hardly identified, either. If we calculate the rms distortion of the lattice functions from many error patterns, its magnitude grows almost as a function of the square root of time. The whole study shows that "resonance" is not the correct physics to explain the orbit and optics distortion in a ring where a beam circulates only 10 to 20 turns [7].

4.6.3.2   *Time of flight depending on transverse amplitude*

In a linear nonscaling FFAG, the revolution frequency cannot be constant even though a muon or an electron is already ultra relativistic. The circumference changes as it is accelerated. On the other hand, there is no way to modulate rf frequency because the whole acceleration process is finished within 10 to 20 turns. Although it is not possible to make the lattice isochronous, it can be nearly isochronous by adjusting optics such that the time of flight over the range of acceleration makes a parabolic shape. With the rf frequency fixed and synchronized with the revolution frequency of an intermediate momentum, phase slip can be minimized. This is a new acceleration scheme which uses the flow outside rf buckets in longitudinal phase space [8].

It is obvious that a particle with large transverse amplitude takes more time to complete one turn. The time of flight dependence on momentum is also a function of transverse amplitude. Taking this into account, the longitudinal dynamics is closely coupled to the transverse amplitude and the acceleration outside rf buckets is not as simple as we first thought.

We did a simulation of a single particle with different transverse amplitudes. Since the emittance of a muon beam is huge, of the order of 30π mm rad, this effect turned out to be significant and some particles were not even accelerated. For a beam, the longitudinal emittance blows up and the momentum spread becomes unacceptable, as shown in Fig. 5.
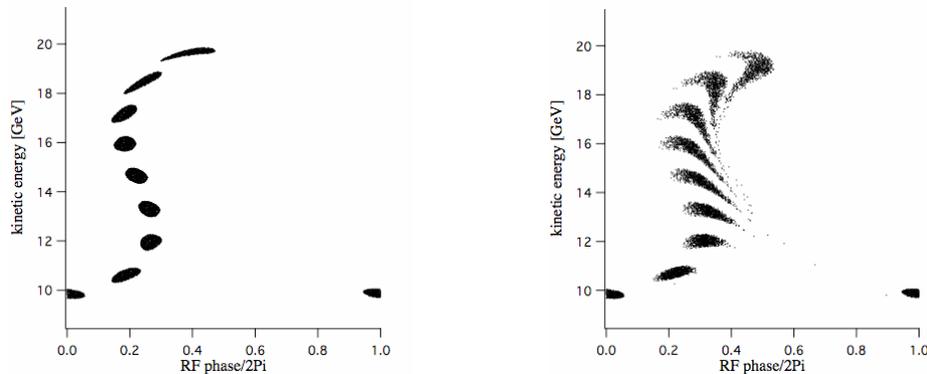
Figure 5: Longitudinal emittance evolution in a 10 to 20 GeV/c muon ring. Left figure shows a beam with zero transverse emittance and right figure shows a beam with 30π mm rad.

The deterioration of the emittance can be cured by correcting chromaticity [9]. One of the side effects is, however, the reduction of dynamic aperture, which we cannot tolerate. Possible remedies are either increasing the rf voltage so that the acceleration should be finished much quicker before the phase slip is accumulated to a noticeable level or introducing a higher harmonic rf component so that the energy gain barely

depends on rf phase. Those remedies certainly work in a single FFAG, but comparatively large momentum spread remains in a cascade of FFAGs. Figure 6 shows the emittance evolution with a 10% increase of rf voltage and a second harmonic rf [10].
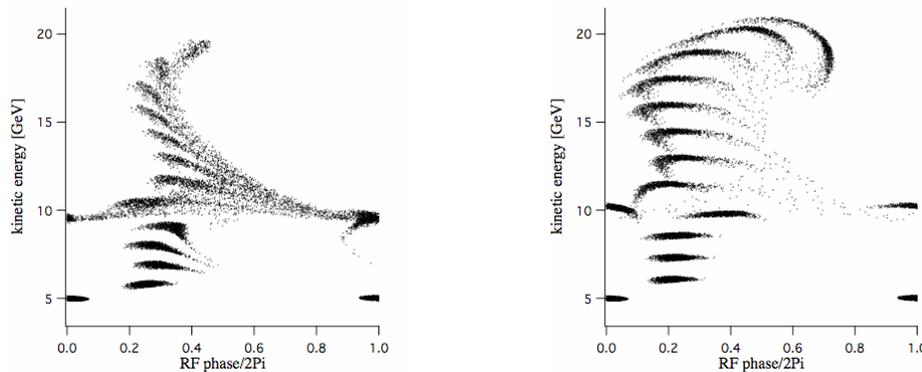
Figure 5: Longitudinal emittance evolution in a cascade of two FFAG with transverse emittance of 30 π mm rad. First FFAG accelerated from 5 to 10 GeV and the second does from 10 to 20 GeV. Left figure uses nominal rf voltage and no higher harmonic rf. Right figure uses second harmonic rf with 10% increase in fundamental rf voltage.

4.6.4   References

1. PTC is another code that can separate element geometry and particle orbits. E. Forest, F. Schmidt and E. Mcintosh, "Introduction to the Polymorphic Tracking Code", KEK Report 2002-3, July 2002.
2. http://mad.web.cern.ch/mad/
3. F. Mills, "Linear Orbit Recirculators", Muon Collaboration Meeting, p. 693, San Francisco, December 13, 1997.
4. C. Johnstone, "FFAG design", Muon Collaboration Meeting, p. 696, San Francisco, December 13, 1997.
5. R. Edgecock, "EMMA – the world's first nonscaling FFAG", PAC'07, Albuquerque, 2007, http://www.jacow.org.
6. J.S. Berg, "The EMMA Experiment", this edition of the ICFA Beam Dynamics Newsletter.
7. S. Machida, "Orbit and optics distortion in fixed field alternating gradient muon accelerators", submitted to Phys. Rev. ST Accel. Beams.
8. S. Koscielniak and C. Johnstone, "Mechanisms for nonlinear acceleration in FFAGs with fixed RF", Nucl. Instr. Methods Phys. Res. Sect. A **523** (2004) 25.
9. J. S. Berg, "Amplitude dependence of time of flight and its connection to chromaticity", Nucl. Instrum. Methods Phys. Res. Sect. A **570** (2007) 15.
10. S. Machida, "Longitudinal emittance blowup in fixed field alternating gradient muon accelerators", Phys. Rev. ST Accel. Beams 9, 104002 (2006).

4.7   The EMMA Experiment

J. Scott Berg, for the EMMA Collaboration
Mail to: jsberg@bnl.gov
Brookhaven National Laboratory[1], Building 901A, P.O. Box 5000,
Upton, NY, 11973-5000, USA

4.7.1   A Brief Description and History of Non-Scaling FFAGs

Fixed field alternating gradient accelerators (FFAGs) are machines that accelerate particles while keeping the magnetic fields unchanged ("fixed field"). By eliminating the synchrotron's requirement to increase the magnetic fields with the total beam momentum, such a machine can in principle accelerate very rapidly while still saving on cost by making multiple passes through the rf cavities. In some applications, the average energy of the particles is not increased, but the FFAG is used as a machine with a fixed reference energy and an extremely large energy acceptance [1–3]. What distinguishes an FFAG from a cyclotron is that alternating gradient focusing is employed to reduce the magnet aperture, at the cost of having to somehow keep the rf synchronized with the beam when the time of flight varies with energy. All FFAGs which accelerate the beam must contend with this time of flight variation.

FFAGs have been discussed since the mid 1950s. While there were some earlier discussions of the machines (see [4] and reference 1 there, references 2 and 3 in [5], references in [6], discussion in [7], references in [8], [9]), the first comprehensive description of the beam dynamics in an FFAG appears in 1956 [5]. This paper describes what is today called a "scaling FFAG." The phase space dynamics at fixed energy in such a machine is the same at any energy, except for an energy-dependent linear transformation. In particular, this means that the tunes and the momentum compaction are independent of energy, and the closed orbits at different energies are geometrically similar. Two electron models were built to "study some of the properties of FFAG accelerators and to confirm theoretical predictions" [10,11].

While there has been newfound interest in scaling FFAGs in recent years [1–3, 12–17], simultaneously there has been an interest in a new type of FFAG, today called a non-scaling FFAG. The application that motivated the consideration of this new type of FFAG was muon acceleration. Because they decay, muons must be accelerated very rapidly; this essentially eliminates the use of any machine with magnets that have time-varying fields, at least at lower energies. Muon beams have very large longitudinal and transverse emittances, and thus require relatively low-frequency rf (around 200 MHz) for acceleration at lower energies. To reduce cost, one desires to make as many passes through the rf cavities as possible during acceleration. A recirculating linear accelerator (RLA), where are pair of linacs are connected by several arcs, and the beam passes through a different arc after each pass through a linac, is limited to making around 4 to 5 passes through each linac [18]. An FFAG seemed to be a promising option for being able to make more passes through the rf cavities.

The non-scaling lattice was developed in hopes of making a more compact lattice than one would have for a scaling FFAG. The energy-independence of the beam dynamics is sacrificed to achieve this compactness. The first forms of these non-scaling

FFAGs were described in 1999 [19, 20], and consisted of simple cells (FODO in that case) with linear magnets.

Since then, a number of authors have proposed using non-scaling FFAGs for various applications. These include medical applications [21–23], high-power proton sources [24–26], and nuclear physics accelerators [27, 28], as well as the original muon application [29]. However, nobody has yet built a non-scaling FFAG to "study some of the properties...and to confirm theoretical predictions" (quoting [10]). EMMA, which is an acronym for "Electron Machine with Many Applications," will be the first non-scaling FFAG.

4.7.2 Experimental Goals of EMMA

EMMA will not just demonstrate that particles can be accelerated in a non-scaling FFAG. It will be used to study the beam dynamics in a non-scaling FFAG, verifying our predictions from theory and simulations. The machine design is similar to the FFAGs used for muon acceleration, since these designs are the most thoroughly studied. There are two broad issues that one must face in the design of non-scaling FFAGs: resonances and longitudinal dynamics. I will describe these issues and describe how EMMA will help us study these issues.

4.7.2.1 Resonances

A scaling FFAG has tunes which are independent of energy. This allows one to choose a working point away from the important resonances and stay there throughout the acceleration cycle. A non-scaling FFAG has a tune which varies with energy. Thus, the beam will pass through a number of resonances during the acceleration cycle. Normally, this would lead to unacceptable beam loss. In a non-scaling FFAG, this is mitigated by several factors:

- The lattice consists entirely of short, identical cells. One can thus consider the resonances of only a single cell, and that will give the resonance spectrum for the entire ring. Assuming that there are no magnet errors, this leads to a resonance spectrum that is considerably less dense than if the symmetry were broken.
- Linear magnets are used (we refer to such lattices as "linear non-scaling FFAGs"). Thus, the nonlinear resonances (the only ones remaining in the error-free lattice) are only weakly driven. The driving terms arise from the nonlinear kinetic terms in the Hamiltonian and the end fields in the magnets.
- Acceleration is rapid, and thus any remaining weakly-driven resonances (either the nonlinear resonances or linear resonances arising from lattice imperfections) are passed through quickly, thus limiting the effect of the resonances on beam growth.

EMMA will be able to study the importance of these conditions. In particular

- We will be able to break the symmetry of the lattice by displacing individual magnets and varying the currents in individual magnets. We are, however, endeavoring to make the magnets as identical as possible and make our magnet placement sufficiently precise to maintain the symmetry of the cells when desired.
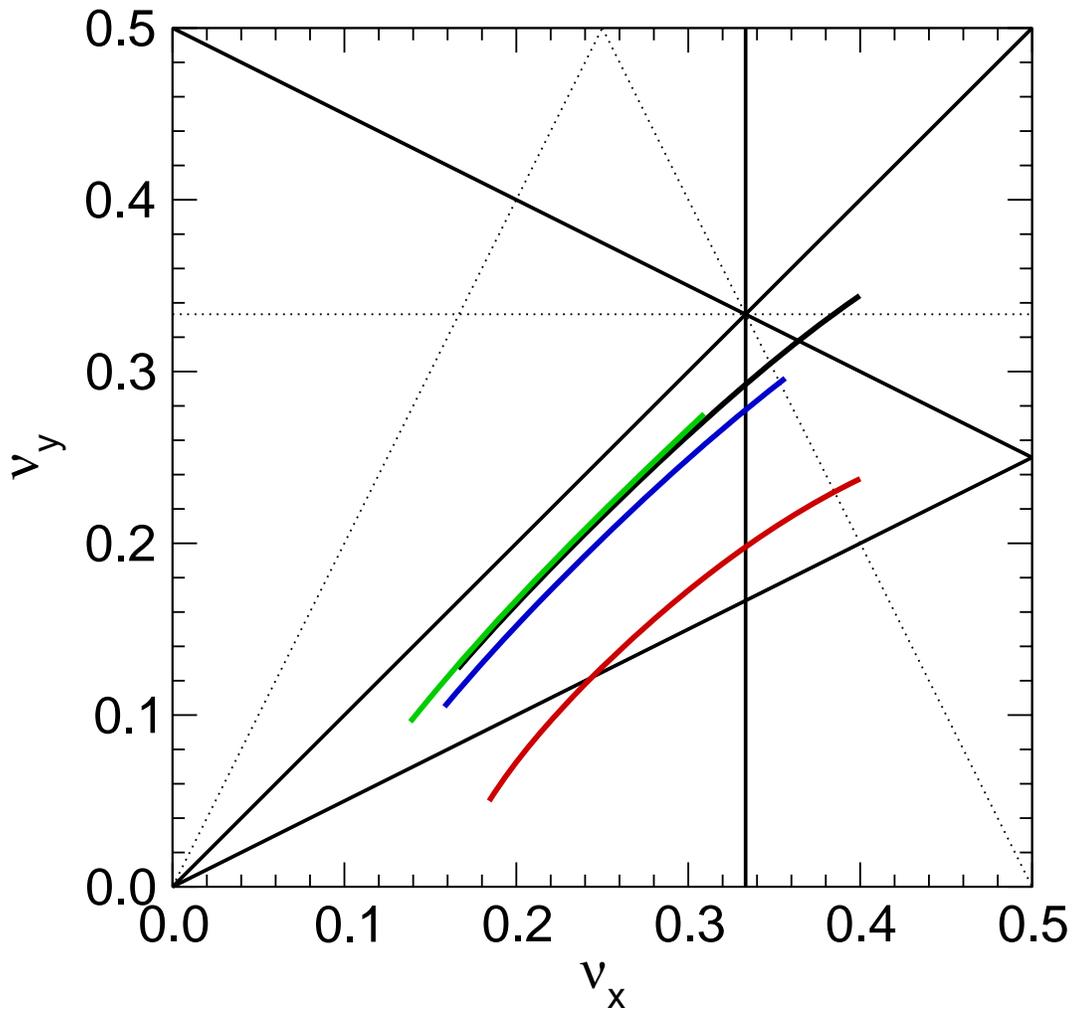
Figure 1: Single-cell tune as a function of energy for four different EMMA lattice configurations. Also shown are resonance lines to third order. Dotted lines are third-order resonances that are driven by skew sextupoles. Higher tunes are lower energy.

- We will vary the range of tunes that the machine passes through during acceleration (See Fig. 1). We can thus see the importance of individual lower-order nonlinear resonances. We will also be able to run in a mode where we pass through an individual resonance at various rates.
- We will be capable of varying the rate of acceleration, and thus the rate of resonance crossing.

4.7.2.2 Longitudinal Dynamics

The disadvantage of using an FFAG over a cyclotron or an RLA is that the time of flight depends on energy. Thus, presumably, if one has fixed-frequency rf, if one spends too much time accelerating, the bunches will eventually shift their rf phase so much that they are no longer accelerated. There are four ways one can deal with this problem:
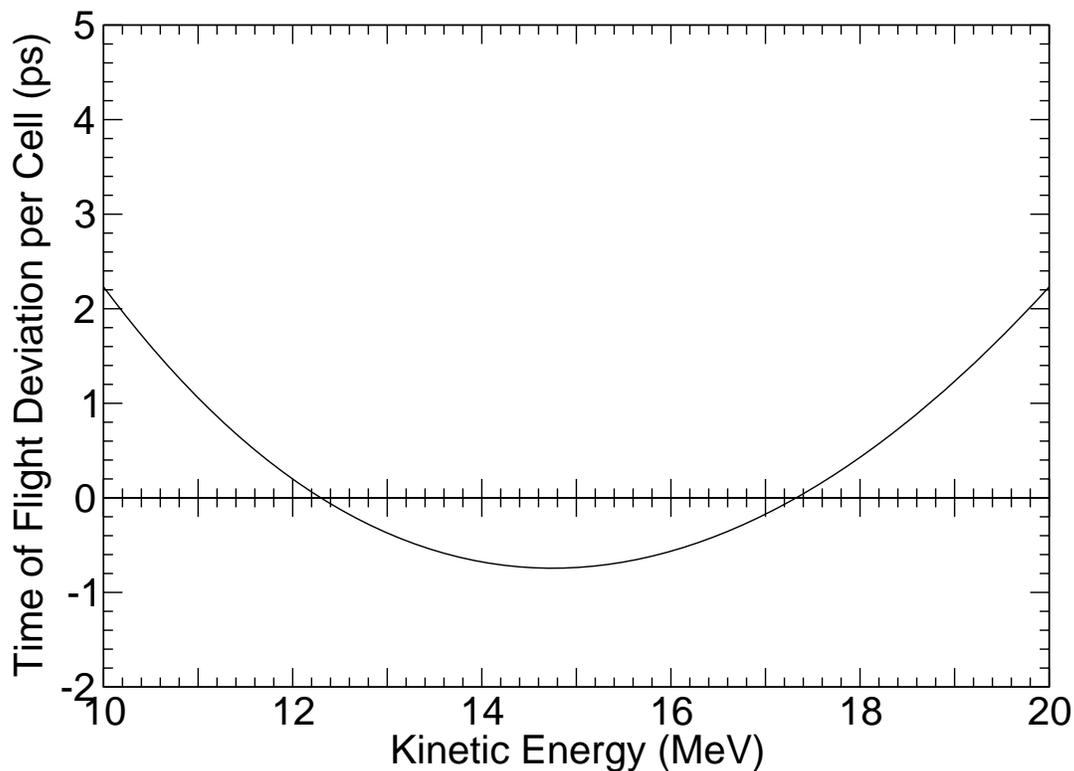
Figure 2: Time of flight as a function of energy in a single linear non-scaling FFAG cell. Zero time of flight deviation means that the time of flight is an integer number of rf wavelengths.

- Accelerate using magnetic induction instead of rf cavities. This was the method used in the original FFAG experiments [10, 11]. This method is typically only used in very low-energy machines.
- Vary the rf frequency as the beam accelerates to maintain approximately constant rf phase. This is typically used when acceleration need not be very rapid, and was used in many of the recent FFAG experiments [12–15]. This method generally gives a significant limitation on the rate of acceleration.
- Craft an rf cavity so that the energy gain as a function of position is such as to make the time of flight an integer number of rf periods on each turn, but that number is different for each turn [30, 31]. This is today referred to as "harmonic number jump."
- Complete the acceleration cycle before the beam has gone too far off of the rf crest. This generally requires the acceleration to be completed in less than 20 turns. It is thus most appropriate when extremely rapid acceleration is required, such as for the acceleration of muons.

It is this latter mode of acceleration that will be studied in EMMA. This mode of acceleration becomes particularly interesting due to the fact that in a highly relativistic linear non-scaling FFAG, the time of flight as a function of energy becomes locally isochronous within the energy range of acceleration (see Fig. 2) when one designs the machine for small aperture. This turns out to give non-scaling FFAGs a significant advantage over scaling FFAGs in this accelerating mode, since the total variation in time of flight with energy becomes significantly smaller in a non-scaling FFAG than in a scaling FFAG, and thus it will take longer for the beam to get far off the rf crest. This
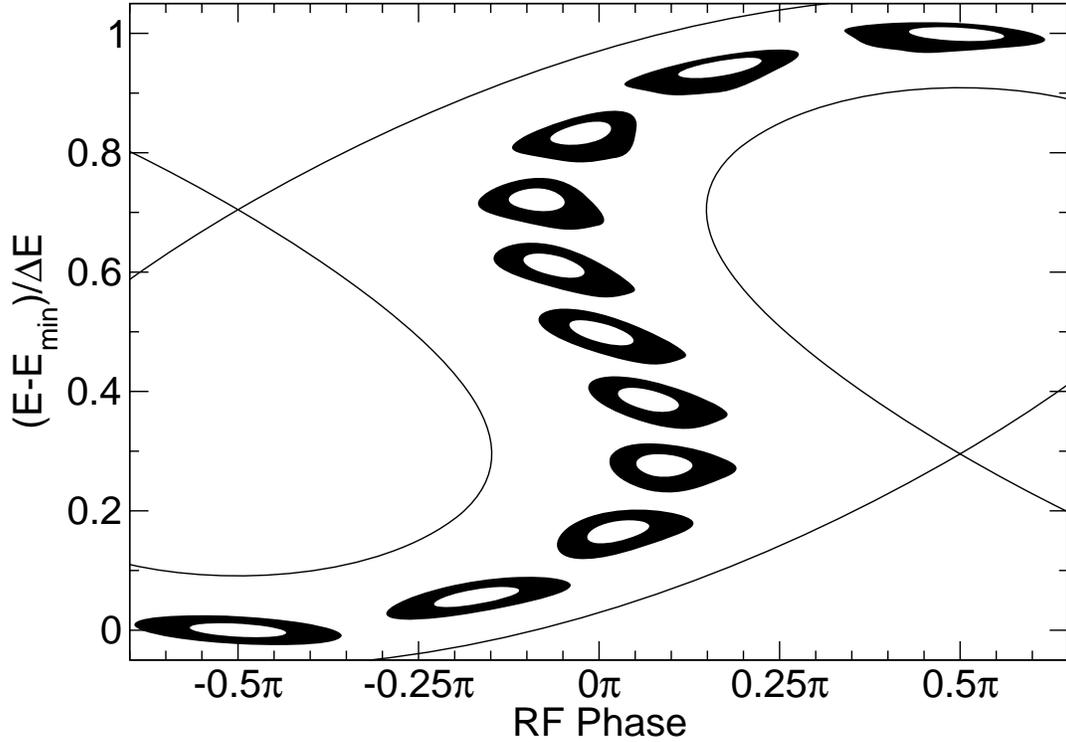
Figure 3: Longitudinal phase space when accelerating in a highly relativistic linear non-scaling FFAG. Bunch is accelerated from bottom to top.

allows the use of higher frequency (and therefore higher gradient) rf in the non-scaling FFAGs which accelerating in this mode.

The dynamics in longitudinal phase space for this time of flight variation with energy is unique; an example is shown in Fig. 3. There have been a number of theoretical studies on the longitudinal dynamics of this system [32], but a machine has never operated in this mode. One of the goals of EMMA will therefore be to study this unique form of longitudinal dynamics. We will modify the machine parameters that govern this acceleration mode: the amount of rf voltage, the rf frequency, and the behavior of the time of flight as a function of energy. Our goal will be to verify that the predictions of our theoretical models are correct, and of course that one can successfully accelerate a beam in this mode.

4.7.3   Machine Description

The longitudinal dynamics of EMMA, as stated earlier, will be similar to the longitudinal dynamics in a muon FFAG. Since one of the most thoroughly studied non-scaling FFAG designs are the muon acceleration FFAGs, EMMA will be similar to those machines in many other ways as well. The machine parameters for EMMA will thus be based on the parameters from a muon FFAG design.

4.7.3.1   *Basic Machine Parameters*

An ring which cannot accelerate by at least a factor of 2 in momentum is somewhat unimpressive. However, because FFAG apertures grow rapidly with the energy range, and the amount of voltage required to accelerate and achieve sufficient longitudinal

Table 1: Basic machine parameters.

Parameter	Value
Minimum kinetic energy	10 MeV
Maximum kinetic energy	20 MeV
Approximate RF frequency	1.3 GHz
Lattice cells	42
RF cavities	19
Lattice type	Doublet
Normalized transverse acceptance	3 mm
Nominal long drift length	210.000 mm
Nominal short drift length	50.000 mm
Nominal D magnet length	75.699 mm

acceptance increases faster than linearly with the energy range, in practice a factor of 2 in momentum is about the right range for an FFAG stage. EMMA will therefore also accelerate by a factor of 2. A higher energy machine is more costly and larger, but the machine must also be highly relativistic. Therefore, we chose a kinetic energy range of 10 to 20 MeV for EMMA.

We chose a doublet lattice, since optimization studies [33] have generally found that to be the most cost-effective configuration. It has the minimum number of individual magnets, and minimizes the cell length. There are arguments that a triplet lattice may have better properties for reducing aperture and the range of the time of flight [34], but the costs of extra magnets, the shorter magnets, and the extra space needed between magnets generally offset any advantage.

Recall that in most cases, the purpose of using an FFAG to accelerate is to obtain the maximum number of passes through the rf cavities, in other words the maximum number of turns. Furthermore, most theoretical studies of FFAG dynamics assume that the energy increases continuously. In practice, however, the energy increases suddenly each time one goes through a cavity. Each one of these energy steps gives a small transverse mismatch, resulting in an effective increase in emittance. Therefore one should complete the acceleration in the largest possible number of steps. Finally, giving a ring more cells improves the ring's characteristics: the magnet apertures decrease, the angles the beam makes with respect to the magnet axes and ends become smaller, and the voltage required to accelerate is reduced. To obtain a goal for these characteristics in the EMMA design, we encapsulated the desired quantities into a single easily-optimized number, the product of the number of cells by the number of turns in the ring. For muon FFAG designs, this number is between approximately 500 and 1500. We chose 500 as the goal for EMMA, using the low end of the range to keep costs down. To approximate the number of turns in the machine, we assumed an *a* parameter (characterizes the available longitudinal phase space volume, see [32]) of 1/12, which is heuristically chosen to be as small as possible while still transmitting an adequate volume of phase space.

We chose between two readily available rf frequencies, 1.3 GHz and 3 GHz. Using 3 GHz would require substantially more lattice cells to achieve our goals, and would have lower stored energy per cavity cell than 1.3 GHz rf (important since beam loading
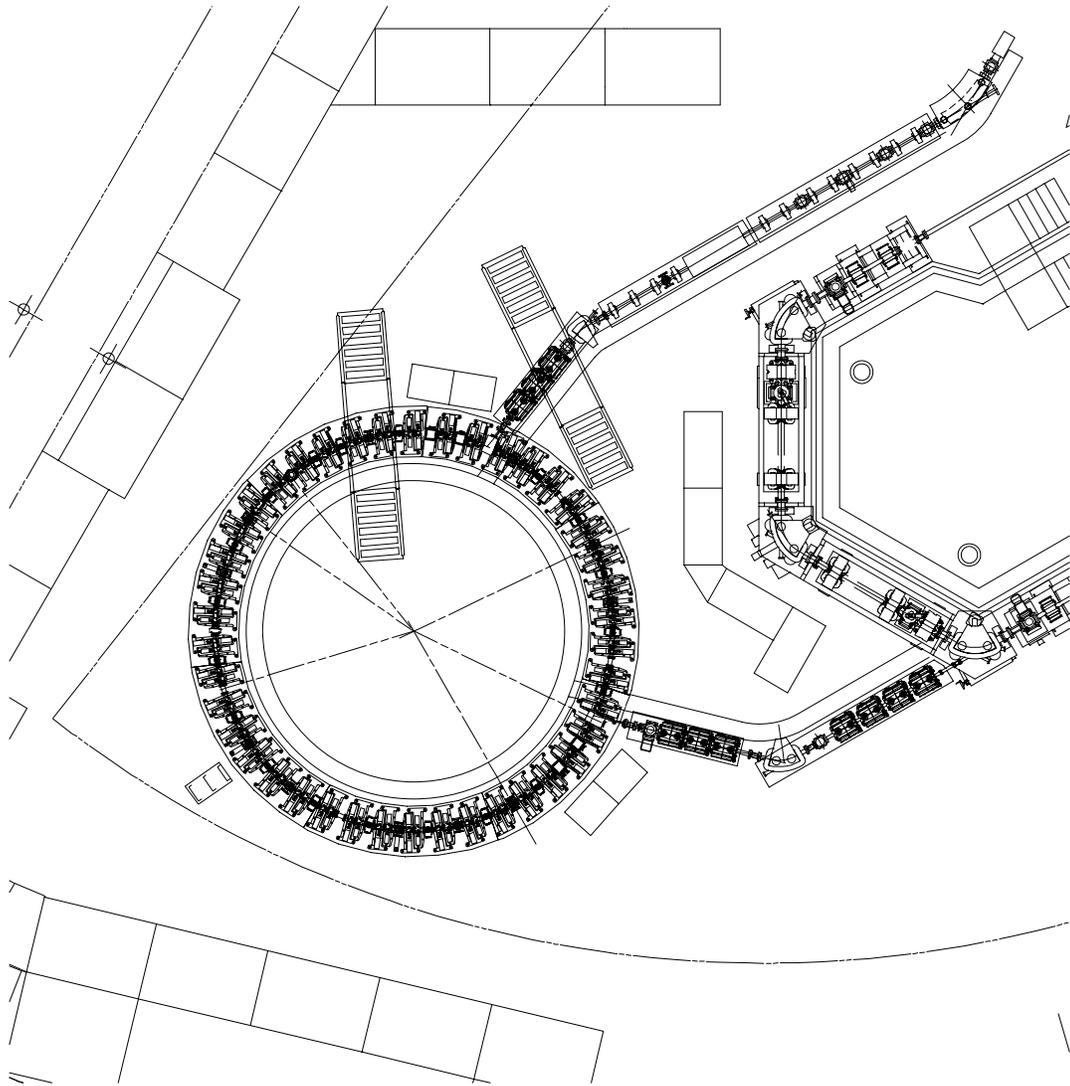
Figure 4: Layout of the EMMA ring (left) relative to ERLP (right).

effects should be small). While rf power transport is more expensive for 1.3 GHz than for 3 GHz, that is not enough to overcome the advantages of the smaller ring.

The scale of the nonlinearities in the machine can be characterized by the fraction of the magnet aperture that the beam occupies and the angle that the beam makes with respect to the magnet ends and axis. To achieve similar levels of nonlinearities to the muon FFAGs, assuming that the beams occupy a similar fraction of the magnet aperture, the emittances should be scaled in proportion to the cell lengths. The normalized transverse acceptance (defined as $a^2mc/\beta p$, where a is the maximum beam half-size, m is the particle mass, c is the speed of light, β is the beta function, and p is the total momentum) of the muon FFAGs is 30 mm, and thus the normalized transverse acceptance of EMMA should be about 3 mm. We are, however, leaving little headroom in the beam pipe beyond that due to the already large magnet and cavity apertures.

As a result of these design decisions, we chose a machine with 42 lattice cells. Using fewer cells would have required shortening the already very short magnets and
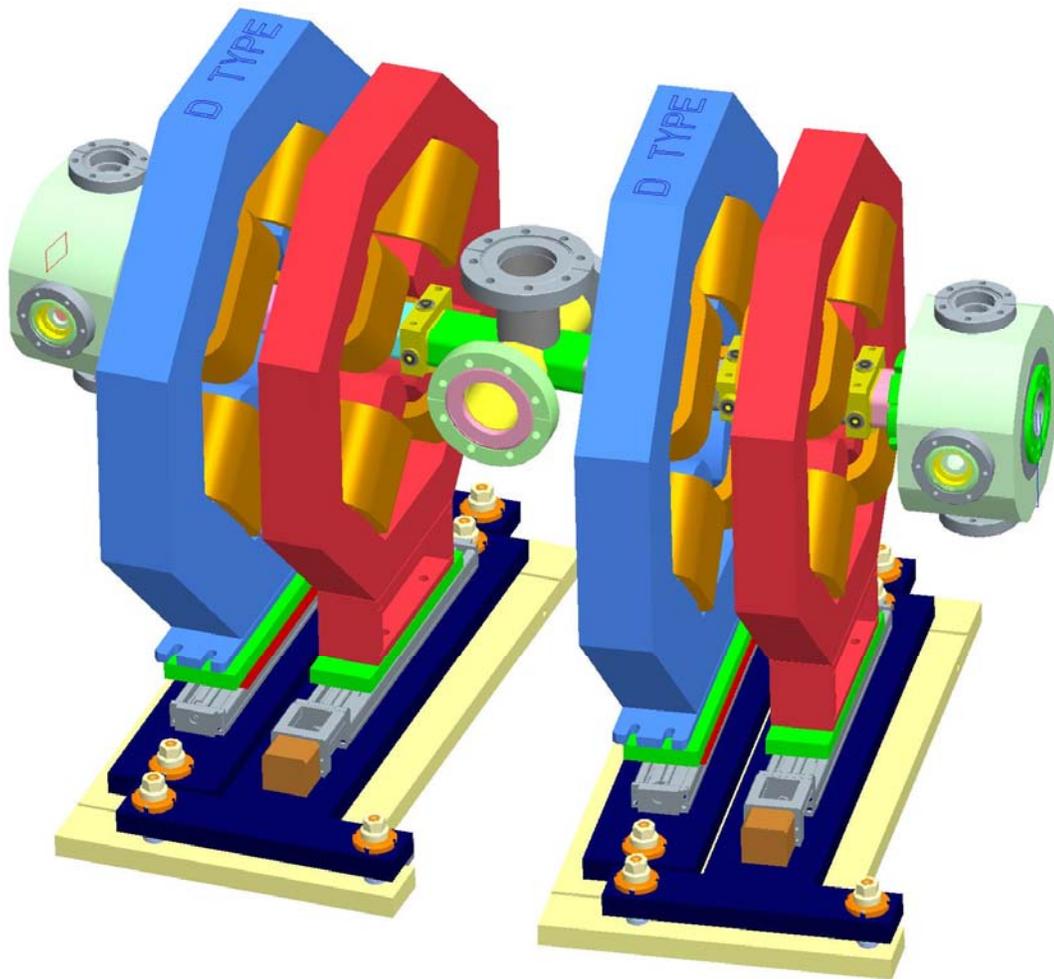
Figure 5: Two cells of EMMA, showing the individual magnets on sliders.

increasing their fields substantially (our goal was 0.2 T pole tip fields in an idealized model). The number of cells was kept as small as possible to reduce the cost of the machine and the ring size.

The machine circumference is adjusted so that the time of flight at some energy within the machine's energy range is an integer multiple of the rf period (as discussed later, the rf frequency will be adjusted to vary that synchronization energy). The long drift must be made long enough for an rf cavity, and sufficient space must be left between the magnets. Given the constraints on the magnet fields, that multiple (the harmonic number) is chosen to be 72, giving a ring circumference of around 16.6 m.

4.7.3.2   *Machine Subsystems*

EMMA will be built at Daresbury Laboratory, using the ERLP [35–38] as an injector. We will be able to adjust the energy of ERLP to inject at any desired kinetic energy from 10 to 20 MeV. Only a single bunch will be injected into EMMA. The beam from ERLP will have transverse and longitudinal emittances which are considerably smaller than the emittance we wish to study (transverse normalized emittances from ERLP are around 2–3 mm.mrad), and so we will use the injection

kickers and steering magnets in the injection line to fully cover the transverse phase space that we wish to explore. Furthermore, to prevent space charge from significantly affecting the dynamics in the EMMA ring, we will take steps to make the beam from ERLP have a slightly larger transverse emittance and bunch length than in the normal ERLP operating mode. We will also keep the beam charge as low as possible, to the extent compatible with being able to get accurate readings from the EMMA diagnostics (about 5×10^8 electrons in the bunch).

Injection into and extraction from the main EMMA ring will be very challenging. Because of our resonance studies, we will be varying the injection tune. Furthermore, our commissioning studies, where we will find fixed-energy tunes and time of flight, require the ability to inject and extract at any kinetic energy in the range 10–20 MeV. This is particularly challenging since the betatron phase advance is different at every energy. The injection and extraction system will also be used to give the beam nonzero horizontal positions and angles. As a result, both injection and extraction will require a septum and two kickers in consecutive cells to be able to create the full range of kicks required. The kickers will have maximum fields of 0.06 T, and will have 35 ns rise and fall times.

The main EMMA ring will contain 19 rf cavities. Since the acceleration in each cavity effectively creates a mismatch from one cell to the next, we would ideally like to have as many cavities in the ring as possible, and to have those cavities placed symmetrically in the ring. Since we need space for injection, extraction, and diagnostics, we cannot place a cavity in every cell. Furthermore, doing so would significantly reduce the amount of stored energy in the cavities, increasing the effect of beam loading. Every other cell would be ideal (making 21 cavities), but we cannot have that everywhere due to the injection and extraction kickers. Thus, we have chosen to have 19 cavities.

To keep costs down, we want to minimize the amount of rf power required. We have therefore designed an rf cavity to maximize the shunt impedance, subject to the requirement of a relatively large aperture and the physical length limitation of the cavity. Originally, a design based on the ELBA buncher cavity design was considered, since that design was chosen for ERLP at least in part due to its lower power requirements [39]. By choosing a toroidal cavity geometry, however, we were able to improve the shunt impedance of the cavity by a factor of 3 over the ELBA buncher cavity [40].

The injection line will contain vertical steering magnets to give the bunches a nonzero vertical amplitude. It will also approximately match the beam from the ERLP (beta functions in the 1–10 m range) to EMMA (beta functions in the 0.2–1.0 m range). Precise matching may not be so important since the beam size will be small compared to the dynamic aperture that we wish to probe. We will also use the injection line to characterize the incoming beam (again, this may not be needed to high precision as long as the beam remains point-like on the scales of interest).

There will be extensive diagnostics in the main EMMA ring. Every cell will have two sets of BPMs (except for cells containing a septum, which will only have one set), each set of BPMs consisting of four button BPMs for obtaining horizontal and vertical position. The BPMs must be kept far from the rf cavities, but doing so places the BPMs in a non-optimal position. Thus, the two sets of BPMs will be placed in different locations in different cells, depending on whether or not the cell contains an rf cavity. Additionally, the main EMMA ring will also have two optical transition radiation
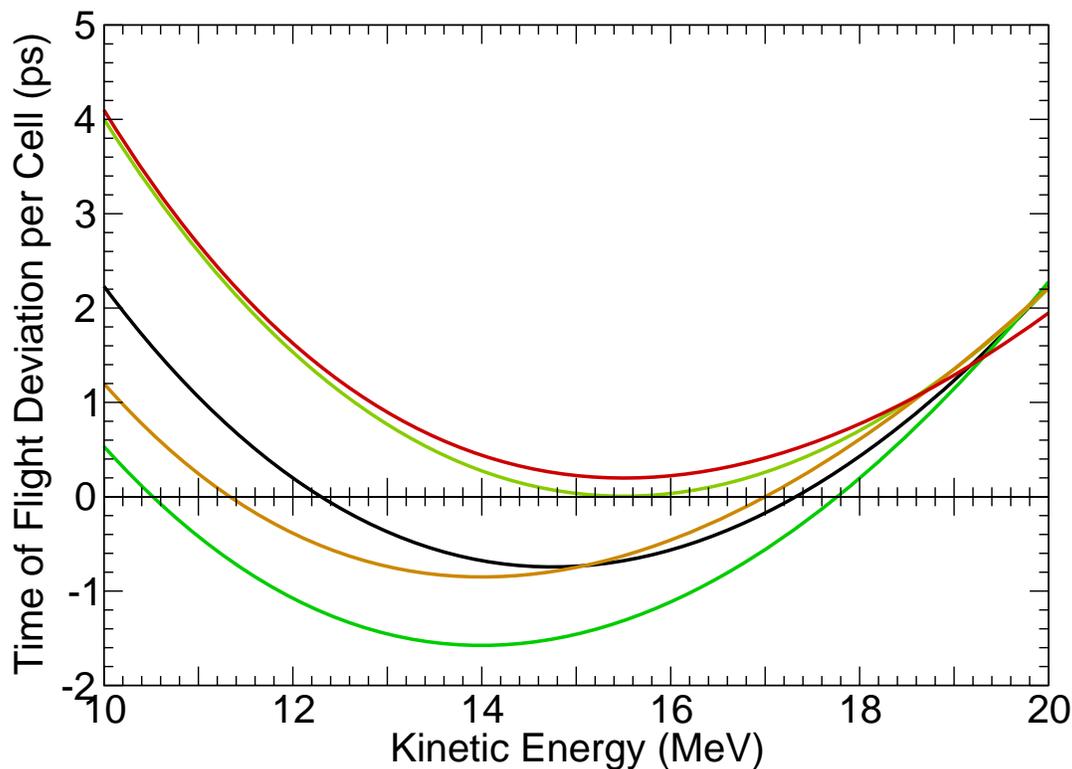
Figure 6: Varying the energy of the minimum time of flight.

screens and two wire scanners which can be inserted and removed as needed, as well as a resistive wall monitor.

The main EMMA ring will also contain 16 vertical corrector magnets to correct any vertical closed orbit distortion. The number 16 is dictated by space considerations: cavities and some other devices in the long straights will not leave room for the vertical correctors. Horizontal closed orbit distortion will be corrected using the mechanisms that we have for adjusting the machine configuration, to be described shortly.

The extraction line from EMMA will also contain extensive diagnostics, so that we can determine the longitudinal and transverse distribution of the beam after acceleration. The goal will not be to measure the distribution in the small emittance ERLP beam, but to reconstruct what happens to a larger emittance beam using several runs with different initial conditions.

4.7.4   Varying the Machine Configuration

The goal of EMMA is confirm our understanding of the dynamics in a linear non-scaling FFAG. To do that, we have designed the machine to be able to vary the machine parameters.

4.7.4.1   *Magnetic Field Variation*

Changing amongst most of the machine configurations requires the ability to independently vary the dipole and quadrupole components of the magnets. For the purpose of changing the configuration, all magnets will be varied in the same way. The best way of obtaining a linear field profile with a dipole component for this machine
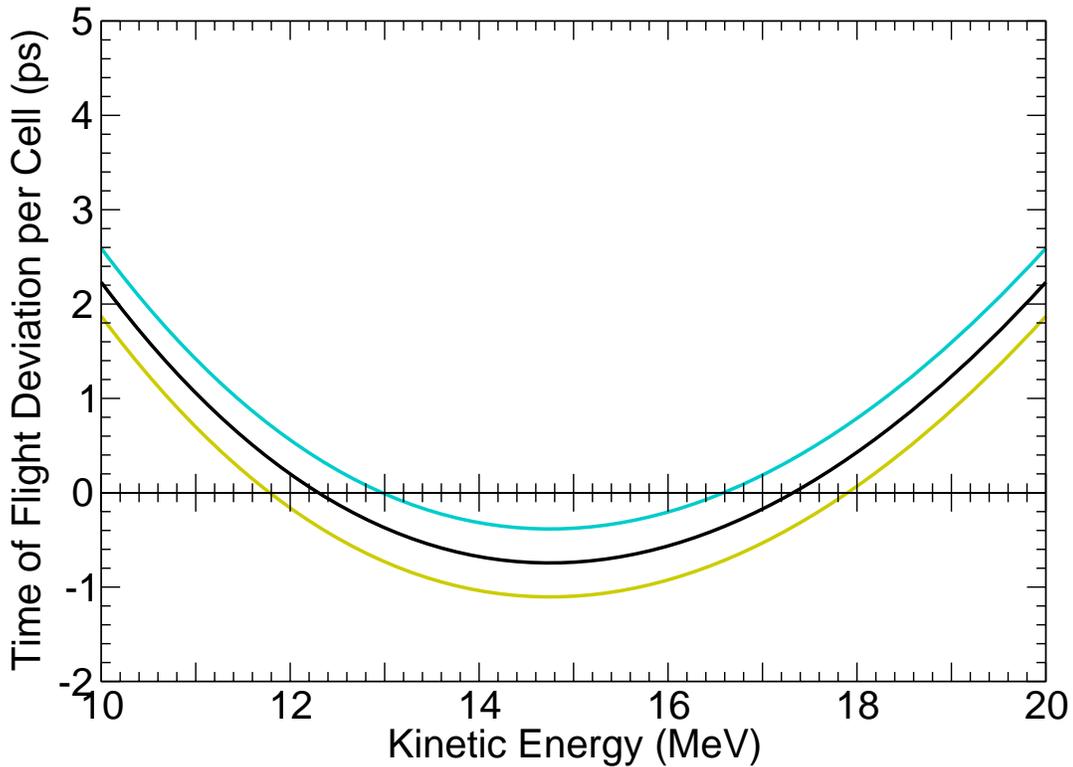
Figure 7: Time of flight as a function of energy, varying the rf frequency. Zero time means that the particle following the energy-dependent closed orbit is synchronized with the rf.

seems to be using quadrupole magnets with their centers displaced horizontally from the beam orbit. The magnets are on horizontal sliders that allow their positions to be controlled, thus allowing the dipole field to be varied relative to the quadrupole field. The quadruople fields can be controlled by the coil currents, thus giving independent control over the dipole and quadrupole fields.

Horizontal correctors are not necessary since the sliders will allow magnet displacements to be corrected and/or dipole corrections to be added directly. Magnets will be powered in series, keeping the fields identical to the extent that the magnets are identical. Any significant gradient errors will be corrected by placing shunts on individual magnets. Dipole and quadrupole errors will be intentionally introduced in the same way to study their effects.

When varying the tune profile with energy (see Fig. 1), the quadrupole components must of course be varied, but the dipole components will also be adjusted to maintain a similar time of flight versus energy profile for all the configurations (similar to Fig. 2). In addition, we will adjust the shape of the time of flight as a function of energy by varying the dipole and quadrupole components, so that the minimum of the time of flight moves to lower or higher energy (see Fig. 6). This is important for studying the longitudinal dynamics: since the time of flight is not precisely a symmetric function of energy, the minimum time of flight will not be at the central energy for the optimal configuration. We should confirm that we understand the effect of changing the location of that minimum. We will only vary the location of the minimum energy for the lattices with the highest horizontal tunes, since doing so for lattices with lower tunes will increase the aperture requirements for the magnets and rf cavities significantly.
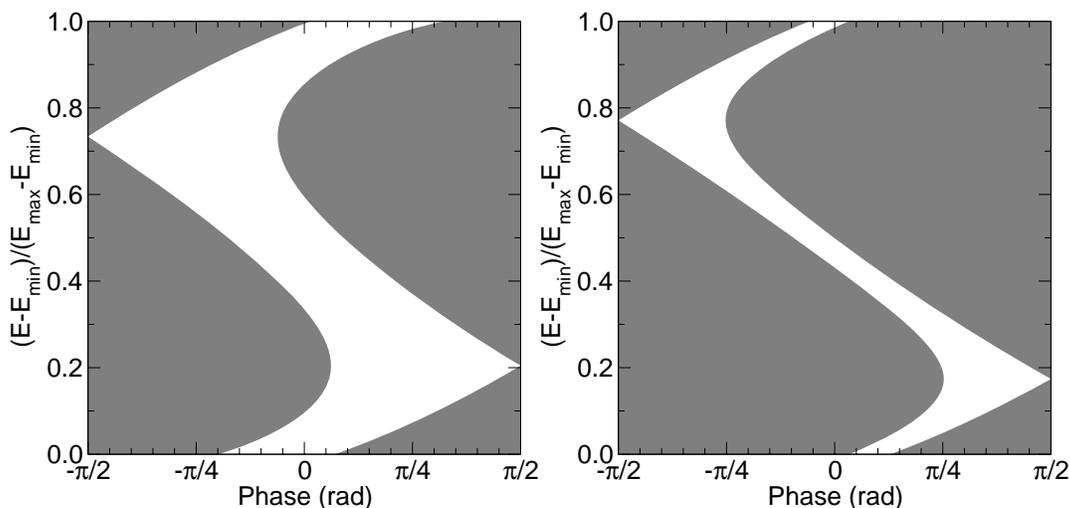
Figure 8: Longitudinal phase space when the time of flight is synchronized with the rf at different energies. The white region is the region of phase space through which particles are transmitted.

4.7.4.2   RF Parameters

Varying the rf parameters is essential for studying the longitudinal dynamics. It will also be important in the commissioning of the machine and other machine studies.

By varying the rf frequency, we can change the energy at which the bunches are synchronized with the rf (see Fig. 7). This is equivalent to varying the *b* parameter in [32], and has a significant effect on the longitudinal phase space (see Fig. 8). Furthermore, during the commissioning process, it will be important to have the rf frequency synchronized to the time of flight at any energy within the operating range of the machine. This will allow running at fixed energy to ascertain the tunes and the time of flight on the closed orbit. It will also allow studies of individual resonances. These considerations determine the range over which the cavity and power source rf frequencies must be varied.

Similarly, we will study the effect of the rf amount of rf voltage on the longitudinal dynamics. One of the parameters determining the dynamics (*a*, see [32]) is proportional to the rf voltage. Since the range of times of flight varies when the machine tune range is changed, and since *a* is inversely proportional to that time of flight range, to have the same longitudinal dynamics, the different tune range configurations will need to have different rf voltages. Furthermore, since we wish to explore how the longitudinal dynamics varies with *a*, we also want to be able to vary the rf voltage for a given lattice configuration. We will have sufficient voltage to double *a* from its baseline value. A later upgrade may supply more rf power to further increase that value, since the phase space changes for values of *a* above 1/6.

4.7.5   Funding and Time Frame

The EMMA machine is part of a larger project for the study of FFAGs known as CONFORM. CONFORM has three parts: EMMA, the design of a proton machine for medical applications, and the study of FFAG applications. More information is available at http://www.conform.ac.uk/.

Table 2: Range of machine parameters required for all configurations.

	D	F	Cavity
Central Axis Shift			
Minimum (mm)	28.751	4.903	0.439
Maximum (mm)	48.559	10.212	0.439
Aperture radius (mm)	55.975	31.850	34.751
Vacuum Chamber Apertures			
Minimum horizontal (mm)	-7.416	-21.638	-16.936
Maximum horizontal (mm)	18.789	20.700	17.814
Half height (mm)	11.676	8.906	10.571
Maximum gradient (T/m)	-4.843	6.847	—
RF Parameters			
Minimum frequency offset (kHz)	—	—	-4019
Maximum frequency offset (kHz)	—	—	1554
Maximum ring voltage (kV)	—	—	2286

The EMMA project itself began in March of 2007, and will take 3.5 years, and the machine will be operating for the last year of that. The total funding for EMMA is £5.6M, of which approximately £3.8M will be for the machine itself, the remainder being for staff.

4.7.6   References

1. Y. Mori, Nucl. Instrum. Methods A **562**, 591 (2006).
2. A. Sato *et al.*, in *Proceedings of EPAC 2004, Lucerne, Switzerland* (EPAC and European Physical Society Accelerator Group, 2004), p. 713.
3. A. Sato *et al.*, in *Proceedings of EPAC 2006, Edinburgh, Scotland* (EPAC and European Physical Society Accelerator Group, 2006), p. 2508.
4. D. W. Kerst *et al.*, Phys. Rev. **102**, 590 (1956).
5. K. R. Symon *et al.*, Phys. Rev. **103**, 1837 (1956).
6. L. J. Laslett, Science **124**, 781 (1956).
7. K. A., At. Energ. **1**(5), (1956) [Atomic Energy (Springer) **1**, 827 (1956)].
8. A. A. Kolomensky, Zh. Eksp. Teor. Fiz. **33**, 298 (1957) [Sov. Phys. JETP **6**, 231 (1957)].
9. A. A. Kolomensky and A. N. Lebedev, *Teoria Cikličeskich Uskoritelej* [*Theory of Cyclic Accelerators* (North-Holland, Amsterdam, 1966), p. 394, Ref. 31].
10. F. T. Cole *et al.*, Rev. Sci. Instrum. **28**, 403 (1957).
11. D. W. Kerst *et al.*, Rev. Sci. Instrum. **31**, 1076 (1960).
12. M. Aiba *et al.*, in *Proceedings of European Particle Accelerator Conference, Vienna, Austia, 2000* (EPS, Geneva, 2000), p. 581.
13. M. Aiba *et al.*, in *Proceedings of the 8th European Particle Accelerator Conference, Paris, 2002* (EPS and CERN, Geneva, 2002), p. 1028.
14. T. Adachi *et al.*, in *Proceedings of the Particle Accelerator Conference, Chicago, IL, 2001*, edited by P. Lucas and S. Webber (IEEE, Piscataway, NJ, 2001), p. 3254.
15. S. Machida *et al.*, in *Proceedings of the 2003 Particle Accelerator Conference,*

edited by J. Chew, P. Lucas, and S. Webber (IEEE, Piscataway, NJ, 2003), p. 3452.

16. M. Tanigaki *et al.*, in *Proceedings of EPAC 2004, Lucerne, Switzerland* (EPAC and European Physical Society Accelerator Group, 2004), p. 2676.

17. M. Tanigaki *et al.*, in *Proceedings of EPAC 2006, Edinburgh, Scotland* (EPAC and European Physical Society Accelerator Group, 2006), p. 2367.

18. N. Holtkamp and D. A. Finley, editors, Fermilab report FERMILAB-PUB-00-108-E (2000).

19. F. E. Mills and C. Johnstone in the transparency book for the 4th International Conference on Physics Potential & Development of $\mu^+\mu^-$ Colliders, Sanfrancisco, CA (UCLA, Los Angeles, CA, 1999), pp. 693–698.

20. C. Johnstone, W. Wan, A. Garren, in *Proceedings of the 1999 Particle Accelerator Conference*, edited by A. Luccio and W. MacKay (IEEE, Piscataway, NJ, 1999), p. 3068.

21. D. Trbojevic *et al.*, in *Proceedings of the Seventh International Conference on Cyclotrons and their Applications 2004, October 18–22, 2004, Tokyo, Japan* (Particle Accelerator Society of Japan, 2005), p. 246.

22. E. Keil, D. Trbojevic, and A. M. Sessler, in *Proceedings of the 2005 Particle Accelerator Conference*, edited by C. Horak (IEEE, 2005), p. 1667.

23. E. Keil, A. M. Sessler, and D. Trbojevic, in *Proceedings of EPAC 2006, Edinburgh, Scotland* (EPAC and European Physical Society Accelerator Group, 2006), p. 1681.

24. A. G. Ruggiero *et al.*, in *Proceedings of EPAC 2004, Lucerne, Switzerland* (EPAC and European Physical Society Accelerator Group, 2004), p. 159.

25. A. Ruggiero, in *High Intensity and High Brightness Hadron Beams: 33rd ICFA Advanced Beam Dynamics Workshop on High Intensity and High Brightness Hadron Beams*, edited by I. Hofmann, J.-M. Lagniel, and R. W. Hasse (AIP, 2005), p. 324.

26. G. Rees, Nucl. Phys. B (Proc. Suppl.) **155**, 301 (2006).

27. D. Trbojevic *et al.*, in *Proceedings of EPAC 2004, Lucerne, Switzerland* (EPAC and European Physical Society Accelerator Group, 2004), p. 932.

28. A. G. Ruggiero, T. Roser, and D. Trbojevic, in *Proceedings of EPAC 2006, Edinburgh, Scotland* (EPAC and European Physical Society Accelerator Group, 2006), p. 1547.

29. J. S. Berg *et al.*, Phys. Rev. ST Accel. Beams **9**, 011001 (2006).

30. A. A. Kolomenskii, Zh. Tekh. Fiz. **30**, 1347 (1960) [Sov. Phys. Tech. Phys. **5**, 1278 (1961)].

31. A. G. Ruggiero, Phys. Rev. ST Accel. Beams **9**, 100101 (2006).

32. J. S. Berg, Phys. Rev. ST Accel. Beams **9**, 034001 (2006). See references therein for earlier studies.

33. J. S. Berg, in *The International Workshop on FFAG Accelerators, October 13–16, 2004, KEK, Tsukuba, Japan*, edited by S. Machida, Y. Mori, and T. Yokoi (2005). URL http://hadron.kek.jp/FFAG/FFAG04_HP/. Preprint NFMCC-doc-309-v1, URL http://nfmcc-docdb.fnal.gov/cgi-bin/DocumentDatabase/.

34. D. Trbojevic and E. Courant, in *Fourth European Particle Accelerator Conference*, edited by V. Suller and Ch. Petit-Jean Genaz (World Scientific, Singapore, 1994), p. 1000.

35. M. W. Poole *et al.*, in *Proceedings of the 2003 Particle Accelerator Conference*,

edited by J. Chew, P. Lucas, and S. Webber (IEEE, Piscataway, NJ, 2003), p. 189.

36. M. W. Poole and E. A. Seddon, in *Proceedings of EPAC 2004, Lucerne, Switzerland* (EPAC and European Physical Society Accelerator Group, 2004), p. 455.

37. M. W. Poole and E. A. Seddon, in *Proceedings of the 2005 Particle Accelerator Conference*, edited by C. Horak (IEEE, 2005), p. 431.

38. D. J. Holder *et al.*, in *Proceedings of EPAC 2006, Edinburgh, Scotland* (EPAC and European Physical Society Accelerator Group, 2006), p. 187.

39. E. Wooldridge *et al.*, in *Proceedings of EPAC 2004, Lucerne, Switzerland* (EPAC and European Physical Society Accelerator Group, 2004), p. 467.

40. E. Wooldridge *et al.*, "RF Cavity Development for FFAG Application on ERLP at Daresbury," to appear in *Proceedings of PAC07, Albuquerque, New Mexico, USA.*

4.8   Design of an Isochronous FFAG Ring for Muon Acceleration

G.H. Rees
Mail to: ghrees@ukonline.co.uk or c.r.prior@rl.ac.uk
ASTeC Intense Beams Group, Rutherford Appleton Laboratory, Chilton, Didcot, Oxon OX11 0QX, U.K.

4.8.1   Introduction

Non-linear scaling, and linear non-scaling, FFAG ring designs may be developed into non-linear, non-scaling designs. The first two types have, respectively, zero and negative chromaticity, but the third may have more non-linearity than the first, allowing a positive chromaticity and the possibility of an isochronous, cyclotron design. Studies for such FFAG rings, one designed as an isochronous, 16 turn, 8 to 20 GeV, muon accelerator for use in a Neutrino Factory, and one for an electron ring model [1], are now outlined.

An FFAG ring allows more beam rotations than an alternative recirculating muon linac and so it needs fewer radio frequency (rf) accelerating systems (201.20 MHz is assumed). Some of the gain may be lost, however, unless the ring is made isochronous, to avoid the beam slipping in phase relative to the assumed, fixed frequency, accelerating fields. Since muon velocities vary little between 8 and 20 GeV, the orbit path lengths have to be nearly constant, scaling with velocity to high accuracy, for the isochronous ring under study.

The requirement for isochronism in a linear magnet lattice is that all 16 orbits have equal gamma-transition (γ_t) and relativistic gamma values, varying from 76.7 to 190.3 between the inner and outermost orbits. For a non-linear lattice, perfect isochronism requires orbits of all energies in the range 8 to 20 GeV, and not just the 16 ones specified, to have gamma equal to γ_t. In practice, use of some correction winding currents may be needed to minimise the effects of non-perfect isochronism.

Further means, beyond just the use of high horizontal betatron tunes, are needed to obtain the γ_t range from 76.7 to 190.3. Methods available to enhance γ_t are use of reverse bending units and (or) resonant excitation of the orbit dispersions. The former has proved adequate and so the latter has not been needed. An example of a resonant

method is the use of 3*n* FFAG cells (*n* integer), with the *n* identical groups of three cells having horizontal tunes just below unity, together with cell bending or focusing perturbations.

Isochronous designs have been sought that minimize the apertures of the superconducting magnets, employed to reduce the size of the ring. Three different magnet types are used in a non-linear lattice cell of five magnets. At 20 GeV, the cell acts like a *bFDFb* triplet with reverse *b* bends and positive bends in the *F* and *D* focusing units, while at the lower energies, the magnet gradients change gradually so that, at 8 GeV, the cell approximates a *dFBFd* triplet, with reverse bends in *d* and *F* units and positive *B* bends.

Each cell has space for both a magnet and a superconducting rf cavity cryostat, and the ends of the former are assumed to fill 0.8 m of the 4.80 m, long straight section provided.

The ring is assumed for use in a Neutrino Factory scenario which includes a low energy, cooling ring ahead of the muon acceleration stages, and where single muon bunches split into three in a 201.20 MHz rf system, receiving longitudinal and transverse cooling. This cooling aspect is desirable, though not essential, for operation of the isochronous ring.

4.8.2   FFAG Lattice Cell

Three different types of magnets are used in a symmetrical, cell configuration as follows:

<p style="text-align:center">O - bd - o - F - o - BD - o - F - o - bd - O</p>

Here *bd* and *BD* are both non-linear, horizontally defocusing, parallel edged, combined function units, but with *bd* and *BD* providing reverse and positive bending, respectively; *F* is a non-linear, horizontally focusing quadrupole, which provides positive and negative bending, respectively, for the muons with energies above and below ~ 11.51 GeV; and the muon orbit lengths at 20 GeV are as shown in the schematic cell drawing Figure 1:
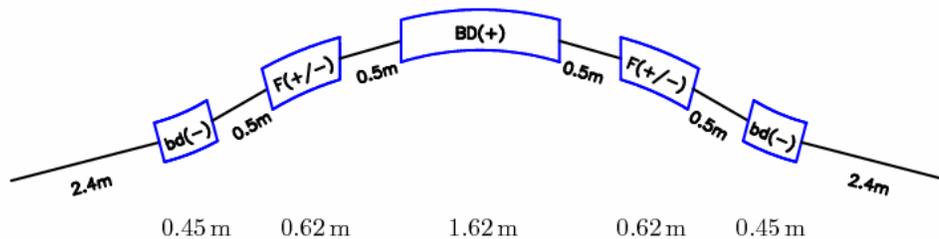
Figure 1: Schematic Layout of the 10.2 m Lattice Cell for the 20 GeV Orbit.

The orbit circumference at 20 GeV is 1254.6 m, assuming there are 3×41, identical cells, each of orbit length 10.20 m, with the multiple three in the number of cells kept to allow the possibility of resonant excitation studies. The sixteen orbits are far from being scaled; *bd*, *F* and *BD* give, respectively, -0.027, 0.0245414 and 0.028 rad muon angular deflections at 20 GeV, and -0.0373548, -0.0493242 and 0.1122204 rad at 8 GeV, with a net bending in each half cell of $\pi/123$ rad, that is ~1.463°.

The gradients of the non-linear bd, F and BD magnets are adjusted for each of the sixteen orbits and for three intermediate low energy orbits. At 20 GeV, the cell betatron tunes are ~ 0.384 horizontally and 0.14 vertically, whilst at 8 GeV, the corresponding tune values are ~ 0.196 and 0.083. Tunes are adjusted to obtain the required γ_t values, and this creates the large tune range. There results a wide orbit separation at low energy, while the orbits are closely packed at high energy.

The 4.8 m, *OO* sections house the injection, extraction and acceleration systems. A kicker for extraction is two cells upstream of a septum unit. There are 41 three-cell, 201.2 MHz rf cavities spread uniformly around the ring, giving an energy gain per turn of 750 MeV. During the acceleration, cavity beam loading is constant, without reactive components, providing a further advantage for an isochronous ring. As errors may arise in muon path lengths and beam rf phase, 13 single-cell, third harmonic rf correction cavity systems may be included for flat-topping the accelerating field waveforms.

4.8.3   Lattice Studies

A full lattice evaluation requires magnetic field simulations over a half cell, using a code such as Opera3D, followed by tracking of the muon input beam, either through the fields obtained or through derived fields, for sixteen ring revolutions. Repeated tracking would be required after any cell changes and, to be feasible, the initial values would have to give approximately isochronous conditions. Much simpler simulations may be used, however, to obtain a first guide to the non-linear field parameters of the cell magnets.

A linear lattice code may be modified to study the problem. Each orbit may be taken as a reference, starting with the orbit at 20 GeV, and searching for the adjacent one of a lower energy or for an intermediate energy. For the new orbit, revised values must be found for the following parameters:

- the magnet bending radii throughout the cell
- the bending angle for each magnet of the cell
- the beam entry and exit angle for each magnet
- the orbit lengths for each cell element, and
- the local value of the magnet field gradients

The lattice dispersion gives a first estimate for the adjacent orbit's position but with some errors due to the field non-linearities. To overcome this problem area, field gradients are assumed to change linearly between each adjacent pair of orbits, corresponding to local sextupolar field variations. New bending radii are then found from the average gradient between orbits and a weighted, momentum-normalized, average dispersion of the second orbit relative to the first and vice-versa, with the weighting chosen for exact orbit closure.

First, small amplitude lattice (Twiss) parameters are found for the 20 GeV, reference cell and these are adjusted as required. Next, for the adjacent or intermediate orbit, cell data is estimated repeatedly until a self-consistent set of output parameters, including the desired orbit γ_t value, is found. A few iterations are usually sufficient but more are needed when proceeding to low energies. Three homing routines are used, one for the tunes, one for exact orbit closure and one, of limited homing range, for the specified γ_t value. An intermediate orbit may be included between reference orbits to

improve the accuracies of the parameter estimates. A small orbit path length correction may be needed to make the orbit exactly isochronous, and the code displays this as output. In practice, it is assumed that such orbit corrections are applied via correction winding currents.

At 20 GeV, the non-linear lattice cell acts like a *bFDFb* triplet with reverse bend *b* units, an advantageous arrangement for reaching a high value of γ_t. It is not an optimum, however, for energies near 8 GeV, as isochronous γ_t values then require the choice of low betatron tunes, resulting in wide orbit separations at low energy. For this reason, *b* units are made as vertically focusing, *bd* magnets of very low gradient for 20 GeV orbits but with larger gradients as the orbit energies decrease, while *BD* units have the opposite gradient changes. At 8 GeV, the cell then acts like a *dFBFd* triplet, with reverse bends in the *d* and *F*, allowing increased betatron tunes and significantly reduced orbit separations.

4.8.4   Practical Issues

Many lattice cells are needed to obtain a γ_t of 190.29 for the 20 GeV orbit while keeping the horizontal betatron phase shift of the cell $\mu_h < 140^o$. An isochronous γ_t range with $\mu_h < 140^o$ is found by using 123 cells with reverse bend units and without any three-cell dispersion excitation. The choice of 123 cells allows a symmetrical ring arrangement for the 41 main accelerating cavities, with one unit in every third cell.

The *bd* units have a sector magnet edge, with a zero beam entry or exit angle at the ends of the long straight section, to ensure that the orbit path lengths in the straight do not vary with energy. The *bd* magnet is 0.45 m long and a shorter, higher field unit is not used as the *bd* length is only 50% larger than its good field aperture.

The lattice is designed so that the *BD* magnet has the maximum field and the smallest separation of reference orbits. The maximum orbit field occurs at 8 GeV, and is chosen at the relatively low value of 4.8 T to ease magnet design, reduce stored energy and increase reliability. In the non-linear *F* quadrupole, the maximum field is 2.66 T at the reference 20 GeV orbit. Despite this low field, an increase in the 0.62 m *F* magnet length is not considered because the local field gradient at the orbit is high (53.55 Tm^{-1}).

The total length for the five magnets in a cell is 3.4 m, but the enclosing cryostat is 6.2 m long. Free space in the 4.8 m straight section reduces to 4.0 m due to the cryostat ends, influencing the design of the injection and the extraction systems. Magnetic fields have to increase in the fast kicker and septum units and there is the added effect of the transverse size of the cryostat. However, the field rise time needed for the kicker magnets is more than a microsecond.

The choice of 4.8 m long straight sections allows the use of three-cell 201.2 MHz rf cavities in 3.0 m cryostats, with ~ 1.0 m left for gate valves, monitors and pumping units. Three cell cavities are chosen in order to reduce the number of main rf systems and their associated costs. In the case of the third harmonic 603.6 MHz rf cavities, used for flat-topping of the fields, single-cell units are proposed due to the higher frequency.

The short muon pulses are accelerated at the peaks of the field waveforms, with rf power needed to control the resistive beam loading. Except for the effect of muon decay losses, the pulsed loading of the cavities remains constant over the sixteen-turns of acceleration. This is in contrast to the case of a non-isochronous ring, where the phase slippage of the beam causes an additional, varying, reactive loading.

An electron ring model may also be considered to test some features of the proposed machine. Non-linear magnets must be used, so the design differs from that proposed for an electron model[1] of a linear, non-scaling, FFAG ring. A magnet lattice design for a 11.0 to 20 MeV electron model is given below, but many aspects of the model require to be studied, including the accuracies needed to obtain isochronous conditions, rf cavity beam loading, the effects of alignment errors, estimates for crossing of betatron resonance lines and the design of various ring systems.

4.8.5   Lattice Results and Summary

Results obtained assume the use of non-linear, superconducting magnets. Each *bd* unit is tilted relative to *BD* for sector entry at the *O* straight section ends, and adjacent edges of the *bd* or *BD* units and the *F* magnets are parallel. The *F* field is almost zero at

Table 1: Reference orbit separations in isochronous FFAG magnets

Energy (GeV)	9.5 to 20.0	8.75 to 20.0	8.0 to 20.0
bd unit (mm)	191.6	230.0	272.3
F quad (mm)	171.5	210.1	253.8
BD unit (mm)	114.6	143.7	177.5

11.51 GeV, and the orbit circumference at 20 and 11 GeV is 1254.60000 and 1254.56060 m, respectively. Examples for the reference orbit separations in the magnets are given in Table 1 corresponding to the cell structure:

O1, (bE1, bd, bE2), O2, (FE1, F, FE2), O3, (BDE, BD, BDE), O3, (FE2, F, FE1), O2, (bE2, bd, bE1), O1.

Details of the 20 and 11 GeV orbits are given Table 2, and results and a tune plot are laid out in Tables 3 and 4 and Figure 2. Here $\mu_h/2\pi$ and $\mu_v/2\pi$ are the local small

Table 2: Details of the 20 and 11 GeV muon orbits

Elements		Length (m)		Angle (rad)		K_v (m^{-2})	
		20 GeV	11 GeV	20 GeV	11 GeV	20 GeV	11 GeV
bd	cb-fun	0.45	0.450014	-0.0270	-0.041990	0.005	0.018
F	quad	0.62	0.618016	0.0245414	-0.004301	-0.79847	-0.4472
BD	cb-fun	1.26	1.260908	0.056	0.143665	0.56517	0.26248
bE1	E end	0.0	0.0	0.0	0.0	0.0	0.0
bE2	E end	0.0	0.0	0.027	0.041990	0.0	0.0
FE1	E end	0.0	0.0	0.027	-0.041990	0.0	0.0
FE2	E end	0.0	0.0	-0.028	0.071833	0.0	0.0
BDE	E end	0.0	0.0	0.028	0.071833	0.0	0.0
O1	straight	2.4	2.4	0.0	0.0	0.0	0.0
O2	straight	0.5	0.500259	0.0	0.0	0.0	0.0
O3	straight	0.5	0.501097	0.0	0.0	0.0	0.0

amplitude horizontal and vertical betatron tunes per cell, respectively; β_{hmax}, β_{vmax} and α_{pmax} are the maxima of the small amplitude cell horizontal and vertical lattice β-functions and dispersion function, in m; and *bd(T)*, *F(T)* and *BD(T)* are the average magnetic fields in Tesla on the closed orbit in the bd, F and BD magnets, respectively.

Table 3: Isochronous muon FFAG optical parameters.

T(GeV)	$\gamma = \gamma_t$	$\mu_h/2\pi$	$\mu_v/2\pi$	β_h max	β_v max	α_p max	bd(T)	F(T)	BD(T)
20.000	190.288	0.384	0.140	6.973	28.690	0.109	-4.024	2.655	2.981
18.500	176.091	0.337	0.130	6.947	27.590	0.130	-4.018	2.319	3.104
17.000	161.894	0.295	0.120	7.268	26.800	0.156	-4.003	1.951	3.253
15.500	147.698	0.261	0.110	7.977	26.260	0.190	-3.966	1.535	3.434
14.000	133.501	0.232	0.100	8.806	25.940	0.232	-3.881	1.046	3.651
12.500	119.305	0.204	0.091	9.836	25.620	0.291	-3.724	0.459	3.912
11.000	105.108	0.180	0.083	11.051	25.190	0.371	-3.456	-0.258	4.220
10.250	98.010	0.170	0.083	11.694	23.830	0.419	-3.263	-0.676	4.390
9.500	90.912	0.170	0.083	12.022	21.900	0.459	-3.006	-1.144	4.561
8.750	83.813	0.176	0.083	11.973	21.220	0.490	-2.663	-1.655	4.711
8.000	76.715	0.196	0.083	11.402	22.320	0.493	-2.244	-2.167	4.806

Table 4: Magnet gradients (normalized) and orbit displacements

T(GeV)	*Bd magnets*		*F magnets*		*BD magnets*	
	$K_v(m^{-2})$	X(mm)	$K_v(m^{-2})$	X(mm	$K_v(m^{-2})$	X(mm
20.000	0.005	130.043	-0.798	112.228	0.5652	71.412
18.500	0.015	120.888	-0.705	105.292	0.5143	67.857
17.000	0.030	108.956	-0.625	95.937	0.4641	62.720
15.500	0.060	93.118	-0.569	83.053	0.4170	55.180
14.000	0.100	71.814	-0.527	65.004	0.3701	44.000
12.500	0.140	42.313	-0.488	38.950	0.3196	26.945
11.000	0.180	0.000	-0.447	0.000	0.2625	0.000
10.250	0.205	-28.042	-0.431	-26.615	0.2322	-19.147
9.500	0.260	-61.547	-0.432	-59.264	0.1934	-43.214
8.750	0.320	-99.957	-0.426	-97.825	0.1385	-72.303
8.000	0.383	-142.269	-0.401	-141.556	0.0558	-106.125

4.8.6 Summary for the 8 to 20 GeV Muon Ring Design

A method has been found for estimating and optimising the magnet parameters of a non-linear, non-scaling, isochronous, FFAG ring for acceleration of muons from 8 to 20 GeV, over 16 turns with 750 MeV energy gain per turn, or over 12 turns with 1 GeV per turn. More rapid acceleration may also be considered by adding further rf cavities in the free straight sections of the ring. Simulation of muon beam acceleration over the energy range using the code Zgoubi [2] show encouraging preliminary results for both the isochronism and the effects due to the non-linear motion.

Each 4.8 m straight section has a 4.0 m free space between magnet cryostat ends, a length which is sufficient for the injection, extraction, vacuum, diagnostic and rf cavity systems. The length allows the use of just 41 three-cell cavities for the main rf systems. Another consequence of the choice of lattice is a ring filling-factor of one-third for the magnets.
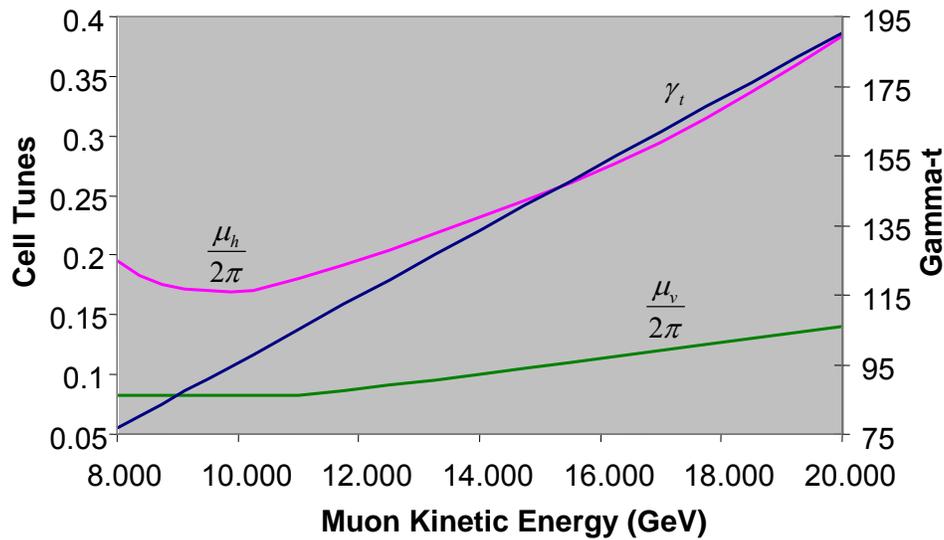
Figure 2: Cell betatron tunes and gamma-transition values as a function of muon energy.

An unusual ring feature is the gradual change of the focusing structure from a *dFd* triplet at 8 GeV to an *FDF* triplet at 20 GeV. This enables the superconducting magnet apertures to be minimised for the desired isochronous conditions, which are obtained by adjusting the local, small amplitude, lattice γ_t values.

There is a gradual change of the cell tunes each turn, as shown by the tune plot. It may be possible, at the lower energies, to reduce the horizontal tune variation and extend the zero vertical chromaticity region. The separations of the 8 and 20 GeV orbits in the *bd*, *F* and *BD* magnets are 272.3, 253.8 and 177.5 mm respectively, with the lowest orbit spacing provided for the magnets of highest field and greatest length, the *BD* units.

The muon kinetic energy range spans a ratio of two and a half to one and, assuming the same range is feasible in earlier acceleration, the following sequence may be considered: a 3.2 GeV muon linac; 3.2-8 GeV and 8-20 GeV, isochronous FFAGs. The final ring circumference of ~ 1254.6 m is larger than for many of the linear, non-scaling

designs for 10-20 GeV FFAG rings. Some of the increase is due to the larger space allocations and some to the use of five magnets per cell in place of a triplet/doublet cell. To describe the cell of five magnets, use is made of the term *pumplet* (pronounced "pimplet"[2]) cell.

The ring circumference may be reduced if it is possible to design matched cell insertions over the full energy range. Similar pumplet cells may be considered for both the arcs and insertions, but with shorter straight sections and changed non-linear fields in the arc cells.

The six-parameter lattice matching has to change for each turn, but this reduces to three-parameter matching because of the cell symmetry. Bending is required in the cells of the insertion to allow the dispersion matching. In addition, it is desirable to make both the arc cells and the insertion cells separately isochronous. Thus, for each FFAG turn, there are five separate requirements, and there are six magnet gradients that may be adjusted in the two types of pumplet cells. This allows for more flexibility than if the cells were based on triplet magnets. It remains to be seen, however, if satisfactory solutions may be obtained.

As an example of the possible reduction in cell circumference, consider an isochronous ring composed of four superperiods, each with twenty-one arc cells and nine insertion cells, for a total of 120 cells (compared to the 123 identical cells of the ~1254.6 m ring). Assuming cells of length 10.2 m (as before) for the insertion, but cells of length 6.4 m in the arcs, the circumference reduces to 904.8 m. There are the benefits of the reduced ring size and of localising the rf systems, but the possible disadvantage of the reduced ring periodicity with more dangerous resonance crossing.

A 45 cell 11-20 MeV electron model of the 123 cell, FFAG ring is presented in the next section, but significant experiments may be made with the following simpler e-models:

The isochronous properties of the cyclotron type design may be tested without having an rf system and complete ring. A linac output matching section may be followed by a number of ring cells, and the matching adjusted for each energy under study. Electron flight times would need to be measured, to better than one part in 10^5 at the energies of the proposed 15 turns. Three types of non-linear magnets, and a decision on the cell number, would be required.

Matching between non-linear arc cells and non-linear insertion cells may be studied downstream of the electron linac matching section. Isochronism tests and matching studies for all 15 proposed orbits would be required.

Resonance crossing studies would require installation of the full ring and rf systems.

4.8.7   A 15 Turn, 11 to 20 MeV, Electron Model for the Isochronous Ring

The same lattice structure is chosen as for the muon ring, but magnet lengths are reduced by a factor ten, and the (*o*) and (*OO*) straight lengths are, respectively, ~ 0.04 and 0.15 m. At 20 MeV, the orbit cell length is 0.65 m and the circumference for 45 cells is 29.250 m. An energy gain of 600 keV per turn allows electron acceleration from 8 to 20 MeV over 20 turns, or from 11 to 20 MeV over 15, and the latter is deemed sufficient.

---

[2] Based on the Welsh for five.

The frequency 3002.1 MHz is proposed for acceleration, at harmonic number 293, which may be compared with 842 for the muon ring (isochronism error relates to the harmonic). Every third cell houses an rf cavity, as for the muons, with each of the 15 units providing 40 keV, peak energy gain per turn. A single klystron powers the 15 units and the resistive beam loading. Straights in adjacent cells are available for both injection and extraction.

In comparison with the electron model proposed for a linear, non-scaling FFAG ring [1], the magnet apertures are similar for 0.3 mm normalised transverse rms emittances, with 3×rms maximum beam sizes of 14.1 mm vertically and 20.1 mm radially. The circumference is larger, however, with 5 magnets per cell instead of three, and 225 units total, as compared with 145. On the other hand, the rf system is much reduced with fifteen 40 kV cavities in place of the forty-five 78.5 kV cavities for the 5-turn linear electron FFAG model.

The nomenclature of the previous section is used for reference orbit separations, basic parameters and more detailed results. Examples of the reference orbit separations in the magnets are:

Energy (MeV)	12.2 to 20.0	11.6 to 20.0	11.0 to 20.0
bd unit (mm)	20.25	23.14	23.16
F quad (mm)	17.37	20.10	253.8
BD unit (mm)	10.5	12.43	14.54

Basic details for 20 and 11 MeV orbit lengths, orbit angles and normalised gradients are given in Tables 5 to 7.

Table 5: Details of the 20 and 11 MeV electron orbits

Elements		Length (m)		Angle (rad)		K_v (m^{-2})	
		20 MeV	11 MeV	20 MeV	11 MeV	20 MeV	11 MeV
bd	cb-fun	0.0225	0.022506	-0.036000	-0.048677	0.6000	39.0000
F	quad	0.0310	0.030428	0.033907	-0.006372	-86.9617	-64.8914
BD	cb-fun	0.0315	0.031642	0.037000	0.089955	62.6300	21.7293
bE1	E end	0.0000	0.000000	0.000000	0.000000	0.0000	0.0000
bE2	E end	0.0000	0.000000	0.072000	0.097354	0.0000	0.0000
FE1	E end	0.0000	0.000000	0.072000	-0.097354	0.0000	0.0000
FE2	E end	0.0000	0.000000	-0.074000	0.179910	0.0000	0.0000
BDE	E end	0.0000	0.000000	0.074000	0.179910	0.0000	0.0000
O1	straight	0.0750	0.075000	0.000000	0.000000	0.0000	0.0000
O2	straight	0.0400	0.040086	0.000000	0.000000	0.0000	0.0000
O3	straight	0.0400	0.040545	0.000000	0.000000	0.0000	0.0000

Table 6: Isochronous electron FFAG optical parameters

T(GeV)	γ = γₜ	μₕ/2π	μᵥ/2π	βₕ max	βᵥ max	αₚ max	bd(T)	F(T)	BD(T)
20.000	40.139	0.313	0.140	0.449	1.659	0.028	-0.109	0.075	0.076
18.800	37.790	0.287	0.130	0.472	1.634	0.031	-0.109	0.067	0.083
17.600	35.442	0.268	0.120	0.493	1.621	0.035	-0.109	0.059	0.086
16.400	33.094	0.251	0.110	0.514	1.617	0.039	-0.107	0.050	0.090
15.200	30.745	0.238	0.100	0.548	1.622	0.043	-0.105	0.040	0.094
14.000	28.397	0.224	0.100	0.580	1.491	0.048	-0.101	0.028	0.098
12.800	26.049	0.213	0.100	0.609	1.360	0.054	-0.095	0.015	0.103
11.600	23.700	0.206	0.100	0.629	1.227	0.060	-0.088	0.000	0.107
10.400	21.352	0.207	0.100	0.626	1.179	0.066	-0.078	-0.016	0.111
9.800	20.178	0.208	0.100	0.637	1.181	0.067	-0.073	-0.024	0.112

Table 7: Magnet gradients (normalized) and orbit displacements for the electron ring

T(GeV)	Bd magnets		F magnets		BD magnets	
	$K_v(m^{-2})$	X(mm)	$K_v(m^{-2})$	X(mm)	$K_v(m^{-2})$	X(mm)
20.000	0.600	13.153	-86.962	10.882	62.6300	6.361
18.800	2.400	11.396	-80.132	9.537	57.9267	5.658
17.600	6.600	9.271	-76.622	7.861	53.7044	4.729
16.400	12.000	6.726	-74.605	5.787	49.4150	3.532
15.200	18.000	3.680	-73.113	3.216	44.6535	1.994
14.000	24.000	0.000	-71.608	0.000	39.8940	0.000
12.800	30.000	-4.487	-69.615	-4.063	34.0099	-2.615
11.600	36.000	-9.983	-66.795	-9.218	26.4637	-6.065
10.400	42.000	-16.651	-62.485	-15.686	16.1550	-10.580
9.800	45.000	-20.432	-60.200	-19.186	11.4000	-13.281

4.8.8   References

1. E. Keil and A.M. Sessler, Muon Acceleration in FFAG Rings, CERN-AB-2004-033.
2. F. Méot and S. Valero, ZGOUBI Users' Guide, CEA DAPNIA SEA-97-1.

4.9   FFAG-based Proton and Heavy-Ion High-Power Drivers[*]

Alessandro G. Ruggiero
Mail to: agr@bnl.gov
Brookhaven National Laboratory, Upton, NY 11973, USA

4.9.1   Introduction

Recently High-Power Proton and Heavy-Ion Drivers have been proposed for a variety of applications, namely: Spallation Neutron Sources; Tritium Production; Nuclear Waste Transmutation; Energy Production by impinging a proton beam on a sub-critical fissionable nuclear core; production of Radio-Isotopes and Exotic Nuclear Fragments; high-intensity secondary beams such as Kaons and Muons for Nuclear and High-Energy Physics; and more. The proton beam energy, as well that of heavy ions, is not exceedingly large for these applications, ranging in the low to medium range from 1 to about 10 GeV. The required average beam intensity though is more demanding, ranging from at least 1 to possibly 10 MWatt, and above. Different modes of operation are also considered: low repetition rate of a few tens of pulses per second (Hz); high repetition rate of a few thousand pulses per second (kHz); and continuous mode of operation (CW), where the beam impinging on the target is essentially continuous, though it may have a microscopic time structure of several hundreds of MHz due to the rf method of acceleration employed.

There are several types of Particle Accelerator that can be used for the acceleration of intense hadron beams. These include Rapid-Cycling Synchrotrons (RCS), Super-Conducting Linacs (SCL), Cyclotrons, and Fixed-Field Alternating-Gradient (FFAG) accelerators. Microtron accelerators and Re-Circulators have an operation mode similar to FFAG accelerators. Also Cyclotrons are similar to FFAG accelerators, but have some major differences: for instance the energy span during acceleration, and the requirement for isochronous condition in the case of Cyclotrons. SCL's represent the ideal configuration for a high-power Proton or Heavy-Ion Driver, and are the most straightforward solution to adopt. However, they require considerable cryogenic and rf systems, and are expensive. RCS's on the other hand are expected to be more economical but are limited in repetition rate and have their performance limited by space-charge effects, especially at injection. FFAG accelerators are expected to perform in between SCL's and RCS's. The rf system needed for acceleration is considerably reduced to a fraction of that of a SCL, since the beam is accelerated in a few revolutions across the same rf cavity system. Whereas the beam is accelerated in one single pass in the SCL, and circulates for several thousand revolutions in the RCS, the beam is accelerated in the FFAG accelerator over a few tens or at most a few hundreds of revolutions. Thus the beam dynamics can differ markedly from one type of accelerator to the other. Recently acceleration of protons in FFAG accelerators has been demonstrated at KEK [1] and KURRI [2], in Japan, up to an energy of 150 MeV. It is the prevailing opinion now that FFAG accelerators are very attractive, compete well with respect to cost and performance, and can certainly be effectively used for the acceleration of high-intensity proton and heavy ions beams.

4.9.2 Main Features of FFAG Accelerators

The most important feature of the FFAG accelerator is that the guiding magnetic field, bending and focusing, is kept constant with time, as in Cyclotrons, Microtrons and Re-Circulators, and thus does not need to be ramped during the acceleration cycle as in the case of RCS. Thus the acceleration rate is not limited by the magnetic field but by the accelerating rf system itself. Because of the higher repetition rate, higher beam power can be achieved with lower beam intensity. Let I denote the average beam intensity on the target and E the final kinetic energy, then the average beam power is $P = EI$. In turn, denoting by N the number of particles accelerated per pulse and f the repetition rate, we have $I = Nef$ or $P = ENef$, which clearly shows that indeed the same power can be achieved with a higher repetition rate and lower intensity per pulse.

At the same time, because the magnetic field is kept constant, and has a limited range across the radial aperture, the momentum excursion between injection and extraction is reduced when compared to the range that can be achieved in an RCS. Depending on the ring lattice choice, the momentum range accepted in the acceleration cycle is at most $\Delta p/p = \pm 30$ to $\pm 50\%$. Thus depending on the application and the required energy range, the accelerator complex can be made of a single or two or even three FFAG rings of the same circumference and structure concentric to each other, to ease the transfer, and all located in the same enclosure. Figure 1 is the actual configuration of the three FFAG rings in the KURRI facility for the final energy of 150 MeV, and Figure 2 is a proposed Proton Driver for a Neutrino Factory also comprising 3 FFAG rings [3] for a final energy of 12 GeV.

4.9.3 Proposed Projects with FFAG Accelerators

Table 1 gives the summary of five proposed proton FFAG accelerators. The first (A) is the 1.5 GeV FFAG proposed as a new injector [4] to the Alternating Gradient Synchrotron (AGS) at Brookhaven National Laboratory (BNL) for the power upgrade program; the second (B) is a pulsed Proton Driver at low repetition rate for the Neutrino Factory as it has been proposed by the International Scoping Study [3]; the third (C) is a very high power Proton Driver operating in CW mode also proposed for the Neutrino Factory but with a different mode of operation to circumvent problems with target and cooling [5]; the fourth (D) is a low energy accelerator, operating at very high repetition rate and also in CW mode, for energy production [6]; and the last (E) is a similar FFAG complex for the acceleration of ions of Uranium 238 for Rare-Isotopes production [7].

Table 1: Examples of proposed FFAG-based Proton and Heavy-Ion Drivers.

Project	A	B	C	D	E
Final Energy, GeV(/u)	1.5	12	12	1	0.40
Inj. Energy, MeV(/u)	400	400	400	50	15
Rep. Rate	2.5-5.0 Hz	50 Hz	CW	1 kHz-CW	1 kHz-CW
Ave. Power, MW	0.050	4	100	10	0.40
Ave. Current, mA(-ion)	0.033	0.33	8.5	10	0.0042
No. of Rings	1	3	3	2	2
Circumference, m	807	807	807	204	204

Figure 1: Kyoto University FFAG for ADSR

The only FFAG project (not shown in Table 1) actually built and being commissioned is the KURRI project [2]. It represents a practical demonstration of the principles of operation of a low-energy FFAG with a well-defined application to generate a proton beam to drive a sub-critical nuclear core, and to study the neutronics for fission power production. There is a plan to complement it in the future with one more FFAG ring to reach the energy of 1 GeV. The present layout is shown in Figure 1. Its massive distribution of magnets is reminiscent of a cyclotron, though with obvious differences in detail.

Project A, in the second column of Table 1, was conceptually studied and proposed as the new injector to the AGS replacing the 1.5 GeV Booster for the upgrade program to an average beam power of 1 MW at 28 GeV [4]. Its design has been taken as the reference for all other similar projects of Table 1 that were derived with convenient scaling rules [8]. Projects B and C are proposals of high-energy Proton Drivers for a Neutrino Factory (and Muon Collider) [3, 5]. They are similar as they share the same magnet lattice design and configuration, and are both made of the same identical FFAG rings shown schematically in Figure 2. But they differ in the mode of operation and handling of the beam. Project C is a very high power proton source proposed for CW operation, whereas project B has a more modest average power pulsed at a relatively lower repetition rate. We shall not discuss here the motivations and the rationalities of these two approaches, but we take them as examples of different acceleration schemes
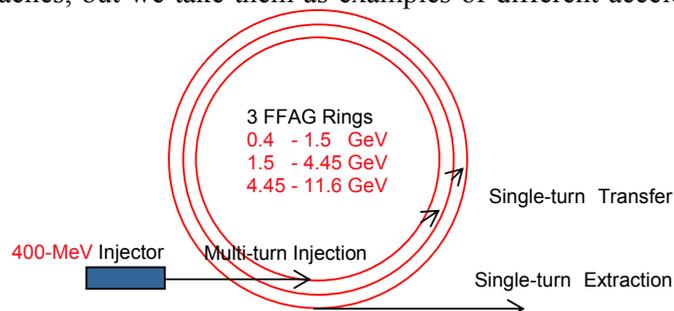
Figure 2: Schematic layout of a proposed FFAG for a Neutrino Factory.

we shall discuss later. Similarly, projects D and E have identical FFAG ring layouts with the same lattice and magnet configurations [6, 7]. They are both for relatively lower beam energy and represent examples of how the same FFAG accelerator complex can be used for acceleration of protons and of heavy ions (Uranium 238). Again the main difference is in the beam manipulation and performance, and in the rf method of acceleration.

Apart from these projects, FFAG accelerators have also been proposed for the acceleration of low-energy protons and light ions for Medical applications [9], and, recently, for the Radiography of sensitive material.

4.9.4   FFAG Magnet Configurations

There are several types of FFAG configuration, but mostly they fall into two categories: *Spiral* and *Radial* FFAG's, and sometime a combination of both [10]. In the *Spiral* configuration the Alternating Gradient (AG) focusing is provided by properly shaping the entrance and exit profiles of the magnets, as focusing is given primarily by the edge effect. In the *Radial* configuration, magnets are typically sector-shaped with a radial field profile in the body of the magnet itself. In the latter case there are two possible choices of magnet configuration: the *Scaling Lattice* (SL) and the *Non-Scaling Lattice* (NSL) [11]. The SL has a hyperbolic field profile with a field index set such that the chromaticity, that is the variation of the lattice functions with beam momentum, is fully compensated. On the other hand, the NSL does not compensate for the chromaticity since the field profile is linear with a constant gradient in each magnet. As a consequence, there is a large variation of betatron tunes with the beam momentum sweeping across several integral and half-integral resonances during the acceleration cycle, some of them even driven by the space-charge forces [12]. There is of course concern about the beam stability and survival in this situation, but conversely one expects that if the acceleration rate is large enough, say a few tens or few hundreds of revolutions, no harm is done to the beam. In contrast to FFAGs with SL that have been demonstrated in practice at KEK and KURRI [1, 2], those with NSL still await a practical demonstration. Recently a scaled-down FFAG model has received DOE funding to be studied simulating the motion of protons with low-energy electrons in the same velocity and space-charge range [13]. All the examples of Table 1 are of the NSL type.

A direct comparison between the two types of lattice has not been carried out yet and certainly needs to be understood. Aside from the beam dynamics issues that are different in the two cases, the FFAG with SL allows fewer magnets but with a larger radial aperture, prefers DFD triplets, and is more compact, smaller in size though at the cost of larger bending field. At the same time the FFAG with NSL has considerably more magnets but with narrower radial aperture, prefers FDF triplets, and allows longer drifts for insertion devices like rf cavities, injection and extraction components, and collimators. FDF Triplets have been proven to be very effective in strong focusing systems with very low amplitude and dispersion functions [14].

Below we shall describe FFAG with NSL and Linear Field profile (LFP), though also cases with Non-Linear Field Profile (NLFP) have been studied to compensate or at least reduce the variation of betatron tunes with the beam momentum [15, 16]. Though these lattices have a good chromatic behaviour, nevertheless because of the field nonlinearities, they may suffer exceedingly high aberration problems when the betatron

tunes and other lattice parameters vary strongly with the amplitude of the betatron motion.

4.9.5   Non-Scaling FFAG Accelerators with Linear Field Profile

Figure 3 shows a sequence of FDF Triplets that make a NLS FFAG with LFP. The beam is injected on an orbit placed on the inside of the ring, spirals during acceleration toward the outside, and is extracted from an outer orbit. There are two major drifts: a long one, *s*, and a minor one, *g*, that separate the magnets. These are sector magnets with parallel entrance and exit faces. The field profile is linear, namely a superposition of a dipole and a quadrupole (shifted) field. The reference orbit is commonly taken to be at injection. Other solutions [17] have also been proposed with periods made of five magnets (dFDFd) called *Pumplets* with either LFP or NLFP (see later articles).

As one can notice from Table 1 there are two distinct circumferences: a major one of 907 m that corresponds to the reference design based on the AGS circumference, and a minor one of 204 m for the lower energy cases. Table 2 gives a list of the main magnet lattice parameters for the two circumference cases. The optimum design, that ensures beam stability over the required momentum range and reasonable magnet size and drift lengths, requires a periodicity as large as possible, compatible with the operation, and also a large circumference to reduce the betatron tune splitting caused by the curvature effect. A lower periodicity makes the lattice unstable at the high-energy end, and a higher periodicity could make the lattice impractical. Two main parameters are the length *s* of the long drift that should be long enough to accommodate rf cavities, collimators, and injection and extraction components, and the radial width *w* required for the momentum excursion during acceleration. The width *w* is to be small enough to match the radial extension of the rf cavities especially in the case of very high frequency.
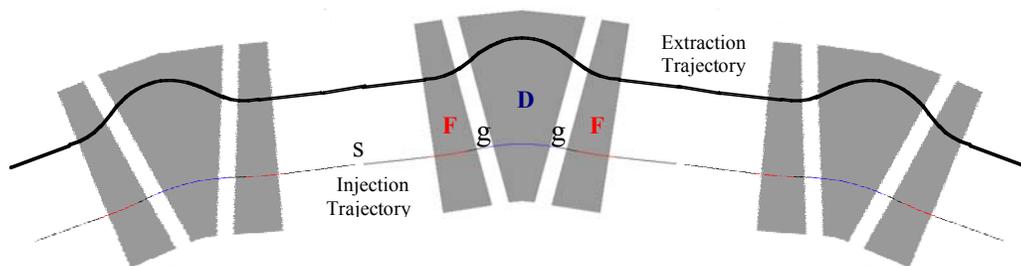
Figure 3: The FDF-Triplet Period of a FFAG Ring.

4.9.6   An Example of FFAG Accelerator

As an example, Figure 4 gives the plot of the lattice functions along the length of one period for the low-energy proton FFAG project D of Table 1. Because of the adoption of the NSL, the lattice functions vary with energy, as is shown by the variation of the betatron tunes during acceleration in Figure 5. To the left of the same Figure, closed orbits are plotted at different momenta in the acceleration cycle along the length of one period. From these plots we can infer the required radial excursion *w*. Figure 6 gives the magnetic field profile in the two sector magnets for both FFAG rings. The off-

momentum variable δ = (p − p_{inj}) / p_{inj} is used as the abscissa of Figure 5, where p is the actual particle momentum and p_{inj} the value at injection. At extraction δ_{ext} = (p − p_{inj}) / p_{inj} = 1.35 corresponding to a relative momentum range Δ ≈ ± 40% in all proposed FFAG rings. The magnetic packing factor, defined as the ratio of the total length of the magnets in one period over the length of the period itself, is 47.2% and the same for all FFAG rings.

Table 2: Structure of the FFAG Rings.

Projects	A, B, C	D, E
Curcumference, m	907	204
Number of Periods	136	80
Period Length, m	5.93	2.55
Long Drift *s*, m	2.534	1.089
Short Drift *g*, m	0.30	0.129
F-Sector Arc Length, m	0.70	0.301
D-Sector Arc Length, m	1.40	0.602
Radial Width *w*, cm	17.3	11.2
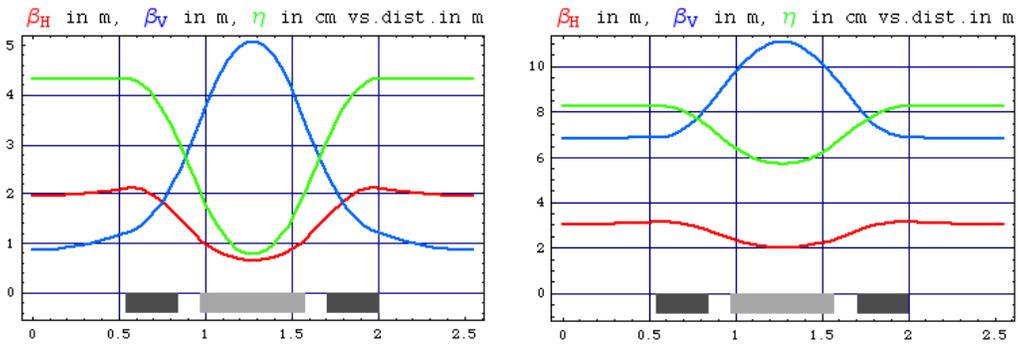
Figure 4: Lattice Functions along the length of a period (Project D).
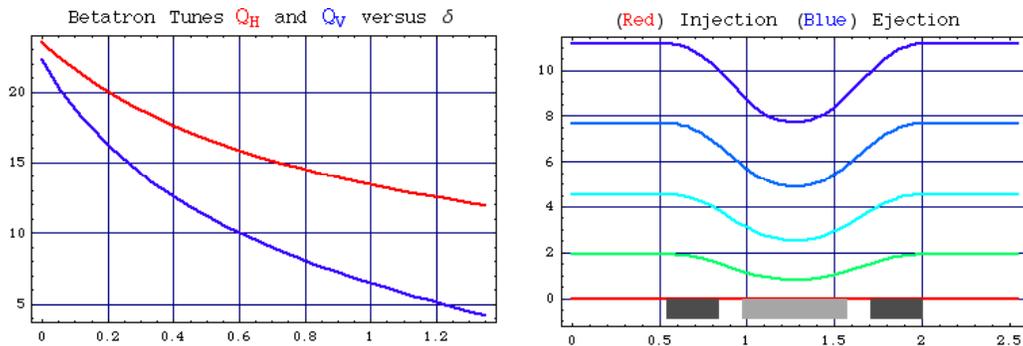
Figure 5: Betatron Tunes and Closed Orbits during the Acceleration Cycle (Project D).
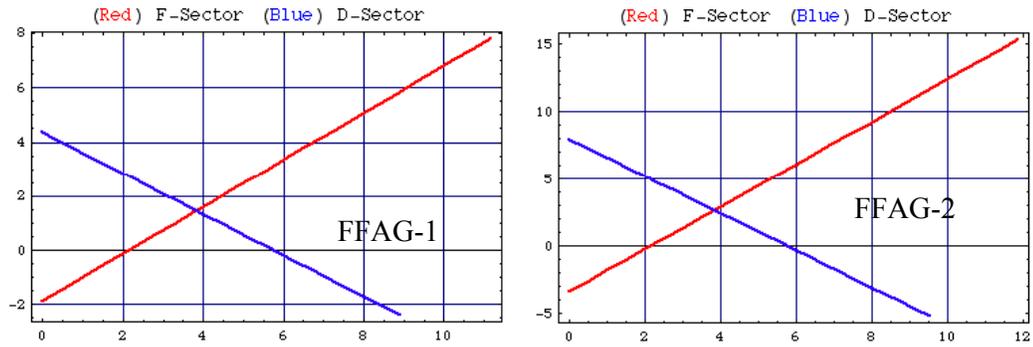
Figure 6: Field Profiles (kG) in the two FFAG Rings vs. Radial location x (cm) (Project D).

4.9.7   Acceleration Methods

In the case of acceleration in the low-energy range of heavy particles like protons and, even more, ions of Uranium, the beam velocity varies considerably during the acceleration cycle. A fast acceleration, frequency-modulated rf cavity system, like those using ferrite, will not do the job well, except for cases with low repetition rates. An alternative is to use broad-band, constant frequency rf cavities, such as those used in the J-Parc accelerator complex [18]. In this case the rf frequency is relatively low (a few MHz), and the voltage is only a few tens of kVolt per cavity. Another approach that would allow a considerably higher repetition rate is the method of Harmonic Number Jump (HNJ) [19]. In this case the cavities have constant frequency in the hundreds of MHz range, and possibly in the GHz range. But this method requires a programmed energy gain per cavity crossing that can be obtained with an almost linear profile across the radial width of the cavity. The HNJ method needs of course to be demonstrated in practice. Ultimately the HNJ method could be used for a continuous beam mode of operation, since on a given orbit the beam is accelerated by a pre-programmed rf voltage, the profile being kept constant across the width of the cavity at all times, and all orbits can simultaneously be occupied by beam.

Another feature that distinguishes NSL FFAG accelerators from Cyclotrons is the lack of synchronous conditions that cannot be satisfied because of the strong focusing of the FDF lattice with transition energy well above the actual beam energy. The transit time between cavity crossings is essentially given by the beam velocity and only marginally by the change of the path length with momentum.

4.9.7.1   *Acceleration by RF Frequency Modulation*

Ferrite-driven rf cavities can be used for acceleration, but have a limitation on the frequency sweep that cannot exceed a few MHz/ms. Definitively they can be easily used for project A of the AGS-Upgrade program where the sweeping rate does not exceed a fraction of a MHz/ms. The rf, matching that of the AGS, is in the range 6 to 9 MHz, over an acceleration period of 7 ms. This applies also to project B with a repetition rate of 50 Hz. In this case, the rf frequency ranges between 36 and 50 MHz, spread over the three rings, and the sweeping rate also does not exceed a few MHz/ms. More problematic are projects D and E if they are required to operate with repetition

rates of about 1 kHz. Such higher repetition rates would boost the beam average power at modest beam intensity per pulse to avoid space charge limitations, but the required sweeping rate in this case is well above 10 MHz/ms, and very difficult to reach.

4.9.7.2   *Acceleration by Broad-Band Cavities*

It may be possible to operate projects D and E at a repetition rate of 1 kHz (or higher) with the use of Broad-Band cavities. Such cavities have been developed at KEK, Japan and operate at constant frequency. They are Finemet cavities (Magnetic Alloy), typically made of few gaps for a total length of about 60 cm, and a peak voltage of 20 kVolt in the middle of the frequency range that can be between 1 and 10 MHz. There is nevertheless a significant drop of voltage ($\sim$ 30%) on both sides of the bandwidth that may need to be compensated either with adjusted phase programs or by increasing the number of cavities. The actual accelerating field achieved in the Finemet cavity is close to 100 kVolt/m, but this value applies to the active region of the core. When the cavity is packaged in a multi-layer pancake, the actual accelerating gradient is diluted [20]. Because of the limited rf voltage that can be achieved in these cavities, a large number of them are required, essentially filling every available long insertion of the FFAG rings. The power consumption dissipated is also excessive. Broad-Band cavities have been proposed for the acceleration to 1 GeV in the future KURRI complex to reach a repetition rate of 120 Hz.

4.9.7.3   *Acceleration by Harmonic Number Jump*

A higher repetition rate not only is desirable to boost the beam power and to avoid problems with space charge and with multiple resonance crossing in the NSL FFAG, but also to ease the performance requirements of the ion source and of multi-turn injection into the first FFAG ring. For a higher repetition rate, we should consider a different rf system for acceleration. This is the method know as Harmonic Number Jump (HNJ) [19]. This method allows the use of superconducting rf cavities at very high constant frequency, in the range of several hundred MHz or even in the GHz range. Acceleration requires a programmed energy gain that varies between cavity crossings, to allow for the change of the transit time between cavities that corresponds to a *jump* of one or more rf harmonics. If f_{RF} is the rf frequency, obviously the relation $f_{RF} = h\beta c/C$ holds where h is the (local, that is between two consecutive cavity crossings) harmonic number, C the distance between cavities, and βc the beam velocity. In a synchrotron, the harmonic number h is kept constant; as the beam velocity βc varies, then the rf frequency f_{RF} is adjusted accordingly. The HNJ method, on the other hand, requires that f_{RF} is kept constant so that as the beam velocity βc changes the harmonic number h will have to vary accordingly. This can be achieved only with a proper program of energy gain between cavity crossings [21]. It should be pointed out that, since the harmonic number h reduces during acceleration, the number of beam bunches at injection into the first ring cannot be larger than then harmonic number at extraction from the second ring. That is, the beam injected into the first ring has a duration that is a fraction of the revolution period, given by the ratio β_1/β_2 of the initial to the final value of the beam velocity. Consequently the average current of the injected beam pulse is larger by the same factor of the average value over the whole circumference.
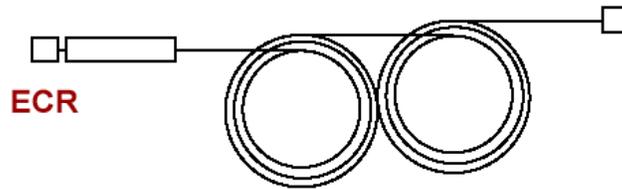
Figure 7: Continuous Mode of Operation for a Chain of two FFAG Rings

The HNJ method is very well suited for projects C, D and E. The method is described with more details in the accompanying paper included in this issue [21]. The HNJ method needs of course to be demonstrated in practice. There is an initiative in this direction at the KURRI complex where a 1 GeV upgrade is also proposed with acceleration by HNJ.

4.9.7.4   CW Mode of Operation

By extrapolation, the HNJ method of acceleration can be used for the more convenient and useful Continuous Wave (CW) mode of operation where the beam is continuously injected, accelerated and transferred to the Target [3, 7, 22]. The continuous injection will require that ions occupy simultaneously all orbits as they move in a spiral way in and out from one ring to the next as shown in Figure 7. No major objection or obstacles are foreseen to this mode of operation that, after all, resembles very closely that adopted in Cyclotrons, with the provision that one requires a method for injection and extraction with beam sitting on different orbits with enough separation from each other. This requires that the beam from the source, prior to injection into the first FFAG ring, is pre-chopped at the injection revolution frequency to allow for the gap corresponding to the ratio β_1/β_2 discussed above.

4.9.8   Outstanding Issues to be investigated with NSL FFAG Rings

The operation of a NSL FFAG needs a practical demonstration for the acceleration of intense proton and heavy-ion beams. Nevertheless no major objections are foreseen, and yet there a number of details that need attention and a closer investigation.

Considering the limited amount of drifts with sufficient length, multi-turn injection of protons by charge exchange into the first FFAG ring needs to be designed and demonstrated. For the case of heavy-ions one needs to resort to the old-fashioned betatron stacking. An alternative is to find a way somehow to transfer the beam from the ECR in a following EBIS structure where it can be stored, and eventually continually ionized, by the electron beam [7]. Then once enough ions have been stored, the beam is extracted from the EBIS in a single pulse and transported through the RFQ and the Linac prior to injection into either one of the FFAG rings. Similarly the beam needs to be extracted, always fast and in a single turn. Space should also be considered for collimators to eliminate uncontrolled beam losses to avoid dangerous activation of ring components.

All the Proton Drivers considered have serious space-charge limitations at injection that need to be investigated. Space-charge forces themselves create systematic low-order resonances that particles may have to sweep through during acceleration [12]. The multiple resonance crossing is also a serious problem that can be overcome with fast acceleration.

Ferrite-driven cavities and broad-band cavities need to be understood better in their performance and limitations for acceleration. Similarly, despite the obvious advantages offered by the HNJ method of acceleration, there are still important issues to be studied, for instance how to create the required field profile, how to design and use a deflecting cavity for such an application.

The CW mode of operation of a proton and heavy-ion driver is possibly the most interesting. Yet it is important to demonstrate that is possible to inject and extract beam with turns sufficiently well separated as they circulate in the FFAG ring.

There are many other topics relevant to the performance, design and operation of a FFAG accelerator, including diagnostics, beam steering, magnet imperfections and misalignments.

4.9.9   References

1. M. Aiba, "Status of 150 MeV Proton FFAG", The Int. Workshop on FFAG Accel., page 3, Dec. 5-9, 2005, KURRI, Osaka, Japan.
2. M. Tanigaki et al., "Status of FFAG complex at KURRI", The Int. Workshop on FFAG Accel., page 1, Dec. 5-9, 2005, KURRI, Osaka, Japan.
3. A.G. Ruggiero, "FFAG Accelerator Proton Driver for Neutrino Factory", Nuclear Physics B (proc. Suppl.) 155 (2006) 315-317. Also BNL report C-A/AP/219, September 2005.
4. A.G. Ruggiero, Invited Talk to EPAC-04, July 2004, Lucerne, Switzerland.
5. A.G. Ruggiero, "An Alternative for the Neutrino Factory with a High-Power Proton Driver", BNL report C-A/AP/66, August 2001. Also in the Proceedings of Snowmass Workshop, Colorado, July 2001.
6. A.G. Ruggiero, "FFAG-based High-Intensity Proton Drivers", Proceedings of ICFA-HB2004, October 18-22, 2004, Bensheim, Germany, page 324.
7. A.G. Ruggiero et al., "Heavy Ion Driver with Non-Scaling FFAG", presented to PAC 2007, Albuquerque, New Mexico, June 2007. Also BNL report C-A/AP/219, June 2007.
8. A.G. Ruggiero, "Design of Proton FFAG Accelerators", The Int. Workshop on FFAG Accel., page 31, Dec. 5-9, 2005, KURRI, Osaka, Japan.
9. D. Trbojevic, "FFAG for Medical Application", contribution to this Issue of ICFA Beam Dynamics Newsletter.
10. A.G. Ruggiero, "Brief History of FFAG Accelerators", The Int. Workshop on FFAG Accel., page 9, Dec. 5-9, 2005, KURRI, Osaka, Japan.
11. J.S. Berg, et al., Invited Talk to the 17th Cyclotron Intern. Conf. Tokyo, Japan, October 2004. Also contribution to this Issue of ICFA Beam Dynamics Newsletter.
12. S.Y. Lee, et al., "Emittance Growth Mechanisms for the Space Charge Dominated Beams in the FFAG and Proton Driver Rings", New J. Phys. 8 291 (2006). See also this edition of the ICFA Beam Dynamics Newsletter.
13. S.M. Boucher, "MINHA", presentation made on the Semiannual 2007 FFAG Workshop, Grenoble, France, April 11-17, 2007, http://lpsc.in2p3.fr/congres/FFAG07/
14. D. Trbojevic and E. Courant, in *Fourth European Particle Accelerator Conference*, edited by V. Suller and Ch. Petit-Jean Genaz (World Scientific, Singapore, 1994), p. 1000.

15. A.G. Ruggiero, "Adjusted Field Profile for the Chromaticity Cancellation in FFAG Accelerators", Proceedings of ICFA-HB2004, October 18-22, 2004, Bensheim, Germany, page 324.
16. G.H. Rees, Nucl. Phys. B (Proc. Suppl.) **155**, 301 (2006).
17. G.H. Rees, contribution to this Issue of ICFA Beam Dynamics Newsletter.
18. Y. Yamazaki, "Approach to a very high intensity beam at J-PARC", HB2006 Proceedings, Tsukuba, Japan, May 29-June 4, 2006.
19. A.G. Ruggiero, Physical Review ST A&B **9**, 100101 (2006).
20. C. Ohmori, presentation made on the Semiannual 2007 FFAG Workshop, Grenoble, France, April 11-17, 2007, http://lpsc.in2p3.fr/congres/FFAG07/
21. A.G. Ruggiero, "Acceleration by Harmonic Number Jump", contribution to this Issue of ICFA Beam Dynamics Newsletter.
22. A.G. Ruggiero "CW Mode of Operation of a Proton FFAG Accelerator" BNL Internal Report, C-A/AP/218, September 2005.

4.10 RF Acceleration by Harmonic Number Jumps in FFAG Accelerators[*]

Alessandro G. Ruggiero
Mail to: agr@bnl.gov
Brookhaven National Laboratory, PO Box 5000, Upton, NY 11973, USA

4.10.1 Introduction

A very important feature of Fixed-Field Alternating-Gradient (FFAG) accelerators, as the name itself implies, is that the guiding and focusing magnetic field is constant during the acceleration cycle, that is, it does not need to be ramped with the beam energy. This greatly simplifies the design and engineering of the vacuum and power supply systems. But most importantly, the constancy of the field eliminates in principle any limitation to the acceleration rate other than that set by the accelerating rf system itself. We have described in a previous note [1] the use of FFAG rings for acceleration of protons and heavy ions with different repetition rates. Some projects have a low repetition rate ranging from a few to 50 Hz; others need to operate at 1 kHz or more; and others even in Continuous Wave (CW) mode. Moreover, the acceleration of protons and heavy ions in the low or medium energy range is characterized by a significant change of the particle velocity during the acceleration cycle. A certain relation between rf frequency f_{RF} and beam velocity βc has to apply for acceleration to be effective, that is

$$f_{RF} = h\,\beta c\,/\,C, \tag{1}$$

where C is the ring circumference, and h the so-called harmonic number, an integer. In a synchrotron, the harmonic number h is kept constant; as the beam velocity βc varies, the rf frequency f_{RF} is adjusted accordingly. This is accomplished with frequency–modulated rf cavities, loaded with ferrite. The frequency range typical with ordinary ferrite is from a few up to 50-60 MHz, beyond which the usefulness of ferromagnetic

---

material (ferrite) drops significantly. Moreover, there is a limitation for the attainable frequency sweep to a few MHz/ms, that in turn limits the accelerator repetition rate.

For higher repetition rates, kHz and more, one has to resort to a constant frequency method similar to that employed historically in Microtrons and Cyclotrons. This method was proposed about a half century ago (see Figure 1). The beam circulates within the gap of a dipole magnet that has also a field profile (gradient) for focusing. The beam crosses periodically the same rf cavity that operates at constant frequency (no ferrite) and voltage. At every crossing, there is an energy gain, and the trajectory path length on the next turn increases accordingly. An isochronous condition needs to be satisfied in order for the particle to experience the same voltage and phase every turn through the same rf cavity. The revolution period is $T = C / \beta c$. Differentiating for infinitesimal quantities around each orbit,

$$\Delta T / T = \Delta C / C - \Delta \beta / \beta. \qquad (2)$$

The isochronous condition requires $\Delta T = 0$ at every turn, that is, the velocity change $\Delta \beta$, caused by the energy gain, is compensated by the increase of the path length ΔC. In this situation, the frequency and the voltage of the rf cavity can be maintained constant. Kolomenskii [2] generalized the isochronous condition by allowing the change in transit time ΔT between two consecutive cavity crossings to be a multiple of the rf period, that is, $\Delta T = m \, T_{RF}$ with m an integer.
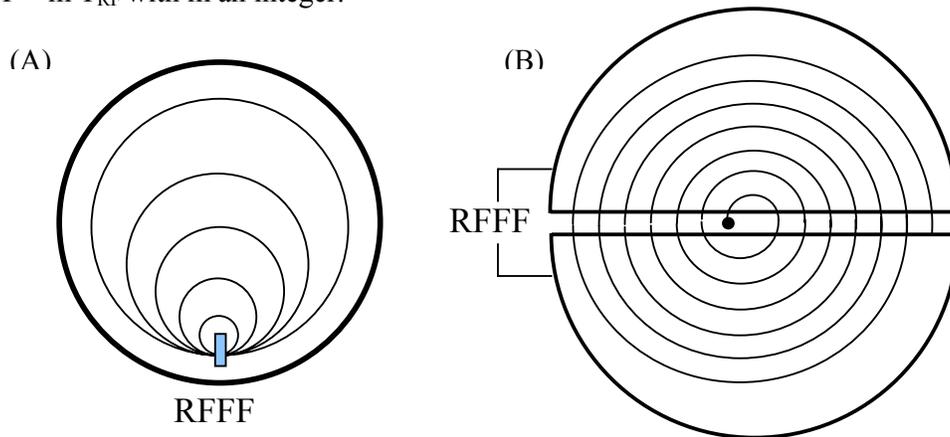
Figure 1: Sketch of a Microtron (A) where all the trajectories with increasing radii go through the same location of the accelerating rf cavity, and of a Cyclotron (B) where the trajectories spiral toward to larger radii and traverse a region where rf accelerating field is applied.

The isochronous condition cannot be satisfied in an FFAG accelerator with *Non-Scaling Lattice* (NSL) and *Linear Field Profile* (LFP), as discussed in the previous note [1]. The lattice, typically made of a periodic sequence of FDF triplets, has strong focusing, and allows only a modest variation of the path length with momentum that cannot compensate the much larger variation of the beam velocity. Thus, in such a ring it may not be possible to accelerate with an rf cavity system that at the same time has constant frequency and voltage. Obviously, to operate at large repetition rate we need an acceleration mode at constant frequency, eventually made of superconducting cavities that also create large accelerating gradients. But we have then to program the

energy gain that varies from turn to turn. We could still follow Kolomenskii's concept, and chose the energy gain per turn in such a way that the transit time between cavity crossings changes by a number of rf periods. This is equivalent to saying that every time beam bunches cross the cavity they skip a number of rf buckets; this is known as Harmonic Number Jumping (HNJ) [3, 4].

4.10.2 Acceleration of Synchronous Particles

The FFAG ring has M equally spaced localized groups of cavities each with N_c cavities, as shown in Figure 2. Each group of cavities applies a local, total energy gain that is a function of the beam energy at the moment of the n-th crossing. If acceleration is carried out with constant frequency, then the product $h\beta$ is also an invariant during acceleration. The variation of h with β can be calculated precisely on a computer, but here we use a linear approximation (a very good one indeed!).

The acceleration cycle can be thought of as a sequence of pair events: an energy kick V_n at the location of the n-th cavity, followed by an arc A_n that takes the beam from that cavity to the next.

Let us start by assuming that all particles have the same energy, and cross the cavities all together at the same instant. These are the *synchronous* or *reference* particles around which all other particles oscillate. The total energy of the reference particle in the n-th arc A_n is $\mathbf{E}_n$, and the period of time that it takes to travel the arc A_n is $\mathbf{T}_n = h_n T_{RF}$, where T_{RF} is the constant rf period, and h_n is the rf harmonic number local to the arc A_n. Here

Figure 2: Multi-Cavity FFAG Layout

and in the following bold face parameters apply to the *reference* particle. The same parameters in plain face apply to the other particles. Let Q and A denote respectively the charge state and the mass number of the ion particle. The energy gain when crossing the n-th cavity is

$$\Delta \mathbf{E}_n = (Q\ eV_n\ /\ A)\ \sin\ (\omega_{RF}\ \mathbf{t}_n) = (Q\ eV_n\ /\ A)\ \sin\ (\boldsymbol{\phi}_n) \tag{3}$$

where V_n is the peak voltage, $\omega_{RF}\ /\ 2\pi$ the rf frequency, $\mathbf{t}_n$ the instant of traversal of the cavity, and $\boldsymbol{\phi}_n = \omega_{RF}\ \mathbf{t}_n$ the rf *synchronous* phase. Both V_n and $\boldsymbol{\phi}_n$ can vary from cavity to cavity, and, in the same cavity, from turn to turn.

The HNJ method requires that the energy gain is adjusted to cause a change in the travel period $\mathbf{T}_n$ in the following arc A_n, so that the *reference* particle is pushed forward or back exactly by Δh rf harmonics and appears in an exactly identical bucket ahead or trailing by Δh rf wavelengths. Thus, denoting

$$\mathbf{T}_n\ =\ h_n\ T_{RF} \tag{4a}$$
$$\mathbf{T}_{n-1}\ =\ h_{n-1} T_{RF} \tag{4b}$$
$$h_n - h_{n-1} = -\ \Delta h, \tag{4c}$$

this is accomplished by requiring, in linear approximation,

$$\Delta\mathbf{E}_n = \beta_n{}^2 \gamma_n{}^3 E_0 \Delta h / h_n (1 - \alpha_{pn}\gamma_n{}^2) \tag{5}$$

where E_0 is the ion particle rest energy, β_n and γ_n the usual relativistic velocity and energy factors, and α_{pn} the momentum compaction factor local to the n-th arc A_n. The HNJ is executed by combining equations (3), (4) and (5).

4.10.3 Acceleration of Non-Synchronous Particles

Let us consider now an off-momentum particle following (or leading) the *reference* particle with a time difference τ_n. It will cross the n-th cavity at the instant $t_n = \mathbf{t}_n + \tau_n$, and the corresponding energy gain is

$$\Delta E_n = (Q\, eV_n / A) \sin (\omega_{RF}\, t_n). \tag{6}$$

Subtracting equation (3) from equation (6) gives the change in the energy difference $\varepsilon_n = E_n - \mathbf{E}_n$ after crossing the n-th cavity

$$\Delta\varepsilon_n = (Q\, eV_n / A) [\sin (\phi_n + \omega_{RF}\, \tau_n) - \sin (\phi_n)]. \tag{7}$$

In the limit of small delay τ_n

$$\Delta\varepsilon_n = (Q\, eV_n / A) (\cos \phi_n)\, \omega_{RF}\, \tau_n . \tag{8}$$

The change of the time delay, in linear approximation, is given by

$$\Delta\tau_n = \tau_n - \tau_{n-1} = (t_n - \mathbf{t}_n) - (t_{n-1} - \mathbf{t}_{n-1})$$
$$= T_n - \mathbf{T}_n = - (1 - \alpha_{pn}\gamma_n{}^2)\, \mathbf{T}_n\, \varepsilon_n / \beta_n{}^2 \gamma_n{}^3 E_0. \tag{9}$$

Combining equations (8) and (9) gives the phase (or energy) oscillation equation in the limit of small amplitude

$$\Delta^2 \tau_n / \Delta n^2 + \Omega_n{}^2 \tau_n = 0, \tag{10}$$

where the oscillation angular frequency [using equations (3), (5), (8) and (9)] is

$$\Omega_n{}^2 = 2\, \pi\, \Delta h / \tan \phi_n \tag{11}$$

4.10.4 Motion within RF Buckets

The two canonical equations, (7) and (9), can be derived from the following Hamiltonian

$$H = (Q\, eV_n / A\, \omega_{RF}) [\cos (\phi_n + \omega_{RF}\, \tau_n) + \omega_{RF}\, \tau_n \sin (\phi_n)]$$
$$- (1 - \alpha_{pn}\gamma_n{}^2)\, \mathbf{T}_n\, \varepsilon_n{}^2 / (2\, \beta_n{}^2 \gamma_n{}^3 E_0) . \tag{12}$$

The motion of all particles is to occur in rf buckets. The simple analogues for the usual equations for bucket fixed points, height and area [4, 5] may be obtained from the Hamiltonian of equation (12). There is though the exception that the energy gain per group of cavities is programmed according to the combination of equations (5) and (6). The rate of acceleration cannot be given *a priori*, but is determined by the required energy gain program. This is most advantageous indeed in FFAG accelerators where the guiding field does not change with time.

4.10.5 Consequences of the Harmonic Number Jump

The procedure we have followed applies correctly to the case when beam energy is constantly below the transition energy, namely when $\alpha_{pn} \gamma_n^2 < 1$. We have set equations (3) to (5) explicitly for this case, requiring a decreasing harmonic number as acceleration proceeds. In the opposite case when beam energy is above the transition energy, when $\alpha_{pn} \gamma_n^2 > 1$, the harmonic number will increase monotonically. Thus equation (4c) is to be replaced with $h_n - h_{n-1} = +\Delta h$, and a minus sign placed in front of the right-hand side of equation (5).

To avoid unnecessary beam loss, the number of bunches (which will be constant during acceleration) ought to be always less than the harmonic number at all times. On the other hand, because of the change of the revolution period due to the beam velocity variation, the number of rf buckets will vary. The actual distribution of the beam bunches with respect to the available buckets during acceleration is shown in Figure 3a for the case of acceleration below transition energy, and in Figure 3b for the case above. It is seen that in the former case the beam longitudinal extension at injection ought to be shorter than the revolution period, and at most equal to the revolution period at extraction. That is, the number of injected bunches cannot be larger than the rf harmonic number at extraction. The situation is different when the beam is injected at energy above transition. In this case the revolution period decreases and the harmonic number increases during acceleration.
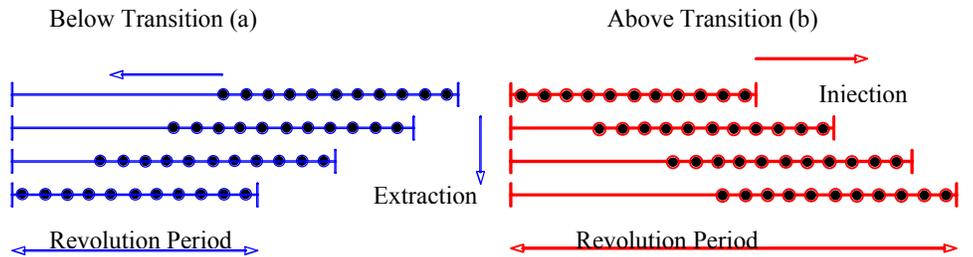
Figure 3: Bunch to Bucket Configuration with HNJ below (a) and above (b) Transition Energy

In the case of interest - below transition energy - the beam pulse at injection must have a duration that is a fraction of the revolution period given by the ratio β_1 / β_2 of the initial to the final value of the beam velocity. In the case of multiple FFAG rings where HNJ acceleration is applied throughout, that ratio is of the beam velocity at injection into the first ring to the beam velocity at extraction from the last ring.

As already stressed above, the energy gain per turn is not a free parameter but is assigned by the requirement of providing the Harmonic Number Jump. As a

consequence the acceleration period, the inverse of which can be taken as the repetition rate, is a result and not a goal.

Again, the beam behaviour can be calculated exactly on a computer, but we want here to show qualitatively the main features of HNJ application. After linearization and integration we derive the maximum energy gain per crossing as:

$$\Delta E_{max} = E_f \, \beta_f \, \gamma_f^2 \, \Delta h \, Mc \, / \, f_{RF} \, C_{tot}, \tag{13}$$

the total number of cavity crossings

$$n_{cr} = f_{RF} \, C_{tot} \, (1 - \beta_i / \beta_f) \, / M\beta_i c \, \Delta h, \tag{14}$$

and the total acceleration period

$$t_f = f_{RF} \, C_{tot}^2 \, (1 - \beta_i^2 / \beta_f^2) \, / \, 2M^2\beta_i^2 c^2 \, \Delta h. \tag{15}$$

The subscript "f" denotes the final values, and the subscript "i" the initial values of the corresponding parameters. C_{tot} is the total ring circumference, and f_{RF} is the rf frequency. ΔE_{max} can be used as an estimate of how much rf voltage is required in the cavities; the larger f_{RF} the lower is the voltage. On the other hand, the acceleration period increases with f_{RF}. The total number of revolutions is given by Mn_{cr}.

4.10.6 An Example

As an example of an FFAG accelerator where acceleration can take place with the HNJ method, we refer to the 1 GeV, 10 MW Proton Driver reported in previous notes [1, 6]. This is a facility comprising two rings each with a circumference of 204 m, concentric to each other and housed in the same enclosure. The rings' NSL with LFP magnet lattice structures are identical, both made of 80 FDF triplets separated by a 1 m long drift. The first ring accelerates from 50 to 250 MeV, and the second from 250 MeV to 1 GeV. Table 1 is a summary of the main acceleration parameters of both rings.

Table 1: RF Parameters for Acceleration with HNJ in two FFAG Proton Drivers.

	FFAG-1	FFAG-2
Cavity Groups	4	2
Cavities per Group	8	16
RF Frequency, MHz	804.9	804.4
h, total	(436 – 223) x 4	(446 – 313) x 2
β_0	0.40	0.80
Cavity Gap g, cm	7.45	14.9
RF Phase	30°	60°
RF Voltage / Cavity, MVolt	6	25
Acceleration Period, μs	87.1	62.7
No. of Revolutions	53 + 1/4	66 + 1/2

Note that the beam travels around each ring for less than a hundred revolutions, fast enough to remove any concerns over beam stability and survival that might be caused by the multiple-resonance crossing that cannot be avoided with a NSL and LFP FFAG. Also the acceleration period is less than 100 microseconds in both rings, permitting a 1 kHz operation rate. The same mode of acceleration with the same rf parameters can also allow a CW mode of operation. A continuous sequence of beam pulses of the right duration, respecting the β_1/β_2 ratio, is injected into the first ring and let spiral so contiguous pulses can circulate together side by side on different orbits. Each pulse time structure is preserved during acceleration and transfer between rings. At the end of acceleration in the final ring, the beam pulses get closer to each other and eventually collapse next to each other as a real continuous beam. The main issue for CW mode of operation is to ensure that there is enough separation between contiguous turns for single-turn injection and extraction.

4.10.7 Energy Gain Program

Several methods have been proposed [2] to reproduce the required energy gain profile according to equation (5). The method we prefer, and we explain here, is the use of a cavity with a radial longitudinal field profile. The required energy gain profile (total peak rf voltage per group of cavities) across the radial width is plotted in Figure 4. It can be seen that the voltage profile is approximately linear with respect to the radial displacement of the beam during acceleration. The cavities are superconducting, all operating close to 805 MHz, which is convenient for the proton driver example we have selected here to illustrate the HNJ method of acceleration. In the same example, cavities have a single cell and are all tuned independently from each other. The gap g is related to the rf wavelength λ_{RF} by the relation $g = \lambda_{RF}\,\beta_0/2$ where β_0 is the nominal value of velocity, kept constant and the same for all the cavities in the same ring; its value is shown in Table 1. During the n-th cavity crossing the peak total voltage V_n is related to the surface axial field ξ_n through the relation $V_n = g\,\xi_n\,TTF\,(\beta_0/\beta_n)$ where TTF is the Transit Time Factor that varies with the beam velocity β_n. The surface axial field ξ_n is plotted in Figure 5.
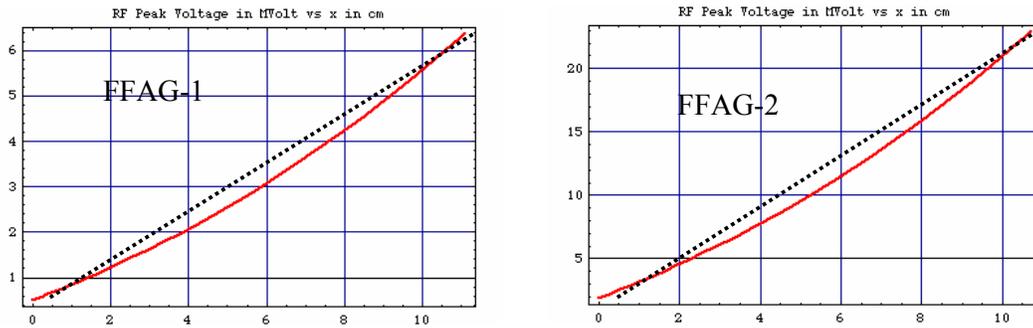
Figure 4: RF Voltage Profile in MVolt vs. Radial Displacement x in cm

The surface axial field is about the same for the cavities of both rings. It can be obtained with three cavities located next to each other, as shown in Figure 6, one operating in a TM_{01} mode at the constant field $\xi = 16$ MVolt/m corresponding to the middle value of the curves of Figure 5, and the other two in TM_{11} mode with a linear

field $\xi = \pm 6$ MVolt/m, corresponding to the slope of the curves also shown in Figure 5. The use of a TM_{11} cavity is problematic, and needs more evaluation and better understanding, especially regarding the deflecting magnetic mode that somehow needs to be compensated without disrupting the beam transverse motion.
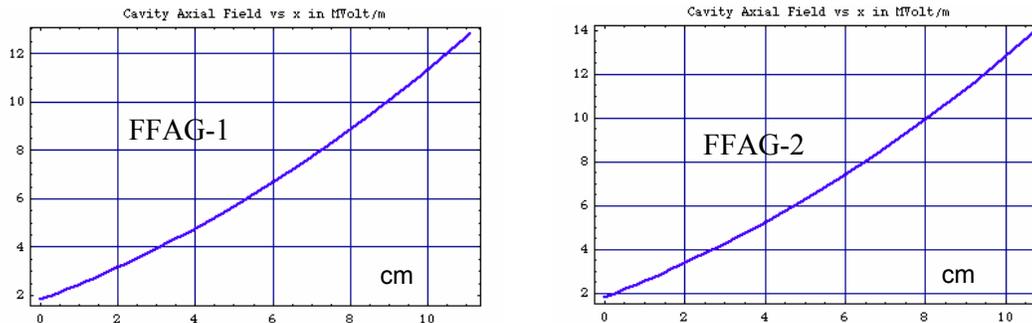
Figure 5: Total Surface Axial Field for each rf Cavity.
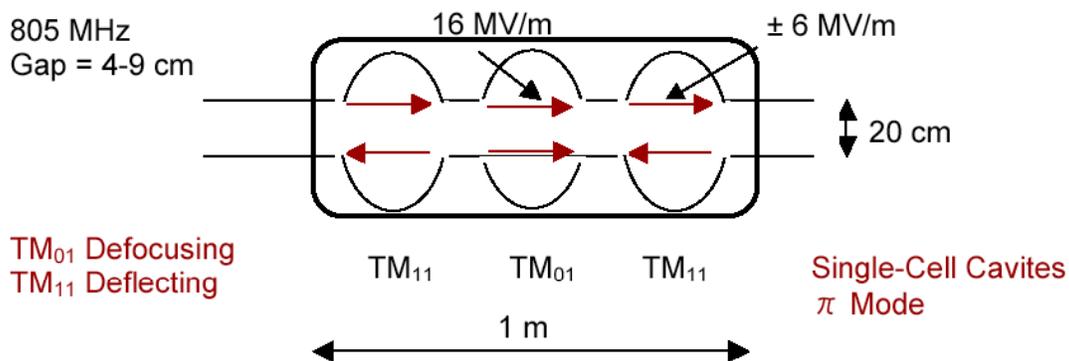
Figure 6: Combination of 3 cavities to reproduce behavior of required axial field profile.

4.10.8 Conclusions

The method of acceleration with the Harmonic Number Jump adds a new dimension to FFAG accelerators and, in opening the path to high repetition rate, and, eventually, CW mode of operation, offers interesting new possibilities. These new features, combined with potentially lower costs, would make the FFAG accelerator very competitive, and a viable alternative to Super-Conducting Linacs for High-Intensity Proton and Heavy-Ion Drivers. The method still needs a practical demonstration, perhaps along the lines of recent proposals at the KURRI FFAG complex. Further important R&D includes the design, manufacture and operation of a combination of TM_{01} and TM_{11} cavities for the attainment of the required energy gain profile.

4.10.9 References

1. A.G. Ruggiero, "FFAG-based Proton and Heavy-Ion High-Power Drivers", contribution to this Issue of ICFA Beam Dynamics Newsletter.
2. A.A. Kolomenskii, "Theory of Motion in the Microtron. An Accelerator with Multiple Periodicity", Soviet Physics - Technical Physics, Vol. 5, No. 11, page 1278. May 1961.
3. A.G. Ruggiero, "rf acceleration with harmonic number jump", Physical Review ST-AB **9**, 100101 (2006).
4. A.G. Ruggiero, "RF Acceleration with Harmonic-Number Jump", BNL Internal Report C-A/AP/#237, May 2006.
5. I. Gumowski, CERN/MPS/Int. RF 67-1.
6. A.G. Ruggiero, "FFAG-based High-Intensity Proton Drivers", Proceedings of ICFA-HB2004, October 18-22, 2004, Bensheim, Germany, page 324.

4.11 An FFAG Proton Driver for a Neutrino Factory

G.H. Rees
Mail to: ghrees@ukonline.co.uk or c.r.prior@rl.ac.uk
ASTeC Intense Beams Group, Rutherford Appleton Laboratory, Chilton, Didcot, Oxon OX11 0QX, U.K.

4.11.1 Introduction

The proton driver for a Neutrino Factory is required to deliver 4 MW of average beam power to a pion production target. The pions are captured and controlled as they decay to muons; the muon beam is then cooled, rapidly accelerated to an energy in the range 20 to 50 GeV and finally stored in a purpose-built storage ring where they decay to intense beams of neutrinos which are directed at far detectors. The recent International Scoping Study (ISS) [1] further refined the parameters and identified the following specifications:

- A pulse repetition frequency of 50 Hz
- A proton kinetic energy of 10±5 GeV
- An rms proton bunch duration of 2±1 ns
- A proton bunch number of either three or five
- A sequential extraction delay of >17μs per bunch
- A pulse duration of $\leq$ 40 μs for a liquid mercury target
- A pulse duration of $\leq$ 70 μs for a solid metallic target

Several synchrotron options had previously been evaluated and also a full energy linac, used in conjunction with an accumulator and a compressor ring [2]. During the Scoping Study, further options included:

- A H⁻ linac with pairs of 50 Hz booster and 25 Hz driver synchrotrons (RCS)
- A H⁻ linac with a 50 Hz booster RCS and a 50 Hz NFFAG driver ring
- A H⁻ linac with a chain of three non-isochronous FFAG rings in series
- A H⁻ linac with two slower cycling synchrotrons and two holding rings

- A full energy H⁻ linac with an accumulator and bunch compression ring(s)

The second is probably the most advanced design and is the one described here. The booster energy range proposed is 0.2 to 3 GeV, and the driver energy range 3 to 10 GeV. The driver is a new type of FFAG accelerator which uses a non-isochronous, non-linear and non-scaling, cell focusing structure. This is referred to as an NFFAG. Either three or five, proton bunches may be used with the design. A low energy electron model of an NFFAG ring needs to be built and tested to confirm viability. In the future, a more detailed comparison with the fifth option is anticipated, as superconducting, high energy H⁻ linacs are under consideration at both FNAL and CERN.

4.11.2 The 10 GeV, NFFAG Proton Driver

Prior to the ISS, a 50 Hz, 10 GeV, 4 MW proton driver [3] had been designed at RAL. During the study, the design has needed to be modified for a three (five), bunch compatibility between booster, driver and 20 (50) GeV muon decay rings.

4.11.2.1 The 200 MeV, H⁻ Injector Linac

For the linac, a 90 MeV design at RAL [4] is extended to 200 MeV by adding a 110 MeV side coupled linac. A stand is being prepared for testing H⁻ sources, a LEBT, an RFQ linac, a two stage beam chopper and a set of diagnostics. The frequency for the design is 324 MHz, and is based on a Toshiba klystron. At the transition energy of 90 MeV, a factor of three increase of frequency is considered. The pulse repetition frequency, peak current, duration, and duty cycle, after chopping, are, respectively, 50 Hz, ~60 mA, ~400 μs, and ~70%.

4.11.2.2 The 200 MeV Achromatic Collimation Beam Line

An achromatic section of beam line is needed between the linac and the booster ring, both for collimation and for diagnostic purposes. Twelve combined function magnets, arranged as four triplet cells, form the achromat. Eight of the magnets have +45° bends and four have -45° for a total bend of 180°. The length is 41.6 m, and the large dispersion and normalised dispersion functions at the central symmetry point are 14.16 m and 5.1 $m^{1/2}$, respectively. Achromatism is obtained by using mirror symmetry about the bend centre, and choosing a (π) horizontal betatron phase shift under space charge for the first two, and last two, triplet cells. The negative bends are in the first and the last magnet of each (π) section.

Upstream of the achromat is a beam line with horizontal beam loss collimators and cavities for momentum spread reduction and correction. In the achromat are more collimators and bunchers. There is vertical collimation for both beam edges at the four FDF triplet centres, and momentum edge-collimation at two places. The main momentum collimation is at the high dispersion centre point, with pre-collimation in the preceding triplet. Stripping foils are used and not conventional collimators. C-shaped cores for the combined function magnets are open on the outer radius for easy exit of the stripped ions to shielded, beam dumps. Bunchers at quarter and three-quarter arc positions restore the upright orientation of the momentum phase space at the arc centre and end.

4.11.2.3   The 50 Hz, 3 GeV Booster Ring

A 50 Hz synchrotron, rather than a 50 Hz FFAG, is used for a booster, as it may have a more efficient H⁻ injection system. The injection scheme dominates the lattice design, which is based on that for the European Spallation Source (ESS) [5]. Seven triplet cells, in each of four superperiods, form the lattice, with three of the seven for a 90° arc and four for a long dispersion-free straight section. All sixteen of the straight cells have a 10.6 m free length. An 8°, 5.4446 m dipole unit is in the centre cell of each arc, and adjacent cells each contain two 20.5°, 4.15 m main dipoles. All of the injection elements are located between the two central triplets of one of the arcs, so providing a fully separated injection scheme. The booster layout is shown in Figure 1.
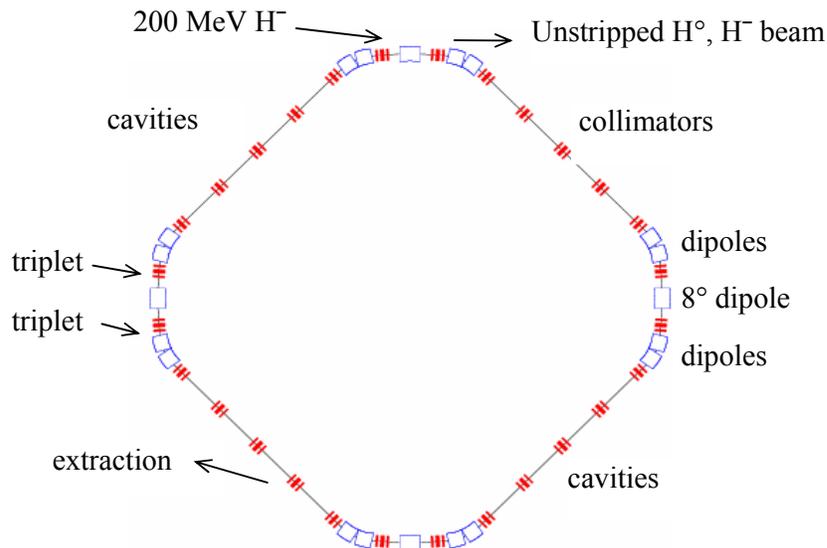
Figure 1: Schematic layout drawing of the 50 Hz, 1.2 MW, 3 GeV, booster synchrotron.

Quadrupole gradients for the symmetrical triplets on each side of a central dipole are set for zero dispersion straight sections. Two other quadrupole types vary the betatron tunes and a fifth type, the normalised dispersion at the arc centre. A common gradient is obtained for all 84 of the quadrupoles by length adjustment of the five different types, simplifying the quadrupole supplies and allowing a single lamination stamping. Parameters are given in Figure 2 and Table 1.

The H⁻ stripping foil is at an 8° arc dipole centre. A normalised dispersion of ~1.9 m$^{1/2}$ allows horizontal phase space beam painting through related rf steering and a momentum ramping of the input beam. An injection chicane is not needed; nor are horizontal painting magnets, nor an injection septum magnet. Longitudinal painting is not as easy as for a dispersion free region, but earlier space charge tracking studies of injection [6] proved satisfactory. A set of symmetrical steering magnets, two on each side of the 8° dipole, provide the vertical beam painting. Either an anti-correlated or a correlated, transverse beam distribution may be obtained. The betatron tune depression at 200 MeV is ~ 0.25, for an assumed 2-D elliptical density distribution.

The dipole magnets are at low β positions in the triplet cells for a low stored energy, which is important in the design of the main magnet power supplies. During

acceleration, the fields in the 8° dipoles cycle between 0.0551 and 0.327 T, and those in the main, 20.5° dipoles, between 0.185 and 1.0996 T, while gradients in the quadrupoles track between 0.9952 and 5.9065 Tm^{-1}. Designs are needed for the magnets and magnet power supplies. In addition to the main magnets, the use of 32 vertical and 32 horizontal steering magnets, and the same number of horizontal and vertical trim quadrupoles, is proposed. Spaces are reserved in the ring for sextupole magnets.
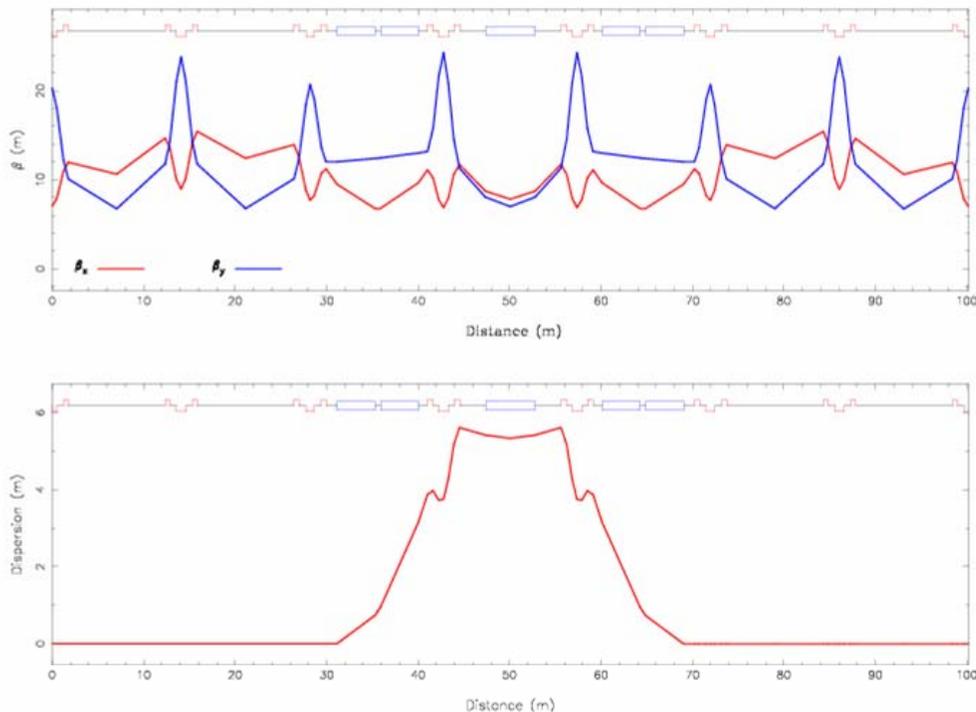
Figure 2: Lattice betatron and dispersion functions for the 400.792 m booster synchrotron.

Ceramic vacuum chambers, with contoured radio-frequency inter-shields, are required for the main and the correction magnets, and these may follow designs used at the ISIS synchrotron [7]. The injection magnet ceramic chamber has a central T-section for mounting and removal of the H⁻ stripping foil and its electron collector. This is a difficult mechanical design area because of the need to reduce eddy current effects. A metal and ceramic uhv standard vacuum system is proposed, using demountable joints with tapered flanges, band clamps and metal seals for quick fitting and removal. Units need careful cleaning, but vacuum baking is not considered necessary. Oil-free turbo-molecular pumps reduce the pressure to $< 10^{-6}$ mbar, before removal from the ring. Ion pumps are then used at the design pump pressures of $< 10^{-7}$ mbar, for long life.

There is a dedicated region for beam loss collimation in one ring superperiod. A momentum collimator protects ring components from longitudinal beam loss, and this is located upstream of the 8° dipole in the arc downstream of the injection arc. Primary and secondary, horizontal and vertical, betatron collectors are used to localise the

transverse beam losses, and these are placed in three, adjacent long straight sections of the superperiod.

The 1.2 MW beam power is higher than in any existing RCS, and more than 100 m is provided for the rf acceleration system. The fields used for the proton acceleration give an adiabatic bunch compression in both booster and driver. The booster uses harmonic h = 5 (2.117 to 3.632 MHz) for five 0.66 eV.sec bunches, or h = 3 (1.270 to 2.179 MHz) for three 1.1 eV.sec bunches. Owing to the bunch compression in the booster, the driver may use higher harmonic numbers (×8). The driver thus has h = 40 (14.529 to 14.907 MHz) or h = 24 (8.718 to 8.944 MHz). For the case of five bunches, the booster needs rf voltages per turn of 0.9 MV for the acceleration and 0.42 MV at 3 GeV, while the driver requires 1.18 MV for an adiabatic bunch compression to ~2.1 ns rms, at 10 GeV. In the three bunch case, the corresponding parameters are 0.85, 0.25 and 1.30 MV per turn for 3.0 ns rms bunches. A hardware issue to be resolved is the choice between Finemet and ferrite for frequency tuning of the rf cavities. Some further compression is envisaged by adding higher harmonic cavities in the driver ring. A possible scheme, using pairs of detuned cavities, at an rf phase shift of π apart to cancel reactive beam loading components, needs evaluation. Use of a multi-pulse kicker, and septum, extraction system and conventional diagnostics is assumed.

Table 1: Details of the 0.2-3 GeV Rapid Cycling Synchrotron Booster

Ring circumference (m)	400.792	No. protons per cycle	5×10^{13}
Betatron tunes (Q_v, Q_h)	6.38, 6.3	Beam power at 3 GeV (MW)	1.2016
Gamma transition	6.57	rf cavity straight sections (m)	11×10.6
Cell lengths (m)	14.6, 14.1	Freq. for h=n=5 (MHz)	2.12-3.63
Transverse acceptance (mm.mr)	400 (π)	Bunch area for h=5 (eV.s)	0.66
Transverse emittances (mm.mr) (maximum, unnormalised)	175 (π)	kVolts at 3 GeV for η_{sc}<0.4	417
D quad lengths (m)	1.07, 0.926, 1.015	kVolts at 5 ms for φ_s = 48	900
F quad lengths (m)	0.511, 0.615		
Quad gradients (Tm^{-1})	0.995-5.907	Freq. for h=n=3 (MHz)	1.27-2.18
Quad inscribed radius (mm)	110.0	Bunch area for h=3 (eV>s)	1.1
No. 20.5° sector dipoles	16	kVolts at 3 GeV for η_{sc}<0.4	247
Length of main dipoles (m)	4.15	kVolts at 5 ms for φ_s=52°	848
Radius of main dipoles (m)	11.599		
Field of main dipoles (T)	0.185-1.0996	No. of 8.0° rect. dipoles	4
Dipole v,h good field (mm)	160.0, 175.0	Length of 8.0° dipoles (m)	5.445

4.11.2.4   The 50 Hz, 10 GeV Proton Driver

A proton driver based on an NFFAG has several advantages. It may have a high duty cycle, and thus lower rf accelerating fields. Adiabatic compression is eased, as bunches may be held at the top energy of 10 GeV. The NFFAG ring may have sturdy,

metallic vacuum chambers, in comparison with an RCS, which has ceramic chambers with rf shields, to limit the eddy currents. Single booster and driver rings and transfer lines may be chosen, whereas two boosters and two drivers are needed, due to practical reasons, for a 50 Hz RCS driver [6]. There is thus a saving in both rings and expensive, transfer lines. Low beam power loss during H⁻ injection, and the compression of three bunches, are more readily achieved than in the option that uses a linac, an accumulator and a compressor ring [6]. The NFFAG concept is considered to need further study, however, and the building and testing of a low energy, electron model to prove its viability.
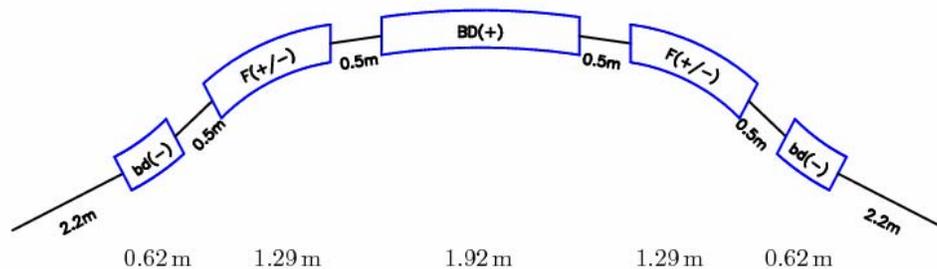
Figure 3: A single lattice cell of the 50 Hz, 4 MW, 10 GeV, NFFAG proton driver ring.

The NFFAG cell layout is shown in Figure 3. Three magnet types are used in the basic cell, which has five magnets (bd, BF, BD, BF, bd, O). The bd and BD units are non-linear, vertically focusing, parallel edged, combined function magnets, but with bd and BD providing reverse and positive bending, respectively. The BF is a non-linear,
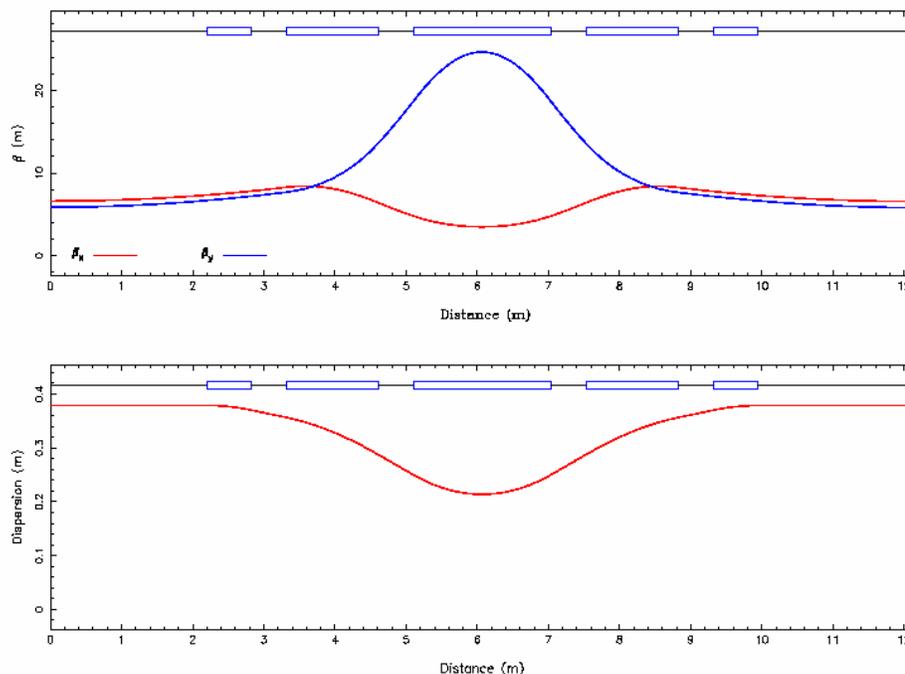
Figure 4: Small amplitude betatron and dispersion functions for the NFFAG 10 GeV orbit

horizontally focusing, positive bending, combined function magnet, whose edges are parallel to those of bd and BF. There is a zero entry and a zero exit angle, respectively, for the upstream and the downstream bd magnets. Betatron tunes are $\nu_h = 4/13$ and $\nu_v = 3/13$ for the zero chromaticity cell. Groups of 13 cells have integer tunes, with non-linear effects up to order 12 cancelled locally. The ring has five such groups and one more cell, so that $Q_h = 20\ 4/13$ and $Q_v = 15\ 3/13$. Non-linear, betatron excitations and structure resonance effects are much reduced owing to the use of the 66 cells. Coupling occurs at $Q_h + Q_v = 7$ for groups of 13 cells, but $Q_h + Q_v = 35\ 7/13$ for the ring, far from any resonance. The NFFAG proton driver is thus expected to have a large dynamic aperture.

Figure 4 shows 10 GeV lattice functions, and Table 2 gives some 3, 5.9 and 10 GeV, orbit data. The 3 and 10 GeV, orbit separations are largest in the *bd* unit, reaching 0.33 m. The *BF* unit has a peak orbit field of 1.75 T, but the full non-linear magnet data is not included. The parameters for the adiabatic bunch compression have been given above. A multi-pulse kicker and septum extraction system is needed, but is less demanding than that for the muon decay rings. The unnormalised beam emittances

Table 2: Respective 3, 5.9 and 10 GeV orbit parameters for the NFFAG proton driver ring.

Parameter	*3 GeV*	*5.9 GeV*	*10 GeV*
Orbit circumference (m)	801.5841	801.0174	801.4474
Length of lattice cell (m)	12.14521	12.13664	12.14314
Length of long straight (m)	4.403143	4.403143	4.403143
Betatron tunes (Q_v, Q_h)	15.231, 20.308	15.231, 20.308	15.231, 20.308
Gamma-transition	18.9302 i	47.6967	21.8563
bd norm. gradient	0.0585	0.0285	0.005
BF norm. gradient	−0.2832148	−0.2724653	−0.2597134
BD norm. gradient	0.273322	0.283943	0.284159
bd bend angle (mr)	−72.484408	−44.293752	−28.8000
BF bend angle (mr)	8.644825	37.82673	61.99989
BD bend angle (mr)	222.8789	108.1338	28.8
Orbit length in bd unit (m)	0.620114	0.620029	0.62
Orbit length in BF unit (m)	1.284787	1.28532	1.29
Orbit length in BD unit (m)	1.923913	1.920869	1.92
Orbit length BF to bd (m)	0.501109	0.500283	0.5
Orbit length BF to BD (m)	0.503069	0.500671	0.5

are similar for protons in the booster and muons in the decay ring, but those for protons in the NFFAG are much less than those for $\mu^\pm$ in the 10-20 GeV ring. The possibility of using a superconducting NFFAG for the $\mu^\pm$ acceleration is of interest, but may not be feasible due to the variation of gamma-transition with energy, as outlined next. Twenty-four reference orbits are defined for a lattice cell of the 3 to 10 GeV proton NFFAG. The magnetic field profiles of the BF and BD units, together with those of the bd units, are set for zero chromaticity at each reference energy. Gamma transition is made ~21.86 at 10 GeV to assist the bunch compression. The non-linear, non-scaling

aspects of the ring cause gamma-t to vary with energy, despite the constant tunes. γ_t is imaginary at low energy, real after mid-cycle, and decreases at high energy. A full analysis needs processing of the non-linear, magnet lattice data, followed by ray tracing in a 6-D simulation program such as Zgoubi [8].   .

Beam loss collimation differs from that in the booster. The momentum loss collector requires the use of a beam-in-gap kicker. Vertical loss collection is simpler, as collimators may be tapered across the aperture. Horizontal beam collimation is made prior to injection and also at extraction. The fractional loss in the collectors must be kept to about 1 part in 10^3, with that in the extraction region and elsewhere in the ring, both less than 1 part in 10^4. Halo growth has thus to be limited. Primary collimators are remotely adjustable, with quick release water fittings and flanges. Use of local shielding helps to reduce the air activation. The collimation is a major design issue.

4.11.3 Summary

A compact, schematic layout for a 50 Hz, 4 MW, 10 GeV proton driver is shown in Figure 5. It consists of a 200 MeV H⁻ linac, a 3 GeV booster synchrotron and a 10 GeV NFFAG driver. The NFFAG uses a non-isochronous, non-linear and non-scaling, cell focusing structure, which differs significantly from that of a traditional, scaling FFAG.
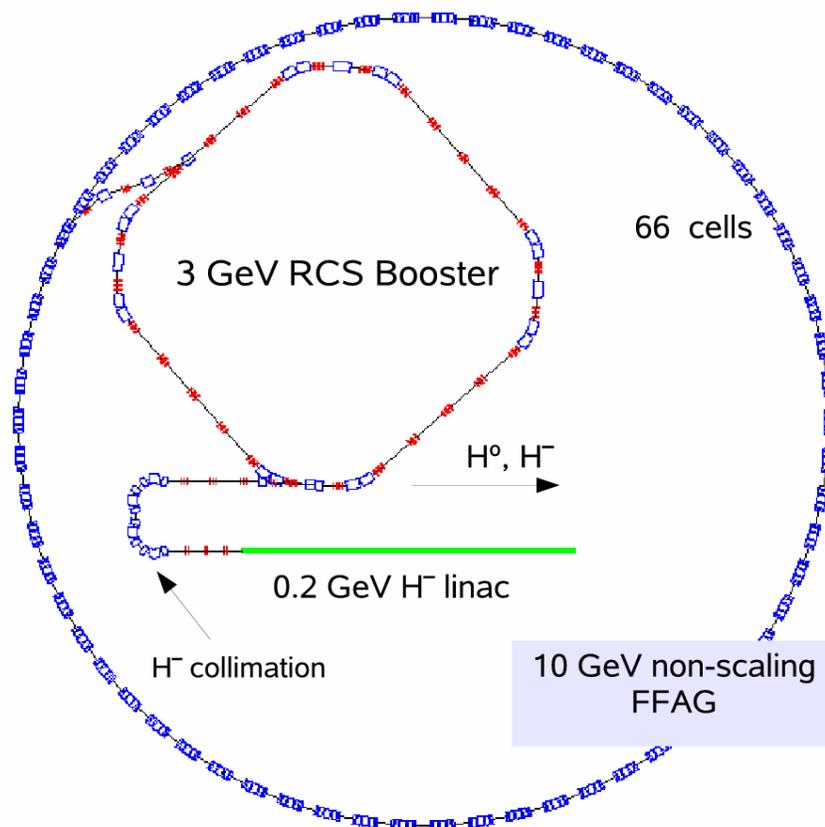
Figure 5: Schematic layout drawing of the linac, booster and NFFAG of the proton driver.

It is recommended that a low energy electron model of the ring be constructed and

tested to confirm the concept viability. An alternative proton driver uses a full energy H⁻ linac with accumulator and bunch compression ring(s). A detailed comparison of the alternatives is anticipated in the future, as superconducting 5 and 8 GeV H⁻ linacs are under consideration at CERN and FNAL, respectively.

4.11.4 References

1. C.R. Prior, "Recommendations from the International Scoping Study for a Neutrino Factory", Proc. U.S. Particle Accelerator Conference, PAC07, Albuquerque NM, June 2007.
2. D. Neuffer, U.S. Neutrino Factory Design Study Report 2A (2004).
3. G.H. Rees, "FFAG Studies for Neutrino Factory Accelerators", Nuclear Physics B, 155 (2006), p 301.
4. C. Plostinar, RAL, private communication (2006).
5. H. Lengeler (ed), The European Spallation Source Study, Vol 3, ESS-96-53-M (1996), pp 3-15.
6. C.R. Prior and G.H. Rees, "Synchrotron-based Proton Drivers for a Neutrino Factory", Proc. 7th European Particle Accelerator Conference, Vienna, Austria, 26-30th June, 2000, p 963. A. Blondel et al. (editors), ECFA/CERN Studies of a European Neutrino Factory Complex, CERN-2004-002 and ECFA/04/230, 13 April, 2004.
7. B. Boardman (editor), "Spallation Neutron Source: Description of ISIS Accelerator and Target", RAL Report RL 82-006, March 1982.
8. F. Méot, "Status of 6-D Beam Dynamics Simulations in FFAGs using Zgoubi", FFAG05, p 47.

4.12 An Electron Model for a 3-10 GeV, FFAG Proton Driver

G.H. Rees
Mail to: ghrees@ukonline.co.uk or c.r.prior@rl.ac.uk
ASTeC Intense Beams Group, Rutherford Appleton Laboratory, Chilton, Didcot. Oxon OX11 0QX, U.K.

4.12.1 Introduction

A 50 Hz, 3-10 GeV, proton driver suitable for a Neutrino Factory [1] was described in the previous article. It uses a new type of fixed-field alternating gradient accelerator, with a non-linear, non-scaling and non-isochronous, cell focusing structure (referred to as NFFAG). Such an accelerator has never been built, and, if construction were ever to be contemplated, an essential pre-requisite would be an equivalent electron machine to check feasibility and examine aspects of the beam dynamics. This article outlines the design of such an electron model of the driver aimed at studying the following features of the NFFAG design:

- The effects of the non-linear magnetic fields
- The constancy of tune at different reference energies
- The halo growth during the 50 Hz acceleration

- The range of momentum for the acceleration
- Adiabatic bunch compression to < 1 ns rms
- Longitudinal space charge limited operation
- The effect of space charge tune shift of $\Delta Q = 0.1$ at the injection energy
- The effect of space charge tune shift of $\Delta Q = 0.1$ for a compressed bunch

In the electron machine, the non-linear lattice cells are designed to have fixed betatron tunes at different reference energies, with the electron model having the same tunes as the proton driver. Other parameters are chosen to allow a reasonably compact ring. In particular, the length and number of lattice cells are reduced from those of the driver, resulting in larger bend angles and smaller bend radii, and a reduced ratio of final to initial gamma (total energy). A blow-up of the longitudinal bunch area is needed after injection so that all design aims of the model may be met, and a scheme to achieve this is discussed.

4.12.2 Electron Model Parameters

In the proton driver, there are 66 cells, each with ($\nu_h = 4/13$, $\nu_v = 3/13$), so that the ring betatron tunes are (20 4/13, 15 3/13) and a group of 65 cells has integer tunes (20, 15). This choice is made to cancel the non-linear effects over most of the length of the closed orbit at each reference energy. A similar scheme is used for the model, but the number of cells is reduced to 27, so that the ring tunes are (8 4/13, 6 3/13), and non-linear cancellations occur for 26 of the 27 cells.

The bend angle per cell in the proton ring is 5.4545°, while that in the electron ring is 13.3333°. Short magnets are used in the model, resulting in increased edge focusing and a restricted energy range: the protons have $\beta\gamma = 4.197$ to 11.658, while the electrons have $\beta\gamma = 6.8708$ to 11.658, for an energy range from 3 to 5.44632 MeV. Use of more cells in the model would result in very low magnetic fields. The NFFAG cell layout is shown in Figure 1. Three magnet types are used in the basic cell, which has five magnets labelled (bd, BF, BD, BF, bd, O). The bd and BD units are non-linear, vertically focusing, parallel edged, combined function magnets, but with the bd and BD providing, respectively, reverse and positive bending. The BF is a non-linear, horizontally focusing, combined function unit whose edges are parallel to those of bd and BF. There is a zero entry and a zero exit angle, respectively, for the upstream and

5.5 cm	5.5 cm	11.0 cm	5.5 cm	5.5 cm
−8.0°	7.5°	14.333°	7.5°	−8.0°
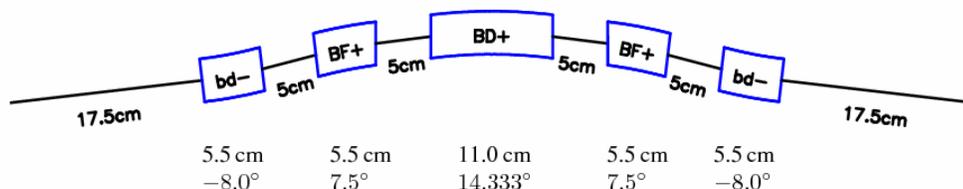
Figure 1: Magnet bend angles and cell lengths for the 5.44632 MeV, electron reference orbit.

the downstream, bd magnets. The orbit circumference for the 27 lattice cells varies from 23.778 m at 3 MeV to 23.760 m at top energy, with the corresponding cell lengths equal to 0.88067 m and 0.88 m.

The magnet bend angles for the maximum energy orbit are given in Figure 1, and are needed for a high gamma-transition value (19.9545). Angles are very different from those of the proton driver, where they are −1.65°, 3.5523°, 1.65°, 3.5523° and −1.65°.

Reference energies (17 in all) are selected at approximately 2 to 4% momentum intervals. At each reference energy, the small amplitude betatron tunes are constant. For the orbits nearby, the tunes vary with the momentum, but return to the set values at the reference energies. There is also a variation of tune with amplitude. Magnet parameters are given in the Table 1 below:

Table 1: Main magnet parameters of the 3.0-5.4465 MeV NFFAG electron model

Electron kinetic energy (MeV)	$3.0000 \rightarrow 5.4465$
Field in bd magnets (gauss)	$411.9239 \rightarrow 502.6101$
Field in BF magnets (gauss)	$72.2348 \rightarrow 471.1970$
Field in BD magnets (gauss)	$582.1691 \rightarrow 450.2549$
Maximum β_v value (m)	$0.8843 \rightarrow 1.4629$
Maximum β_h value (m)	$0.7044 \rightarrow 0.6047$
Maximum dispersion (h) (m)	$0.0793 \rightarrow 0.0635$
Full normalised emittance ε_n (π mm.mrad)	$10.000 \rightarrow 10.000$
Maximum vertical beam size (mm)	$2.2811 \rightarrow 2.2445$
Maximum horizontal beam size (mm)	$2.9082 \rightarrow 2.4591$
Maximum aperture height (mm)	4.500
Maximum orbit separation (mm)	38.500
Magnet vertical×horizontal gap size (mm×mm)	10.0×45.0

4.12.3 Gamma-t and Acceleration Frequencies

In Table 2, the proton driver and the model are compared for both gamma-t values and rf frequencies, at nearly equal γ. The gamma-t values are imaginary at low energies, real in mid cycle, decrease at high energies and are set at approximately 20 for the compression studies at top energy. The frequency ranges are comparable.

The non-linear lattice program used for the model calculates the values of $L(\delta)$ and α_o $(= \gamma_t^{-2})$, where $L(\delta)$ is the orbit length for the $p = p_o(1 + \delta)$ closed orbit, and

$$L(\delta) = L_0\left(1 + \delta\alpha_0\left(1 + \alpha_1\delta + \alpha_2\delta^2 + \ldots\right)\right)$$

Hence it is possible to solve for the non-linear, longitudinal motion parameters, α_1 and α_2. For example: $L_o(3 \text{ MeV}, \gamma = 6.871) = 0.88067033$ m, $L(3.15 \text{ MeV}) = 0.88040339$ m, and $L(3.3 \text{ MeV}) = 0.8801886$ m, so that α_o $(= \gamma_t^{-2}) = -0.00711816$, $\alpha_1 \approx 0.277441$ and $\alpha_2 \approx -18.79563$. For the bunch compression stage, $\alpha_o = 0.0025114$, $\alpha_1 \approx 8.02196$ and $\alpha_2 \approx 73.9689$, with α_1 and α_2 approximately twice the values for the proton driver.

The frequency, $F + \Delta F$, between the (p_o, C_o) reference orbits is $F = hc\beta(\delta)/C(\delta)$, with the rf harmonic number h=3; $c\beta(\delta)$ is the particle velocity and $C(\delta) = 27 L(\delta)$. The frequency ratio may be written:

$$\Delta = \frac{\Delta F}{F_0} = \left(\gamma_0^{-2} - \alpha_0\right)\delta + \left(\gamma_0^{-2}\left(\alpha_0 - 1 - \frac{1}{2}\beta_0^2\right) - \alpha_1\right)\delta^2$$

$$- \left(\alpha_2 + \gamma_0^{-2}\left(\alpha_0\left(1 + \frac{1}{2}\beta_0^2\right) + \alpha_1 + \frac{5}{2}\beta_0^2 - \frac{1}{2}\beta_0^4 + \gamma_0^{-4}\right)\right)\delta^3 + \ldots$$

Δ is a function of δ alone, but is less accurate than a direct use of the expression $F = hc\beta(\delta)/C(\delta)$.

4.12.4 Bunch Area Blow-Up, Space Charge Levels and Bunch Compression

The model needs to be able to simulate the proton driver betatron tune shifts of $\Delta Q = 0.1$ at compression and injection, and longitudinal space charge η_{sc} values > 0.1

Table 2: Gamma-t and acceleration frequencies in the proton driver and the electron model.

Proton Driver (h=40)			Electron Model (h=3)		
$\gamma=E/E_0$	γ_t	F(MHz)	$\gamma=E/E_0$	γ_t	F(MHz)
11.658	21.6563	14.90741	11.658	19.9545	3×12.57103
10.805	23.1154	14.90039	10.980	22.4864	3×12.56150
10.379	23.9225	14.89598	10.393	24.2936	3×12.56150
9.953	24.8996	14.89082	9.806	28.9955	3×12.55509
9.100	27.6544	14.87762	9.219	51.1918	3×12.54676
8.673	29.7066	14.86920	8.632	34.7566 i	3×12.53577
8.247	32.5945	14.85921	8.045	19.6996 i	3×12.52101
7.608	40.0939	14.84049	7.458	14.2350 i	3×12.50091
6.968	64.0158	14.81571	6.871	11.8527 i	3×12.47367
4.197	18.9302 i	14.52924	-	-	-

during the initial acceleration. Bunching factors must be found and, for these, Hofmann-Pederson longitudinal beam distributions are assumed for 5×10^9 electrons in a single $h = 3$ beam bunch. The same beam momentum spread, $\delta = \pm 8\times10^{-3}$, as for the compressed beam bunches in the proton driver, is assumed, together with a final bunch time duration of < 1 ns rms. This sets the longitudinal bunch area, and allows the rf voltage to be found for the required bunch compression. The same bunch area is assumed at injection, and this enables the rf voltage to be determined for an injection tune shift of 0.1 at a value of $\eta_{sc} < 0.4$.

At compression, when $\gamma = 11.658$ and the above conditions hold, a space charge ΔQ of 0.1 occurs at a bunching factor of $B_f = 0.0322$, assuming Gaussian transverse distributions. The bunch phase and time extents needed for $h = 3$ at 37.713 MHz are then: $\Delta\varphi = \pm 0.425$, $\Delta T = \pm 1.899$ ns (~ 0.85 ns rms) and the resulting bunch area $A(\Delta E, \Delta T)$ is 0.266554×10^{-3} eV sec. Assuming that the inductive wall fields cancel the longitudinal space charge forces, the required bunch compression voltage is found to be 195.3 V.

At injection, when $\gamma = 6.870$ and the above conditions hold, a space charge ΔQ shift of 0.1 occurs at a bunching factor of $B_f = 0.0934$, assuming Gaussian transverse distributions. The bunch phase and time extents needed at 37.421 MHz are $\Delta\varphi = \pm 1.159$, $\Delta T = \pm 4.93$ ns (~ 2.2 ns rms). The longitudinal space charge fields are not cancelled and $\eta_{sc} = 0.1004$ for the assumed bunch area, with a peak voltage per turn at injection of 44.0 V and a $\Delta p/p$ of $\pm 5.5\times10^{-3}$. To achieve this $\Delta p/p$, it appears necessary to blow up the longitudinal bunch area by a sideband excitation scheme, such as that proposed [3] at TRIUMF.
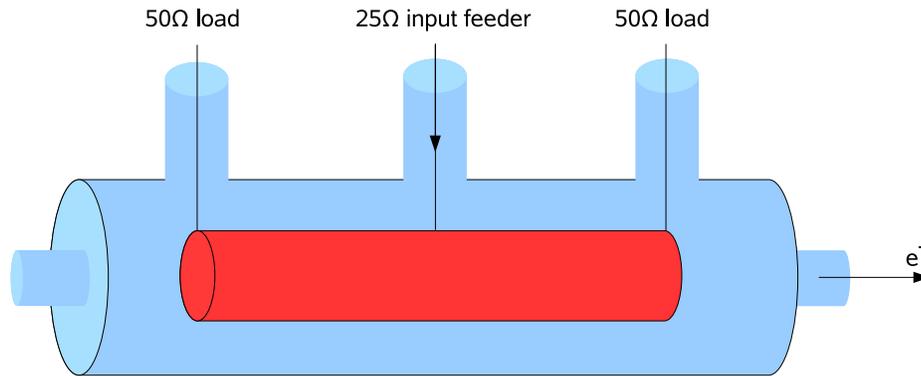
Figure 2: Broadband, centre-fed (or travelling wave), drift tube rf system.

The use of three broadband mini-drift tubes is proposed, located in cells 1, 4 and 7 (120° apart in rf phase for $h = 3$). Each unit is in a 0.35 m straight section, and a schematic drawing of the 0.29 m long drift tube, of phase extent ± 6.59°, is given in Figure 2. The voltage gain reduction due to the short phase extent is 0.2281, so each drift tube needs 285 V for compression and 64 V at injection. Alternatively, a single system at 193 V may be used at injection, freeing two drift tubes for the emittance blow-up.

Bunch mode excitation is proposed for the blow-up, using synchrotron sidebands of a high revolution frequency harmonic k [3]. Since only one bunch is involved, k need not be an integer multiple of $h = 3$, and $k = 31$ is chosen, with a drift tube phase extent of ±68.1° at 386.684 MHz. Most efficiency is found by omitting a carrier frequency and using just two sidebands, $(k - mQ_s)f_0$, where Q_s is the synchrotron tune, f_0 is the revolution frequency and mode number $m = 4$ stimulates motion at the bunch centre, while $m = 8$ affects the periphery. Varying the ratio of the mode amplitudes gives tailoring of the bunch shape. The small amplitude Q_s value at injection is 0.00109 but, during bunch blow-up, the ensemble average value of Q_s falls, and the sideband frequencies have to follow in step to obtain large emittance growths. Tracking of longitudinal bunch motion is planned to define the mode amplitudes and the specifications of the (commercial) broadband distributed amplifiers, needed for powering the drift tube systems.

4.12.5 Summary

An electron model is proposed for a 50 Hz, 3-10 GeV NFFAG proton driver. The model has 27 cells, in comparison with the 66 of the driver, and a circumference of 23.76 m. The cell tunes at each reference energy are as in the driver, but the smaller bending radii restrict the model energy range to 3-5.446 MeV. A space charge simulation code is needed to study beam blow-up, acceleration and compression and to confirm that model design aims are all met. The studies have raised the question of whether an NFFAG ring is feasible for rapid muon acceleration.

4.12.6 References

1. International Scoping Study, Neutrino Factory Design Report; Proton driver section, November 2006.
2. G.H. Rees, FFAG Studies at RAL in 2005; The International Workshop on FFAG Accelerators, KURRI, Osaka, Japan, December 5-9, 2005, p.77-80.
3. S.R. Koscielniak and G.H. Rees, Studies of Techniques for Longitudinal Emittance Blow-Up in the Kaon Factory Collector Ring, Proc. of 2nd European Particle Accelerator Conference, Nice, 1990.

4.13 Non-scaling FFAG Accelerators and Gantries for Medical Purposes

Dejan Trbojevic[1], Eberhard Keil, and Andy Sessler[3]
Mail to: dejan@bnl.gov
Brookhaven National Laboratory, Upton, New York 11973, USA ,
CERN, Geneva, Switzerland , and
Lawrence Berkeley National Laboratory, Berkeley, California 94720, USA

4.13.1 Introduction

Interest in hadron therapy has seen unprecedented growth in recent years. This is due to the clear advantages with respect to the other existing radiation treatments – x-rays, γ rays, or electrons (as shown in Figure 1 below). A major advantage of hadron therapy with respect to "photon" therapies is localized energy deposition at the tumor position. The photon therapies, as shown in the figure, cannot avoid radiation of the healthy tissue, while this is significantly lower with hadron therapy. The present "photon" therapies have side effects like: creating cancers children (that develop many years later), and creating serious cardio-vascular problems, from the unavoidable radiation to which healthy body cells are exposed.

Hadron therapy is growing rapidly, but a simple comparison of the present number of patients treated by hadrons is of the order of 50,000 while 4 million are treated by photons. This is mostly due to the higher cost of a hadron facility. We think that non-scaling FFAG machines (NS-FFAG) could reduce the cost in acceleration as well as in the gantries. The gantry's weight reduction should be of two orders of magnitude. Also any solution like cyclotrons, synchrotrons, or scaling FFAGs should be compared with respect to the size and weight.

4.13.1.1   Hadron facilities and clinical requirements for treatment

Neutrons were the first hadrons to be used for radiation treatment around 1930. Later, in 1946, R. R. Wilson [1] wrote a paper suggesting the use of protons or light ions emphasizing the Bragg peak advantage; that is, that most of the energy is deposited in a narrow region around it. Pioneering work in hadron therapy was developed at Harvard and Berkeley. Careful heavy ion studies were developed at the Bevalac in the 70's. The important parameters in radiation therapy are Relative Biological Efficiency

(RBE) and Oxygen Enhancement ratio (OER). A comparison of the preferable highest RBE's and lowest OER shows that carbon and neon ions have advantages with respect to protons.
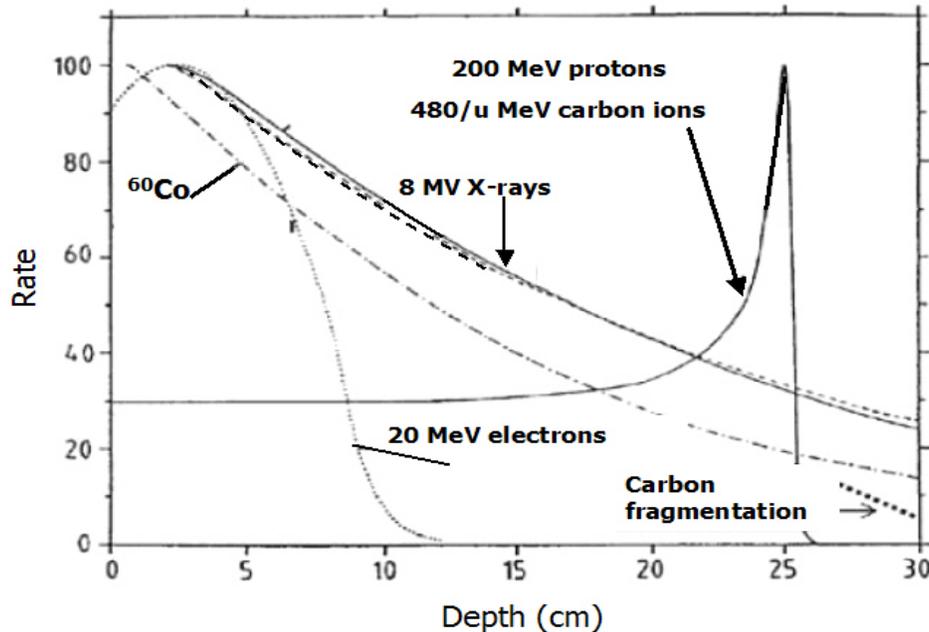
Figure 1: A comparison of the photon and electron therapies with hadron therapy.

The first dedicated facility in carbon cancer therapy was developed in Japan. The first hospital-based proton therapy facility opened in Loma Linda in California in 1990, using a small four dipole synchrotron built at Fermi National Laboratory. This facility has treated the largest number of patients until now. Cyclotrons are used in a very large number of facilities due to their compactness and lower cost. Energy degraders need to be used, as in the first proton treatments in Uppsala in the late 1950's [2]. This is an unavoidable problem with present-day cyclotrons due to the neutron radiation created at the degraders, and beam spread (both transverse and longitudinal energy spread from the beam interaction with the degraders). A reduction of cyclotrons' weight from ~230 tons to ~35 tons came through the use of superconducting cables. These machines produce protons of adequate energy for treating any tumor while keeping a small size ~3 m. Advantages of synchrotrons are smaller emittance beam, energy variation without degraders, easier point-scanning due to smaller beam size, and better duty factor – smaller beam loss. Rapid cycling synchrotrons, with single turn extraction by fast kickers, might improve the beam degradation arising from the slow extraction problem in synchrotrons. They will be capable of making repetition rates of the order of 25-60 Hz [2]. In fast cycling synchrotrons, problems are strong eddy currents and a large frequency swing of the rf in a short time.

The important clinical requirements in hadron therapy today are [2]:

- Accelerators and gantries need to be easy to operate due to the limited number of staff.

- Intensity, energy and position are programmable. Pencil scanning beam delivery is essential for the best treatment.
- Smaller accelerator size is important due to limited space and cost.
- Availability of the system has to be grater than 95%.
- Proton energies in a range of 100-250 MeV or carbon 150-400 MeV/u are necessary to cover the required penetration depth depending on the tumor position.

4.13.2 Properties and advantages of non-scaling FFAGs

The NS-FFAGs form extremely strong focusing accelerators or beam lines in the case of gantries. The strong focusing is a consequence of very small magnets. The NS-FFAG is made of repetitive identical cells using triplet or doublet combined function magnets with a linear variation of the magnetic field along the transverse axis. The strongest focusing and smallest dispersion is achieved using combined function magnets [3]. A larger magnet, with a defocusing gradient, provides major bending. Two smaller opposite bends surround it. They are combined function magnets with a focusing gradient. The dispersion and Courant–Snyder amplitude functions are very small for the relatively large kinetic energy range, for example for protons of 30-250 MeV or $\delta p/p = \pm 50\%$.
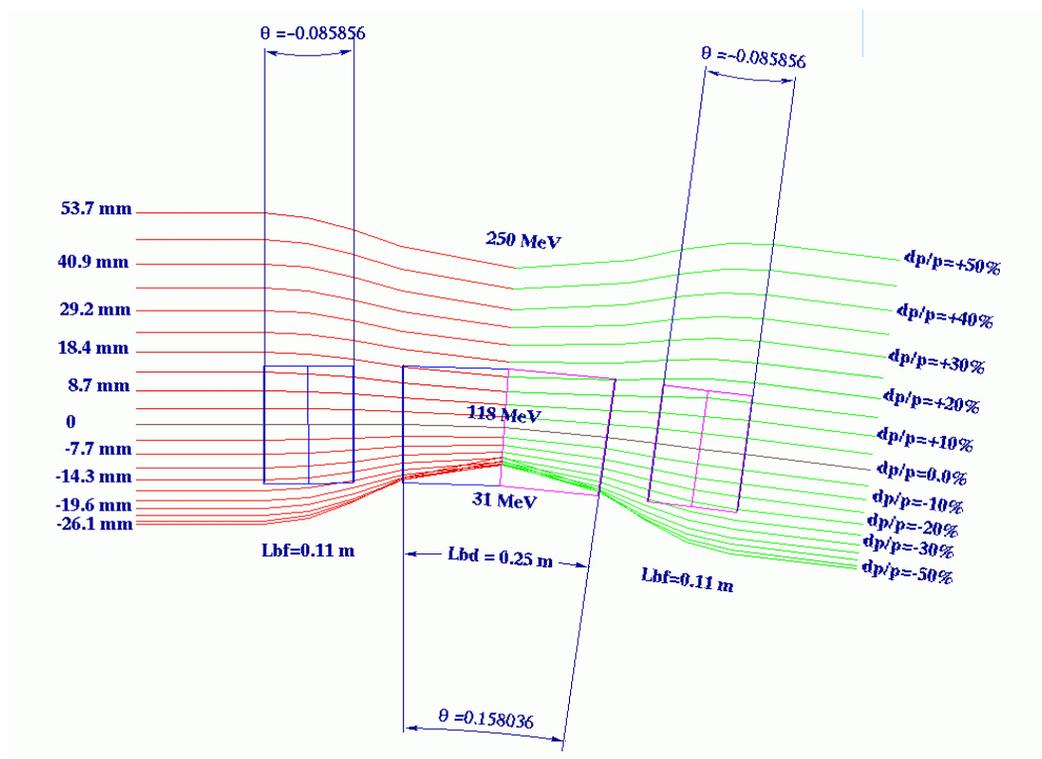
Figure 2: Orbit offsets in a single cell in the non-scaling FFAG for proton therapy. The cell length is 0.9 m; there are 48 cells with circumference 43.2 m. Drift lengths between the magnets are 6 cm long, while drifts for the extraction/injection and cavity length are 31 cm. Orbits are obtained from the Polymorphic Tracking Code (PTC) [4].

Particles with the central momentum make a circular orbit around the ring. Orbits of the lower energy particles oscillate mostly on the inner part of the aperture, while above the central energy orbits grow in radius towards the outer end of the aperture. Major differences between scaling FFAGs, or the combined non-scaling and scaling FFAG [5] with respect to the NS-FFAG, are the maxima of the orbit offsets during acceleration. The orbit offsets are the order of 40–60 cm in the case of radial and spiral scaling FFAGs, or of the order of 1 m in the case of combined scaling/non-scaling FFAGs for carbon ion acceleration. The NS-FFAG orbit offsets are in a range of 20-54 mm for the proton/carbon accelerator (the doublet NS-FFAG makes a slightly larger offset, up to 70 mm [6]).

We would like to show a few major properties of the proton therapy NS-FFAG accelerator and the advantages they provide in acceleration and for the gantry application:

- Small magnet size and linear variation of the fixed magnetic field implies reduction of cost, simplicity in construction, no eddy current problems as in the fast cycling synchrotron,and easier operation.
- Fast treatment of patients with a beam repetition rate of the order of ~1 kHz is possible. The variable harmonic jump could be applied in proton acceleration, with a fixed 1.3 GHz RF frequency (as explained in detail in the acceleration section). This would allow acceleration within ~100 turns.
- Tunable energy by using the extraction kickers at appropriate times without requirement for degraders.
- In the gantry application there is a dramatic reduction of the isocentric gantry weight from ~130 tons to ~1.5 tons. This reduces the overall weight of the whole structure with a support from the order of 630 tons.
- Three-dimensional spot scanning: two transverse and the longitudinal Bragg peak positioning.

The magnet sizes are shown in Figure 2 in the basic NS-FFAG cell description. Previously we selected 48 periods-cells and the whole complex of three NS-FFAG accelerators was presented in detail in [6]. In this report we present for the first time the triplet-based proton NS-FFAG ring. Our previous selection was the doublet option, mostly due to a smaller number of magnets. In the triplet design there are 48·3=144 magnets, while the doublet uses 48×2=96 magnets. The whole triplet ring is presented in Figure 3, while magnet properties are presented in Table 1. In Figure 3, the orbit offsets are magnified by a factor of 10 as is the size of the magnets. The circumference of the triplet NS-FFAG ring is the same as previously published for the doublet lattice, namely 43.2 m.

Table 1: Magnet properties in the triplet proton therapy design.

Magnet	L (m)	B_c (T)	A_p (mm)	G (T/m)	B (T)
BD	0.25	0.8578	-11.6 <–> +45.1	-23.7	−0.21 <–> 1.13
BF	0.11	-0.0100	-26.1 <–> +53.7	30.9	−0.82 <–> 1.65

The combined function magnet properties shown in Table 1 are: the length of the magnet "L" (m), the bending field at the central momentum, a range of the maximum

and minimum orbit offsets at the magnet aperture, the gradient and the variation of the magnetic field in the transverse direction.

Circumference 43.2 m
radius 6.8755 m
48 cells, l = 0.90
l cavity= 0.31 m

r_min= ro - 0.00799
ro=6.8755 m
r_out = ro + 0.0406

Orbits magnified 10 times
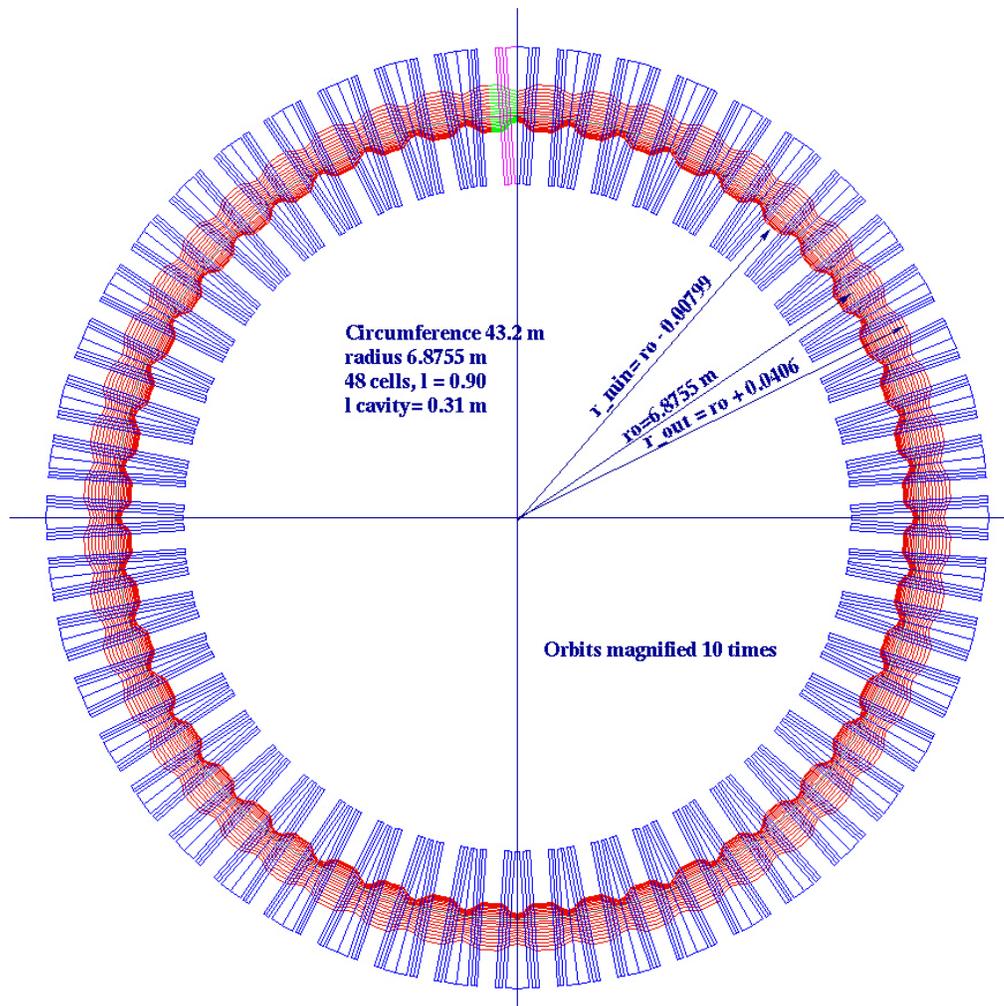
Figure 3: The proton therapy accelerator NS-FFAG made of 48 cells. The ring accelerates protons from a kinetic energy of 30 to 250 MeV. Acceleration is over 116 turns using the harmonic number jump method with an RF frequency of 1.3 GHz. Particle orbits are obtained using PTC tracking [4].

4.13.2.1   *Tune dependence on momentum and amplitude functions*

The NS-FFAG has to accelerate particles very rapidly as the tunes vary with momentum. Particles used in hadron therapy are accelerated in the non-relativistic regime and the variation of the path length with energy is dominated by change in velocity or the $\gamma\beta$ relativistic factors. In muon acceleration – the ultra-relativistic case – one of the major concerns is to make as short a path length variation as possible due to the fixed frequency. This is of no concern in hadron therapy. The scaling FFAGs have very small tune variation if there is any at all and the acceleration could be done in a larger number of turns. The tune dependence on momentum for this example is shown in Figure 4. There is crossing of the vertical and horizontal tunes at the beginning of
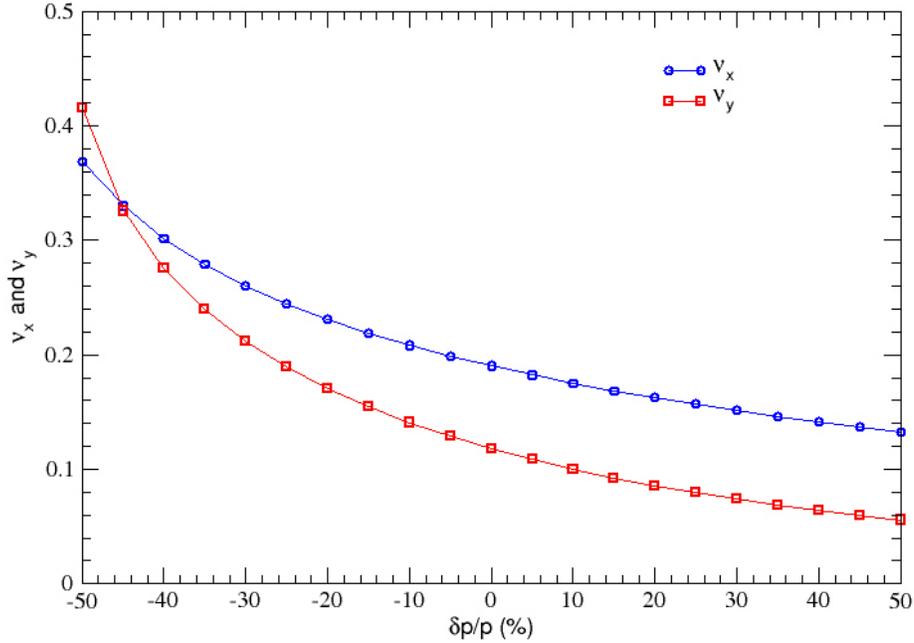
Figure 4: Tunes vs. momentum per single cell. It is important to avoid half-integer and integer tunes.

acceleration. We do not consider this to be a problem, as there is not enough time for a coupling "resonance" and in any case, the beam may be round.

The amplitude functions vary with momentum, especially close to end of the available momentum range as shown in Figure 5.

4.13.2.2 Acceleration

We adopt acceleration using the harmonic number h jump technique [7]. The energy gain in a turn ΔE is adjusted such that the change in $c\beta$ causes a change of the revolution period by an integral number of rf cycles, and hence corresponds to an integral step Δh in h. Since $\Delta\beta/\beta = -\Delta h/h$, and $d\beta/d\gamma=1/\beta\gamma^3$, it follows that $\Delta E=-E_0\beta^2\gamma^3\Delta h/h$, where E_0 is the rest energy of the particle. The smallest ΔE is achieved with $\Delta h=-1$ and large h. During acceleration, h decreases, since the revolution period decreases because of the increasing speed $c\beta$. At fixed Δh, ΔE increases rapidly during acceleration. Its variation can be reduced by starting acceleration with $|\Delta h|>>1$, gradually decreasing $|\Delta h|$, and switching to $\Delta h=-1$ towards the end [7]. Bunches are arranged in a train. The train occupies a fixed time interval ΔT, which is a small fraction of the revolution period at injection. This fraction of the revolution period grows during acceleration. The fraction of the circumference not occupied by the bunch train is useful for at least two purposes: one is for the rise time of kicker magnets, and the other for the rf manipulations outlined below. As can be seen in the example that follows, the harmonic number scheme involves a significant change in the energy gain per turn during acceleration. This variation can be accomplished in several ways. One possibility is a rapid change of the rf cavity voltage (implying inefficient low Q rf cavities).
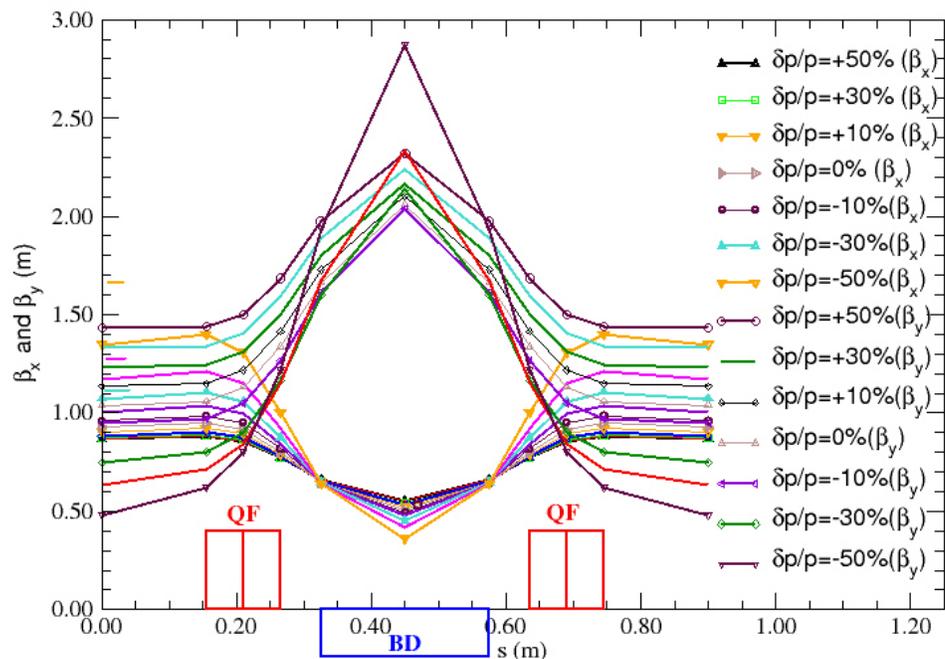
Figure 5: Dependence of betatron function on momentum for the proton non-scaling FFAG ring. Protons are accelerated from a kinetic energy of 30 MeV to a maximum energy of 250 MeV.

The harmonic number jump scheme has an energy gain per turn that is much larger than in a synchrotron. The high rate of acceleration ensures fast crossing of the resonances. Table 2 shows the main parameters of the rf system. The number of turns is significantly smaller than the difference h_i-h_f, because of the initial step $|\Delta h| > 1$, and it is much smaller than it is in a synchrotron.

Table 2: Proton acceleration in the non-scaling FFAG: $f_{RF} \sim 1.3$ GHz, initial and final harmonic numbers h_i and h_f, initial step $|\Delta h|$, number of turns, and maximum circumferential voltage V.

	h_i	h_f	$|h|$	turns	V(MV)
H^+	745	305	25	116	2.4

4.13.3 Another example of a medical NS-FFAG ring

Another example of the triplet NS-FFAG cell, as a part of a possible ring in a future Oxford facility, is shown in Figure 6. The maximum kinetic energy is 100 MeV. If the ring can accelerate within the momentum range of $\delta p/p = \pm 50\%$, then the lowest kinetic energy is 11.6 MeV. The magnetic fields are kept to be within the permanent magnets' capabilities with the maximum field on the transverse axis of 1.98 T. The maximum and minimum orbit offsets are: $x_{off} = +49.5$ mm and $x_{off} = -24.5$ mm, respectively. The magnet properties are shown in Table 3.

A picture of the NS-FFAG ring for the medical studies at the Oxford facility (made to fit between existing poles) is shown in Figure 7. The drift length for the cavity and injection/extraction kickers is 25.3 cm.
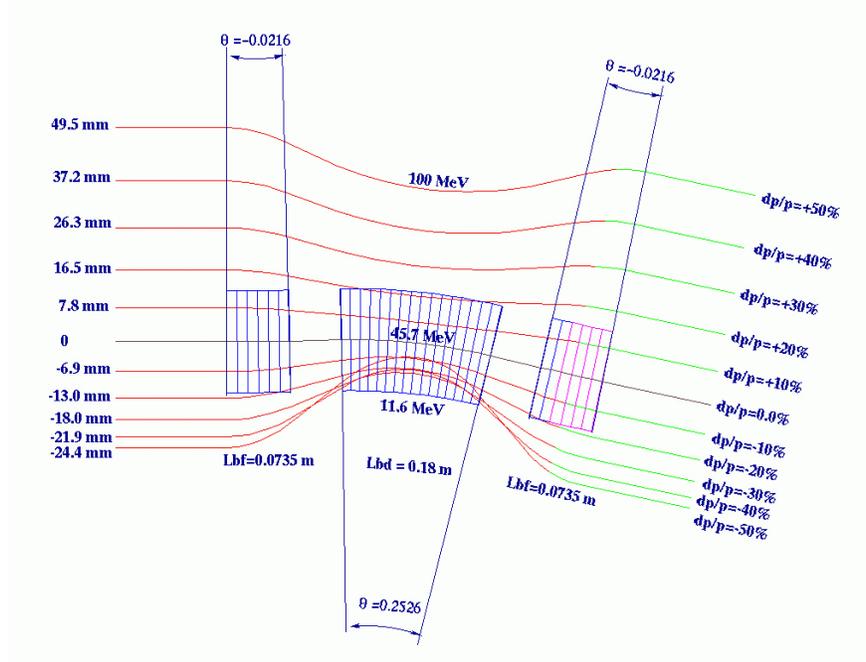
Figure 6: Orbits in a cell for a possible NS-FFAG at Oxford University, U.K. The proton beam is accelerated from a kinetic energy of 11.6 MeV to a maximum energy of 250 MeV. The circumference of the ring is 21 m.
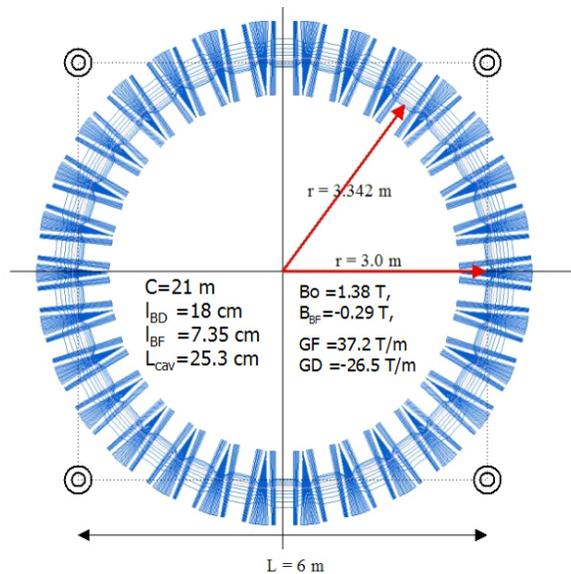
Figure 7: Non-scaling FFAG ring with triplet magnet cells as a possibility for the Oxford University proton medical accelerator. The protons are accelerated from the kinetic energy of 11.6 to 100 MeV.

Table 3: Magnet properties in the triplet proton therapy design:

Magnet	L (m)	B_c (T)	A_p (mm)	G (T/m)	B (T)
BD	0.1800	1.38	-23 <–> +25.1	-26.5	0.71 <–> 1.98
BF	0.0735	-0.29	-24 <–> 49.5	37.2	1.18 <–> 1.55

4.13.4 A NS-FFAF gantry

A major challenge and cost in present and future hadron therapy facilities is the beam delivery system. In almost all facilities, at least one of the patient delivery rooms is equipped with an isocentric gantry system. An isocentric gantry system is becoming a necessity for each facility; it is especially important for treating hard-to-reach tumors especially around the spine (chordomas, low grade chondro-sarcomas, unresectable sacral chordomas). Hadron therapy treatment requires different incident angles to avoid damage to sensitive areas (such as the spine) by radiation. The gantry must deliver a
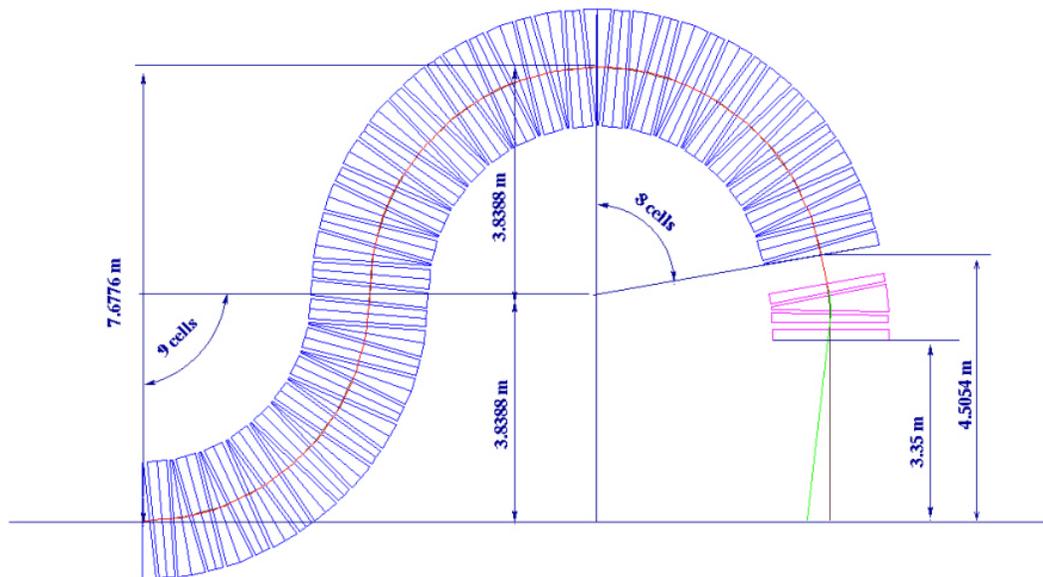
Magnet dimensions:
BD = 25 cm GD =-33.7 T/m, B=1.5 T + 33.7 T/m*0.012 mm = 1.9 T
BF = 30 cm GF =+35.5T/m, B=-0.25 T -+ 35.5 m*0.028 mm = 1.2 T

Figure 8: Proton gantry made of non-scaling FFAG cells with a magnetic field sufficiently small that permanent magnets can be used. Superconducting magnets made without any iron could be used to reduce the size (perhaps by as much as a factor of two).

precise ion dose to the patients with very good reliability and stability. Larger cancerous tumors require transverse position scanning at different beam energies and an angle variation around the patient provided by gantry rotation. The newest state-of-the-art gantry for hadron therapy made of standard warm magnets is in the facility in Heidelberg [8]. In the NS-FFAG gantry [9], the necessary drifts for the rf cavities and injection/extraction kickers for the accelerator are not required at all. This further reduces the orbit offsets and makes it more compact. Reduction of the orbit offsets

makes the magnets even smaller than any other known FFAG application. A design for the proton gantry application is shown in Figure 8.

The very large momentum acceptance of the NS-FFAG allows the gantry to transfer ions with fixed magnetic field over the whole of the energy range required for treatment. The weight of the transport components in the gantries for hadron therapy ranges over the order of 140 tons [9]. The NS-FFAG concept reduces the overall gantry weight to a few tons because elements could be made of small permanent magnets for the proton machine, or of superconducting magnets without any iron in either the proton or carbon case. The transverse scanning is provided at the end of the gantry ~3-4 m above the patient.

The gantry cell consists of two types of combined function magnets: the major bend with horizontally defocusing gradient and the opposite bend with a focusing gradient.

4.13.5 Possible further developments

There are a few disadvantages in the NS-FFAG concept for a medical facility using hadron acceleration. They are: the tune variation with momentum, relatively large number of repetitive cells (~40), and a smaller energy range than the scaling FFAG. There are possible compromises with respect to present NS-FFAG designs:

- The size of the aperture could be larger. This would allow reduction of the number of cells. The argument for the smaller size magnets might still be valid if the aperture size is not dramatically raised. This could be of the order of ~20 cm with a circumference of ~20 m and a radius of 3.6 m, an energy acceptance of $\delta p/p = \pm 60\%$, with the number of cells equal to 16. This work is still in progress.
- A reduction in circumference from 42.2 m to 28 m is possible. The medical NS-FFAG, without reducing the total number of cells, could be obtained by a combination of two rings: one with smaller radius and without any drifts for cavities with the other a regular NS-FFAG with cells to allow cavity and extraction/injection kicker placement. The first racetrack attempts have already been reported [10].

4.13.6 Summary

The NS-FFAG represents a competitive solution for hadron therapy. The concept will enjoy wider acceptance as soon as the first proof-of-principle machine is completed. Very small superconducting magnets used for the NS-FFAG carbon/proton acceleration represent a possible solution. A reduction in the time for patient treatment by the faster 1 KHz hadron ion delivery rate, the fixed magnetic field (assumes simpler and easier operation with no eddy current problem as in fast cycling synchrotrons), simple and possibly low cost combined function magnets are all positive arguments.

The NS-FFAG gantry application with two orders of magnitude reduction in the gantry weight has already obtained very strong interest within the hadron therapy community.

4.13.7 References

1. R. R. Wilson, "Radiological use of fast protons," Radiobiology 47, p. 487-491, 1946.
2. S. Peggs, T. Satogata, and J. Flanz, "A Survey of Hadron therapy Accelerator Technology", invited talk at Particle Accel. Conference, Albuquerque, 2007.
3. D. Trbojevic, E. Courant, and M. Blaskiewicz, Phys. Rev. Spec. Topics – Accelerators and Beams **8**, 050101 (2005).
4. E. Forest, E. Mcintosh and F. Schmidt, KEK Report 2002-3, CERN-SL-2002-044 (AP), 44, 3 (2002).
5. C. Johnstone and S. Koscielniak, "New Non-Scaling FFAG for medical applications", Proceedings of PAC07, Albuquerque, New Mexico, USA, 2007, THPMN103.
6. E. Keil, A. M. Sessler, and D. Trbojevic, "Hadron cancer therapy complex using non-scaling fixed field alternating gradient accelerator and gantry design", Phys. Rev. Spec. Topics Accelerators and Beams, **10**, 054701(2007).
7. A.G. Ruggiero, "RF acceleration with harmonic number jump", Phys. Rev. Spec. Topics – Accelerators and Beams, **9,** pp. 100101(2006). See also article in this issue of ICFA Beam Dynamics Newsletter.
8. U. Weinrich, "Gantry Design for Proton and Carbon Hadrontherapy Facilities", Proceedings of EPAC'06, Edinburgh, UK, 964, (2006).
9. D. Trbojevic, E. Keil, and A.M. Sessler, "Carbon/proton therapy: A novel gantry design", Phys. Rev. Spec. Topics – Accelerators and Beams, **10**, 053503(2007).
10. D. Trbojevic, "Muon acceleration with a racetrack non-scaling FFAG", PAC07, Albuquerque, New Mexico, June 26-29, (2007).

4.14 A New Non-scaling FFAG for Medical Applications

C. Johnstone, S. Koscielniak
Mail to: cjj@fnal.gov
Fermilab[*], Batavia, IL 60510, U.S.A.
TRIUMF[†], Vancouver, BC 60439, Canada

4.14.1 Introduction

A hybrid design for a linear-field, non-scaling FFAG accelerator has been invented which uses edge and alternating-gradient focusing principles applied in a specific configuration to a combined-function (CF) magnet to stabilize tunes through an acceleration cycle which extends over a factor of 6 in momentum. By using fixed, rather than ramped, magnetic fields the machine proposed here has the high current advantage of the cyclotron yet retains important features of the synchrotron: smaller

radial aperture, variable energy, and both kicker-based and resonant extraction. Using normal conducting magnets, the highest, extracted energy from this machine slightly exceeds 400 MeV/nucleon and thus supports, without modification, both a proton and a carbon ion beam in the energy range of interest for cancer therapy. Competing machines for this application include superconducting cyclotrons [1], synchrotrons [2], and, more recently, FFAGs [3]. As such this machine represents a significant and broad innovation in therapy machines.

In recent years, linear-field FFAG accelerators have been successfully designed for applications requiring rapid acceleration, where a variation of optics with momentum can be tolerated. Historically [4], these non-scaling FFAGS, accelerate a factor of 2-3 in momentum, and execute on the order of ten turns. Slow acceleration, where beam executes hundreds to thousands of turns in the machine, greatly reduces rf requirements and expense, but requires, at a minimum, a stable tune in order to avoid resonances and associated beam blow up and loss. Since position in a fixed field accelerator is always energy dependent, the integrated magnetic (focusing) strength must scale with the energy of the beam, and accurately track the position of the beam as it moves outward across the magnetic aperture during acceleration. In scaling FFAGs strong, high-order multipole fields are incorporated directly into the magnetic field profile to achieve this change (as in the radial sector [5] FFAG), or through elaborate edge shaping (as in the spiral sector [6] FFAGs). All such scaling-type magnet designs require sophisticated 3D field modelling to ensure accurate scaling optics.

The new concept proposed here is to stabilize tunes without directly introducing nonlinear field components by using a linear-gradient magnetic field to provide the bulk of the transverse beam confinement (or tune) combined with a significant edge angle to compensate for the energy change. The field in the body of the magnet has only a linear dependence on transverse position, i.e. a CF magnet with both quadrupole and dipole components. Using only linear fields and associated edge-focusing means that not all of the optical functions can be constrained as a function of energy – but, most importantly, the tune can be. Since this design is based on an ultra-short FODO cell, other optical parameters (beta functions) are slow functions of momentum and experience with non-scaling FFAGs has shown that such adiabatic changes of optical functions do not contribute significantly to transverse beam blow up [7].

4.14.2 Discussion

Despite applying only constant and linear gradient field profiles, the dynamics do not strictly obey linear optics. A sextupole component [7] arises when the quadrupole body field is combined with an edge angle. Still, this approach provides a unique and advantageous combination of multipoles which cannot be achieved through the introduction of individual multipole fields. Further, there is only one magnetic-field configuration which works when one considers both quadrupole focusing and edge-focusing effects on the transverse beam envelope, and that is the one described here. The background and rationale for the new transverse beam confinement scheme will be discussed in the following.

4.14.2.1 Stability

Tune is perhaps the most important optical indicator of stable particle motion, since it determines when particles in the beam, executing periodic motion around the

accelerator, return to the same transverse position relative to a central, or reference orbit in the machine. In a fixed-field machine such as an FFAG or cyclotron, this reference orbit moves with energy. In a synchrotron, the magnetic field increases proportional to energy and therefore particles are confined about a laboratory-based reference trajectory independent of energy.

In a scaling FFAG design, the beam optics remain constant with energy – the beam envelope and tunes along with all other optical parameters remain fixed. The non-scaling FFAG relaxes this condition and aims only for stable beam during acceleration. If the acceleration is quick, then tune variations can be tolerated. If the acceleration is slow the tune must be more controlled (although some tune variation can be accommodated or compensated for if the acceleration cycle is slow enough).

4.14.2.2 Tune and Transverse Envelope Control

Three conventional methods exist for controlling the beam envelope and phase advance using linear fields, i.e. dipole and quadrupole fields. (Here we refer to the linear lattice functions and the linear tune.) One is the weak focusing principle used in classical cyclotrons in which changes in path-length through the magnetic field as a function of transverse position focus the beam, but only in the bend plane (which is typically horizontal). Vertical control is achieved by radial shaping of the pole-tip and this is weaker than focusing from path-length differences.

By alternating the sign of both constant (dipole) and gradient (quadrupole) fields, two strong-focusing techniques can be applied: edge focusing which occurs in the fringe fields of a dipole and constant-gradient, or quadrupole, focusing which is the main technique used in a synchrotron. Strong-focusing techniques are capable of focusing equally in both planes with much stronger focusing strength, particularly in the case of the quadrupole field. As is well known, stronger focusing results in larger phase advances, shorter focal lengths, and corresponding higher machine tunes than achievable in weak-focusing machines, i.e. stronger envelope control.

Both principles are generally applied in FFAGs—scaling machines specifically require edges plus quadrupole and higher multipole fields to achieve constant optics. A new type of FFAG, a linear-field non-scaling FFAG which does not use edge-angle focusing specifically nor nonlinear field gradients was proposed by the authors for rapid acceleration. Constant optics are not a requirement for rapid acceleration, however, the beam envelope must exhibit stability across all energies, or beam particles are bent out of the ring by the main fields. This implies constraints on the range of phase advance across a unit cell: typical tune stability limits are $\sim 0.7\pi$ - 0.2π radians per cell for realistic magnets and machines. Both practical magnet apertures and stable phase advances further limit the achievable momentum range of linear-field non-scaling FFAGs for rapid, or muon, acceleration to a factor of 2-3. In these applications magnets are generally simple rectangular ones. Clearly the short acceleration cycle requires a tremendous amount of radio-frequency accelerating cavities to be installed in order to accelerate the beam quickly and there are no fine controls over the beam. This design is therefore not suitable for many applications. However, if the tune were more stable, then the momentum reach of the machine increases, and acceleration can progress slowly – over thousands of turns as in a conventional cyclotron or synchrotron with a modest rf system. A new non-scaling approach therefore is proposed here: one which constrains the tune to allow for a longer acceleration cycle. The new concept entails combining weak and strong focusing principles in a specific configuration to a fixed-

field (DC) combined-function magnet to stabilize the tune over a very large energy range (currently a factor of 6).

4.14.3 Tune-stable, Linear-field non-scaling FFAG

4.14.3.1 General Principles

Combining the different focusing principles can mitigate tune variations with energy in a non-scaling FFAG yet maintain smaller apertures without the nonlinear fields used in scaling FFAGs. However, only one magnetic-field configuration succeeds and that is the one derived and applied here.

To hold the tune constant and confine a finite beam transversely as its energy increases by applying linear gradients only, i.e. quadrupole fields, require the beam to traverse longer and longer paths through the magnet. (Here we are addressing transverse-amplitude focusing, not the net curvature of the central or reference-particle orbit which is determined by the constant, or net dipole, field.) This can be accomplished by a wedge magnet since higher-energy particles follow outer radii orbits.

The problem, however, is not as simple as scaling path-length with energy since, when a vertically-oriented (horizontally-bending) dipole field is present, the physical magnet edge angle brings with it a horizontally focusing or defocusing effect, or no effect in the case of a rectangular magnet. Weak focusing by the dipole field in the body of the magnet does not affect the vertical plane. However, focusing by the fringe field of the magnet depends on the angle through which the beam traverses the fringe field. This effect is essentially equivalent to a quadrupole located at each magnet edge: it can be either focusing horizontally and defocusing vertically, or the reverse. (A normal entrance angle has no focusing effect.) The fringe-field traversal angle can be utilized to work with the body quadrupole field in the magnet or against it. Further as the energy changes in a non-scaling FFAG so do the reference orbits and entrance/exit angles. Hence the sign of the effect can be changed within the acceleration window. This combination of the different magnet edge and entrance/exit angle effects indicate that the problem is not straightforward, but, in principle, a preferred and optimal solution exists. The solution proposed here is to use different combined function magnets (dipole + quadrupole) for the horizontally-focusing element and the vertically-focusing element. In the horizontally focusing element the combined function fields can be configured such that weak plus fringe-field focusing effect adds with quadrupole focusing, increasing the net horizontal focusing of the beam envelope in the outer-radii region of the element. In this way, the factor of 6 increase of path-length through a quadrupole field from injection to extraction can be reduced to approximately a factor of two and still constrain the tune.

For the vertical plane, the same is true in the vertically-focusing element, but from the fringe field effect alone. In this magnet the field configuration is such that the net vertical focusing also increases with radius and again the required path-length difference is mitigated from injection to extraction

4.14.3.2 Matrix Expansion

To understand the interplay between weak and alternating strong focusing, a simple linear, thin-lens matrix model serves as a guiding example. The approach is most easily

examined using sector magnets, then adding quadrupole fields and edge angles. The following low order matrix is used for a horizontally-focusing sector magnet:

$$M = \begin{bmatrix} \cos\Theta & \dfrac{1}{\sqrt{K}}\sin\Theta \\ -\sqrt{K}\sin\Theta & \cos\Theta \end{bmatrix} \approx \begin{bmatrix} 1 & l \\ -Kl & 1 \end{bmatrix}$$

where $\Theta = \sqrt{K}l$ and $K = k_0 + \dfrac{1}{\rho_0^2}$ for a C.F. sector magnet. Note that $Kl = \dfrac{1}{f}$ where f is the focal length of the magnet. If one adds an edge angle, where we adopt the sign convention to be opposite the norm ($\eta > 0$ is outward, or away from the body of the magnet and increases net horizontal focusing in all magnets), then the matrices from the center of the quadrupole to the end of the magnet to lowest order are:

$$\begin{bmatrix} 1 & 0 \\ -\tan\dfrac{\eta}{\rho_0} & 1 \end{bmatrix}\begin{bmatrix} 1 & l \\ -Kl & 1 \end{bmatrix} \approx \begin{bmatrix} 1 & 0 \\ -\dfrac{\eta}{\rho_0} & 1 \end{bmatrix}\begin{bmatrix} 1 & l \\ -Kl & 1 \end{bmatrix} = \begin{bmatrix} 1 & l \\ -(k_F l + \dfrac{l}{\rho_0^2} + \dfrac{\eta}{\rho_0}) & -\dfrac{\eta l}{\rho_0} + 1 \end{bmatrix}$$

$$\cong \begin{bmatrix} 1 & l \\ -(k_F l + \dfrac{l}{\rho_0^2} + \dfrac{\eta}{\rho_0}) & 1 \end{bmatrix} = \begin{bmatrix} 1 & l \\ -(k_F l + \dfrac{(\vartheta + \eta)}{\rho_0}) & 1 \end{bmatrix}$$

since $\dfrac{l}{\rho_0^2} \cong \dfrac{\vartheta}{\rho_0}$, where ϑ is the sector bend angle and now the length l is the half-magnet length.

One can immediately see that the sector angle and edge angle term increase the focusing in the horizontal plane for a positive bend angle or dipole component. The choice of dipole component – which changes at each reference orbit as a function of energy – has very important consequences. If the dipole component is chosen correctly, then focusing increases with energy relative to injection with the sector-angle term and the edge-angle one adding constructively with the quadrupole term at the extraction energy. Both planes are not identical, however, for in the vertical only the net edge angle contributes to a change in focusing strength.

4.14.3.3 Lattice Design

The ring must be completely periodic and here a FODO cell containing two CF magnets was chosen as the base structure. A minimum 0.5 m length has been imposed on the two drifts in each FODO cell to accommodate the acceleration cavities. A target cell tune of 90° was chosen to facilitate injection/extraction from the ring, and the observed variation, without optimization, was calculated to be ~0.24 ± 0.06 between the injection and extraction points, considering both the horizontal and vertical. A graph of the tunes as modeled using MAD at different momentum values is shown in Figure 1. Comparison with the tune variation/cell for the non-scaling FFAG for rapid acceleration is also provided.

Many simulation codes are presently inadequate to find closed orbits and optics for the far off-momentum orbits encountered. Therefore, solutions for individual magnetic-field configurations at different points in the acceleration cycle had to be obtained via a set of simplified equations and the results placed into MAD for each point plotted. Both the tunes which are solutions of the simplified equations (approx) are compared with the results from the MAD model.
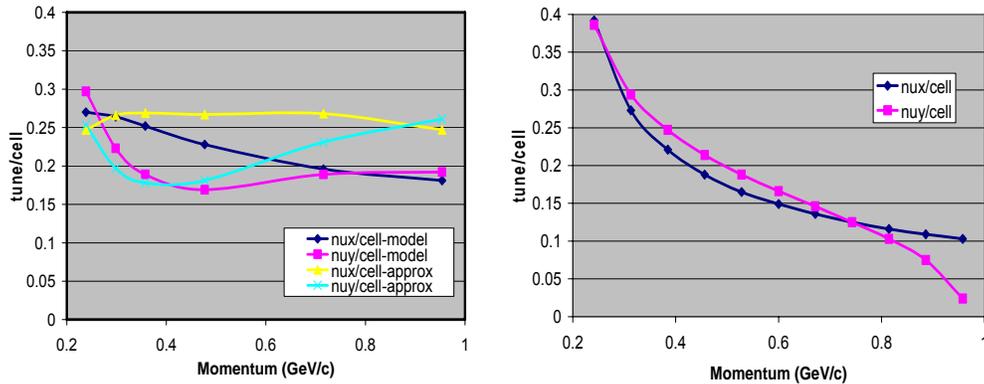
Figure 1: Dependence of cell tune on momentum in a non-scaling, linear-field FFAG which is tune-stabilized for medical therapy. In the legend, 'approx' means the solution obtained from solving a set of approximated optical equations and 'model' means the tune as modeled in MAD using solutions found for the CF magnetic fields. Dependence of cell tune on momentum in a linear-field FFAG designed for rapid, or muon, acceleration is shown on the left.

Note that the tunes are not perfectly flat in the current design with the horizontal tune exhibiting less variation than the vertical tune due to the additional contribution from weak focusing. More elaborate edge contouring would be required to flatten particularly the vertical tune further. In the new application, the components are non-superconducting with solid iron cores (no laminations) so that accurate edge or even pole-face contouring – a standard technique in cyclotrons – can be used.

Orbits in a non-scaling FFAG are not parallel as in a scaling one, and are drawn together in a configuration that decreases the relative magnet aperture and cost. This is true also for this new non-scaling design, although not as efficiently as in the muon accelerators. However, aperture is less of a concern with non-superconducting, solid iron-core magnets. A cartoon of "thin-lens" orbits in this new non-scaling FFAG is given in Figure 2 and again compared with a "muon"-type accelerator. Tables 1 and 2 offer additional comparative information.
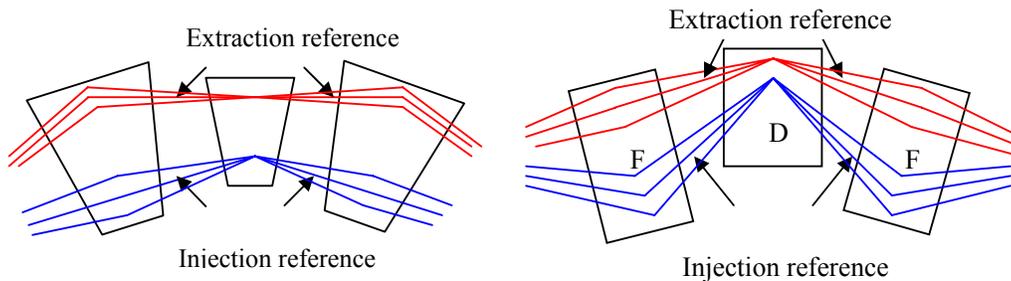
Figure 2: 1½ cells of a non-scaling, linear-field FFAG which is tune-stabilized for medical therapy (left) compared with 1½ cells of a doublet-based non-scaling FFAG (right) for muon acceleration.

4.14.3.4 Tracking

At this point, using the MAD code, it is not possible to track over the large momentum offsets and change in optics and edge effects reliably. Therefore, this lattice

Table 1: General Parameters of the 400 MeV non-scaling FFAG design for medical applications.

Parameter	Unit	Injection	Extraction
Energy Range	MeV/nucleon	18	400
Tune/cell (ν_x / ν_y)	2π-rad	0.27 / 0.30	0.18 / 0.19
Circumference	m	40	
No. cells		14	
Straight	m	>1	0.5
Peak field	T	1.5	
Apertures	m	~1	

was tracked at the injection energy, which has the largest geometric emittance, in order to demonstrate the limiting dynamic aperture. Tracking over 4,000 turns at this energy

Table 2: General Parameters of an equivalent muon non-scaling FFAG.

Parameter	Unit	Injection	Extraction
Energy Range	MeV/nucleon	114	400
Tune/cell (ν_x / ν_y)	2π-rad	0.39 / 0.39	0.10 / 0.02
Circumference	m	41	
No. cells		16	
Straight	m	0.5	
Peak field	T	1.5	
Apertures	m	~1	

gives the phase space portraits of Figure 3, which, in turn, correspond to a dynamic aperture of 10-20π mm.mr (geometric emittance, ~95%).

Clearly in the complete machine using only linear edges, the beam passes through some resonances. However the resonances resemble more those through which beam in cyclotrons pass than the large number and types of resonances which are traversed in the muon version of this accelerator.
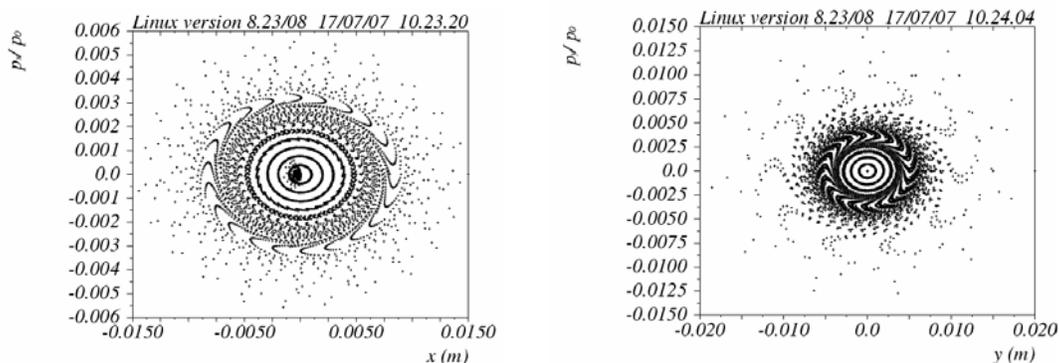
Figure 3: Phase space portraits which correspond to 4,000 turns of the proposed machine at the injection energy.

4.14.3.5 Injection and Extraction

Like a synchrotron, drifts between magnets allow for multiple injection and extraction ports. One could, for example, have different injection ports for proton and carbon beams, respectively, thus eliminating the need to change out sources. The injection energy of 18 MeV/nucleon was chosen to correspond to an industry-standard proton cyclotron. Likewise, different extraction ports could also feed different beamlines to different treatment rooms or again for different ions.

A very strong advantage of this design is the potential for synchrotron-like extraction. Variable energy and multi-port extraction is possible along with fast and slow resonant extraction. These extraction options greatly enhance the applications of this new non-scaling FFAG. For a kinetic energy of 400 MeV/nucleon, the kicker strength is modest: only 5 mr or 0.5 kG is required to divert beam ~1 cm into a septum magnet. The FFAGs also exhibit the low loss extraction characteristics of the synchrotron.

4.14.4 Summary

A hybrid design for a FFAG accelerator has been developed which successfully applies weak, edge, and linear-gradient focusing principles to a fixed-field (DC) combined-function magnet to stabilize tunes. In this approach, the momentum reach has been enlarged from a factor of 2-3 to a factor of 6 when compared with an equivalent muon accelerator design. The quadrupole gradient provides the majority of the phase advance per cell and weak and edge focusing from dipole fields provide the change in focusing strength needed to track the change in momentum during acceleration. With stabilized tunes, this FFAG behaves more like a synchrotron with multiple energies available for extraction and use, and with the attractive low-loss feature characteristic of synchrotrons. With its fixed fields, the magnets and power supplies are simple and this machine can be effectively operated continuously with potentially high output beam current which is the noted strength of the cyclotron. The designs here specifically apply only to normal conducting fields and still attain carbon therapy kinetic energies of 400 MeV/nucleon. Lower energy proton beams are simultaneously supported. Also like the synchrotron and unlike the cyclotron, there are multiple places to extract beam supporting multiple treatment rooms or other applications.

4.14.5 References

1. M. Schillo, AIP Conf. Proc. 600, Cyclotrons and Their Applications 2001, 16th Int. Conf., M.S.U., E. Lansing, MI, USA, pp. 37-39.
2. NuPECC Report on Impact, Applications, Inter-actions of Nuclear Science (2002). Nuclear Physics European Collaboration Committee http://www.nupecc.org/iai2001
3. E. Keil, Phys. Rev. ST-AB, 10, 054701 (2007).
4. C. Johnstone et al, Proc. of 1999 Particle Accelerator Conference, New York NY, 1999, pg.3068

5. T. Misu et al, Phys Rev Special Topics - AB, Vol 7, 094701 (2004). A. Wolski and M. Woodley, "The NLC Main Damping Ring Lattice" NLC LCC-0113, LBNL CBP Tech Note-276, February 2003.

6. M. Tanigaki et al, Proc of 2005 Particle Accelerator Conference, Knoxville, Tennessee, pp. 350-352.

7. S. Machida, Proc. U.S. Particle Accelerator Conference PAC07, Albuquerque NM, 2007. See also this edition of ICFA Beam Dynamics Newsletter.

8. S. Koscielniak et al, Proceedings of PAC07, June 25-29, TUPAN001, Albuquerque, NM.

5   Activity Reports

5.1   ICFA Beam Dynamics Panel Meeting Minutes

Date and time: June 25, 2007, 6:00 pm – 8:00 pm

Place: Albuquerque, New Mexico, U.S.A. during PAC07

Attendees: C. Biscari (INFN), S. Chattopadhyay (Cockcroft), W. Chou (Fermilab, Chair), M. Furman (LBL), S. Henderson (SNS, invitee), I. Hofmann (GSI), K-J. Kim (ANL), I.S. Ko (PAL), E. Malamud (Fermilab, retired, invitee), C. Prior ((RAL), D. Rice (Cornell), A. Takagi (KEK, invitee), J. Urakawa (KEK), J. Wang (IHEP/China), R. Wanzenberg (DESY), M. Yoshii (KEK, for Y. Mori)

Sixteen people attended the meeting, including panel members and invitees. Chou chaired this meeting. The agenda is in the Appendix 1.

Panel and Working Group Reports

The Panel Chair gave a report, summarizing panel activities over the past two years. The Panel organized seven *ICFA Advanced Beam Dynamics Workshops* (ABDWs) and several *ICFA Mini-Workshops*. Beginning in 2006, ABDW proceedings have been published by JACoW. Seven issues of the *ICFA Beam Dynamics Newsletter* were published. All newsletters from no. 1 through no. 42 have now been archived and are available online. The Panel also participated with the ILC GDE to organize the successful first *International Accelerator School for Linear Accelerators*. The second school is now being organized and will be held in Erice in October 2007.

Four working group leaders – Biscari, Kim, Rice and Mori (represented by Yoshii) – gave reports on working group activities. There was discussion of the FLS workshop series and the ERL workshop series. Both have been well attended (120 – 150 people). Although there was overlap in subject matter between the two series, it was agreed that both series should continue because of their importance to the beam dynamics community. The remote accelerator physics experiment working group was discussed.

This group has not been active in recent years. Rice (group leader) said it was difficult to carry on the group's mission. He suggested changing the mission to facilitation of communication within the accelerator community if the group is to continue to exist.

Length of Terms on the Panel

Biscari introduced a discussion on membership and working group leadership turnover. She emphasized the importance of getting fresh blood on the Panel. People can become tired and bored by remaining on the Panel for too long a period. Although the formal invitation letter to become a panel member defines a 3-year term, no formal mechanism exists to enforce this. Rice made the following proposal: after the 3-year term ends, the Panel Chair will write to the Panel member whose term is expiring, either informing him/her that the term is ending or inviting him/her to continue to serve for another 1, 2 or 3 years. The maximum extension will be 3 years for a total period of service of 6 years, i.e., 2 full terms. The Panel unanimously approved this proposal.

PAC Cycle

The Panel discussed a proposed letter from the Panel to Stan Schriber, Chair of the PAC Organizing Committee, concerning the cycle of PACs. The letter urges the PAC OC to support the creation of IPAC, a 3-year cycle of PAC, EPAC and APAC. The Panel unanimously approved this letter (Appendix 2). It will be sent to Schriber immediately, in time for the PAC OC meeting on Tuesday June 26, 2007. (Note added: The letter was e-mailed to Schriber after the panel meeting.)

Open Access Publishing

Open Access (OA) Publishing was discussed. This is a topic currently on the table for discussion by ICFA. The Panel believes OA would be good for the HEP community. ICFA should play a leading role in a campaign to accomplish this major paradigm shift. The focus is on 6 journals in which 90% of all papers relevant to HEP and beam physics are published.

New Workshops

The following were described and discussed:
- HB2008, September 2008 in Nashville, U.S.A. (Henderson)
- e^+e^- workshop, March 2008 in Novosibirsk, Russia (Biscari)
- FLS workshop, May 2009 at SLAC (Kim)
- ERL workshop, spring or fall of 2009 at Cornell (Rice)
- Collective effects in damping rings in 2008 at BNL (Kim)
- Deflecting cavities for light sources and colliders, April 2008 in Shanghai, China (Kim)

Proposals for these workshops will be prepared by panel members for ICFA approval. Chou pointed out that the proceedings for all new workshops must be published by JACoW. The alternative is to hold ICFA mini-workshops, which only need the Panel's approval and publication of formal proceedings is not required.

Future Newsletters

The following people volunteered to edit future newsletters:
- No. 43, August 2007: Chris Prior (RAL)
- No. 44, December 2007: Ajay Ghodke (RRCAT)
- No. 45, April 2008: Rainer Wanzenberg (DESY)
- No. 46, August 2008: Miguel Furman (LBL)
- No. 47, December 2008: In Soo Ko (PAL)
- No. 48, April 2009: Dave Rice (Cornell)
- No. 49, August 2009: Jiuqing Wang (IHEP, China)

Biscari suggested holding the next panel meeting during EPAC'08. At that time there may be new Panel members who can become newsletter editors.

Appendix 1: Meeting Agenda

1. Report from the Panel   W. Chou
2. Report from the Working Groups   C. Biscari
                                                     K-J. Kim
                                                         D. Rice
                                                         M. Yoshii (for Y. Mori)
3. Membership and WG leadership turnover   C. Biscari
4. PAC and 3-year cycle
5. Open Access Publishing
6. New workshop proposals
7. Newsletter editors for the next two years
8. Any other business

Appendix 2: Letter to Stan Schriber and the PAC Organizing Committee

June 25, 2007

Dr. Stan Schriber
Chair, PAC Organizing Committee

Dear Dr. Schriber and members of the PAC Organizing Committee,

There have been many discussions over the past year in our community about a proposed merging of the three major particle accelerator conferences – PAC, EPAC and APAC – into one international conference alternating between the three regions on a 3-year cycle. We, the ICFA Beam Dynamics Panel, are writing to urge the PAC OC to support this proposal.

Our panel consists of about 20 accelerator physicists representing the international beam dynamics community. This panel publishes the *ICFA Beam Dynamics Newsletter*, organizes *ICFA Advanced Beam Dynamics Workshops* and *ICFA Mini-Workshops*, and endorses various working group activities including light sources, high

intensity and high brightness hadron beams, high luminosity e+e- colliders and remote experiments in accelerator physics. At today's biennial panel meeting, we discussed the 3-year cycle proposal and unanimously decided that our panel will give endorsement to this proposal. As stated on the panel web site (http://www-bd.fnal.gov/icfabd/) the mission of our panel is "*to encourage and promote international collaboration on beam dynamics studies for present and future accelerators*." The 3-year cycle proposal is in agreement with the panel's mission. A combined International Particle Accelerator Conference (IPAC) in lieu of PAC, EPAC and APAC is most appropriate for the future of our field, which is more internationalized than ever with new and proposed projects such as LHC, ILC, J-PARC, XFEL and LCLS.

We note that both EPAC and APAC have agreed to the 3-year cycle and EPAC decided not to have a conference in 2010 so that APAC2010 can be the only international particle accelerator conference in that year. We hope the PAC OC will reach a similar agreement and start a 3-year cycle at the earliest possible date.

Thank you for your consideration.

Sincerely,
ICFA Beam Dynamics Panel

6 Workshop and Conference Reports

6.1 Report on the 18th Meeting of the International Collaboration on Advanced Neutron Sources

Stuart D. Henderson
Mail to: shenderson@ornl.gov
Oak Ridge National Laboratory, Neutron Sciences Directorate,
Spallation Neutron Source, Research Accelerator Division.
P.O. Box 2008, MS 6462, Oak Ridge, TN 37831-6462

6.1.1 Introduction

The 18th Meeting of the International Collaboration on Advanced Neutron Sources (ICANS XVIII) was held April 25-29, 2007 in Dongguan, Guangdong Province, China. The Meeting, chaired by Dr. Jie Wei, was hosted by the Institute of High-Energy Physics and the Institute of Physics of the Chinese Academy of Sciences in Beijing. Whereas the Meeting was devoted to the broad range of technical issues of importance for accelerator-based neutron sources, this report summarizes only the accelerator aspects of the Meeting.

This Meeting attracted many accelerator scientists and engineers not only from accelerator-based neutron sources, but also from the larger field of high-power proton and ion beams. The meeting was attended by approximately 50 accelerator scientists

and engineers from 10 countries. There were 45 oral presentations and 8 poster presentations presented in 11 sessions on topics ranging from accelerator-driven spallation neutron sources, to high-intensity proton and hadron accelerators for high-energy physics, radioactive ion beams, accelerator driven systems and fusion material irradiation, to medical applications, to reports on other accelerator projects in China. Meeting information and the proceedings are available at the conference website: http://www.icans-xviii.ac.cn/ .

The plenary session program included status reports on the major operating or planned facilities: ISIS by A. Taylor, the Spallation Neutron Source (SNS) by the author, the J-PARC Project by Y. Ikeda, the Swiss Spallation Source by W. Wagner, the Los Alamos Neutron Science Center by K. Schoenberg, the Intense Pulsed Neutron Source (IPSN) by J. Richardson, SPIRAL2 at GANIL by J.M. Lagniel, IFMIF by P. Garin, the European Spallation Source (ESS) by P. Tindemans, the Proton Engineering Frontier Project (PEFP) by B.H. Choi, China Spallation Neutron Source (CSNS) by J. Wei, and conceptual studies for a spallation neutron source in the Basque region by G. Bauer.

The breakout sessions were focused on the following broad range of topics (the conveners are also noted):

1. Accelerator system development (front-end and linac): D. Faircloth (RAL), K. Hasegawa (JAEA) and H.F. Ouyang (IHEP)
2. Accelerator system development (ring): S. Henderson (ORNL), A. Chao (SLAC) and S. Wang (IHEP)
3. Accelerator commissioning and operations: D. Findlay (RAL), J. Galambos (ORNL), and S.N. Fu (IHEP)
4. Medical Applications: L. Teng (ANL), S. Peggs (BNL) and Q. Qin (IHEP)
5. Accelerator Projects in China: Z. Zhao (SSRF) and J. Xia (IMP)
6. Accelerator and target/experimental interface: G. Murdoch (ORNL) and J.Y. Tang (IHEP)
7. Accelerator Driven Systems, Radioactive Ion Beam Accelerators and Drivers: J. Lagniel (CEA), W.T. Weng (BNL) and X.L. Guan (CIAE)

6.1.2 Operating Spallation Neutron Sources

Table 1 shows a comparison of the operating spallation neutron sources, with parameters as presented at this Meeting. The PSI cyclotron remains the world's highest power source, as well as the highest power proton accelerator in operation, delivering 1.2 MW from the cyclotron, 800 kW of which is directed to the SINQ neutron production target. The ISIS accelerator is the world's highest power pulsed spallation neutron source, routinely delivering 160 kW to the neutron production target. The Spallation Neutron Source at Oak Ridge National Laboratory is in the initial operating phase, delivering nearly 100 kW to the production target. The Proton Storage Ring (PSR) at Los Alamos operates at 80 kW. Finally, the Intense Pulsed Neutron Source (IPNS) at Argonne National Laboratory operates at a beam power of 7 kW.

M. Seidel reported on the operation of the Megawatt Proton Beam Facility at PSI. Through a continuous program of improvements over the last 30 years, the cyclotron has reached 5000 hours of operation per year, a beam power of 1.2 MW, and an availability of 85-90%. The facility has a long history and much experience in handling

Table 1: Summary of operating Spallation Neutron Sources

Facility	Time Structure	Type	Intensity [μC] Current [μA]	Beam Energy [MeV]	Neutron Production Beam Power [kW]
PSI	DC	Cyclotron	N/A 1400 μA	590	800 (1200)
ISIS	Pulsed	Linac+Synchrotron	4.0 μC 200 μA	800	160
SNS	Pulsed	Full Energy Linac + Accumulator	6.7 μC 100 μA	890	90
LANSCE	Pulsed	Full Energy Linac + Accumulator	5.0 μC 100 μA	800	80
IPNS	Pulsed	Linac+Synchrotron	0.5 μC 15 μA	450	7

high-power proton beams, beam loss management and active component handling, as well as the recent success in operation of the first Megawatt-level liquid metal target as demonstrated in the MEGAPIE experiment. A continuous upgrade program continues with the goal of achieving 3 mA, 1.8 MW operation.

D. Findlay and D. Adams reported on the operation and recent improvements at ISIS. In a program of continual improvement over the past 20 years, the beam current has increased to 200 μA (160 kW). A. Letchford reported on a new RFQ that was recently installed and commissioned, which provided an increase in injection current to 20-30 mA. A new dual-harmonic RF system to improve the bunching factor was installed in the synchrotron. This system should allow an increase in current to 300 microamps at fixed beam loss. Recent successful tests demonstrated an increase in the capture efficiency from 93% to 97% with a subsequent measured reduction in beam loss. A second ISIS target station is presently under construction. An operational scenario is envisioned in which the first target station receives beam at 40 Hz, 240 μA and the second target station receives beam at 10 Hz, 60 μA. Plans to upgrade ISIS to 1 MW beam power, enabled by a new 3 GeV rapid-cycling synchrotron, were reported.

K. Jones and R. McCrady reported on operation of LANSCE and the PSR at Los Alamos. LANSCE has a rich history of sophisticated operation in the LAMPF-era with acceleration and transport of three beam species to 34 experimental stations. LANSCE achieved the world record for beam power delivered by a proton linac in 1983 with a 1 MW demonstration run, and operated routinely at 800 kW for LAMPF. Continuous improvements to the PSR in the 1990s resulted in a significant increase in charge delivered to the Lujan Center.

Valuable experience at the mature operating facilities (ISIS, LANSCE/PSR, IPNS, PSI) has informed all next-generation designs. Many issues first encountered, identified and studied in these facilities are crucial to the successful design and ultimate operation of the newer facilities. In particular, the identification of beam-loss mechanisms, such as halo development, the role of space-charge dynamics, beam-stripping foil interactions and formation of metastable excited states, the electron-proton instability and its mitigation, are central issues that must be understood in great detail to achieve

MW-level performance. Valuable experience from PSI, ISIS and LANSCE related to beam loss management and beamline activation monitoring and interlocks, incorporation of active handling of accelerator components, beam collimation, and the operation and handling of high-power beams has been incorporated into the recent pulsed spallation source designs for the SNS, CSNS and J-PARC. In particular, these new designs make use of dual-harmonic RF systems for improving the bunching factor, collimation systems to control beam loss, sophisticated machine protection systems, and incorporate measures to guard against the electron-proton instability. Finally, these mature facilities are extremely important testbeds for beam dynamics calculations and benchmarking that is crucial to validate tools used to complete a modern design.

Recent spallation neutron source designs have benefited from experience at the other operating proton facilities, such as the Proton Linac at the Institute for Nuclear Research, Moscow, which operates at 140-400 MeV with 150 µA output current, the Brookhaven Linac/Booster, Fermilab Linac/Booster, CERN complex and the KEK-PS.

The availability of mature operating facilities provides essential information and guidance for the new facilities and was therefore a subject of active discussion. Table 2 summarizes the availability history of the mature facilities. Newer facilities are striving for ultimate availabilities in the 90-95% range. Based on experience, this goal will be a very challenging one.

Table 2: Availability of Mature Spallation Neutron Sources

Facility (Time Period)	
IPNS (2006)	96%
PSI	85-90%
ISIS (1998-2007)	88%
Lujan Center (1995-2007)	80%

Initial SNS operating experience and beam commissioning results were presented by the author and by John Galambos. It is anticipated to take three years to ramp-up the performance of the SNS accelerator complex to 1.44 MW, 5000 hours of operation per year and >90% availability. Already in this initial operating phase, a number of important performance goals have been achieved. The linac has reached the design beam energy of 1.0 GeV in a demonstration run; the single-pulse intensity of 6 kJ/pulse in routine operation makes the SNS the "brightest" pulsed source, and a world-record beam intensity of 0.96×10^{14} protons/pulse was accumulated and extracted from the ring. Routine operation is now at a beam power of 90 kW. Beam loss in most of the accelerator is in line with expectations. Features incorporated in the design are already paying-off: the flexibility and low beam loss of the superconducting linac; the low-loss ring design features such as the dual-harmonic RF system, collimation and the careful beam-dynamics design.

6.1.3 Spallation Neutron Sources Under Construction, in Design, or Proposed

Several reports on spallation neutron sources under construction, in the design phase or proposed were presented. A summary of parameters for these facilities is shown in Table 3.

Ikeda, Hasegawa, Ikegami and Kinsho reported on progress at J-PARC. The linac commissioning is progressing well. The design beam energy of 181 MeV was

Table 3: Parameters for Spallation Neutron Sources under construction, in the design phase or proposed

Facility	Type	Energy [GeV]	Initial Beam Power /Upgrade [kW]
J-PARC	Linac (181/400 MeV) +RCS	3	600/1000
CSNS	Linac (81/132 MeV) +RCS	1.6	120/240/500
European Spallation Source	Linac	1.3	5000 (long pulse)
SNS in Basque Region	Linac (50 MeV)+RCS	2.0	250

achieved. Six of eight beam commissioning cycles were complete at the time of the meeting. The basic commissioning of the linac at low current has been accomplished, and higher intensity and higher power commissioning and operation is planned in the next runs. Installation of the 3 GeV rapid-cycling synchrotron is nearly complete with commissioning scheduled for September 2007. Goals include reaching 4 kW at 3 GeV by March 2008, and delivering first beam to the Materials/Life Science Facility in mid-2008.

Progress in the design and planning of the China Spallation Neutron Source was presented by J. Wei, S. Wang and S. Fu. The CSNS design calls for an advanced facility with initial operation at 120 kW, incorporating a straightforward upgrade path to 240 kW, with ultimate capability of 500 kW. The design strategy incorporates mature, proven technology and design choices to achieve low risk and high availability. The design utilizes an 81 MeV Drift Tube Linac, upgradeable to 132 MeV, and a 1.6 GeV, 25 Hz rapid cycling synchrotron. The first-order physics design is complete; sub-system design is nearly complete and prototyping is in progress. The start of construction is planned for 2008 with first beam in 2013. Impressive results from an RFQ developed at IHEP for ADS applications demonstrating 50 mA, 6% duty factor, 3 mA average current at 3.5 MeV were presented by H.F. Ouyang.

D. Faircloth and A. Letchford reported on the Front-End Test Stand project at RAL which is intended to demonstrate key technologies for the front-end of next generation high power accelerators, namely high-quality, high current chopped H⁻ beams. Recent development of the ISIS H⁻ Penning Surface Plasma Source has achieved impressive performance: 78 mA peak current in 500 μs pulses at 50 Hz. Chopper switch development has achieved the required ±1.4 kV with rise and fall times of less than 2 nsec.

6.1.4 Other proton/ion facilities

Since spallation neutron sources have proton beam requirements also shared by high-power injectors for high-energy physics (proton/anti-proton collisions, neutrino sources, neutrino factories, muon colliders), accelerator-driven subcritical systems, ion

linacs for production of radioactive ion beams and drivers for fusion material irradiation, reports on the various projects in these areas were reviewed. Table 4 summarizes the parameters of these facilities presented at the Meeting.

Table 4: Parameters for high power proton/ion accelerators presented at this Meeting.

Facility	Application	Type	Energy [GeV]	Beam Power [kW]
PEFP	Multipurpose	NC Linac	0.1	160
SPIRAL-2	RIB	CW SC Linac	0.040 Deut	200
CERN SPL	HEP	SC Linac	5.0	4000
IFMIF	Fusion Materials Irradiation	CW RT Linac	0.040 Deut	5000

Spiral-2 at GANIL, presented by J.M. Lagniel and T. Junquera, is under construction. Contracts for the injector and cryomodules will be complete this year with conventional construction and installation in the 2009-2011 timeframe. The driver linac makes use of CW 88 MHz quarter-wave resonators with geometric-beta of 0.07 and 0.12 to accelerate a 5 mA deuteron beam to 40 MeV, providing 200 kW beam power.

R. Garoby reported on plans for the CERN Superconducting Proton Linac and LINAC4 project. A normal conducting linac utilizing DTL/CCDTL structures produces a 90 MeV H⁻ beam which is further accelerated to 5 GeV in a superconducting linac. One set of design parameters calls for 40 mA average pulse current for 400 μs pulse length at 50 Hz providing 4 MW of beam power.

Design parameters for accelerator-driven systems with a goal of demonstrating concepts related to transmutation were discussed by J.L. Biarrotte, Z. Jie and others. The EUROTRANS parameters call for a 600 MeV, 2.5 mA CW proton source with less than 20 trips per year exceeding 1 second. An industrial transmuter is expected to require 800 MeV, 20 mA proton beam with less than three beam interruptions exceeding one second each year. These parameters require reliability many orders of magnitude beyond present performance. This will only be possible through use of highly reliable, sophisticated digital RF controls for SC cavity fault recovery.

G. Rees (RAL) was asked to consider the question of how to take the next order-of-magnitude step in beam power for short-pulse spallation neutron sources. He presented options for a 50 Hz, 10 MW short pulse spallation source based on FFAGs. He concluded that ultimately, one would design such a facility based on a 1 GeV H⁻ linac and compressor ring with two 3.2 GeV, 5 MW NFFAG (non-linear, non-scaling, non-isochronous, fixed-field alternating gradient) machines.

Impressive progress and growth in accelerator-based science in China was described in a dedicated session. Accelerators in all phases are represented in China, from the operation of a mature light source at Hefei, to the commissioning of the new Beijing Electron-Positron Collider II, to the construction of a state-of-the-art third generation

light source in Shanghai, to the design of a new high power proton accelerator for neutron scattering (CSNS).

One working group focused on medical applications of accelerators. To highlight the importance, it was noted that in Europe, one in three people will confront some form of cancer in their lifetime; it is the second most frequent cause of death. On the positive side, radiation therapy using protons, carbon ions and neutrons is the second most successful form of treatment after surgery. As a result, particle therapy is undergoing a period of rapid growing demand throughout the world with 22 particle therapy centers in operation treating 40,000 patients per year. There is interest in China to leverage the construction of CSNS to incorporate fast neutron therapy capabilities and in addition to build a rapid-cycling medical synchrotron for proton therapy.

6.1.5   Conclusion

This 18th ICANS Meeting reflected the present vigorous activity in the field of spallation neutron sources. As evidence of the healthy state of accelerator-based neutron sources one need only consider the variety of facilities and machines in all phases of operational life: very mature and mature facilities (IPNS, LANSCE, ISIS, PSI) have been operating for more than 20 years, one new facility (SNS) is beginning to operate, another (J-PARC) is in commissioning and nearing completion of construction, while others are being designed and planned (CSNS, ESS).

6.2   41st Advanced ICFA Beam Dynamics Workshop on Energy Recovery Linacs, "ERL07"

Mike Poole, Susan Smith, Bruno Muratori
Mail to: m.w.poole@dl.ac.uk s.l.smith@dl.ac.uk
ASTeC, Daresbury Laboratory, Warrington, WA4 4AD, UK

6.2.1   Introduction

The Advanced Beam Dynamics Workshop on Energy Recovery Linacs "ERL07" was held at the Cockcroft Institute, Daresbury Laboratory, Warrington, UK, from May 21-25, 2007. The workshop attracted 91 registered participants, with representatives present from a total of 24 different laboratories and institutes world wide. The first day comprised 11 plenary talks covering the status of ERL projects, prototypes development and the major technology areas for these accelerators. The next three days were reserved for break out sessions with around 100 presentations being made in the four workgroups. The final half day was used to present the conclusions and summarize the work of these groups.

6.2.2   Plenary Talks

Overviews of all the major ERL activities around the world were given. These included status reports from some of the leading experts in their field. These were:

Operating ERL Based FELs, L. Merminga (JLab)
Future ERL Based FELs, J. Clarke (ASTeC Daresbury)
ERLs as Hard X-ray Sources, G. Hoffstaetter (Cornell)
ERLs in HENP, V. Litvinenko (BNL)
High Current Research and Development ERLs, I. Ben-Zvi (BNL)
ERL Prototype at Daresbury, S. Smith (ASTeC Daresbury)
New Developments in Injectors, J. Lewellen (ANL)
High Current Superconducting RF and RF Control, T. Grimm (Niowave/MSU)
Synchronization, G. Hirst (CLF RAL)
Diagnostics, K. Jordan (JLab)
Drive Lasers for Photoinjectors, I.Will (MBI Berlin)

6.2.3   Working groups

There were four working groups, namely: injectors; optics; synchronization, diagnostics and instrumentation; and superconducting RF. All working groups had charges to look at the latest developments and possible common problems facing the accelerator community in specialized areas in the ERL laboratories around the world. The conveners and co-conveners for the working groups were:

WG1: Injectors: convener - A. Burril (BNL), co-convener - M Poelker (JLab)
WG2: Optics: convener - R. Hajima (JAEA), co-convener - H. Owen (ASTeC Daresbury)
WG3: Superconducting RF: convener - T. Smith (Stanford), co-convener - R. Rimmer (JLab)
WG4: Diagnostics, Synchronisation and Instrumentation: convener - K. Jordan (JLab), co-convener - S. Simrock (DESY)

Working Group 1:   Injectors

The charge for WG1 required status reports from the principal existing and planned injectors worldwide. It also requested an update on the progress made in this area since the previous Workshop in 2005 (ERL05). In particular vacuum problems, field emission, load-locked designs, photocathode cooling, HV breakdown, beam management and photocathode degradation were looked at in detail. This working group was also to examine the latest developments in the identification of appropriate laser wavelengths and the required laser power to achieve 100 mA average current as well as drive laser candidates and pulse shaping techniques.

In WG1 there were 22 talks including two joint sessions with WG2 and WG3. Considerable activity was reported across a broad range of DC, RF and SRF gun projects. From a single DC gun operational in 2005 a total of 5 high voltage DC guns now exist (> 250kV). There are also many functioning normal conducting RF guns, for example at FLASH, PITZ, BNL ATF, LANL, CTF (CLIC), KEK, PAL etc. The group heard reports from the two healthy SRF gun projects at FZD Dresden and BNL. The implementation of new modelling tools was discussed, including the advancement of parallelization of *elegant* and genetic optimization algorithm and simulations using VORPAL. Finally several viable laser options for current ERLs as well as future high current ERLs were presented and their merits discussed.

Working Group 2:   Optics

The charge for WG2 included status reports on some of the latest beam optics designs throughout the world for high injection/final energy ratios, an analysis of ERL merger designs compatible with emittance compensation, lattice designs for magnetized beams, bunch flattening schemes and practical multi-turn configurations. It also required an update on the progress made since ERL05, in particular linear optics for the main linac section, optics for different ERL applications, nonlinear optics, current dependent effects like BBU and CSR, other sources of emittance growth, halo development and collimation, and instrumentation and commissioning techniques.

In WG2 there were 30 talks including joint sessions with the other three groups. Several summaries of ongoing projects were given, including 4GLS, the planned test ERL at KEK, a possible ERL upgrade to the APS and a survey of optics issues for an ERL-based electron cooler at BNL. Many talks addressed the essential issue of emittance preservation, for example at BNL and KEK. The uses of multi-variant optimisation and parallelisation were reported on, in particular the use of these techniques in both injector design and for the tracking and matching code *elegant.* Several developments in the design of special optical elements were looked at. These included a method of overlaying the two main 4GLS machines with a system consisting of a spreader dipole and two solenoids together with a novel path length correcting method which used to ensure the returning bunch enters the linac with the correct phase with respect to the RF. Several talks on instabilities were also given. These included the investigation of beam loss, Touschek scattering, ion instabilities in ERLs, CSR and BBU.

Working Group 3:   Superconducting RF

The charge for WG3 also required status reports as well as assessment of the parameter space covered by ERLs currently being considered from an RF viewpoint. SRF-related ERL-specific challenges, and what optimization criteria should be used in designing the main linac, were also a charge. Participants were also asked to consider solutions that have already been developed for the SRF-specific challenges and to identify those components and topics for which further R&D work was now needed, together with the possibility of organizing this effort at an international level.

Between normal and joint sessions there were 24 talks. WG3 had two joint sessions, one with WG1 and one with WG2. Several status reports were given on experimental cryomodules and design aspects, for example from JLab and Cornell, as well as reports on investigations into optimal running temperatures. Cavity design was also investigated and discussed. This included presentations from JLab, JAEA, KEK, LBNL and Cornell as well as 4GLS. The status of tuners, microphonics and RF control was also reported on, as were RF power sources and couplers.

Working Group 4:   Diagnostics, Synchronization and Instrumentation.

The main topics to be addressed by WG4 were: procedures for commissioning and operations, transverse orbit measurements and beam profiles, longitudinal beam instrumentation for energy spread and time profiles, beam-based machine diagnosis and feedback systems, synchronization and timing systems for operations and users, and passive and active machine protection systems. These topics can be subdivided into the specifics that each proposed diagnostic method should address, including operation

phase, beam mode and location. Participants were asked to give presentations on each diagnostic method proposed which should address the measurement resolution, the dynamic range and limitations of the system due to physical, technical or noise reasons. A further question asked was whether the method discriminates between the accelerating and decelerating beams

WG4 had two joint sessions with WG2 and had a total of 18 talks. These included a status report on synchronization at LBNL together with initial results and a report on synchronization activities in ERLP, 4GLS, JLab and KEK. Several talks were given about beam instrumentation specific to ERLs, for example from JLab and the coronagraph for halo measurement at KEK. A great deal of discussion was centered on operational procedures and how to best set things up. As a result, a repository of procedures was agreed to be set up, to be hosted by ASTeC at Daresbury Laboratory.

6.2.4 ERL07 participants group photo

6.3 Report on the International Workshop on Electron Cloud Effects (ECLOUD07)

K. Ohmi[1], E.S. Kim[2] and H. Fukuma[1]
Mail to: kazuhito.ohmi@kek.jp
[1]KEK, Tsukuba, Japan
[2]KyungPook National University, Daegu, Korea

The international workshop on Electron Cloud Effects was held from 9th to 12th April 2007 at Hotel InterBurgo in Daegu, Korea. Details of arrangements in place for the workshop can be found on the web site at http://chep.knu.ac.kr/ecloud07/. Forty participants attended from China, Europe, India, Japan, Korea and USA. The workshop was organized in single sessions, and included summaries of related workshops as well as covering topics such as observations in existing accelerators, measurements and treatment of surface properties, electron cloud build-up, theory and simulation of electron cloud instabilities, and ion effects. There were 40 talks presented in the four days of the workshop, all of which are linked at:

http://chep.knu.ac.kr/ecloud07/upload/ECLOUD07_Program_ver_2_3.pdf

The scientific program was arranged as follows:

A. **Summary of related workshops:**
   e-p feedback mini-workshop (R. Macek)
   ECL2 Mini-Workshop (W. Fisher)

B. **Measurements of electron cloud effects:**
   Observation at KEKB: multi-bunch instability (M. Tobiyama)
   Observation at KEKB: single bunch instabilities (J. Flanagan)
   Observation at BEPC and BEPC-II (Y.D. Liu),
   Dust Effects in the BEPC, (Z. Deming)
   Observation at SNS, proton transverse microwave instability (S. Cousineau)
   Emittance growth in RHIC (S.Y. Zhang)
   ANKA heat load at cold undulator (S. Casalbuoni)

C. **Electron cloud build-up**
   TEVATRON MI, simulations and measurements (M. Furman, R. Zwaska)
   RHIC pressure rise and cures, molecular disorption (W. Fisher, S.Y. Zhang)
   EC trapped in quads in PSR (R. Macek) and its simulation (Y. Sato)
   EC dynamics in solenoid/quad transport (A. Molvik)
   EC density measurement at HCX (M. K. Covo) and KEKB (K. Kanazawa)
   Clearing electrode, its impedance (M. Pivi)
   SEY < 1 for conditioned surfaces (L. Pimpec, M. Pivi, S. Kato, M. Nishiwaka)
   Groove's result at SLAC (M. Pivi)
   Photoelectrons can dominate in wigglers (C. Celata, ECL2)

D. **Instabilities**
   Analysis of synchro-beta sideband (J. Falanagan, H. Jin)
   Simulation codes for single bunch effect (K. Sonnad, A. Markovik, G. Poeplau)
   Longitudinal single bunch instability (Y.D. Liu)
   Moving frame method towards self consistent simulation (J-L. Vay)

Tune shift measurements, KEK (T. Ieiri) and CESR (M. Palmer), and theory (L. Schachter)
Analytical treatment of EC induced wake force (S. Heifets)
Tune shift limit and dynamic aperture (J. Gao)
Physical and artificial noise effects in PIC simulation (K. Ohmi)
Ion instabilities in ILC (E.S.Kim) and Super KEKB (H. Fukuma)

The next ECLOUD workshop is expected to be held at Indiana University.

7   Recent Doctoral Theses

7.1   Collection and Muon Acceleration in the Neutrino Factory Project

Franck Lemuet
Mail to: lemuet@lpsc.in2p3.fr or meot@lpsc.in2p3.fr
LPSC, Grenoble, France

Name: Franck Lemuet
University: University Paris-Sud 11, France
Institution: Faculty of Sciences
Thesis Title: Collection and Muon Acceleration in the Neutrino Factory Project
Graduation date: 3 May 2007
Supervisor: Dr. F. Méot, CEA and IN2P3, LPSC Grenoble

Abstract:
The thesis represents a study of muon collection in a quadrupole channel and an analysis of muon acceleration in a fixed-field alternating gradient accelerator (FFAG) in the context of a Neutrino Factory.

The work starts by exploring beam dynamics in a 4-horn assembly, proposed in the CERN Neutrino Factory study, to funnel the beam from the pion production target into a channel where the pions decay to muons. Results for the transmission demonstrate that the use of alternating gradient focussing is a viable alternative to the solenoid channel generally favoured for muon capture. The necessary computational codes are developed and tested in the thesis and are now available for investigation of related problems.

The principal aim of the work is to provide modelling tools that can be used to study muon acceleration in re-circulating linear accelerators (RLA) and FFAGs, with the emphasis being placed on FFAGs. As a consequence of the developments, the ZGOUBI [1] code is now able to model all types of FFAG and has become one of the major tools for examining particle trajectories and studying machine parameters in these types of accelerator.

Simulations of an isochronous FFAG lattice have identified the degree of muon loss during acceleration and the dynamic aperture limitations due to non-linearities in the

magnetic fields. Techniques developed in ZGOUBI have also facilitated study of an electron model of a non-scaling FFAG designed for protons, using the same type of lattice structure.

The code may also be applied to the non-scaling electron FFAG, EMMA, under construction at the Daresbury Laboratory in the U.K. Beam dynamics issues in scaling FFAGs have also been addressed, and the RACCAM project is under study in order to develop spiral FFAG lattices with applications to medical therapy.

7.2 Investigations of Non-Destructive Emittance Measurements of a Negative Ion Beam

Christoph Gabor
Mail to: c.gabor@rl.ac.uk
ASTeC Intense Beams Group, STFC Rutherford Appleton Laboratory, U.K.

Name: Christoph Gabor
University: University of Frankfurt, Germany
Institution: Institute for Applied Physics
Thesis Title: "Untersuchungen zur zerstörungsfreien Emittanzmessungan einem negativen Wasserstoffstrahl", published in German;
English title: Investigations of non-destructive emittance measurements of a negative ion beam
Graduation date: 3 May 2007
Supervisor: Professor Ulrich Ratzinger (u.ratzinger@iap.uni-frankfurt.de)

Abstract:
For diagnostic studies, non-destructive measuring devices provide minimum influence on the ion beam. In addition, for applications like High Power Proton Accelerators (HPPA), problems often arise due to the power deposition on wires, pinhole or slit plates used for different types of beam diagnostics. Diagnostic devices without any mechanical part inside the ion beam therefore promise a large improvement.

An H⁻ ion beam offers the opportunity for non-destructive diagnostics based on the principle of photo detachment. By the interaction of light with H⁻ ions, the additional electron can be detached and a small number of neutrals will be produced. A magnetic dipole field can then be used to separate the detached electrons and neutrals from the ions. In terms of a slit-slit emittance instrument, the first slit (determining the position) is then replaced by a laser beam and at the 2nd measurement plane, where the angle (x', y') is determined, a particle detector with spatial resolution can be used.

Based on this principle, a transverse emittance measurement device has been developed and tested on a small ion beam line with a beam energy of 6 keV and an ion current of $I_{H^-} \sim 1$ mA. The beam line consisted of an ion source, a differential pumping tank and an electrostatic lens system to focus the H⁻ beam. For the "proof of principle" experiment, a thin-disc laser (because of its very good beam propagation parameters) with a wavelength of 1030 nm, a dipole magnet with 30° deflection angle and a P43 scintillator with Al-layer including a LN2 cooled CCD camera were used. Measurements with photo neutralized particles were possible as well as comparisons

between photo detachment and traditional emittance measurements. In the expected range of misalignment, the latter experiments showed good agreement.

It was also possible to study further aspects of the new diagnostic method. Compared with traditional 2-D emittance instruments, the photo detachment method offers more information about the phase space. Instead of using a so called slit-slit transfer function, like the 2-D emittance scanner, the photo detachment method based on a slit-point principle resulted in better information especially about the aberrations. This aspect was verified with experimental data as well as particle simulation.

7.3 Beam Dynamics in an Ionisation Cooling Channel

Christopher T. Rogers
Mail to: c.rogers@rl.ac.uk
ASTeC Intense Beams Group, STFC Rutherford Appleton Laboratory, U.K.

Name: Chris Rogers
University: Imperial College University of London, UK
Affiliation: Blackett Laboratory, Department of Physics
Thesis Title: Beam Dynamics in an Ionisation Cooling Channel
Graduation date: 21 August 2007
Supervisor: Professor K. Long

Abstract:

This thesis gives a detailed exposition of the simulation used in the Muon Ionisation Cooling Experiment (MICE) at the Rutherford Appleton Laboratory, U.K. The accuracy of the simulation is studied and the cooling and emittance measurement performance of the experiment is simulated.

MICE uses a custom-built simulation tool, G4MICE, based on the GEANT4 physics modelling library. In G4MICE electromagnetic fields are simulated using realistic maps while the physical apparatus is simulated using complex curved shapes, enabling particle tracking to arbitrary precision. The relationship between tracking accuracy and the modelling of these elements of MICE is examined. This enables various features of the beam optics to be simulated in G4MICE. With knowledge of the accuracy of such simulations, the full six dimensional beam dynamics of the cooling channel is examined. The cooling performance of the final MICE configuration is then simulated in six dimensions to high precision.

MICE uses a particle-by-particle technique for the emittance measurement, which introduces unique challenges in achieving the unprecedented precision that the experiment demands. In the final chapter of the thesis the effect of these errors on the six-dimensional emittance measurement is simulated and compared with the expected cooling performance.

MICE begins data-taking in Autumn 2007.

7.4 Electron-Proton Dynamics for Long Proton Bunches in High Intensity Proton Rings

Yoichi Sato
Mail to: yoichisato@postman.riken.jp
Accelerator Division, Nishina Center for Accelerator-Based Science, RIKEN, Japan

Name: Yoichi Sato
University: Indiana University, Bloomington, Indiana, USA
Thesis Title: Electron-Proton Dynamics for Long Proton Bunches in High Intensity Proton Rings
Graduation Date: 16 December 2006
Supervisor: Professor S.Y. Lee

Abstract:
   Electron clouds have been found to play an important role in the stability of high intensity beams. This dissertation presents the development of the new electron cloud module and its implementation in the ORBIT code, including benchmarks demonstrating its capability to examine the effects of the electron cloud on the proton beam and simulation studies of electron cloud dynamics. The thesis studies the sensitivity of the electron cloud properties to different proton beam profiles. Using the secondary electron yield (SEY) and primary proton loss as free parameters, the thesis tries to reproduce the experimental data on the electron cloud recovery, prompt and sweep electron vs the beam intensity, obtained from the PSR at the Los Alamos National Laboratory.

8 Forthcoming Beam Dynamics Events

8.1 Workshop on FFAG Accelerators

Yoshiharu Mori
Kyoto University – Reactor Research Institute (KURRI), Osaka, Japan
Mail to: mori@KL.rri.kyoto-u.ac.jp

   The next workshop on Fixed-Field Alternating Gradient (FFAG) accelerators will be held at Kyoto University Reactor Research Institute, KURRI from Nov 5-10, 2007. KURRI is located in Kumatori, Osaka, Japan.
   The meeting will be the last in the series of twice-yearly FFAG workshops, before switching to an annual event. The previous workshop was held in Grenoble, France, in April 2007 (http://lpsc.in2p3.fr/congres/FFAG07) and attracted over 50 participants. The programme for Osaka is expected to be similar and cover theory, experiment and application of all types of FFAG accelerators. Details will progressively appear during the next few weeks at http://hadron.kek.jp/FFAG/FFAG07_HP

8.2 Workshop on Sources of Polarized Electrons and High Brightness Electron Beams (PESP2008)

Matt Poelker
Mail to: poelker@jlab.org
Thomas Jefferson National Accelerator Facility
12000 Jefferson Ave., Newport News, VA 23606

Workshops on Polarized Electrons have been conducted since 1988. These workshops provide an excellent venue for reporting progress in the field of polarized electron beam generation, and have contributed significantly toward development of successful physics programs at today's nuclear and high energy accelerator facilities. New initiatives such as the International Linear Collider, the CERN Linear Collider, and electron/ion collider proposals ELIC and eRHIC will likely also benefit from the creative spirit of these workshops.

Jefferson Lab will host the next polarized electron source workshop, October 1-4, 2008 (preceding the International SPIN Symposium, as is customary). Besides the usual status reports from laboratories and research groups worldwide, the workshop agenda will focus on recent developments related to high polarization photocathodes, UHV/XHV vacuum research, support for parity-violation experiments, drive lasers, gun and photo-injector modeling, load-locked gun designs, high voltage handling, field emission suppression and electron beam polarimetry. Workshop organizers expect to attract participants from the research field known as "spintronics" which hopes to exploit the spin nature of electrons to develop commercial applications such as enhanced data storage and optical computing. Sessions will be devoted to programs using high current unpolarized GaAs photoguns, a field with many shared technological challenges.

Registration information will be made available in the next ICFA newsletter and at the PESP2008 web page http://conferences.jlab.org/pes2008/index.html, which is under development.

9 Announcements of the Beam Dynamics Panel

9.1 ICFA Beam Dynamics Newsletter

9.1.1 Aim of the Newsletter

The ICFA Beam Dynamics Newsletter is intended as a channel for describing unsolved problems and highlighting important ongoing works, and not as a substitute for journal articles and conference proceedings that usually describe completed work. It is published by the ICFA Beam Dynamics Panel, one of whose missions is to encourage international collaboration in beam dynamics.

Normally it is published every April, August and December. The deadlines are 15 March, 15 July and 15 November, respectively.

9.1.2   Categories of Articles

The categories of articles in the newsletter are the following:

1. Announcements from the panel.

2. Reports of beam dynamics activity of a group.

3. Reports on workshops, meetings and other events related to beam dynamics.

4. Announcements of future beam dynamics-related international workshops and meetings.

5. Those who want to use newsletter to announce their workshops are welcome to do so. Articles should typically fit within half a page and include descriptions of the subject, date, place, Web site and other contact information.

6. Review of beam dynamics problems: This is a place to bring attention to unsolved problems and should not be used to report completed work. Clear and short highlights on the problem are encouraged.

7. Letters to the editor: a forum open to everyone. Anybody can express his/her opinion on the beam dynamics and related activities, by sending it to one of the editors. The editors reserve the right to reject contributions they judge to be inappropriate, although they have rarely had cause to do so.

The editors may request an article following a recommendation by panel members. However anyone who wishes to submit an article is strongly encouraged to contact any Beam Dynamics Panel member before starting to write.

9.1.3   How to Prepare a Manuscript

Before starting to write, authors should download the template in Microsoft Word format from the Beam Dynamics Panel web site:

http://www-bd.fnal.gov/icfabd/news.html

It will be much easier to guarantee acceptance of the article if the template is used and the instructions included in it are respected. The template and instructions are expected to evolve with time so please make sure you always use the latest versions.

The final Microsoft Word file should be sent to one of the editors, preferably the issue editor, by email.

The editors regret that LaTeX files can no longer be accepted: a majority of contributors now prefer Word and we simply do not have the resources to make the conversions that would be needed. Contributions received in LaTeX will now be returned to the authors for re-formatting.

In cases where an article is composed entirely of straightforward prose (no equations, figures, tables, special symbols, etc.) contributions received in the form of plain text files may be accepted at the discretion of the issue editor.

Each article should include the title, authors' names, affiliations and e-mail addresses.

9.1.4 Distribution

A complete archive of issues of this newsletter from 1995 to the latest issue is available at

http://icfa-usa.jlab.org/archive/newsletter.shtml.

This is now intended as the primary method of distribution of the newsletter.

Readers are encouraged to sign-up for electronic mailing list to ensure that they will hear immediately when a new issue is published.

The Panel's Web site provides access to the Newsletters, information about future and past workshops, and other information useful to accelerator physicists. There are links to pages of information of local interest for each of the three ICFA areas.

Printed copies of the ICFA Beam Dynamics Newsletters are also distributed (generally some time after the Web edition appears) through the following distributors:

Weiren Chou	chou@fnal.gov	North and South Americas
Rainer Wanzenberg	rainer.wanzenberg@desy.de	Europe++ and Africa
Susumu Kamada	Susumu.Kamada@kek.jp	Asia**and Pacific

++ Including former Soviet Union.

** For Mainland China, Jiu-Qing Wang (wangjq@mail.ihep.ac.cn) takes care of the distribution with Ms. Su Ping, Secretariat of PASC, P.O. Box 918, Beijing 100039, China.

To keep costs down (remember that the Panel has no budget of its own) readers are encouraged to use the Web as much as possible. In particular, if you receive a paper copy that you no longer require, please inform the appropriate distributor.

9.1.5 Regular Correspondents

The Beam Dynamics Newsletter particularly encourages contributions from smaller institutions and countries where the accelerator physics community is small. Since it is impossible for the editors and panel members to survey all beam dynamics activity worldwide, we have some Regular Correspondents. Their task is to identify interesting activities and either report on them themselves or find appropriate persons to provide reports. We hope eventually to create a "compact and complete" list providing coverage worldwide. The present Regular Correspondents are as follows:

Liu Lin	Liu@ns.lnls.br	LNLS Brazil
Sameen Ahmed Khan	Rohelakan@yahoo.com	SCOT, Middle East and Africa

We are calling for more volunteers as Regular Correspondents.

9.2 ICFA Beam Dynamics Panel Members

Name	eMail	Institution
Caterina Biscari	caterina.biscari@lnf.infn.it	LNF-INFN, Via E. Fermi 40, C.P. 13, Frascati, Italy
Yunhai Cai	yunhai@slac.stanford.edu	SLAC, 2575 Sand Hill Road, MS 26 Menlo Park, CA 94025, U.S.A.
Swapan Chattopadhyay	swapan@dl.ac.uk	The Cockcroft Institute, Daresbury Laboratory, Daresbury, Warrington WA4 4AD, U.K.
Weiren Chou (Chair)	chou@fnal.gov	Fermilab, MS 220, P.O. Box 500, Batavia, IL 60510, U.S.A.
Yoshihiro Funakoshi	yoshihiro.funakoshi@kek.jp	KEK, 1-1 Oho, Tsukuba-shi, Ibaraki-ken, 305-0801, Japan
Miguel Furman	mafurman@lbl.gov	Center for Beam Physics, LBL, Building 71, R0259, 1 Cyclotron Road, Berkeley, CA 94720-8211, U.S.A.
Jie Gao	gaoj@ihep.ac.cn	Institute for High Energy Physics, P.O. Box 918, Beijing 100039, China
Ajay Ghodke	ghodke@cat.ernet.in	RRCAT, ADL Bldg. Indore, Madhya Pradesh, India 452 013
Ingo Hofmann	i.hofmann@gsi.de	High Current Beam Physics, GSI Darmstadt, Planckstr. 1, 64291 Darmstadt, Germany
Sergei Ivanov	ivanov_s@mx.ihep.su	Institute for High Energy Physics, Protvino, Moscow Region, 142281 Russia
Kwang-Je Kim	kwangje@aps.anl.gov	Argonne Nat'l Lab, Advanced Photon Source, 9700 S. Cass Avenue, Bldg 401/C4265, Argonne, IL 60439, U.S.A.
In Soo Ko	isko@postech.ac.kr	Pohang Accelerator Lab, San 31, Hyoja-Dong, Pohang 790-784, South Korea
Alessandra Lombardi	Alessandra.Lombardi@cern.ch	CERN, CH-1211, Geneva 23, Switzerland
Yoshiharu Mori	mori@kl.rri.kyoto-u.ac.jp	Research Reactor Inst., Kyoto Univ. Kumatori, Osaka, 590-0494, Japan
Chris Prior	c.r.prior@rl.ac.uk	ASTeC Intense Beams Group, STFC RAL, Chilton, Didcot, Oxon OX11 0QX, U.K.
David Rice	dhr1@cornell.edu	Cornell Univ., 271 Wilson Laboratory, Ithaca, NY 14853-8001, U.S.A.
Yuri Shatunov	Yu.M.Shatunov@inp.nsk.su	Acad. Lavrentiev, prospect 11, 630090 Novosibirsk, Russia
Junji Urakawa	junji.urakawa@kek.jp	KEK, 1-1 Oho, Tsukuba-shi, Ibaraki-ken, 305-0801, Japan
Jiu-Qing Wang	wangjq@mail.ihep.av.cn	Institute for High Energy Physics, P.O. Box 918, 9-1, Beijing 100039, China
Rainer Wanzenberg	rainer.wanzenberg@desy.de	DESY, Notkestrasse 85, 22603 Hamburg, Germany
Jie Wei	wei1@bnl.gov	BNL, Bldg. 911, Upton, NY 11973- 5000,U.S.A.

The views expressed in this newsletter do not necessarily coincide with those of the editors.
The individual authors are responsible for their text.